FUNDAMENTAL INVESTIGATIONS INTO THE FACTORS AFFECTING RESPONSE OF LACCASE-BASED ELECTROCHEMICAL BIOSENSORS

A Thesis submitted in fulfilment of the requirements for the degree of

Doctor of Philosophy

of

RHODES UNIVERSITY

by

RONEN FOGEL

January, 2011

General Abstract:

Given their widespread effects and distribution in both natural and industrial environments, the monitoring of phenolic compounds is of considerable analytical interest. Electrochemical biosensor technologies, in particular those comprising laccase enzymes, afford many potential benefits to address this analytical need. However, several key factors affecting sensor response currently limit their applicability.

This Thesis reports on the fabrication and optimisation of an electrochemical laccase-based biosensor towards the application of the monitoring of phenolic compounds. Selected factors considered to affect sensor response were investigated using the optimised biosensor. These included: electrochemical, biochemical and substrate-dependent factors, which were found to intersect in modulating biosensor response signals. Through the application of transducer-dependent and substrate-dependent parameters, the selective and simultaneous detection of a mixture of different phenolic analytes is successfully demonstrated.

This Thesis also investigates the use of Quartz-Crystal Microbalance with Dissipation (QCM-D) technology, an analytical technique that measures physical parameters of thin-film structures, towards the successful monitoring of enzyme immobilisation strategies. These strategies are fundamental to the successful fabrication of biosensors, and the real-time monitoring of immobilised film formations is of considerable research interest. In the studies reported on in this Thesis, QCM-D technology was demonstrated to be an effective complementary technology in the prediction of film immobilisation techniques on the resultant biochemical kinetics of immobilised enzymes.

To my beloved family,

who must have surely called off the search for me by now.

Sorry, I meant to call, but I've been writing this.

"This is how you do it: you sit down at the keyboard and you put one word after another until it's done. It's that easy – and that hard." – Neil Gaiman.

Acknowledgements

This thesis would not have been possible without the following people:

Firstly, to the grand-parents of this body of work: both to my familial parents, Mr D. and Mrs. J. Fogel, and my academic supervisor, Prof. J. L. Limson. Words cannot adequately convey my gratitude to them for their constant support, advice, loving guidance and care which ensured the completion of this project.

Secondly, to Ms. K. T. Sealy-Fisher, for everything she's done and continues to do. From throwing herself into a car to pick me up from work at 4 a.m., shoring up my caffeine-riddled nervous system with rest and food, having ideas bounced off of her, to sticky-taping my sanity together during the writing-up phase, her selfless and essential help throughout all the phases of research were always imbued with love.

Thirdly, the Biosensor Research Group - a better group of colleagues is impossible to imagine. Thanks for all the help and work-related commiserations, especially those occurring beyond 8 p.m. In the same breath, the enormous social support network of my friends and sometimes-digsmates who have, for years in some cases, stoically put up with my odd views on Life-as-interpreted-by-Science and the other Just-plain-Odd views. The shared conversations and teachings for both of these aforementioned categories are dearly remembered. While there are far too many names to mention, I have thought of all of you while writing this paragraph. If you fall into this category and are uncertain – just ask me.

Finally, my sincerest thanks to the following, for the funding disbursed throughout the duration of this project – the Deutscher Akademischer Austausch Dienst (DAAD), the DST/Mintek Nanotechnology Innovation Centre (NIC), the East London Chevra Kadisha, Mintek/AuTEK, the National Research Foundation (NRF) of South Africa and Rhodes University, especially their Research Office.

Table of Contents

Table of Contents

Table of Contents

Table of Contents

Table of Contents

Table of Contents

Table of Contents

FIGURES and TABLES

List of Figures occurring in this Thesis:

Figures and Tables

Figures and Tables

Figures and Tables

Figures and Tables

Figures and Tables

Figures and Tables

List of Tables occurring in this Thesis:

Figures and Tables

Figures and Tables

EQUATIONS and SCHEMES

The following equations and schemes are referenced in-text.

Scheme 2.1:

$$E + S \underset{k_{-1}}{\overset{k_1}{\rightleftharpoons}} ES \xrightarrow{k_2} E + P$$

Equation 2.1:

$$\frac{d[P]}{d(t)} = v = k_2[ES]$$

Equation 2.2:

$$\frac{d[P]}{d(t)} = v = \frac{k_2[E]_{tot}[S]}{([k_2 + k_{-1}]/k_1) + [S]}$$

Equation 2.3:

$$\frac{d[P]}{d(t)} = v = \frac{v_{max}[S]}{K_m + [S]}$$

Equation 2.4:

$$K_m = \frac{([E]_{tot} - [ES])[S]}{[ES]}$$

Equation 2.5:

$$v = \frac{v_{max}[S]^{nH}}{K' + [S]^{nH}}$$

Equations and Schemes

Scheme 2.2:

$$O + ne^- \underset{k_b}{\overset{k_f}{\rightleftharpoons}} R$$

Equation 2.6:

$$y = d + \frac{(a-d)}{(1+(x/c)^b)}$$

Equation 2.7:

$$y = d - \frac{d}{(1+(x/c))}$$

Equation 2.8:

$$y = \frac{(d)(x)}{(c+x)}$$

Equation 3.1:

$$i_{DL} = \frac{\Delta E}{R_S} \; e^{\frac{-t}{(C_{DL})(R_S)}}$$

Equation 3.2:

$$i_{ch} = A_{surf} C_{dl} \nu$$

Equation 3.3:

$$\nu = \frac{\Delta A}{\Delta t.\varepsilon.[C].L.dl}$$

Equation 4.1:

$$I_p = 0.4463 \left(\frac{F^3}{RT}\right)^{1/2} n^{3/2} A D_O^{1/2} C_O^* \nu^{1/2}$$

Equations and Schemes

Equation 4.2:

$$\nu_{max} = k_2.[E_{tot}]$$

Equation 5.1:

$$dE = E_{p,a} - E_{p,c}$$

Equation 5.2:

$$\%I = \frac{I_{p,a}}{I_{p,c}}$$

Equation 5.3:

$$\%Q = \frac{Q_{p,a}}{Q_{p,c}}$$

Equation 5.4:

$$Q_{w,c} = \Delta Q_{w,red} - \Delta Q_b$$

Equation 5.5:

$$\text{Sensitivity} \propto \frac{i_{max}}{K_m} = \left(\frac{\nu_{max}}{K_m}\right)\left(\frac{\text{Phenol oxidised}}{\text{Quinone produced}}\right) = \left(\frac{k_2(P/Q)}{K_m}\right)[E]_0$$

Equation 5.6 :

$$1/K_m = \frac{k_1}{k_2} + \frac{k_{-1}}{k_1}$$

Equation 5.7:

$$1/K_m^{app} = \frac{k_1}{k_2(P/Q)} + \frac{k_{-1}}{k_1}$$

Equation 5.8:

$$\%I \sim \left(\frac{\text{Quinone produced}}{\text{Phenol oxidised}}\right)$$

Equation 5.9:

$$\frac{\%I}{K_m} \sim 1/K_m \propto \text{Sensitivity}$$

Equation 6.1:

$$i_t = \left(\frac{dQ}{dt}\right) = nF\left(\frac{dN}{dt}\right) = nFAD_O\left(\frac{\delta \mathbf{O}}{\delta x}\right)_{x=0,t}$$

Equation 6.2:

$$i_t = \frac{nFAD_O^{1/2}C_O^*}{\Pi^{1/2}t^{1/2}}$$

Equation 6.3:

$$I_{l,c} = \frac{nFAD_O[C_{O^*} - C_{O(x=0)}]}{\delta_O}$$

Equation 6.4:

$$\delta_O = 1.61D_O^{1/3}\omega^{-1/2}\nu^{1/6}$$

Equations and Schemes

Equation 7.1:

$$\Delta m = \Delta f \times C / n$$

Equation 8.1:

$$V.I. = \Delta f_{tot} / \Delta D_{tot}$$

List of Symbols and Abbreviations

Usual values are bolded, if other values occur elsewhere in this Thesis. Absent Chapter Reference indicate common usage throughout this Thesis.

Symbol	Meaning	Usual Units	Chapter Reference
	Biochemical and biosensor parameters		
I	Current	A	
i	current density (I / surface area)	$A.m^{-2}$	
I_{max}	Maximal current	A	2, 4
i_{max}	Maximal current density	$A. m^{-2}$	2-6, 8
U	Enzyme activity	Unit ($\mu mol.min^{-1}$)	
v_{max}	Maximal enzyme velocity	$mol.s^{-1}$	2-6,8
v /K	Enzymatic specificity constant	$mol.s^{-1}.M^{-1}$	2, 4,5
i/K	Electrochemical specificity constant	$A.m^{-2}.M^{-1}$	2,4,5
n_H	Hill's coefficient	-	2,4
K_m	Michaelis constant	M	2-6,8
S	Substrate concentration	M	2
P	Product concentration	M	2
E	Enzyme	-	2
ES	Enzyme-substrate complex	-	2
k_1	Enzyme-substrate assembly rate constant	s^{-1}	2-6,8
k_{-1}	Enzyme-substrate disassembly rate constant	s^{-1}	
k_2 (k_{cat})	Catalytic rate constant	s^{-1}	
Sensitivity	Biosensor sensitivity at linear range	$A.m^{-2}.M^{-1}$	
	Modelling parameters		
a	Minimum current density asymptote	$A.m^{-2}$	
b	degree of sigmoidality	-	
d	Maximal current density asymptote	$A. m^{-2}$	
c	Sigmoidal Function mid-point	M	
SSD	Sum of Squared Differences	$\mathbf{A^2}$	
χ^2	Chi-Squared Statistic	**A**	

List of Symbols and Abbreviations

Electrochemical parameters

Symbol	Meaning	Usual Units	Chapter Reference
E	Potential vs. reference electrode	V	3-5, 7
$E_{p,a}$	Oxidative peak potential	V	3-5,7
dE	$\lvert E_{p,a} - E_{p,c} \rvert$	V	5
$E_{p,c}$	Reductive peak potential	V	3, 5-6
$E_{1/2}$	Half-wave potential	V	6
$I_{p,a}$	Oxidative peak current	A	3,
$I_{p,c}$	Reductive peak current	A	5
%I	Current yield ($I_{p,a} / I_{p,c} \times 100$)	%	5
$Q_{p,a}$	Oxidative peak charge	C	5
$Q_{p,c}$	Reductive peak charge	C	5
$Q_{w,c}$	Reductive wave charge	C	5
%Q	Charge yield: $\lvert Q_{p,a} / Q_{p,c} \times 100 \rvert$	%	5
	: $\lvert Q_{p,a} / Q_{w,c} \times 100 \rvert$	%	5
C_{DL}	Double-layer charging capacitance	F	3
dI	Separation distance of anodic and cathodic current/s	A	3
ν	Scan rate	$V.s^{-1}$	4
E_D	Analyte-detecting potential	V	6
E_R	Resting potential	V	6

Piezoelectric Measurements

QCM-D	Quartz-Crystal Microbalance with Dissipation		7-8
f	Frequency	Hz	7-8
D	Dissipation	-	7-8
V.I.	Viscoelastic Index (f/D)	Hz	7-8
M_s	Sauebrey Mass	$ng.cm^{-2}$	7-8
M_v	Voigt-element Modelled Mass	$ng.cm^{-2}$	7-8
μ	Viscosity		7-8
G	Shear modulus		7-8

List of Symbols and Abbreviations

Commonly-used acronyms and abbreviations

Abbreviation	Meaning	
[A]	Concentration of substance A	M
t	time	s
pH	logarithm of proton concentration, H^+	$\log_{10}[H^+]$
ε	Molar extinction co-efficient	$M^{-1}.m^{-1}$
R^2	Pearson's Product-Moment Correlation Coefficient	-
C.V.	Co-efficient of variation (Uncertainty of observation / mean of observation x 100)	-
	Transducers	
GCE	Glassy Carbon Electrodes	
AuE	Gold Electrodes	
	Proteins and Reagents	
BSA	Bovine Serum Albumin	
SLB	0.1 M succinic acid - 0.1M lactic acid buffer	
PHE	Phenol (Phenol)	
CAT	Catechol (o- diphenol)	
3-MC	3-methyl catechol (3-methyl o-diphenol)	
HQ	Hydroquinone (p- diphenol)	
BZT	1,2,4-benzenetriol (o-, p- triphenol)	
2-AP	2-aminophenol (o-amino phenol)	
P-CL	p-cresol (p-methyl phenol)	
GOL	Guaiacol (o-methoxy phenol)	
GA	Gallic acid (p-carboxy, o-triphenol)	
ABTS	2,2'-azino-bis(3-ethylbenzthiazoline-6-sulphonic acid)	
	Electrochemical Waveforms	
CV	Cyclic Voltammetry	
CA	Chronoamperometry	
MPCA	Multiple-Pulse Chronoamperometry	

Chapter 1: General Introduction

1.1 Chapter Overview

This chapter aims at contextualising the research reported on in this Thesis. To this end, a literature review is presented, followed by the identification of current knowledge gaps pertaining to this research.

The literature review provided outlines the necessity for, and methods by which, monitoring of phenolic compounds occurring at the time of writing, before giving an overview of biosensor technology in general, and the current state of research in laccase-based electrochemical biosensors for phenolics detection.

The identification of current knowledge gaps is centred on laccase-based biosensor processes. In this section, the various factors that currently contribute to limit the application of this technology are briefly discussed, in order to motivate for the proceeding research reported on in this Thesis.

1.2 Literature Review:

1.2.1: Phenolic compounds

1.2.1.1Chemical and physical properties of phenolic compounds

Phenolic compounds are a class of compounds, characterised by the presence of a benzene ring onto which a hydroxyl substituent is attached (McMurry, 2000a; Stalikas, 2007). The hydroxyl substituent makes phenolic compounds weakly acidic (McMurry, 2000a; Schweigert et al., 2001). Figure 1.1 depicts the generalised chemical structure of a phenolic compound.

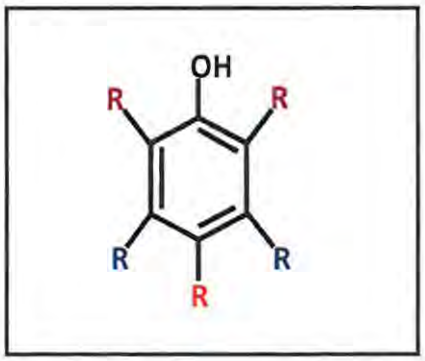

Figure 1.1: Generic structure of a phenolic compound.

R represents any substituent. In the parent compound, phenol, R is a hydrogen substituent. Red represents the *ortho*-position, blue the *meta* position and orange the *para* position of the substituents, relative to the hydroxyl group.

The aromatic nature of the benzene ring onto which substituents are anchored provides a high degree of stability, decreasing the reactivity of the phenolics towards many organic chemical interactions and enhancing their residence time in environmental systems. The conjugated bonds of the benzene ring carbons provides a resonance structure that delocalises Π electrons throughout the benzene molecule, providing an evenly-distributed electron density around the ring, which precludes many substitution and elimination reactions from occurring (McMurry, 2000b). Conjugation allows for intra-molecular electron transfer to occur, both within the ring between the substituents and the ring, providing a further stability when an electron is abstracted from the compound (McMurry, 2000b). This mono-electron removal results in the formation of a carbocation radical that is stabilised by the resonance intermediates, as electron donation within the ring structure stabilised the positive radical charge (McMurry, 2000c). Further stability of the resonance forms is also noted with the inclusion of substituents with electron-donating resonance effect, such as halogens and amino substituents, and further hydroxyl and alkoxyl substitution. It is important to note that many of these substituents are electron-withdrawing groups (from an electronegativity inductive perspective), withdrawing some of the electron (i.e. electron density) from the benzene ring and destabilising it. This, in some cases (such as halogens), may counteract their electron-donating effects towards the resonance structure. Other electron-withdrawing groups (notably carbonyl, cyano and nitro substituents) are also classed as electron-withdrawing groups, further helping to destabilise the resonance structure (McMurry, 2000c).

Many of the physical and chemical properties attached to specific phenolic compounds are dependent on, and modulated by, the nature of the substituents attached to the conjugated ring. Phenolic compounds are cited as being volatile or semi-volatile, at room temperatures, dependent on their substituents (Soares et al., 2008) and the aromaticity of phenolics makes them readily absorb UV (i.e. < 280 nm wavelength) light (Robbins, 2003). Due to the presence of the benzene ring, many simple phenolic compounds are weakly soluble in aqueous solutions, albeit slightly more soluble in alkaline solutions, due to their acidity. The presence of polar (e.g. –OH) and ionic (e.g. –COOH. –X, $–NH_2$) groups tend to increase the aqueous solubility, while the presence of non-polar groups (e.g. $–CH_3$) tends to achieve the converse.

The reactivity of phenolics is generally initiated by, and results in alterations of, the substituent groups attached to the benzene ring. The hydroxyl substituent, in particular, is a strongly-activating ortho- and para-directing substituent (Figure 1.1) due to the donation of electrons via the Π-bonds overlapping from the oxygen substituent to the benzene ring (McMurry, 2000b). The directing effect of the hydroxyl group permits the relatively easy attachment of halogens to the benzene rings at the *ortho* and *para* positions of the benzene ring. When oxidised, phenolics can reversibly form cyclic, non-aromatic quinone compounds. Figure 1.2 depicts the relevant chemical forms. (McMurry, 2000b)

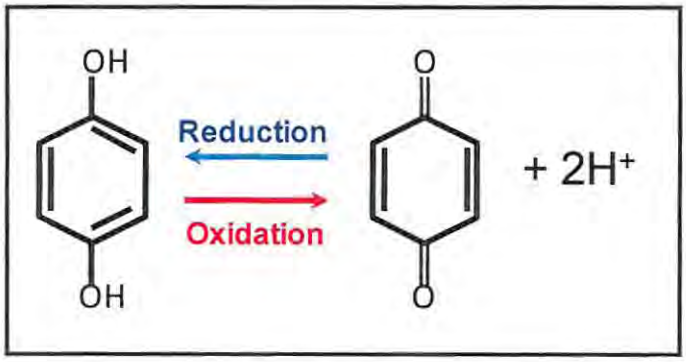

Figure 1.2: Chemical structures of hydroquinone (1,4-dihydroxybenzene) and its corresponding quinone, *p*-quinone.

Note the alteration of the double-bond structure within the benzene ring. Adapted from McMurry, 2000b.

1.2.1.2: Distribution and effect of phenolic compounds

Two broad classifications of phenolic compounds are apparent when considering both the effects and the distribution of phenolic compounds in the environment and, by inference, in human contact. Generally, anthropogenic phenolic compounds are produced in great quantities and act as harmful xenobiotic compounds which are manufactured by-products of industrial processes. Naturally-generated phenolics are generally found in lesser quantities and possess numerous food and medicinal applications.

This broad, almost antithetical, gap between the two classes of phenolic compounds defined above arises from the initial chemical definition of a phenolic compound (Section 1.2.1). The classification of phenolics encompasses a vast number of chemical compounds, from the essential roles tyrosine and dopamine play in mammals (Garrett and Grisham, 1999c) to the toxic effects of pentachlorophenol (Oikari et al., 1992), ranging in size from humic acids ($\leq$ 22.6 kDA, Smith et al., 2000) to the simplest, phenol (94 Da) (Stalikas, 2007). Phenolic compounds must contain at least one aromatic ring to which a hydroxyl substituent is attached, but the presence of this defining structure does not govern the effects, mode of biological action of same and other relevant properties of a given phenolic (Schweigert et al., 2001, Aptula et al., 2005). Of far more importance, in terms of assaying the detrimental/beneficial effects of a phenolic group are the other, secondary substituents, the presence and number of other aromatic / aliphatic groups and the degree of halogenation of the aromatic moieties of a given compound.

Even beneficial properties conferred by consumption of phenolic compounds may still constitute pollution – it has been reported that contamination of more than 1μg/L of phenolics adversely affects the colour and odour of water (Martínez et al., 2000).

a. Anthropogenic phenolics:

Anthropogenic phenolic compounds have found application as the following: precursors to bulk antioxidant manufacture for both food/beverage industries (Karovičová and Šimko, 2000) and for industrial applications (Soares et al., 2008); lubricants (Soares et al., 2008); surfactant precursors (Soares et al., 2008; Lian et al., 2009); precursors in the manufacture of pharmaceutics (Schweigert et al., 2001);

plastics (Schweigert et al., 2001) and adhesives manufacture (Schweigert et al., 2001; McMurry, 2000b) and the petrochemical industry (Quintana and Ramos, 2008). Chlorophenolic compounds are released as by-products of the paper and pulp industries (Oikari et al., 1992; Schweigert et al., 2001) and in agrochemical industries, phenolics are present as intermediates of the degradation of pesticides (Quintana and Ramos, 2008) and certain fertilizers. Pentachlorophenol, a priority pollutant, is still widely used as a wood-preservative, and chlorinated phenolics are widely applied as herbicides, pesticides (Barceló and Hennion, 1995) and antiseptic agents (McMurry, 2000b). The anti-oxidant effects of anthropogenic phenols are also exploited within the food industry as preservatives (McMurry, 2000b) and as anti-corrosives (Sugama, 2000).

To emphasise the wide production of phenolic compounds, nonylphenols, which act as precursors for compounds used in many other industrial processes are presented as an example of the manufacturing scope: an estimated 500 000 tons are manufactured yearly around the globe, 60% of which is eventually distributed into water systems (Ying et al., 2002). The chemical structure of 4-nonylphenol is depicted below (Figure 1.3).

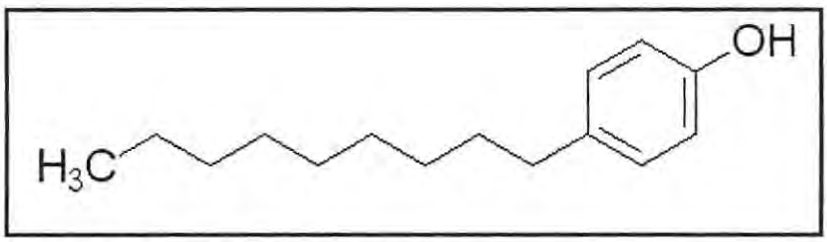

Figure 1.3 Chemical structure of 4-nonylphenol (Sigma-Aldrich, 2010)

Due to the large quantities of manufacture and use, phenolic-originating compounds generally reach wastewater streams in significant quantities where they are imperfectly degraded (Soares et al., 2008) to produce a phenolic compound, whereupon they are discharged into the environment.

The dual polar and aromatic natures of phenolic compounds allow them to pass easily into organisms and through cell walls. Phenolic compounds are thereby taken up by living organisms, both micro- and macro-organisms (Ferrara et al., 2001), entering the food-chain of the local environment and enhancing the exposure probability in humans. The following detrimental effects of exposure to phenolic compounds are noted, with some notable examples included: endocrine disruption, notably of the

oestrogenic pathways e.g nonylphenol (Soares et al., 2008) and other alkylphenols (Ferrrara et al.,2001; Santos and Galceran, 2003); disruption of intracellular metabolic pathways (Aptula et al., 2005) and protein inactivation (Schweigert et al., 2001); acute toxicity (Oikari et al., 1992); cytotoxicity (Soares et al., 2008); hepatotoxicity (Wang et al., 2001); mutagenicity (hydroquinone, Smith et al., 2000, Roza et al., 2003); teratogenicity; genotoxicity (catechols and chlorocatechols, JEM, 2003, Gaskell et al,. 2005; phenols and chlorophenols, Rothman et al., 1998; Farré et al., 2005; Soares et al., 2008), carcinogenicity (Smith et al., 2000; Soares et al., 2008) and increased oxidative cellular stress (Schweigert et al., 2001; Wang et al., 2001). Specifically cited is the acute toxicity towards aquatic organisms following contamination of water systems by phenolic systems (Matthiessen and Law, 2002; Chen et al., 2009), which is indicative of their ability to circulate within water systems despite their non-polar properties. Polyaromatic hydrocarbons (PAHs) in particular, a class of aromatic compounds within which some phenolics are also classified, are considered to be exceedingly toxic to aquatic life (Matthiessen and Law, 2002).

Due to the chemical stability of phenolic compounds conferred by the properties of both the benzene ring and the substituents attached to it (McMurry, 2000c), phenolic compounds are recalcitrant pollutants, resisting degradation by both biotic (Goi et al., 2004; Soares et al., 2008) and abiotic processes (Soares et al., 2008), as well as by anthropic methods e.g. bulk electro-oxidation (Anandhakumar et al., 2010) or catalytic chemical oxidation (Hamoudi et al., 1999).

In addition, the partial degradation, or metabolism, of a phenolic compound may only result in the release / alteration of substituents (e.g. oxidation to the quinone form, or semi-quinone radical) – the resulting compound itself possessing toxic qualities, sometimes more so than the parent compound (Schweigert et al., 2001; Wang et al., 2001; Aptula et al., 2005; Soares et al., 2008). Similar transformations and partial metabolisms of phenolic compounds have been noted within mammalian models (Davies, 1999; Mudnic et al., 2010). Phenol has been shown to be metabolised to form hydroquinone and catechol (Davies, 1999), and phenolic compounds are excreted in urine as -glucuronide (Malaveille et al., 1998), -O-glycoside (Heim et al., 2002), -sulfate (Malaveille et al., 1998)

and -glutathione (Davies, 1999) complexes of the same. Chemical disinfection of phenolic-contaminated drinking water has been reported to result in the formation of chlorophenols (Martínez et al., 2000).

Remediation of contaminated sites is further complicated by the tendency of phenolic compounds to associate with environmental matter. Through a combination of hydrogen bonding, Π-Π interaction and hydrophobic binding (Li et al., 2009) many phenolics can bind strongly to matter within the environment, such as humus (Soares et al., 2008), humic acids (Oikari et al., 1992), microbial biomass, (Soares et al., 2008; Lian et al., 2009), soil (Llorca-Pórcel et al., 2009; Chen et al., 2009), metal ions (Schweigert et al., 2001; Ferrat et al., 2003) and clay particles (Razee and Masujima, 2002). Soil, in particular, is cited as a favourable binding substrate for phenolic compounds (Llorca-Pórcel et al., 2009). These effects are also affected by the nature of the substituents attached to the benzene ring (Li et al., 2009).

The binding kinetics of phenolics to environmental matter has the effect of decreasing the possibility of degradation through physicochemical means (e.g. photolysis, oxidation, ozonation (Goi et al., 2004) and situates them favourably from many microbial degradation methods (Lian et al., 2009) through e.g. partitioning in areas with decreased oxygen availability; Soares et al., 2008). In some cases, this increases the detrimental effect of exposure to phenolics (Oikari et al., 1992). This preferential partitioning further increases their recalcitrance (Oikari et al., 1992; Soares et al., 2008) and improves their rate of circulation throughout the biosphere under examination. In addition, their low aqueous solubility provides a long-term, chronic circulation of the contaminant between water and soil mediums (Soares et al., 2008).

In summary, due to the high levels of phenolic production, the wide-ranging adverse effects of contamination to both human and environmental well-being, coupled with phenolics' inherent recalcitrance, their incomplete degradation kinetics and their interaction with environmental matter, it is of extreme importance to monitor levels of hazardous phenolics within industrial, household and environmental contexts. The following section outlines the effects that naturally-synthesised phenolics possess, primarily in human health and nutrition.

b. Natural phenolics

As secondary metabolites produced by plants, phenolic compounds have been widely studied (Ferrat et al., 2003) and have numerous structural and protective functions within plants. Approximately 8000 distinct compounds classified as phenolics have been identified from plant matter (Stalikas, 2007). Phenolics comprise the largest group of non-nutritive compounds found within the plant kingdom and are synthesised from ubiquitous precursor compounds found within most cells e.g. phenylalanine and acetylcoenzyme A (Sakihama et al., 2003; Harnly et al., 2007). Phenolics are classifiable by the number of phenol moieties: relatively simple compounds are present i.e. compounds comprising a single phenolic ring, but phenolics are also present in other configurations; from dimeric and oligomeric phenols up to very complex, much larger polymeric molecular forms of polyphenols, such as lignins, are present in plant matter (Robbins, 2003; Stalikas, 2007). Within the plants, they afford protection against: pathogens, browsers and UV-mediated oxidative damage (Stalikas, 2007; Harnly et al., 2007), and form pigmented compounds in order to attract pollinators and seed-distributors e.g. anthocyanins (Heim et al., 2002; Harnly et al., 2007) and impart organoleptic qualities to edible plant matter (Robbins, 2003; de Pascual-Teresa et al., 2010) and are widely distributed and varied according to tissue (Heim et al., 2002).

Flavonoids (Firuzi et al., 2005, specifically flavonones and flavonols, González-Molina et al., 2010) , phenolic/benzoic acids (González-Molina et al., 2010; Mudnic et al., 2010; Rodríguez-Bernaldo de Quirós et al., 2010) tannins (Ferrat et al., 2003; Rodríguez-Bernaldo de Quirós et al., 2010), polyphenols (Rodríguez-Bernaldo de Quirós et al., 2010) and lignins are groups of phenolic, or phenol-comprising, compounds and are widely distributed throughout the plant world (Ferrat et al., 2003). Humus (semi-degraded plant matter) and humic substances are themselves highly complex phenolic compounds with widely-varied chemical constructions, functional groups and isomers (Lin et al., 2001), while lignin is a phenolic polymer of irregular size and structure that is a component of cell walls (Rabinovich et al., 2004). The structure and distribution of phenolics varies from tissues and species of producing plant (Ferrat et al., 2003). As such, phenolics are also present as intermediates in the microbial degradation of plant-based polyphenolic compounds (Schweigert et al., 2001). The chemical structure of an example of a flavonoid, (-)-epicatechin gallate, is presented below (Figure 1.4)

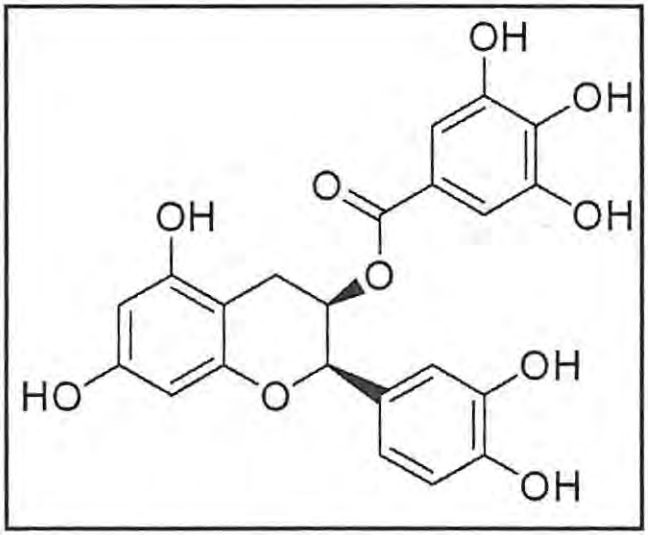

Figure 1.4: Structure of (-)-epicatechin gallate, an example of a flavonoid. (Sigma-Aldrich, 2010)

Many beneficial phenolic compounds are taken in by humans as components of food products (Schweigert et al., 2001) or beverages (Mudnic et al., 2010). Their beneficial properties as a food component includes: cardioprotective function (Céspedes et al, 2008; de Pascual-Teresa et al., 2010); antimutagenicity and antigenotoxicity (Heim et al., 2002; Malaveille et al., 1998), anti-tumour activity (Robbins, 2003) and possess vasodilatory (Mudnic et al., 2010), anti-allergenic (Léger et al., 2009), antimicrobial, antiviral (Robbins, 2003) wound-repair stimulation (albeit indirectly, Gouthamchandra et al., 2010) as well as anti-inflammatory properties (Heim et al., 2002; Robbins, 2003). As with anthropogenic phenolics, the effect and degree of effect noted with intake of dietary phenolic is strongly influenced by the substituents and structure (Arora et al., 1998; Heim et al., 2002; Firuzi et al., 2005) of the phenolic compound.

The most well-known and well-studied properties of plant-originating phenolics are as radical-scavenging antioxidants i.e. decreasing the amount of free radical-induced damage to cells through the donation of one or more protons to a free radical source, stabilising it (Arora et al., 1998; Heim et al., 2002; Robbins, 2003). A great diversity of simple phenolic compounds from whole foods and food extracts have been demonstrated to delay and minimise oxidative damage to cells, not only within the producing plant source (Heim et al., 2002; Céspedes et al, 2008), but also within mammalian models and tissues (Heim et al., 2002; Céspedes et al, 2008; González-Molina et al., 2010; Gouthamchandra et al., 2010; Mudnic et al., 2010) and the *in-vitro* stabilisation of free-radicals (Heim et al., 2002; Firuzi et al.,

2005; Malaveille et al., 1998; Gouthamchandra et al., 2010; Mansoor et al., 2010; Moyo et al., 2010; Mudnic et al., 2010; Xu et al., 2010). The increased uptake of phenolic-based antioxidants by humans is itself implicated in many protective functions against chronic diseases, such as carcinogenesis (Malaveille et al., 1998; Heim et al., 2002; Céspedes et al, 2008), neurodegenerative diseases (Céspedes et al, 2008; de Pascual-Teresa et al., 2010) and cardiovascular diseases (de Pascual-Teresa et al., 2010), either through direct antioxidant interaction with radical species, or through the chelation and neutralisation of metal ions implicated in cellular oxidative damage (Heim et al., 2002; Firuzi et al., 2005). Free-radical interaction and proton donation is considered to be primarily a function of the hydroxyl substituents (Heim et al., 2002).

The correlation existing between the antioxidant capacity of a given foodstuff is so high that a separate determination of the phenolic content of a foodstuff is generally measured as an indication of the total antioxidant activity (Huang et al., 2005; Xu et al., 2010; Rodríguez-Bernaldo de Quirós et al., 2010), in conjunction with other assays.

1.2.2: Detection of phenolic compounds

The variety, distribution and wide-ranging health implications of phenolics within the contexts of both natural environments and human prosperity strongly indicates that quantitative analysis of phenolics is essential when considering monitoring strategies. Since the detrimental/beneficial properties of phenolic exposure are strongly influenced by the substituents present, it may be insufficient from an analytical perspective to merely determine the phenolic content of a given sample.

In the case of detrimental, pollutant phenolics: Due to the aforementioned reasons of detrimental exposure effects, excellent inter-medium partitioning and persistence within natural environments, many phenolic compounds, or compounds that degrade to phenolics, have been classified as priority pollutants by the United States Environmental Protection Agency (Buckman et al., 1984). A total of 12 phenolics are classified as priority pollutants, and numerous other compounds that have a phenolic degradation intermediate, or final degradant, are included within this list. Thus, there is a pressing need to monitor their levels within the environment within a number of analytical matrices. This intimates the necessity

for *in-situ* (portable) and rapid analytical methods to be implemented in the monitoring of sites suspected of phenolic contamination.

In addition to the characterisation of the extent of contamination in polluted sites, quality-assurance procedures of treatment processes require that phenolic levels require extensive characterisation and monitoring to ensure that safe levels of pollutants are achieved prior to industrial effluent discharge into municipal, or natural, treatment pathways. This is also an important measuring priority when determining the efficacy at which treatment of contaminated sites is occurring, and requires medium- to long-term analysis taking place.

Quality-assurance is also necessary for ensuring synthesis reproducibility in those industries/applications for which these phenolic precursors are essential – this is of especial importance in those phenolic compounds for which pharmaceutical applications have been exploited and human exposure is expected.

A similar rationale for phenolic monitoring is anticipated for those phenolics classified as beneficial / nutritive. Both quantitative and qualitative analysis of these are required in order to standardise process streams in the food, beverage and phyto-medicinal industry. Extensive research has been performed on determining both the structure and the level/s of phenolics within a variety of samples. The following section describes the conventional methods of determining phenolic contents within these analytical matrices and a critical evaluation of their efficacy in being applied to phenolics monitoring. The call for a profiling method that comprehensively and rapidly detects all separate phenolics within a food source has previously been made (Harnly et al., 2007). In terms of process control and quality assurance, in the combined spheres of human health and human nutrition, it is essential to not only identify and monitor beneficial phenolics within food sources, but also the biokinetic information derived from *in-vivo* transformation of beneficial phenolics.

Hence, the following analyte matrices are to be considered when considering the potential areas at which monitoring of both beneficial and detrimental phenolics is important: soil, water, foodstuffs, bacterial and macro-organism tissues and secretions.

1.2.2.1 Conventional, non-electroanalytic detection methods:

The following techniques have been used in order to detect and monitor phenolic products. These have been categorised by the medium in which detection of phenols has been investigated.

Due to the aforementioned effects of phenolic contamination, much research has been expended on the monitoring of priority aromatic pollutants (including phenolic compounds) in water systems and soil systems. In environmental soil samples, sample extraction followed by Gas-Chromatography-Mass-Spectroscopy (GC-MS) has been used extensively, as the degree of separation coupled with the qualitative/quantitative information gained by this technique lends itself well to the initial characterisation of chemical species present in complex samples suspected of contamination (Santos and Galceran, 2003, Farré et al., 2005; Llorca-Pórcel et al., 2009). GC-MS has also been used to characterise phenolics present in various fractions of petroleum (Wasinski and Andersson, 2007)

Water samples containing phenolic compounds are routinely analysed with High-Performance Liquid Chromatography, HPLC (Suliman et al., 2006; Lian et al., 2009). This is a technique that lends itself well to the detection of phenolics, as they strongly absorb UV light (Robbins, 2003). Since a common detection mode of HPLC is a UV/Vis spectroscopic detector, this makes non-derivatised detection of phenolics much easier for this technique. Samples of water contaminated by chlorinated phenols have been analysed with Liquid Chromatography (LC) with solid-phase extraction (Barceló and Hennion, 1995), as well as by GC-MS (Eisert and Levsen, 1996; Heberer and Stan, 1997; Lian et al., 2009) and CE (Martínez et al., 2000). For the purposes of initial characterisation, in cases of suspected phenolic contamination of water sources, the use of model organism toxicity/inhibition studies has been employed, primarily bacterial (Farré et al., 2005). Toxicity/inhibition studies of macroscopic aquatic organisms (Aptula et al., 2005; Ferrara et al., 2001) is also studied for an assessment of the medium-to-long term detrimental features of site-specific phenolic-specific contamination. These techniques suffer from a lack of specificity, but remain useful for a comprehensive overview as to the general toxicity of the sample under examination.

In mammalian serum sampling, microdialysis has been used as a preparative pre-analysis treatment in order to improve detection specificity, coupled with LC or Capilliary Electrophoresis (CE) (Davies, 1999). Other analyses conducted on samples, or extracts of animal tissues include: GC-MS (Ferrara et al., 2001, Ahn et al., 2007a; Rothman et al., 1998), typically with Solid-Phase Extraction to screen out interferents. HPLC has been used in order to analyse liquid samples, such as blood or urine (Malaveille et al., 1998).

Antioxidant assays, primarily of foodstuffs, fruits and beverages are classed separately. HPLC has been employed as a preparative separation technique (Malaveille et al., 1998; Karovičovà and Šimko, 2000; Robbins, 2003; Harnly et al., 2007; González-Molina et al., 2010), followed by a variety of detection methods - typically UV/VIS or flourimetric spectroscopy (Robbins, 2003; Győrik et al., 2003) or MS. Extraction, followed by derivitization and GC-MS detection has also been routinely used to analyse phenolic contents of food (Robbins, 2003).

Biomolecular detection techniques focus primarily on immunoaffinity assays, such as Enzyme-Linked Immuno-Assay (ELISA), offer portable, highly specific and sensitive (0.05 to 1 µg/L sensitivity, depending on the chemical species and matrix properties under consideration) assays for various phenolic compounds with samples obtained in complex matrices (Farré et al., 2005).

The advantages of many of these techniques are the principles of easy separation between chemical species (Buckman, et al., 1984), detection efficiency of phenolics (Llorca-Pórcel et al., 2009) down to the ng level (Buckman et al., 1984), short sample preparation times and the ability of preanalytical techniques to further concentrate and purify analytes of interest (Karovičov à and Šimko, 2000).

However, the drawbacks of applying these techniques to phenolics monitoring are: the lack of portability, high unit-cost of detection equipment, lack of robustness for much of the equipment, requirements of skilled technical sample preparation, which combine to make on-site analyses very difficult, especially within an environmental monitoring paradigm, but also affecting industrial process monitoring, such as effluent quality assurance. This requires that samples be transported to analysing centres, increasing the time-of-analysis and making real-time monitoring difficult to deploy, further

decreasing the information-gathering efficiency that is necessary to enact relevant alterations to processes to improve pollutant regulation.

Due to the high toxicity of many phenolics, many detection techniques require that standardised procedures must be emplaced for the extraction and concentration of environmental samples prior to analysis (Eisert and Levsen, 1996), many of them complex in themselves (Rothman et al., 1998; Ahn et al., 2007a; Quintana and Ramos, 2008; Lian et al., 2009), the use of which might lead to a lack of representative sampling. In addition, the need for derivatisation of analytes prior to analysis, which in some techniques is required to enhance, or generate, a signal (Robards, 1992; Heberer and Stan, 1997; Suliman et al., 2006; Wasinski and Andersson, 2007) necessitates the use for skilled operators and data analysts to perform the dual qualitative-quantitative analysis. Many of these pre-analytical concentration and separation techniques suffer the same drawbacks, and entail the use of toxic reagents/solvents in both preparative and analytical stages of determination (Lian et al., 2009; Llorca-Pórcel et al., 2009), and their use raises the issue of destructive sampling that occurs during these procedures. This makes disposal of analysed samples difficult *in situ*. The addition of the requisite solvents and reagents used in the detection/pre-detection procedures (such as the generation of monoclonal antibodies in ELISA, highly-pure solvents for sample extraction, or the flourophoric derivatising compounds in some variants of GC) greatly increases the per-sample cost of analysis.

While equipment portability for GC-based equipment is improving, and commercially-available portable detection systems are available, the degree of portability is limited by "power, weight and analytical capability issues" (Santos and Galceran, 2003) and the more cost-effective and powerful models are still limited to vehicle-transported units.

1.2.2.2 Electroanalysis:

a. Basic principles

Electroanalysis is the measurement of electric potential, current (and its integral, charge) and/or resistivity, typically following an alteration of one or more of the aforementioned parameters. Electrochemistry, a subset of this analytical discipline, studies the chemical changes created by the passage of current and/or the production of electrical energy by chemical reactions. In brief, it relates the reduction, or oxidation, of analytes at an electrode/electrolyte system to provide information on the analyte (Bard and Faulkner, 2001a). The governing principle of electrochemistry is that generation of a suitable potential difference between electrodes immersed in an electrolyte solution (the sum of these components referred to as the electrochemical cell) containing an electroactive analyte generates a current, based on the reduction/oxidation of the analyte.

For the purpose of this Thesis, the electrochemical cell is comprised of a three-electrode electrochemical cell. Electrodes are distinguished by their purposes: a reference electrode maintains a constant potential to maintain or control the potential difference between a working electrode and an auxiliary electrode via external energy input. The working electrode's potential allows it to generate the desired reduction/oxidation reaction at its surface and the auxiliary electrode completes the circuit by performing the other half-cell reaction/s as a counterpart to the processes undergone at the working electrode (Bard and Faulkner, 2001a).

Categories of electroanalysis are based on which property of the electrochemical cell is being measured – amperometric devices measure current (usually relative to a set potential); coulometric devices measure charge (relative to a set potential), potentiometric sensors detect potential shifts (relative to a fixed current) and impedimetric sensors measure the impedance/admittance of an electrochemical cell (usually to a frequency-dependent AC potential shift) (Bard and Faulkner, 2001a).

Electrochemistry has several benefits when viewed for its consideration as an analytical technique. The following advantages of employing electrochemical analysis have been cited: extreme sensitivity of

signal detection, and the resultant low detection limits (Bakker and Telting-Diaz, 2002; Ashley, 2003), ruggedness (Ashley, 2003), portability (Farré et al., 2005), ease-of-miniaturisation of detection platforms (Bakker and Telting-Diaz, 2002; Ashley, 2003), leading to the possibility of *in-vivo* analyses (Bakker and Telting-Diaz, 2002), excellent compatibility with a number of analytical matrices (Ashley, 2003); rapid analysis timeframes, potential for real-time analysis, non-destructive sampling, the easy, low-cost mass-production of most of components, such as disposable screen-printed electrodes (Ashley, 2003; Farré et al., 2005), allowing for disposable components to be manufactured (Farré et al., 2005) and low cost of analysis relative to other analytical techniques. Through the use of specific potentials, or the fabrication of sensor arrays (Ashley, 2003), the simultaneous presentation of both quantitative and qualititative multicomponent detection of analyte(s) is also made possible under real-time monitoring conditions. All of these advantages lend themselves to the concept of electroanalysis as a method of monitoring *in situ* (Ashley, 2003) and in the paradigm of continuous-monitoring, both of which are of paramount importance in the context of phenolics monitoring (Sct. 1.2.2).

Some of the disadvantages to using electroanalysis include the generation of false-positives by the presence of electroactive substances present in the matrix (Farré et al., 2005). Since many analytes within a given matrix undergo oxidation/reduction at specific potentials, this imparts a degree of selectivity to the analytical procedure that obviates the separation/exclusion protocols cited in Sct 1.2.2.1. However, there is a general lack of selectivity noted using electroanalysis as a quantitative technique – hence much research has been focused on the alteration of electrode surfaces to impart further selectivity to detection methods (Bakker and Telting-Diaz, 2002)

b. Electroanalysis in phenolics detection

Due to the absence of specificity, coupled with the vast array of phenolic pollutant species, electroanalytical detection of phenolics is commonly coupled with a separative technique, such as HPLC, in order to apply the extreme detection sensitivity of electroanalysis together with the selectivity of the separation technique. Detection limits for phenolic compounds assessed by electroanalysis are routinely within, or below, the 10^{-6} M range, in a variety of matrices (10^{-9} M, (Farré et al., 2005)). Table 1.1

displays a short overview of selected electroanalysis detection of various pollutant phenolics. These were selected to display the scope and compatibility of electrochemical detection with various sample matrices and phenolic species under investigation.

Table 1.1: Examples of phenolics monitoring and detection using electroanalysis:

Phenolic species	Detection Method	L.O.D (M)[1]	Matrix (Transducer)[2]	Reference
Chlorophenols	EC[a]	$10^{-4,b}$	Lipid/Water Micelles	Anandhakumar et al., 2010
Flavanoids, phenolic acids	CE[c]-EC	0.25-2.5 µg/ml	Ethanolic tinctures	Peng, et al., 2005
o-cresol, chlorophenols	Electrochemical "tongue"[d]	$> 10^{-5}$	Aqueous	Gutés et al., 2005
Beneficial phenolics	HPLC-EC	> 1 mg/L	Liqueur extracts	Rødtjer et al., 2006
Beneficial phenolics	HPLC-EC	< 4 µg/L	Mead extracts	Kahoun et al., 2008
Alkylphenols, oestreonic phenols	HPLC-EC	0.98×10^{-7} – 3×10^{-7}	Water samples (nanotube-modified electrode)	Vega et al., 2007
Dopamine, catechol	CE-EC	$< 10^{-7}$	Acidic buffer (microchip platform)	Ding et al., 2007
Priority phenolic pollutants	HPLC-EC	< 0.1 µg/L	Contaminated water (preconcentration)	Pocurull, et al., 1996

[1] - Limit of Detection.

[2] - If of interest.

[a] - Electrochemistry

[b] - Not specifically mentioned, but inferred from the presented data

[c] - Capillary Electrophoresis

[d] - Artificial neural networks' modelling of electrochemical data to provide simultaneously-acquired detection and signal separation during 1 electroanalysis.

As Table 1.1 displays, the electrochemical detection of phenolics couples high sensitivity with a broad selection of matrices and samples in which detection takes place. The combined separation-electrochemical detection methods, while improving the limits of detection, have the same drawbacks to those outlined in the previous section, limiting its effectiveness for deployment *in-situ*. However, a very important advantage to electroanalysis that differs from the conventional analytical paradigms outlined previously is the tendency of research in this field towards the modification of the sensor platform and not of the analyte (or the analyte matrix) in order to generate/amplify detection signals and to improve analyte detection selectivity (Bard and Faulkner, 2001b; Ashley, 2003), which alone can improve

environmental and *in-situ* monitoring strategies by addressing the concerns involved with pretreatment of samples. The modification of electrode surfaces in order to improve response to a given analyte has been widely researched for a vast number of applications (Bard and Faulkner, 2001b; Ashley, 2003).This strategy is most effective when tailored towards the analyte under concern within the analytical matrix in which it is found.

In order to improve both the analyte specificity, and the detection sensitivity, biomolecules are routinely applied in conjunction with electroanalysis to produce a composite sensor – an electrochemical biosensor. The following section details the basic principles and applications of biosensors, before exploring biosensors researched for phenolics monitoring, specifically.

1.2.3 Biosensors:

Biosensors are sensors that composite biological macromolecules into a biorecognition element, to which a transducer is coupled. In this configuration, the biorecognition element provides analyte specificity and signal amplification through bioaffinity reactions, while the transducer measures alterations to the biorecognition layer caused by said bioaffinity reactions and relates the changes to the biorecognition layer to a measurable signal. Figure 1.5 provides a pictorial overview of the primary elements in a biosensor.

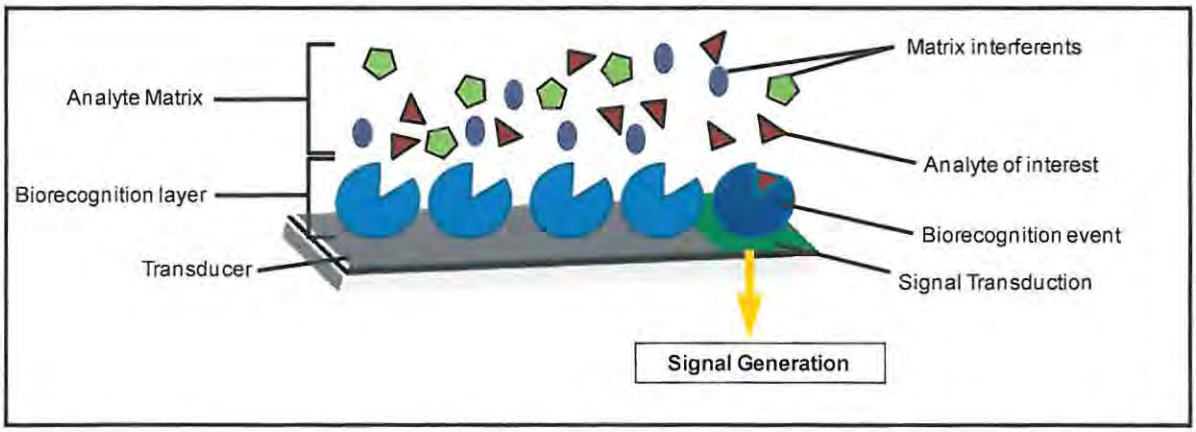

Figure 1.5: Primary components in biosensors and governing principles. Adapted from *Göpel and Heiduschka, 1995.*

As displayed in Figure 1.5, upon the occurrence of a biorecogntion event the biorecognition layer alters (e.g. a change in conformation, the release of enzyme-catalysed product, an alteration in pH), an event that is detected by the transducer. The transducer then corresponds this change with a signal, which is then processed accordingly. The two broad classifications of biorecognition events that exist are bioaffinity and biocatalytic events. In the former, the affinity of a biomolecule (e.g. DNA, antibodies, whole cells) for a desired analyte is exploited and differences between the bound and unbound biomolecule are measured by the transducer. In the latter, the catalytic conversion of a substrate to a product by biomolecules (e.g. enzyme, ribozymes, whole cells) is applied – i.e. the transducer measures the depletion of substrate(s), generation of product(s) or alteration of co-factor(s) (Göpel and Heiduschka, 1995).

Biosensors themselves are primarily classified according to the nature of the transducer employed, and secondarily according to the type of biomolecule comprising the biorecognition element. Thus, optical biosensors exploit optical changes (such as the production of a chromatic product), thermal biosensors measure changes occurring through biorecognition events and electrochemical biosensors measure the production / depletion of electroactive components during biorecognition events. Gravimetric, impedimetric and thermal transducers also measure biorecognition events.

By alteration of the biorecognition element, much of the specificity is altered. The core concept underpinning biosensor fabrication is that of the biorecognition event i.e. the interaction of a biomolecule with an acknowledged specificity/affinity for the analyte of interest with the analyte under consideration. To this end, biosensors have been fabricated using DNA, RNA, and bioaffinity proteins, which include both enzymes and antibodies. The binding affinities that these molecules have towards the analyte of interest are exploited and the resultant change, be it an alteration of conformation, the release of products, or the alteration of co-factors (e.g. NADH) and co-substrates, is monitored to provide quantitative information as to the analyte of interest.

The choice of both the transducer type and the biomolecule are key to the limitations of the biosensor. Transducer selection is typically based on the choice and type of the biorecognition element employed in

a biosensor, due to the dependence of the signal upon the biorecognition event under measurement. For these purposes, electroanalysis, primarily due to the sensitive measurement of electrochemical information has been commonly applied as a transducer platform for biosensor fabrication. Enzymes are particularly suited as biorecognition sensors. Their catalytic action promotes signal generation and, in the absence of inhibitory mechanisms or molecules, providing a continuous generation of signal in the presence of substrate through the monitoring of product formation / substrate depletion (Byfield and Abuknesha, 1994). In addition, the high substrate selectivity normally employed in natural catalysis can be exploited toward the production of a high degree of analyte specificity (Byfield and Abuknesha, 1994).

Biosensors (and bioanalytical techniques in general) possess numerous benefits that lend themselves superbly to environmental monitoring. As biomolecules, they function under mild chemical conditions, thus requiring little in the way of solvents or oxidative elements. Biocatalytic events enhance signal response and biorecognition the selectivity of analyte detection, which is highly applicable to the analysis of complex matrices, such as environmental samples. The monitoring of phenolic compounds has been explored in this context – laccases and tyrosinases are commonly attached to electrochemical transducers to produce electrochemical biosensors for phenolics monitoring. The following section describes laccase-based biosensors, from the characterisation and properties of laccases to their function as biosensors.

1.2.4 Laccases:

1.2.4.1: Distribution, structure and function:

a. Distribution, structure, mechanism and role in nature

Laccases (EC code: 1.10.32) are a class of enzymes that are widely expressed in a number of eukaryotes i.e. fungi, insects and plants (Call & Mücke, 199; Claus, 2004) and more recently, in prokaryotes (Claus, 2004). Laccases are oxido-reductase enzymes, catalysing the transfer of electrons from an oxidisable substrate (usually a phenolic compound), to an electron-acceptor (diooxygen, in the natural state),

catalysing its reduction. Figure 1.6 is a simplified schematic depicting the electron transfer occuring between phenolic substrate and diooxygen when catalysed by laccase.

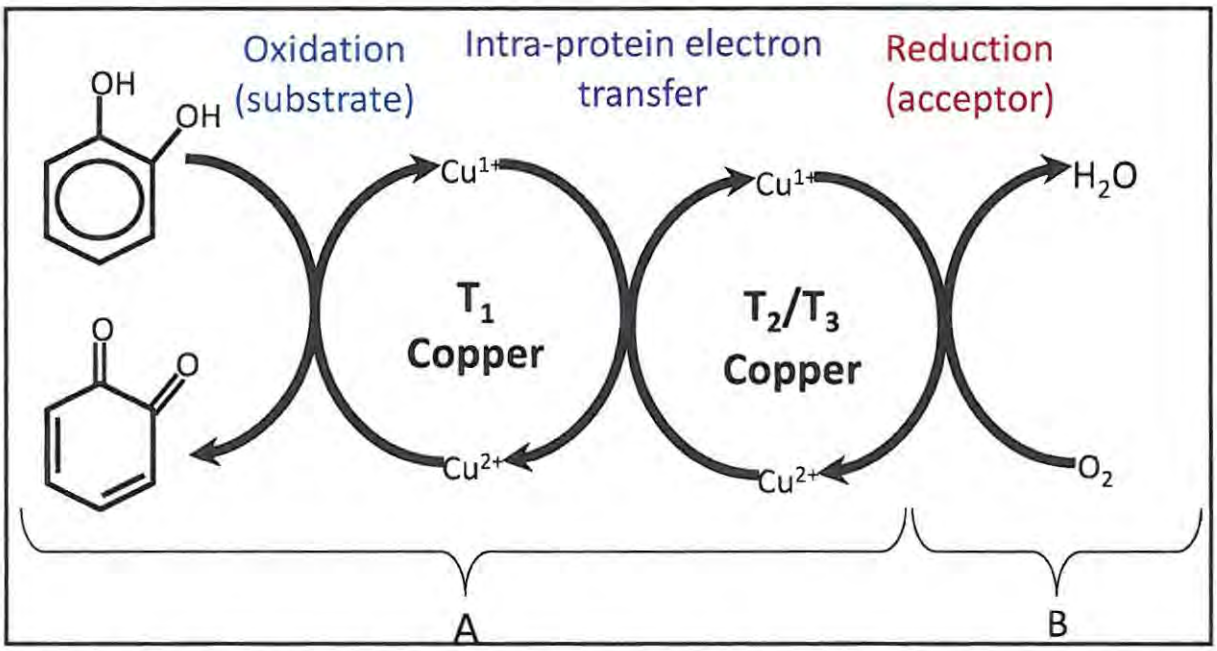

Figure 1.6: Simplified schematic of the flow of electrons between the phenolic substrate and electron acceptor .

In this example, catechol or 1,2-dihydroxybenzene is the substrate and diooxygen, O_2, the acceptor. Type 1 copper (T_1) abstracts an electron from the phenolic substrates and transfers it to the Types 2 or 3 (T_2/T_3) sites situated within the laccase monomer's active site and trinuclear cluster, respectively. Once 4 electrons have been abstracted and stored in this manner, they are transferred to oxygen, producing water. This results in the formation of 1,2-benzoquinone and water as the products of the catalytic cycle of laccase. The cycles grouped as "A" occurs 4 times prior to the occurrence of "B", resulting in regeneration of the active enzyme form.

The active sites of laccases typically include between 3 and 4 copper atoms that reduce and oxidise between the Cu^{1+} and Cu^{2+} state. These copper atoms are themselves broadly categorised as either Type 1 or Type 2/3 atoms, based on their wavelengths of maximal absorption (Claus, 2004) which differentiates their respective roles in the catalytic activity of the enzyme. Types 2 and 3 typically associate within the active site to form a "trinuclear cluster" (Claus, 2004). Type 1 copper atoms are involved in the initial abstraction of electrons from the substrate, followed by transfer of that electron to the trinuclear cluster until 4 separate electrons are stored within the active site (Claus, 2004). These 4 electrons are then transferred to the final electron acceptor, diooxygen, generating water as the final product of this catalysis (Claus, 2004). While the electron-transfer between Type 1 copper atoms and the phenolic substrates occurs in a typical 'ping-pong' enzyme mechanism, the mechanism governing electron-

transfer and their subsequent accumulation at the trinuclear cluster has not yet been fully elucidated (Shleev et al., 2006b).

Laccases are characterised by having a very broad range of substrates that can be oxidised (Claus, 2004). The following compound classes have been cited as suitable substrates which laccase can oxidise: ortho- and para-diphenols; aminophenols; polyphenols; polyamines; lignins; aryl diamines and some inorganic ions (Couto and Herrera, 2006). In addition, it has been noted that during the destruction of larger molecules (such as the biopolymer, lignin), steric hindrances occurring between the enzyme and the substrate preclude direct oxidation of the substrate. Here, the efficacy of the enzyme is considered to be due to the use of smaller compounds that act as electron-transfer mediators. When oxidised, these form stable reactive products that diffuse to the larger substrate and oxidise it, regenerating the mediator. A list of naturally-occuring mediators can be found in Bourbannais et al., 1995 and Claus, 2004, but are not pertinent to the research purposes reported in this Thesis. These diffusional mediators can be used to further increase the apparent substrate range of laccase.

In nature, laccases perform a diverse array of functions including: the formation and degradation of complex natural polymers (e.g lignin (Call & Mücke, 1997; Claus, 2004), initiating the cross-linking of chitin precursor molecules (Claus, 2004), and the oxidation and sedimentation of foreign, toxic phenolic compounds (Leontievsky et al., 2000;Claus, 2004). Laccase is also expressed as an important virulence factor in the human fungal pathogen, *Cryptococcus neroformans* to produce immune-modulating compounds targeting the host (Zhu and Williamson, 2004).

A wide variety of laccases are abundantly secreted by saprophytic fungi which, along with other oxidoreductase enzymes, allows for the degradation of lignin to as a carbon source for the secreting organism (Bourbannais et al., 1995; Rabinovich et al., 2004). For lignin-degradation, laccase is a mandatory enzyme – laccase-free mutants lose the ability to degrade lignin and it is postulated that the degradation of xenobiotic phenolics is due to the incomplete degradation of lignin, which leads to the localised accumulation of phenolics (Rabinovich et al., 2004) .

Fungal laccases, the primary focus of this research, are commonly secreted as a range of isozenymzes (ranging between 50 kDa and 100 kDa in size when expressed by the same organism), which can further aggregate into multimeric complexes in the surrounding medium (Claus, 2004). The fungal laccase monomer is organized in three sequentially arranged domains, with overall dimensions of about 65 × 55 × 45 Å (Shleev et al., 2006). At least 3 separate laccases have been separated from a single culture of *Coriolus versicolor* alone (Bourbannais et al., 1995), each with their own preferred substrate range and optimal operational physico-chemical conditions. In at least one study, the differences occurring between the rate of oxidation of simple phenolics is the same for these isozymes (Bourbannais et al., 1995), but vastly different oxidation rates have been reported for both polyphenols (Bourbannais et al., 1995) and between simple phenolic compounds.

b. Industrial applications of fungal laccases

Given the previous background for laccases provided, the most obvious application of laccase, and associated phenoloxidases is in the bioremediation of water and soil sources and sites contaminated with phenolic and other xenobiotic pollutants (Durán and Esposito, 2000; Xu, 2005; Couto and Herrera, 2006; Shleev et al., 2006). For these purposes, complete degradation/detoxification of the compound is not the primary objective – rather, it is the covalent coupling of the xenobiotic to other substances to neutralise their effect (Couto and Herrera, 2006), or the polymerisation of the xenobiotic. In this capacity, laccases, both immobilised onto various supports and 'free' i.e. dissolved into solution, have been used to degrade: dyes, halogenated phenolics, benzopyrenes, phenols, plastics, petrochemical pollutants and other xenobiotic compounds (Xu, 2005). In some cases, the use of an electron-transfer mediator was necessitated in order to achieve high degradation rates and to increase the apparent substrate range of the laccase (Durán and Esposito, 2000). Other phenoloxidase-like enzymes used in this application include, but are not limited to: tyrosinases, lignin peroxidise, manganese peroxidise, polyphenoloxidase and horseradish peroxidise (Durán and Esposito, 2000).

It is in this capacity that the most widely-researched, non-biosensor, laccase application is during the delignification and bleaching of plant pulp for paper fabrication, which has been touted to both greatly decrease the process' capital costs and increase the environmental palatability of the waste effluent/s (Call & Mücke, 1997; Couto and Herrera, 2006). This is primarily due to the chemically-mild conditions under which enzymes operate (Call & Mücke, 1997; Couto and Herrera, 2006), compared to the chemically harsh conditions under which chemical-based bleaching occurs. A secondary class of the aformentioned application is the degradation of food-based phenolics to improve the quality of the food or beverage in question (Xu, 2005).

In addition to bioremediative efforts, a lot of research has been expended in the application of laccase in the cathodic compartments of biofuel cells (Shleev et al. , 2006) to facilitate the reduction of oxygen. Biobleaching i.e. the decolourisation of chromatic compounds (Couto and Herrera, 2006) and the converse, the activation of dye precursors has also been mentioned as an ancillary application (Xu, 2005). Laccase has also been researched as an alternative to chemical catalysts in the synthesis of novel phenolic polymeric compounds (Tranchimand et al., 2006) and similar molecular assemblies.

It is, however, as a component in biosensor-based technologies for the monitoring of pollutants that laccase has been widely investigated. The proceeding section outlines the mechanisms that laccases, in particular, employ in the detection of phenolic compounds and the advantages that it possesses over alternative biorecognition elements.

1.2.4.2 Laccases as biosensor components

Four major laccase biosensor configurations are available, namely: measuring the decrease of solution diooxygen concentration due to the exposure of phenolics, re-reduction of oxidised substrate at the electrode surface, the electro-oxidation of laccase active sites, and the re-reduction of oxidised mediators at the electrode surface. The first and third of these configurations, respectively, rely on an inference of the data – the levels of oxidised mediator and diooxygen are indicative of laccase activity, and hence, the

presence of reducible substrate. The third configuration, in particular, is reliant on the mediator's ability to reduce the analyte under consideration – chemical limitations are the precluding factor in this method of detection. Figure 1.7 depicts the participants within laccase oxidation that are amenable to electrochemical detection.

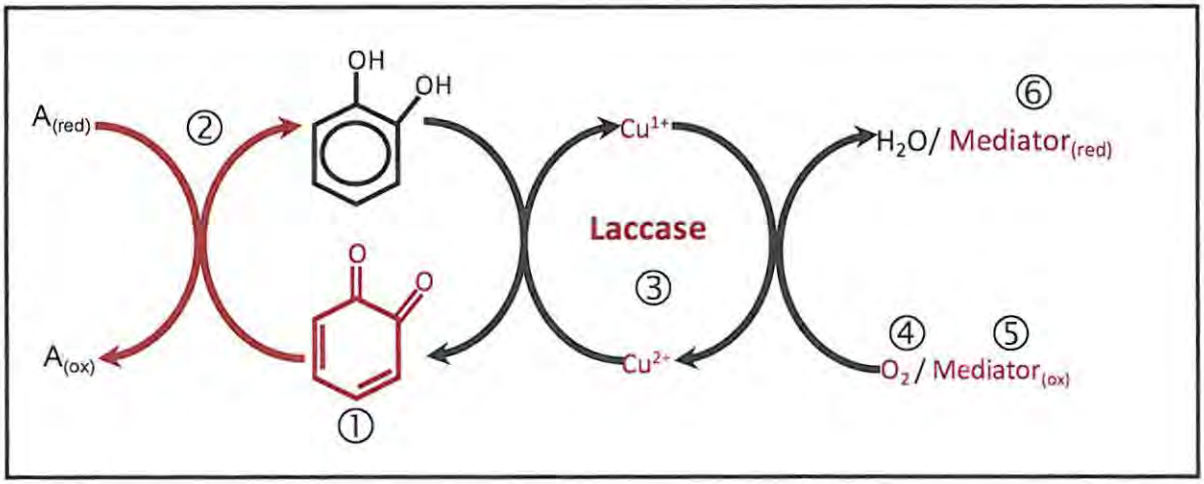

Figure 1.7: Diagram of the molecules and processes within the laccase catalytic cycle that can be electroanalytically detected.

These processes are indicated in red, while those processes that do not for the governing principles of laccase biosensors, are indicated in black.

Figure 1.7 depicts the mechanisms in the laccase catalytic cycle that can be detected electrochemically. ① The direct detection of the oxidised substrate, regenerating the substrate at the electrode surface (e.g. Jarosz-Wilkołazka et al., 2005); ② the use of a substrate in acting as an electron-transfer mediator to oxidise the desired analyte, and the monitoring of the corresponding increase in reduced substrate concentrations (e.g. Shleev et al., 2006b); ③ Detection of the electrons abstracted from the substrate through direct electron transfer occuring between the electrode and the copper centres of the active site of laccase (Xu, 2005); ④ The detection of diooxygen depletion caused by oxidation of a suitable substrate (Xu, 2005) and ⑤ and ⑥, the electrochemical detection of oxidation/reduction of a suitable electron-transfer mediator that re-reduces the active sites in laccase in much the same manner as diooxygen.

1.2.4.3 Difficulties associated with electrochemical phenolic detection and laccase-based biosensors:

Laccase- and tyrosinase-based biosensors have been researched for their applicability towards phenolic monitoring for a great many years and extensive research has been expended towards this end. However, to date, a consistent, reliable, reproducible commercial product has yet to be realised. This is due to a number of considerations that pertain to biosensor fabrication and deployment in general, to the electrochemical detection of phenolics and to the mechanism-of-action that laccases (and enzymes that act in a similar manner) use to detect phenolic compounds. These issues must be adequately addressed prior to the succesful deployment of such a sensor. The following section deals specifically with a number of important considerations when constructing and fabricating laccase-based biosensors, which not much literature has, to date, been concerned with.

Concerns regarding the immobilisation strategies of enzymes, in general, will be covered in Chapters 4, 7 and 8 of this Thesis.

a. Oxidative alterations in chemical structure of both substrate and product:

Figures 1.6 and 1.7 of this Chapter are overly-simplistic views of the fate of the phenolic substrate once an electron is abstracted. Due to the mono-electron oxidative activity of the laccase, the phenolic substrate is generally released in a radical form, which allows it to participate in a number of non-enzymatic reactions, either with the surrounding solvent, other semi-aromatic substrates, or allowing it to participate in further enzymatic reactions with laccase. In addition, the aromatic nature of the phenol permits intramolecular rearrangements of electrons, placing the positive-radical at areas of the molecule other than the hydroxyl-bearing carbon atom. (Call & Mücke, 1997). Figure 1.8 shows the possible reactive sites produced by catechol following the removal of the hydroxyl-situated electron.

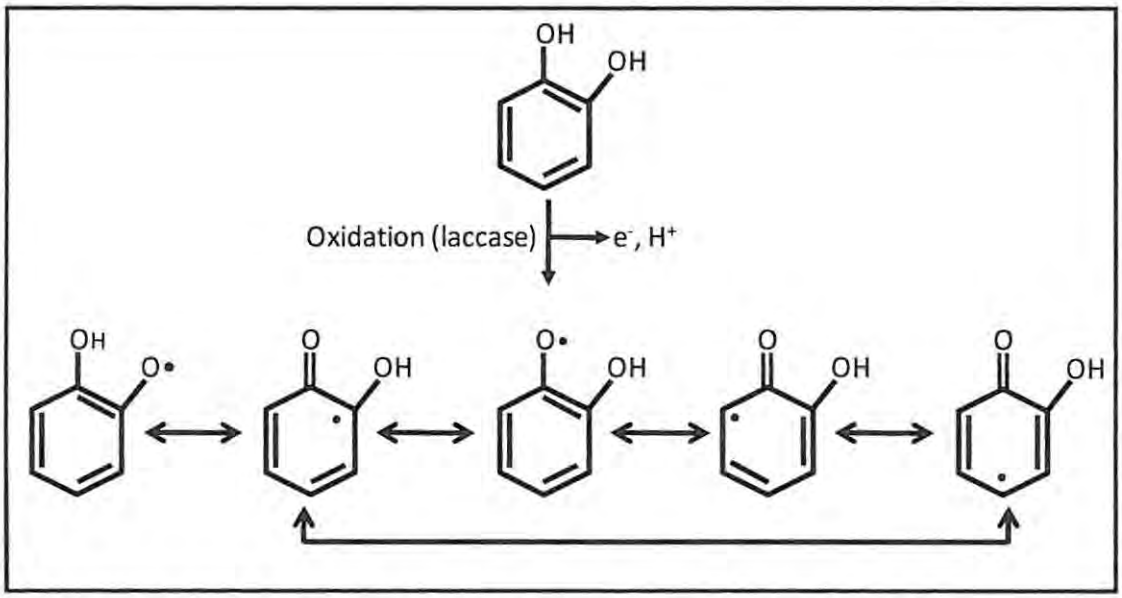

Figure 1.8: Possible forms of free radicals produced by the mono-electron oxidation of catechol by laccase.

Free radical sites are formed not only at the oxygen atom of the hydroxyl site, but also at the carbon atoms at the *ortho* and *para* position (relative to the first hydroxyl), as well as at the adjacent hydroxyl group, where it can undergo a similar molecular rearrangement to that already depicted. Adapted from Dec et al., 2003.

The radical nature of phenolic substrate oxidation allows it to participate in a great number of chemical reactions, and produces an array of products. The number of potential products are further increased by the resonance-stabilised intermediates that can direct reactions at several points around the benzene ring (Figure 1.8), resulting in a variety of enantiomeric products. The phenoxy radical itself is highly reactive, participating in both intra- and inter-molecular reaction while in the semi-quinone intermediate. Possible reactions noted after oxidation of phenolic compounds are: degradation, polymerisation (inter-molecular, both with radicalised and non-radicalised phenolics), solvent-reduction, molecular rearrangements, radical substitutions, intra-molecular dehalogenation (Dec et al., 2003), carboxyl/methyl cleavage (Dec et al., 2003), and oxidation via diooxygen (Tokmakov et al., 2005). It was reported that decarboxylation, demethylisation and dehalogenation was achieved through a common mechanism that is determined by whether or not the moiety in question is attached to a carbon radical cation that participates in further reactions with other radicalised phenolic compounds during coupling reactions (Dec et al., 2003). Electron-withdrawing groups (-COOH and halogens) are more easily detached from the benzene-ring, while electron-donating groups ($-CH_3$, $-OCH_3$, $-NH_2$) are more difficult.

It has been reported that these reactions are more dependent on solvent conditions than they are on the laccase type and composition, indicating that laccase is responsible for the formation of the phenoxy

radical and that ancilliary reactions are not dependent on it, although different rates of oxidation of substrates by the laccase may affect the composition of the final products (Tranchimand et al., 2006).

The vast amounts of conceivable products arising from phenolic oxidation, both electrochemically, and when mediated by laccase may lead to the generation of unanticipated redox products in and around the electrode surface during application of the biosensor (Anandhakumar et al., 2010). This may result in a signal complicated by the formation of new redox cycles occurring between the electrode and the enzyme, or the preferential formation of products that are not electrochemically-detectable. Polymerisation itself is a large concern and presents itself as a passivating coating of the electrode surface in a phenomenon known as 'fouling'. This is addressed in the following section of this Chapter.

b. Electrochemical fouling mechanisms:

Fouling occurs through polymerisation of the parent compound/s due to oxidation. Oligomeric, or polymeric, oxidation products deposits on surfaces, hindering further analyses (Berríos et al., 2009), or catalytic conversion of substrate (Hamoudi et al., 1999). In many instances, this is the single largest drawback against the direct (anodic) electroanalytical detection of phenolic compounds, as surface re-cleaning / catalytic modification makes the detection of phenolic compounds extremely time-consuming, and in the instance of catalytic resurfacing, expensive. Various strategies, both electrochemical and solution-based have been postulated to minimise electrode fouling, to varying degrees of success.

c. Absence of inter-substrate specific discriminatory methods:

Electroanalysis and biosensor technology has been successfully applied for the selective monitoring of phenolic compounds. However, due to the wide variety of chemical species that are both phenolic compounds and suitable laccase substrates, there is a lack of specificity within this class. Substrates that are suitable laccase substrates and the products of which are electroactive may function as interferents when trying to determine analytes of interest, especially considering the breadth of variety of chemical

composition, distribution and exposure effect of phenolics. Hence, it may be analytically important to detect one harmful phenolic compound within a matrix comprising of several other, harmless phenolic compounds. Amperometric biosensors, in particular, suffer from this analytical shortcoming.

1.3 Identified Knowledge Gaps:

Phenolic compounds, both anthropogenic and natural in origin, are of extreme analytical importance due to their widespread production and varied effects on environmental and human health. While biosensor technology, electroanalytical laccase biosensor technologies in particular, possess numerous properties beneficial to this research need, several severe shortcomings remain that require addressing before such technologies find successful application. These are summarised as the following:

(1) Biochemical – immobilisation strategies. The crucial concept underpinning biosensor technology is the localised concentration of signal-generating biomolecules in an area in order to generate a sensitive and selective signal through biorecognition events (Byfield and Abuknesha, 1994). Typically, especially in the case of non-catalytic biorecognition events, this site is located near the signal transducer, but other configurations are available in which the biorecognition site is detached from the transducer. In both cases, however, localisation of biomolecules is typically achieved through the immobilisation of said biomolecules (Byfield and Abuknesha, 1994), and seldom by the addition of the biomolecules to the bulk detection matrix. Immobilisation of biomolecules cannot be applied in a ubiquitous manner: several broad categories and numerous immobilisation strategies exist for individual biomolecules, or even classes of biomolecules, but their effects cannot be generalised when considering the vast array of structures and functions that constitute biomolecules. The broad categories, benefits and drawbacks of their application and a review of techniques applied to fungal laccases is presented in the following section. A main aim of the research presented in this Thesis is the optimisation of immobilisation strategies to produce a biosensor of at least comparable performance to those that have been reported on in the literature.

(2) It is widely acknowledged that the detection of chemically-distinct phenolic compounds is achieved with varying degrees of success. While a principal factor governing the success of detection in laccase-biosensors is due to the efficiency with which laccase acts as a biorecognition element for a given substrate, a further complicating factor is the extent to which the phenolic compound, once oxidised, acts as an efficient carrier of signal to the electrode surface. While a search through literature has revealed that studies on both of these factors have been previously performed, no research, to date has been performed on the interrelatedness of the two within the context of biosensing. Articles concerning the relative laccase-based oxidation rates of specific phenolic compounds have been published (Xu, 1996), as well as investigations probing the mechanisms by which this occurs (Xu, 1997). Other research has been focused on the suitability of specific phenolic compounds as analytes for laccase-based biosensors, without explicitly investigating the connection between sensor response, the fate of oxidised phenolic compounds and the rate at which these oxidised compounds are generated by the laccase biorecognition element. Research in this Thesis aims to unify these two factors, by providing both an electrochemical and biochemical explanation for the detection of different substrates through the same immobilisation stage.

(3) Intra-phenolic specificity. A search of the literature has revealed that very little research has been performed on the specific detection of phenolics in a mixed sample using electroanalytical chemistry. Of the limited research: preanalytical purifications; neural-network detection and alteration of electrochemical waveforms to favour detection of a limited range of present phenolics are the main research concerns. To this end, it is proposed that, through manipulation of the electrochemical waveforms used for the detection of phenolic species, that an enhanced degree of specificity can be obtained during the deployment of the biosensor, providing simultaneous, real-time detection of multiple phenolic species present in the same analyte. The two most important descriptors of a biosensor are the selectivity and sensitivity of response to the target analyte (Byfield and Abuknesha, 1994). These are, in turn, determined from the two main components of a biosensor:the biorecognition layer(s), comprised of biomolecules and the support onto which biomolecules are immobilized onto, and the signal transducer. Their influences on the generated signal may be inferred from their use – biorecognition elements

primarily confer signal selectivity, through the generation of a selective signal in conjunction with a specific analyte (or class thereof), or the enhancement of signal response, as in the case of enzymes (Byfield and Abuknesha, 1994). Transducers are primarily employed in the transduction, or the enhancement of transduction of the biorecognition-originating signal. Biosensor sensitivity is usually controlled through a mixture of the properties of the transducer and the biorecogntion layer (e.g. biorecognition element density) (Byfield and Abuknesha, 1994). These definitions are less distinct than stated – e.g. a degree of selectivity can be conferred by the transducer; such is the case with the selection of a specific potential for the reduction/oxidation of specific analytes with the use of electrochemical transducers, but relatively little research is performed on this aspect of the biosensor fabrication. Tranducers also usually function as the solid support structure onto which enzyme immobilization takes place

Thesis overview:

To these ends, we have examined the following core aspects of laccase biosensor design: reproducibility, immobilisation, sensitivity and specificity as below.

1. Reproducibility: In Chapter 3, investigations were conducted on the various methods improving and predicting inter-electrode reproducibility and enhancement of substrate detection sensitivity through alteration of the surface properties of the transducer. In Chapters 4 and Chapter 5, fouling considerations were in particular taken into account in an effort to address some of the common problems associated with sensor passivation due to oxidation of phenolic compounds in order to assess and assign causal properties to the factors (biochemical, substrate-dependant and transducer-originating) result in sensor passivation via fouling mechanisms.

2. Considerations regarding the role of biomolecules immobilisation on the function of laccase-based biosensors: Using a combined approach that monitored both the analytical properties of the biosensor and the biochemical/electrochemical parameters that govern the analytical properties, various methods of protein immobilisation strategies and their resultant optimisations were examined. The effects of these immobilisation strategies were assessed on the bases of both kinetic and physical properties, and the relevant investigations detailed in Chapters 4, 7 and 8, respectively.

3. Sensitivity and specificity of detection: The respective roles of the: analysis pH, the selection of laccase substrate under investigation and the detection waveformused during the application of biosensors was assessed with an aim to enhance both substrate specificity and sensitivity. Chapter 5 details the investigations of electrochemical and biokinetic considerations for laccase biosensors when considering the detection of chemically-different phenolic substrates via electrochemical biosensors. A proof-of-principle study demonstrating simultaneous monitoring of three selected phenolic substrates via multiple-pulse chronoamperometry is reported in Chapter 6.

4. This Thesis also examines the application of the Quartz-crystal Microbalance with Dissipation (QCM-D) as a tool for monitoring enzyme immobilisation strategies and assessing the fate of immobilised biomolecules at a fundamental molecular level. Chapter 7 examines the role of QCM-D in monitoring the immobilisation of a monolayer Glucose Oxidase, used here as a model enzyme, onto the surface of a biocomposite sensor and the comparison of these findings with enzyme kinetic parameters established for this particular sensor configuration in the literature. In Chapter 8, a more in-depth investigation of the same was performed using laccase as the enzyme under considerations. Comparisons between the physical film parameters established using

QCM-D and the apparent enzyme kinetics of the immobilised film were performed. The principles of QCM-D technology are outlined in the relevant sections.

5. Chapter 2 outlines the general methodologies and principles outlined in this Chapter. Enzyme kinetics and modelling of enzyme kinetics under biosensor paradigms forms a key component of this Thesis and is outlined in this Chapter.

6. Chapters detailing the results of investigations reported on in this Thesis (i.e. Chapters 3 to 8) are prefaced by individual Abstracts, providing a convenient summary of the key findings of each Chapter, as well as contextualising the key purposes of the studies presented.

Chapter 2: General Methodologies and Principles

This Chapter outlines some of the commonly-used apparatuses, reagents, preparation methodologies and data treatments that take place in the proceeding Chapters, as well as the principles of the techniques and models underpinning the biosensors kinetics and electrochemistry used henceforth. Chapter-specific methods and methodologies are detailed in the relevant Chapters.

2.1 Apparatus:

2.1.1 Electroanalysis:

1. Electroanalytical equipment

All electroanalysis was performed on an Autolab Potentiostat/Galvanostat (PGSTAT 30, EcoChemie, Netherlands). Electrodes were positioned and held within a VA stand (Metrohm) and attached via crocodile clips to the PGSTAT 30. Timed stirring control was provided via the IME663 (Metrohm) attachment connected to the PGSTAT 30. Stirring was provided by a Teflon®-coated steel rod and adjustable in 500 rpm increments up to 3 000 rpm, as set by the VA stand.

2. Electrodes

The reference electrode used throughout these studies was a Silver/Silver chloride/saturated chloride reference electrode (Bioanalytical Systems, USA - BAS) and is henceforth referred to as an Ag/AgCl electrode.

Working electrodes for cyclic voltammetry and chronoamperometry were either glassy carbon electrodes (henceforth referred to as GCEs), or gold (AuE), both of which were sourced from BAS. GCEs had an active electrode diameters of 3 mm and AuEs had diameters of 1.6 mm.

2.1.2 UV/Vis Spectroscopy:

1. Equipment

UV/Vis spectroscopy was performed on a PowerWave (Gold) UV/Vis spectrometer. Control of the apparatus, data collection and analysis was perfomed using KCJunior™ software, v4.12. The various protocols are outlined in the appropriate Chapters.

Disposable, UV-transmissible Powerwave plates (96 wells, 300 µl volume wells) were used when UV/Vis spectroscopy was employed.

Data obtained from spectroscopy was exported to Excel spreadsheets following analysis using KCJunior software, owing to software incompatibility.

2.1.3 QCM-D analysis:

Crystals used for QCM-D analyses were AT-cut quartz crystals, QSX-301, surfaced with gold. These were mounted in titanium QCM-D flow chambers, which were in turn housed in a Q-Sense E4 QCM-D sensor system. All of the above were sourced directly from Q-Sense®, Sweden.

Flow of solutions through the chambers was regulated by an Ismatec® peristaltic pump. Flow rate was regulated at 50 $\mu l.min^{-1}$ and the chamber temperature was set at 20C ten minutes prior to the start of QCM-D analysis and maintained throughout.

2.1.4 Glassware

All glassware used to store buffers, cleaning agents or electrolytes, as well as electrochemical cells, were soaked in dilute (~5%) HNO_3 solution overnight, followed by repeated rinsing and air-drying. Between analyses, electrochemical cells were repeatedly rinsed with alternating solutions of 60% ethanol solution and milliQ water.

2.2 Reagents:

2.2.1 General

All reagents used were of analytical purity, unless stated otherwise. Purity indices of reagents was taken into account when formulating reagents, and concentrations were calculated to provide the desired concentration.

2.2.2 Solvents

Water used in cleaning and dissolving of reagents was of double-distilled quality and purified using MilliQ, to a total resistivity of > 18 $M\Omega.cm^{-1}$. Ethanol was of absolute (> 96%) purity and all organic solvents used were of HPLC-grade.

2.2.3 Electrode storage and cleaning.

Reference electrode cleaning and storage was performed using saturated chloride solution, which was formulated using a solution of 3 M KCl and then saturating the solution with NaCl. 3 M KCl was prepared from KCl crystals (99+% pure, Sigma-Aldrich) and then diluted to the desired concentration when used as an electrolyte.

Working electrode surfaces were polished on a Buĕhler felt pad (Bioanalytical Systems) using a small aqueous slurry of aluminium oxide powder (<10 μm diameter, 99.7% pure), sourced from Sigma-Aldrich. Treatment of electrodes thereafter varied – cleaning procedures for GCEs are outlined in Chapter 3 and those for AuEs outlined in Chapter 6. Unless otherwise stated, all electrodes were cleaned between analyses during electrochemical investigations.

2.2.4 Buffers and electrolytes: preparation and storage

Electrolytes and buffers were formulated by dissolving the relevant salts/acids in water. In the case of buffers, the solution was then dissolved with 2.0 M NaOH until the desired pH was obtained before the desired concentration was reached with water. Formulation and titration of buffers occurred at room

temperature. Buffers were stored at 4 °C and aliquots were warmed to room temperature prior to use. Fresh buffers were prepared once every two weeks.

The primary buffer/electrolyte utilised throughout this thesis was succinic-lactic acid buffer (SLB). Succinic acid (Sigma-Aldrich) was of 99+% purity and lactic acid (Sigma-Aldrich) was of 85% purity. A solution comprised of equimolar concentrations of succinic acid and lactic acid was prepared and titrated to the desired pH with NaOH.

2.2.5 Potential laccase substrates (Phenolics):

Phenolic substrates were dissolved in water at the desired concentration and stored in the dark. Fresh substrate was prepared daily, unless a discolouration of the solution was observed, in which case fresh substrate was immediately prepared. In the case of certain phenolic compounds, solubilisation was aided through the addition of less than 5 μl of 2.0 M NaOH to the solution.

2.2.6 Solution De-aeration

Nitrogen (>99% purity, sourced from Afrox) was dehydrated and purified by flowing through a mesh comprised of calcium sulphate and cobalt chloride (sourced from CRS) and Drierite® Molecular Sieve (Sigma-Aldrich) before use.

De-aeration of solutions took place via bubbling nitrogen through the solution for 10-20 minutes. De-aerated solutions were thereafter sealed and any amendments to the solution thereafter were followed by de-aeration.

2.3 General overviews and principles of enzymatic and electrochemical techniques

2.3.1 Biochemical kinetics

The study of chemical kinetics seeks to measure and interpret rates of chemical reactions by monitoring the rate of formation of a given chemical product, or the rate of depletion of a chemical reactant (Atkins,

1997). Thus, the effects of the presence or absence of catalyst/s (which accelerate chemical reaction rates) can be monitored by assessing the relative rates of product formation / reactant depletion (Atkins, 1997). Enzymes are defined as protein-based biocatalysts, enhancing the reaction rates of specific chemical reactions by as much as 10^{16}-fold (Garrett and Grisham, 1999b). Biochemical kinetic studies seek to measure the catalytic effect of designated chemical reactions that are gained through the presence of biomolecules, such as enzymes.

Throughout this thesis, the response of biosensors has been related in the form of a variety of parameters commonly used for relating the biochemical rates and constants of the enzymatic system within the biosensors to the various conditions under which it was fabricated or applied.

To this end, this section has been provided to outline both enzyme kinetics and the techniques used to derive rate parameters describing enzyme-substrate interactions. In the first subsection, the generally-reported case, that of Michaelis-Menten enzyme behaviour, is outlined and the principle biochemical parameters of this paradigm (K_m and v_{max}) defined. Subsections dealing with two special cases that pertain to the description of biochemical behaviour of the biosensors reported on in this Thesis are presented below that. The former case outlines the conventional methods of relating biochemical constants when assessed through electroanalytical means; the latter provides a description of enzyme kinetic determinations that deviate from conventional (i.e. Michaelis-Menten-like) behaviour.

2.3.1.1 Michaelis-Menten kinetics

All steady-state biochemical relationships attempt to define a graphical relationship between the velocity i.e. reaction rate of an enzyme-catalysed reaction (symbolised as **v**, also known as activity) of a specified amount of enzyme and the concentration of substrate that it is exposed to (**[S]**) (Miller and Tanner, 2008).

Under catalytic conditions, enzyme and substrate molecules associate to form intermediate substrate-enzyme complexes that catalyse the conversion of a substrate to a product. Following catalysis, the enzyme-substrate complex degrades, releasing the product and allowing a new catalytic process to take place (Miller and Tanner, 2008) as depicted in Scheme 2.1, below. In classic enzyme kinetics (Briggs-

Haldane), the most simplistic representation of the relative rates of enzyme-substrate complex formation and the degradation of this complex into the product/s – enzyme state is dictated by the following rate formalisms, depicted in Scheme 2.1:

$$E + S \underset{k_{-1}}{\overset{k_1}{\rightleftharpoons}} ES \xrightarrow{k_2} E + P$$

Sch. 2.1

Where E represents the enzyme, S the substrate, P the product and ES refers to the enzyme-substrate complex intermediate stage (Miller and Tanner, 2008). The rate constants k_1, k_{-1} and k_2 refer to the rate of substrate-enzyme association to form ES, the non-catalytic dissociation of ES and the combined rate/s of catalysis and product release from ES, respectively (Miller and Tanner, 2008).

This model assumes only a single substrate interacting with the enzyme and the irreversible formation of product arising from the formation of the enzyme-substrate complex, which is relatively uncommon in enzyme kinetics (Miller and Tanner, 2008). However, by maintaining all other conditions, including the concentrations of co-substrates, as constant, this remains a viable model for monitoring multi-substrate enzyme kinetics under those conditions (Miller and Tanner, 2008).

Activity studies seek to elucidate key rates of biocatalysis by monitoring the rate of product formation, or the rate of substrate consumption in order to assess the rates governing the kinetic behaviour of a given enzyme system. For the purposes of this description, substrate depletion or product formation is considered interchangeable, as either represents the velocity of an enzyme-catalysed reaction. Since the velocity of the enzyme-catalysed reaction is the rate of change of product concentration over time, v, velocity can therefore be defined by the following rate equation:

$$\frac{d[P]}{d(t)} = v = k_2[ES]$$

Eq. 2.1

Where [P] is the concentration of enzyme-catalysed product, thus d[P]/d(t) is the rate of product formation and the other symbols have their usual meaning, as in Scheme 2.1 (Miller and Tanner, 2008).

However, [ES] is not equivalent to the total concentration of enzyme present in the system under investigation. This is accounted for by the rate constants k_2 and k_{-1} (Scheme 2.1), which correct for the inter-conversion between the various states of enzyme at a given concentration of substrate. Accounting for the differences between the amount of bound enzyme i.e. ES and the total amount of enzyme present (E_{tot}) leads to the following rate equation, Eq. 2.2 (Miller and Tanner, 2008):

$$\frac{d[P]}{d(t)} = v = \frac{k_2[E]_{tot}[S]}{([k_2 + k_{-1}]/k_1) + [S]} \qquad \text{Eq. 2.2}$$

Eq. 2.2 is further simplified to yield the classic Michaelis-Menten equation (Eq. 2.3).

$$\frac{d[P]}{d(t)} = v = \frac{v_{max}[S]}{K_m + [S]} \qquad \text{Eq. 2.3}$$

Where v_{max} is the maximal rate of substrate turnover at saturating concentrations of substrate ([S] $\rightarrow\infty$, $k_1 \rightarrow\infty$, therefore [ES] ~ $[E]_{tot}$ and thereafter, using Eq. 2.1) and K_m represents the Michaelis constant = $[(k_2/k_1) + (k_{-1}/k_1)]$, as in Eq. 2.2 (Miller and Tanner, 2008). Eq. 2.3 describes a hyperbolic dependence of v on [S] which is graphically depicted in Figure 2.1 below:

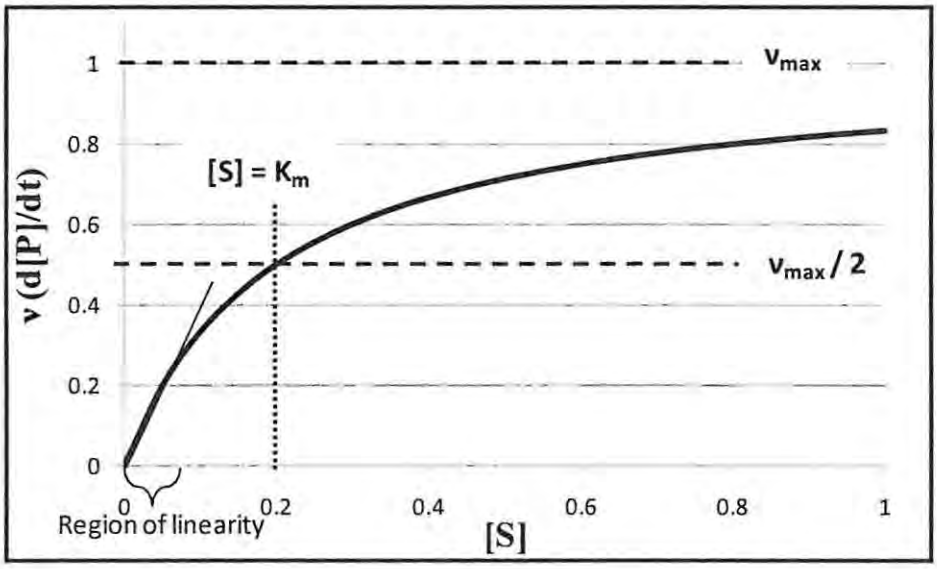

Figure 2.1: Graphical depiction of the Michaelis-Menton plot generated using dimensionless model data. Kinetic parameters inputted: v_{max} = 1 d[P]/dt and K_m = 0.2 [S]

As depicted in Figure 2.1, re-arrangement of Eq. 2.3 shows that K_m is mathematically equivalent to the concentration of substrate required to produce an initial catalysis rate equivalent to $v = v_{max}/2$ (Garret and Grisham, 1999). The interpretation of K_m warrants further exploration at this juncture, as it is used frequently as a relative indication of substrate-binding ability during biokinetic characterisations of enzymes. Through Scheme 2.1 and Eq. 2.2, it is apparent that K_m is the sum of the enzyme-substrate complex degradation rates (k_{-1} and k_2), divided by the assembly rate of said complex (k_1). This, in turn means that K_m can be resolved in terms of the concentrations of the various participants from which the rates themselves are derived. In the simple scheme outlined in Scheme 2.1, K_m is equivalent to:

$$K_m = \frac{([E]_{tot} - [ES])\,[S]}{[ES]} \qquad \text{Eq. 2.4}$$

(Miller and Tanner, 2008)

From Eq. 2.4, $K_m = [S]$ when the difference between the concentrations of total and bound enzyme equals that of the bound enzyme-substrate complex (Garrett and Grisham, 1999b), i.e. when $½[E]_{tot} = [ES]$. Thus, K_m itself can be considered to be a global equilibrium dissociation constant of the enzyme-substrate complex (Garrett and Grisham, 1999b; Miller and Tanner, 2008) i.e. the substrate concentration at which half the enzymes present in the system are in an enzyme-substrate complex. From this understanding of K_m, the inverse of the K_m is often taken as an indication of the substrate-binding efficiency of a given enzyme system (Garrett and Grisham, 1999b). A more intuitive definition of K_m is that it is the concentration of substrate at which the average time of substrate capture by the enzyme is equivalent to that of product generation and release (Northrop, 1998). Viewed from this perspective, v_{max} is then the reciprocal of the time required to generate and release product (Northrop, 1998) by the enzyme system under investigation.

Through use of Eq. 2.1, v_{max} in Eq. 2.3 can be resolved to produce the k_2 constant, if the concentration of enzyme within a given system is known. k_2, often also referred to as k_{cat}, is known as the catalytic constant, or turnover number. The catalytic rate constant, k_2, provides a definition of the maximum catalytic rate at which an enzyme system proceeds under conditions of substrate-saturation (Miller and

Tanner, 2008). A further useful parameter is derived from k_2 and K_m. The specificity constant (k_2/K_m) is a measure of the rate of enzyme reaction velocity at very low concentrations of substrate ([S] << K_m) (Miller and Tanner, 2008) and provides a means of comparing efficiency of enzymatic catalysis under these conditions (Garrett and Grisham, 1999b). Under this substrate concentration range, the velocity is linear (as indicated in Figure 2.1), since K_m becomes the predominant term in the divisor in the Michaelis-Menten formalism (Garrett and Grisham, 1999b).

The above three parameters (k_2, K_m and k_2/K_m) are the most commonly reported values when describing and comparing enzyme kinetics. The following section (2.3.1.2) details the conventions in reporting enzyme kinetics data when electroanalysis is used as the basis of assaying enzyme activity.

2. Enzyme kinetics within an electroanalytical context

Assays and analyses of enzyme kinetics have been performed using an array of techniques to detect the formation of products, or the depletion of substrates. These commonly include, but are not limited to: UV/VIS spectrophotometry; Mass Spectrometry; High-Performance-Liquid-Chromatography and electroanalysis (Miller and Tanner, 2008). Due to the nature of the research presented in this Thesis, kinetic characterisations of enzymes and enzyme systems using electroanalytical techniques is of particular interest. While kinetics analyses of 'free' (i.e. unimmobilised) enzyme systems using electrochemical monitoring techniques takes place under the same principles that other forms of enzyme assays undergo i.e. as a means of monitoring product formation / substrate depletion (e.g. Ciolkosz and Jordan, 1993; Klis et al., 2007a), additional concerns arise when assessing immobilised enzymes for the purposes of biosensor fabrication and application.

When considering enzymatic biosensors, it is the respective velocity of the enzyme-substrate interaction/s that drives signal generation, and thereby, determines the efficiency of analyte detection. The act of immobilising enzymes onto transducers often has the effect of distorting the enzyme structure, affecting its kinetic ability and making predictions of the immobile enzyme kinetics from analyses of the mobile enzyme state analytically inconsistent. This is a subject that is outlined in greater detail in Chapter 4 of this Thesis. Biosensors are further complicated by other operational factors affecting signal

generation: diffusional constraints are often found to be imposed on the transport of the substrate within the biorecognition layer due to the dense packing of catalyst on the transducer surface and on the transport of the product to the transducer surface (Chapter 4 of this thesis). In addition, product-transducer kinetics and side-reactions involving the product may also affect both the quantity and quality of signal (Chapter 5 of this thesis). These factors further distort the apparent rate constants from which signal generation is derived. As such, all further kinetic parameters reported in this thesis (K_m, v_{max}) should be considered as apparent rate constants.

Hence, separate characterisation of the rate kinetics governing immobilised-enzyme systems are essential for assessing the efficacy of biosensors under different conditions (both during fabrication of the biosensor and during its operation), in order to allow for meaningful comparisons between these conditions to be made. From a biosensor-fabrication perspective, the interpretation of sensor responses though biochemical kinetics models is invaluable to understand the mechanisms influencing sensor response. This is useful, both from a fundamental analysis perspective and during optimisation of sensor response, as well as for the meaningful interpretation of other alterations to the sensor performance under different conditions e.g. assessing reasons behind attenuation of sensor response during storage (Bartlett and Pratt, 1993).

From an applications perspective, a linear relationship between the analyte of interest and the sensor's response is desirable, if only for the purposes of ease-of-interpretation by the end user. Commonly used criteria for evaluating sensor performance in the absence of a kinetics-based model include: signal response to changing substrate concentrations (termed "detection sensitivity") and the linear dynamic range under which detection sensitivity is applicable ("linear response range") (Bartlett and Pratt, 1993). Some examples of published findings using these parameters as the prime parameters underpinning biosensor efficiency include, but are not limited to: Gomes et al., 2004; Jarosz-Wilkołaska et al., 2004 and Montereali et al., 2009.

Non-linear sensor modelling processes extends the range under which meaningful sensor response can be extracted from the sensor response, beyond the linear range. As Figure 2.1 shows, the apparent linear response range of a purely Michaelis-Menten-like sensor behaviour is very narrow (in this example,

between [S] = 0 and [S] = ½.K_m). By decreasing reliance on the purely linearly-behaving portions of sensor-current functions, a much greater substrate range can be interpreted; again, in the example provided in Figure 2.1, the non-linear response region covers a much greater range of substrate concentrations (to at least [S] ≈ $4K_m$) before the sensor response approaches zero-order behaviour.

Amperometric sensors assessed in a bio-kinetic method are typically characterised by the following parameters: maximal current, I_{max}, equivalent in this context to the apparent v_{max} parameter in Eq. 2.3 and by their apparent Michaelis constants, K_m (e.g. Kulys and Vidziunaite, 2003; Jarosz-Wilkołaska et al., 2004; Tan et al., 2009; Wang et al., 2009). From these parameters, k_2 and k_2/K_m values can be readily established, as explained in the preceding section (Sct. 2.3.1.1) and interpreted as equivalent indications of the various rates governing the substrate-enzyme kinetic system under investigation. They are considered to be apparent rate constants, for the reasons (both biochemical and operational) that may affect how representative a transduced signal is of the biorecognition event that initiates the signal.

It is now common practice that both the aforementioned aspects of the biosensor's performance be reported on (Kulys and Vidziunaite, 2003; Yan et al., 2009), to present both a biosensor's analytical performance and on the biochemical kinetics that govern said performance.

3. Deviations from non-hyperbolic behaviour: sigmoidal velocity-concentration profiles and entailments

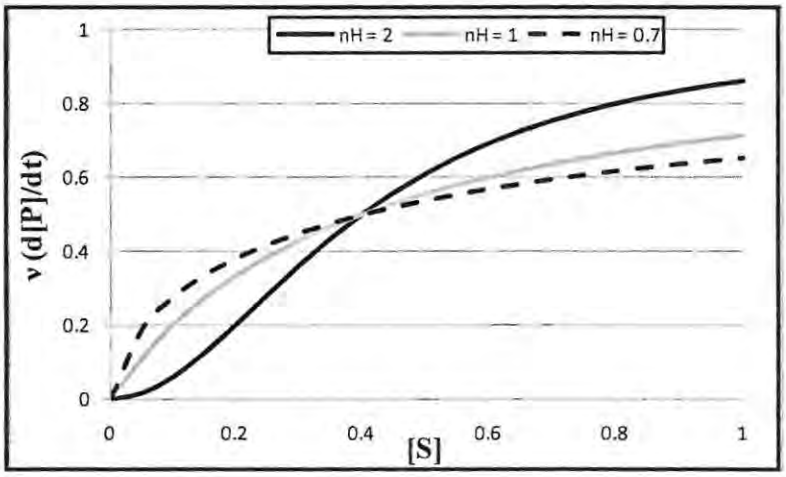

Figure 2.2: Influence of positive and negative cooperativity on velocity-substrate concentration functions.
Graphical representations of kinetic data comprised of different Hill coefficients (nH) generated using dimensionless model data.
v_{max} = 1 and K_m = 0.4 for all graphed functions.

Sigmoidal velocity-substrate behaviour (Figure 2.2) is interpreted as characteristic of co-operative enzyme kinetics, commonly observed in enzyme systems possessing multiple substrate-binding sites. Cooperativity, and allostericity in general, entails an oligomeric organisation of the enzymatic system under investigation, and/or multiple substrate-binding sites per polypeptide chain (Garrett and Grisham, 1999b). Certainly, the most commonly-cited model, the Monod-Wyman-Changeux (M-W-C) model is generated under the assumption that more than one substrate-binding site per discrete biomolecule (which includes oligomeric complexes thereof) occur (Garrett and Grisham, 1999b). Under this paradigm, the formation of an enzyme-substrate complex may alter the affinity of subsequent enzyme-substrate binding kinetics at other substrate-binding sites. In addition to this, the binding of non-substrate compounds to areas of the enzyme other than the active site may also alter substrate-enzyme kinetics. Both of these phenomena are classed as allosteric effects.

From the model of Monod-Wyman-Changeux (schematically represented in Figure 2.3 below) describing allosteric enzyme kinetics, two conformational/catalytic states of the enzyme in a given oligomer are present in equilibrium. They are represented, respectively as R (relaxed i.e. substrate-binding) and T (taut i.e. a conformation with a lesser, or no, substrate affinity). In the absence of substrate, these exist in equilibrium with R↔T. The addition of substrate (S) to this system adds a further equilibrium between R and the substrate-bound R, R↔RS. This, in turn, depletes the relative proportion of R in the system, driving the formation of a new T↔R equilibrium, increasing the effective proportion of active enzyme within the system (Garrett and Grisham, 1999b). Similarly, the binding of an allosteric effector, A, alters the equilibrium in the same manner as binding of S does.

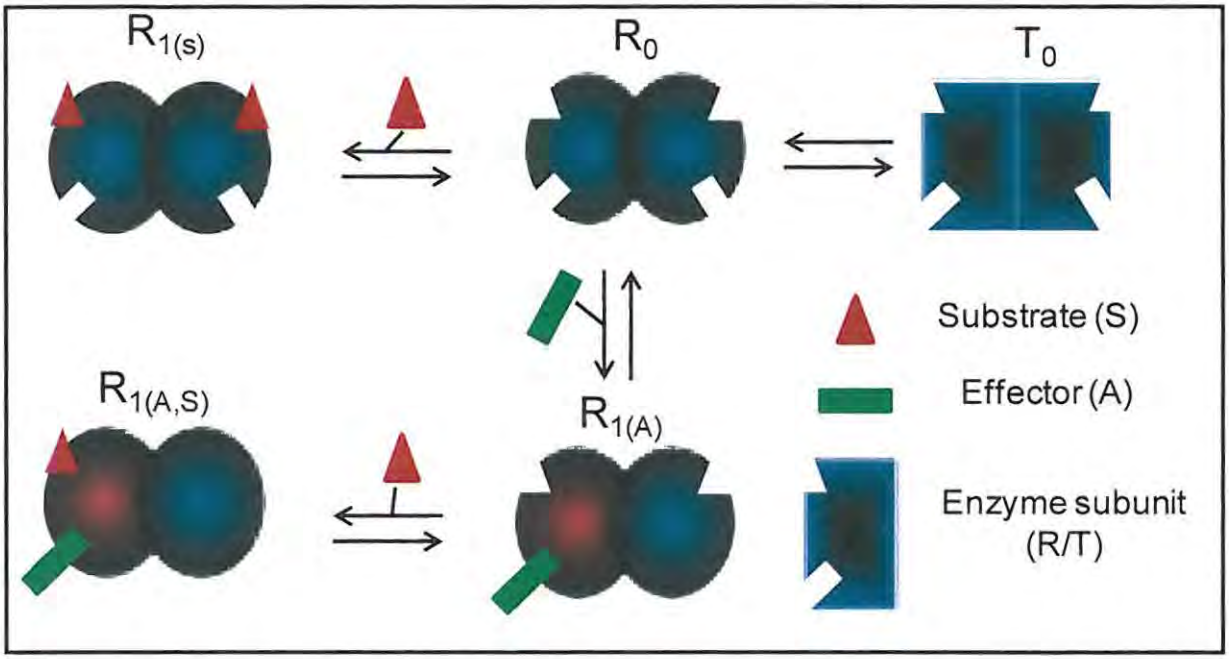

Figure 2.3: Schematic depiction of the M-W-C model of allostericity for an enzyme with a dimeric quarternary conformation.

Separate intra-subunit binding sites for an effector (A) and substrate (S) are also depicted. As adapted from Garrett and Grisham, 1999b.

Empirically, sigmoidal velocity-substrate reactions are fitted to the Hill Equation (Eq. 2.5), which describes a sigmoidal dependence of velocity on substrate concentration.

$$v = \frac{V_{max}[S]^{nH}}{K' + [S]^{nH}} \qquad \text{Eq. 2.5}$$

Where n_H is the Hill coefficient, $K' = (K_m)^{nH}$ fulfilling the same mathematical relation that K_m does, and the other symbols have their usual meaning as in Eq. 2.3 (Miller and Tanner, 2008). Comparison of Eq. 2.5 and Eq. 2.3 show that the Michaelis-Menten equation can be considered as a special case of the Hill Equation, with nH = 1. With nH > 1 a sigmoidal curve is described, and with nH < 1, a flattened hyperbolic dependence, similar in shape to the Michaelis-Menten curve, is described (Figure 2.2).

There are several shortcomings preventing the description of enzyme kinetics using the Hill co-efficient. Most importantly, the Hill Equation is only an empirical formula, to which many sigmoidal curves may

be fitted to equally. For complete description of enzyme kinetics, more stringent models (such as M-W-C) are required (Weis, 1997). Even within the context of enzyme kinetics analysis in well-defined systems, it is that n_H is rarely an exact indication of the number of substrate-binding sites present per catalytic unit: this only occurs under rare conditions of extreme cooperativity (Weiss, 1997). Under normal conditions of positive cooperativity n_H indicates the minimum, and not the total, number of binding sites required to describe the extent of cooperativity in a given system (Weiss, 1997). Generally, it appears to be used mainly as a diagnosis of global cooperativity in a given system not conforming to normal Michaelis-Menten kinetics (such as the systems described above); when $n_H > 1$, positive cooperativity is assumed to occur and when $n_H < 1$, negative cooperativity is presumed (Goldbeter, 1975; Acerenza and Mizraji, 1997). A value of $n_H = 1$ indicates conventional Michaelis-Menten kinetics predominating the enzyme system under examination (Whitehead, 1978; Acerenza and Mizraji, 1997). No further mechanistic analyses may be performed using this system for determining cooperativity.

2.3.2 Electroanalysis

2.3.2.1 Overview of principles governing electroanalysis

The principles governing electroanalysis are concerned with the measurement of electrical variables of charge (more commonly its first-order derivative, current) and potential difference (referred to as potential henceforth) occurring at an electrode (Wang, 1994; Kissinger and Heineman, 1996). By altering one measurable parameter (e.g. potential) away from the pre-existing equilibrium state and measuring the response of the system another parameter (e.g. current), dynamic electroanalytical measurements may be performed. During the research reported on henceforth, potential was usually altered and the charge/current was measured.

Potential and charge may be explained through the example of the classic generic-compound Nernstian reaction (Kissinger and Heineman, 1996). Consider the reaction of O and R occurring at the surface-solution interface of a working electrode at a fixed potential:

$$\mathbf{O} + ne^- \underset{k_b}{\overset{k_f}{\rightleftharpoons}} \mathbf{R}$$

Scheme 2.2

Where ne^- represents a stoichiometric addition of n electrons to the oxidised form **O** to generate the reduced compound **R**. k_f is the forward rate constant (i.e. rate of conversion of O to R) and k_b the reverse rate constant (Kissinger and Heineman, 1996).

The rate constants (k_f and k_b) in the above example are potential-dependent. Alteration of the potential of the working electrode thus alters the equilibrium of k_f/k_b and dictates which reaction becomes prevalent at the surface. The addition/release of electrons to **O** by the electrode is measurable as the charge leaving/entering the electrode (Kissinger and Heineman, 1996). By convention, oxidative current/charge (electron abstraction from **R**) is measured as a positive value and reduction (electron donation to **O**) is designated as negative. Thus, measurement of the current measures the proportional conversion rate of O→R and vice versa.

The potentials at which oxidation/reduction occurs are indicative of the thermodynamic/ kinetic favourability of that reaction. For the purposes of oxidation, less positive potentials indicate more favourable electron donation to the electrode by the analyte. The converse is true for analyte reduction (Bard and Faulkner, 2001).

Since electrochemical reaction rates are potential-dependent, alteration of the potential drives the reaction rate away from the initial equilibrium to a favoured overall direction of oxidation / reduction. As these reactions occur at the electrode-solution interface, current is then driven by the transport of the reactant of the favoured reaction to the interface. At potentials by which the reaction is no longer kinetically-limited by potential (i.e. equilibrium strongly favours a given reaction direction), current is then limited by the rate at which reactant reaches the electrode (mass transport limitations). Diffusion, electrostatic migration and convection are all modes of transport by which the reactant arrives at the electrode surface and are of varying importance depending on the desired outcomes of the electrochemical reaction (Kissinger and Heineman, 1996).

Electroanalytical waveforms used throughout this thesis assess the reduction/oxidation of specific analytes measureable through electrode-analyte current exchange. Two main waveforms, cyclic voltammetry and chronoamperometry are used throughout this Thesis and as such, are briefly outlined in the following subsections (2.3.2.2 and 2.3.2.3).

2.3.2.2 Cyclic Voltammetry

Cyclic Voltammetry (CV) is an electrochemical waveform whereby the potential difference extant at a working electrode surface is linearly altered with respect to time; this alteration occurs in either towards more positive potentials (anodization, promoting oxidation of analytes) or towards more negative potentials (cathodisation, promoting reduction of analytes). As the potential approaches a value whereby a Faradaic reaction (such as outlined in Scheme 2.2) becomes favoured, electron-transfer reactions between the analyte and the electrode generate charge, which is recorded and displayed as a function of potential. At a predetermined potential, the electrode potential is then altered in the opposite direction to the initial direction, promoting the opposite reaction(s) (Bard and Faulkner, 2001). Figure 2.4 below displays this in a graphical format.

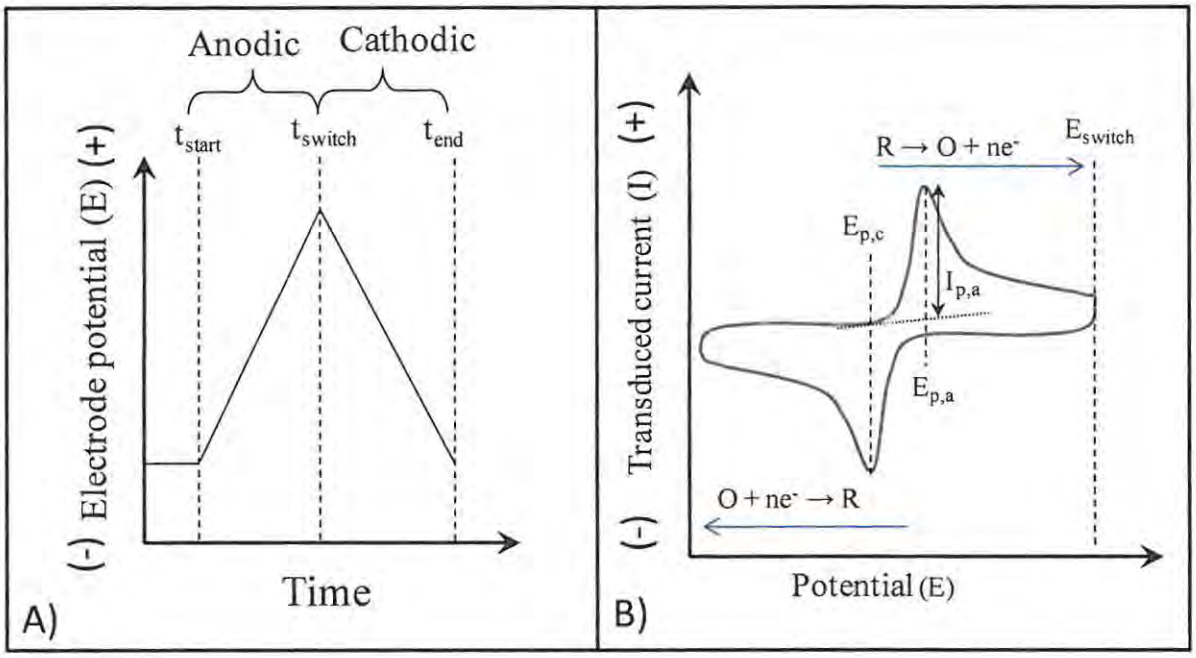

Figure 2.4: Representational diagrams of principles of cyclic voltammetry using the participants outlined in Scheme 2.2

A) Potential-time waveform, moving towards positive values (anodic sweep) and returning to the starting potential (cathodic sweep)

Legends: t_{start} - time of start of application of potential-time cycle, t_{switch}, time at which reverse (cathodic, in this instance) sweep was initiated, t_{end} – time of end of application of potential-time cycles.

B) Transduced current arising from oxidation of R and reduction of O due to the imposed potential-time waveform in A)

Legends: $E_{p,a}$ – peak oxidation (anodic) potential, $I_{p,a}$ – peak oxidation current, $E_{p,c}$ – peak reduction (cathodic) potential.

Single-ended arrows show potentials at which the attached reaction schemes are kinetically favourable.

Figure 2.4 displays that, as electrode potential increases to a point at which the reaction under examination is less limited by electron-transfer kinetics i.e. becomes less kinetically-limited, current becomes increasingly restricted by the amount of analyte present near the electrode surface. Mass-transport limitations, which increase as kinetic limitations decrease, give current responses arising from CV their characteristic peak shapes. The peaks themselves are the basis for information regarding the system: common measured parameters include, but are not limited to, the peak current (I_p) and peak potentials (E_p), indicated for the anodic (oxidation) and cathodic (reduction) peaks, respectively in Figure 2.4 (Bard and Faulkner, 2001). Several data treatments exist for extracting both quantitative and qualitative information regarding electrode processes observed during CV (Bard and Faulkner, 2001).

Electrochemical parameters and data treatments are presented and discussed in the relevant Chapters where pertinent.

2.3.2.3 Chronoamperometry

Similarly to the principles outlined in the preceding section concerning CV (Section 2.3.2.2), Chronoamperometry (CA) involves the stationary positioning of working electrode potential to a predetermined level and subsequent measurement of the current transduced from potential poising.

As an example, consider the Nernstian Scheme 2.2, in which only O was present. By altering the potential cathodically, to a level at which the reduction reaction becomes kinetically favourable, reductive current caused by the conversion of O→ R is transduced. As in cyclic voltammetry, this current rapidly becomes limited by the mass-transport considerations under which the electrochemical system finds itself.

While linear diffusion of analyte to the electrode system results in an exponential decay of current (as in the classical Cottrell Equation for planar electrodes in static solutions), convection of the solution through stirring (classed as hydrodynamic analyses) permits more stable current-time behaviour (as in the classical Levich equation, for a rotating disc electrode undergoing a Faradaic process) (Heineman and Kissinger, 1996).

2.4 Data Treatments of biosensor responses and general modelling considerations:

All enzyme kinetics studies performed were analysed using computer-driven modelling systems to elucidate relevant parameters governing the phenomenon under examination. Data was not linearised prior to modelling in e.g. Hanes-Woolf plots or Eadie-Hofstee plots (Miller and Tanner, 2008).

The use of computer-driven non-linear regression has been previously postulated (Sagnella, 1985; Leatherbarrow, 1990) and subsequently used in a number of biochemical studies (Coons et al., 1995),

including enzyme kinetics (Stojan, 1997; Gooding et al., 2000; Johnson, 2003; Goudar et al., 2004; Walsh et al., 2007). It has the distinct advantage of objectively weighting errors in the modelled data over the whole dataset, rather than exaggerating errors at low substrate concentrations (as occurs when data is normalized to the Lineweaver-Burke and Eadie-Hofstee plots (Leatherbarrow, 1990; Miller and Tanner, 2008), providing more robust overall estimations (Sagnella, 1985). The use of reiterative minima-seeking algorithms, such as those found in Microsoft® Office's "Solver" add-in for non-linear regression curve-fitting has been previously performed (Walsh and Diamond, 1994; Lin et al., 2006) and the various adjustable parameters explained (Walsh and Diamond, 1994).

Rather than create and subsequently rely on specialised modelling programs, the majority of data analyses presented in this Thesis was performed using only the simple and widely-available program Microsoft® Excel 2007, in order to demonstrate the wide-ranging applicability of the systems characterised and analysed in this manner. Data treatments used in assessing biosensor response are available in Sections A1.2 of Appendix 1 of this thesis. The criterion and Microsoft-Excel®-based procedure for assessing the goodness-of-fit between modelled data and experimental data is outlined in Sections A1.3 and A1.4, respectively, of Appendix 1.

2.4.1 Sigmoidal/Hyperbolic model used in describing biosensor kinetics

Sensor response was often resolved into a sigmoidal shape when current response (I_{tot}) at a given substrate concentration [S] was compared to the substrate concentration. For definitions of I_{tot}, refer to Section A1.2 of Appendix 1. In these cases, this necessitated the use of a different model to that typically used in enzyme kinetics modelling, the Michaelis-Menten relation. In order to extract the relevant parameters governing sensor response, a sigmoidal model of the following four-parameter formalism (Eq. 2.6) was used (Pauliukaite et al., 2006, Lee et al., 2000):

$$y = d + \frac{(a-d)}{(1+(x/c)^b)} \qquad \text{Eq. 2.6}$$

Where $y = I_{tot}$ and $x = [S]$ and the other model parameters are explained below. This function provides a very flexible model for sigmoidal (and hence, logistical) plots (Lee et al., 2000). For the purposes of

display, Figure 2.5 demonstrates the effects on the plotted curves that alterations of these parameters has on the overall function using hypothetical data generated between x = 0 and x = 1 (dimensionless units).

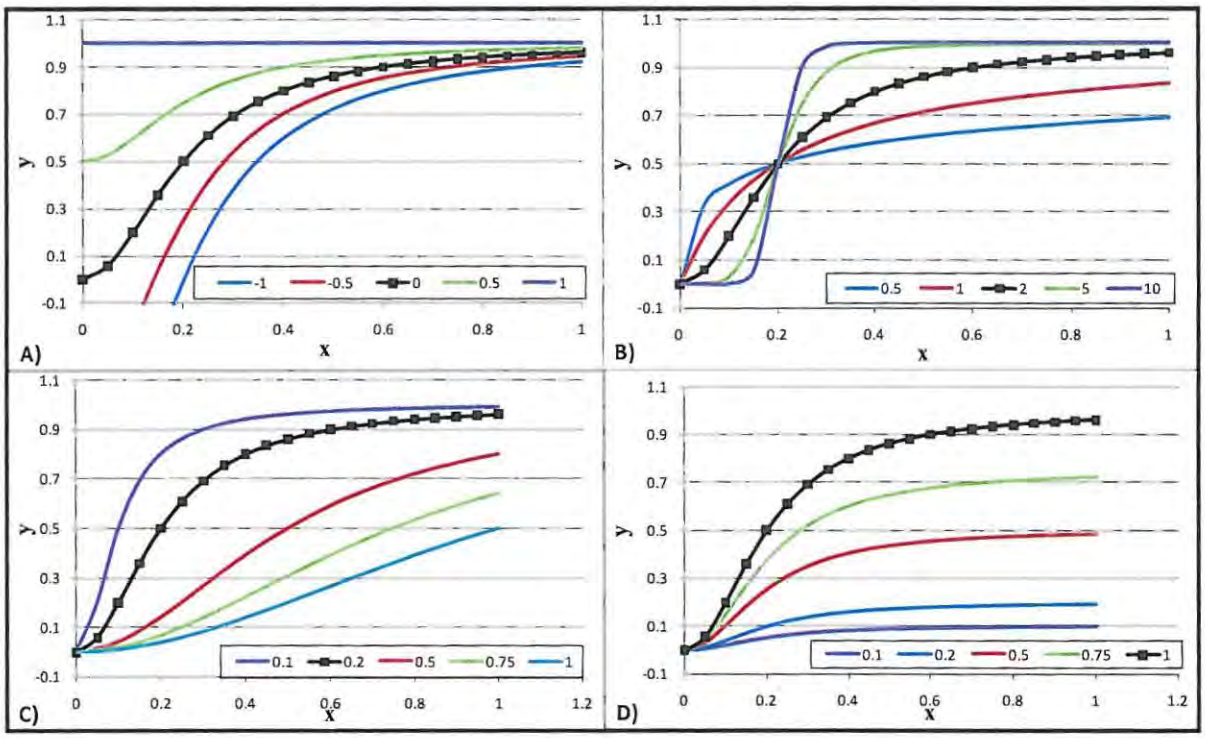

Figure 2.5: Computer-generated model data governed by sigmoidal model, as described by Eq. 2.6.
This was performed using starting values of a = 0, b = 2, c = 0.2 and d =1, using dimensionless x and y values. Legends indicate parameter values substituted into the original equation, while maintaining all other parameters as outlined above. Separate plots are displayed for each alteration of a given parameter: A - parameter a, B - parameter b, C - parameter c and D - parameter d.

For the purposes of comparison, the original function using the aforementioned parameters is displayed within all graphs in Figure 2.5 as —■—. Hence, a is the lowest asymptote of the sigmoidal graph function (Figure 2.5**A**), d is the higher asymptote of the sigmoidal shape (Figure 2.5**D**), c is the mid-point of response (the value of x at which y is half the response of d) and b is the degree of inflexion of the graph - when the function is linearised in a logit-log plot this value equates to the slope of the linearised plot (Lee et al., 2000).

Several notable properties of the model parameters need to be stated at this point in order to equate them to the enzyme kinetic equations outlined in the previous section. Both a and d are asymptotic values, rather than absolute values – at lower and higher values of x, respectively, values of y *tend* towards that value, rather than assume it. Secondly, that when b is set to a value of 1 and a to a value of 0, this

equation becomes analogous to that of the Michaelis-Menten value (see Figure 2.5**B**, b = 1). Upon setting these parameters as aforementioned, the equation governing the function alters to Eq. 2.7:

$$y = d - \frac{d}{(1+(x/c))} \qquad \text{Eq. 2.7}$$

Which, when rearranged, becomes:

$$y = \frac{(d)(x)}{(c+x)} \qquad \text{Eq. 2.8}$$

Which, given the above meanings of these parameters, is equivalent to the classic Michaelis-Menten equation (Eq. 2.3). Similarly, using a value of b not set as b = 1 gives mathematical equivalence between Eq. 2.6 and the Hill's Equation (Eq. 2.5). As expected, model data generated using arbitrary values showed no difference when outputs obtained by Eq. 2.8 when compared to Eq. 2.3, or when comparing Eq. 2.6 to Eq. 2.5. As the same number of parameters is fitted by either of these equations, they are also equal in their exactness of model fitting and computing ability. Thus, this model can be used to predict both the sigmoidal and hyperbolic biosensor behaviour, both of which were commonly found and reported on in later Chapters.

Chapter 3: Transducer surface pretreatments (glassy carbon electrodes) and enzyme activity

3.1 Abstract:

The requirement for a consistent transducer surface for biosensor attachment and transduction is an obvious one for the successful application of biosensor technology. Significant differences in electrode response, both between individual electrodes and between amendments of the electrode surface (i.e. cleanings and modifications), are often noted in studies within this area. These deviations are due to differences arising between electrode surfaces – both due to the differences in the chemical composition between moieties present on electrode surfaces and/or differences in surface roughnesses of the electrodes between cleanings and modifications. Heterogeneity of response is common to carbon-based electrodes; due to their inexpensive fabrication and presence of functional groups, they are desirable transducer surfaces for both biosensor fabrication and operation. Hence, the selection of a rapid pre-analytical treatment of the transducer surface that minimises electrochemical variance between electrodes was investigated. The selection of this cleaning procedure was performed on the basis of both non-Faradaic electrochemical investigations into electrode behaviour and Faradaic behaviour of the electrodes, with respect to catechol. Of the methods reported on in this Chapter, an anodic pretreatment of the electrode in 0.1 M NaOH, in addition to other mechanical pretreatment methods was found to produce a high degree of consistency in the aforementioned categories, both between electrodes and between cleanings of individual electrodes.

Concurrent to this was the research need to provide a means of rapidly assessing the surface of an electrode in order to determine the suitability of a given glassy carbon surface as a transducer for biosensor studies. Several requirements were posited. Firstly, the methods of determination should make use of the same technology as the biosensor (in this case, electroanalysis), in order to decrease the amount of equipment, processing-time and training required to effectively use the biosensor. Secondly, determinations should not substantially interfere with the functionality of the sensor following estimation of the surface area, either through alteration of the transducer or of the attached enzyme-layer.

Additionally, in the case of long-term, or continuous monitoring, such a method should be implementable between analyses, if not ideally during. In the following chapter, an electroanalytical method of determining the electrochemically-active surface area of glassy carbon electrodes is postulated, that of measuring the degree of charging current separation (dI). dI was validated against several, more-established non-Faradaic electroanalytical techniques of determining surface area and found to be partially successful at addressing the need for a rapid means of assessing electrode state.

Finally, in this Chapter, the methods, results and rationales for assaying laccase activity by spectrophotometrically monitoring the oxidation of catechol is described. One of the often-overlooked aspects of enzymatic biosensor fabrication is the standardisation of the quality and activity of the sourced enzyme. This is true both when considering differences in the commercial source/s of the enzyme in question and when determining consistency in quality between sourced batches of the enzyme. The inclusion of a standardised method of assaying enzyme activity under consistent conditions is essential in order to ensure consistency between biosensor fabrications, and thus, consistent results between biosensors. As several individual batches of laccase of varying laccase contents (and therefore, activities) were sourced from the supplier over the course of this research, consistent enzyme activity needed to be maintained throughout the experiments reported on in this Thesis. Enzymatic activity of non-immobilised laccase batches was therefore assessed via spectrophotometric activity assays repeatedly during the course of the research reported on in this Thesis – both when using a new batch of laccase stock and, periodically, to ensure that the laccase retains activity during storage. Assaying of laccase activity was found to be complicated by the non-linear behaviour existing between the concentration of enzyme and the assayed activity determined spectroscopically. This non-linearity was considered to be due to the auto-reduction exhibited by laccases in the absence of substrate, following solubilisation. On the basis of these findings, assays to test the activities of received and stored laccases were standardised through the velocity of oxidation of 0.05 M catechol by a laccase stock concentration of 1 $mg.ml^{-1}$.

3.2: Introduction

3.2.1 The relevance of surface area determinations in biosensor transducers:

For effective biosensor deployment and application a means of either standardising the fabricated transducer's surface area (in both composition and physical area) or, more realistically, a means of incorporating surface area/composition determinations with the biosensor response is essential for consistency and reproducibility of biosensor response.

Most electrochemical parameters and equations make explicit use of surface area (A_{surf}) as a variable in their determinations. Hence, the estimation and determination of real electrode surface area is of paramount importance in relating electrochemical information. Since, for any given experiment presented onward in this Thesis, at least 3 separate experiments are performed on at least 3 separate electrodes, estimation of the real electrode surface area is of great importance when determining and minimising inter-electrode variability and ensuring that proceeding phenomena recorded are evaluated independently of considerations of surface area.

Surface area determinations are still a problematic area in most electrochemical analytical paradigms which has not yet readily been solved, with particular regard to carbonaceous materials such as pyrolytic carbon-based electrodes (e.g. glassy carbon or highly-ordered pyrolitic graphite electrodes). Various research papers have compared the merits/demerits and limitations afforded by the many different methods of determining the active electrode surface area and the results provided may vary substantially through slight changes in the analytical variables; electroanalytical (Marozzi and Chialvo, 1996), chemical, (e.g. solvent composition and purity) the type and state of the electrode surface employed in this determination (Trasatti and Petrii, 1991) have been shown to significantly alter the calculated electrode surface area.

It should be stressed at this point that the main aim of evaluating surface area during the course of this research was merely to standardise the sensor responses to a given surface area. The scope of this research does not entail an exhaustive comparison as to the various merits and informative yield provided by various methods used in determining the real surface area. Since the value of the apparent real

electrode surface area is dependent on the analytical method used to evaluate it (Jarząbek and Borkowska, 1996), there is little value to be gained in a comparison of multiple analytical methods.

By including these measurements as part of the preliminary cleaning stage of the electrode, prior to any electroanalysis, this effectively includes an approximate measurement of surface area of the electrode within the same analysis-scheme, allowing for a time-efficient, individualised analysis on a per-electrode basis.

3.2.2 Methods of determining surface area:

Surface area determinations for solid macro-electrodes may be generally categorised into variations within three discrete groups: (a) mass transfer of redox probes under diffusion control, (b) adsorption processes at the electrode surface (usually with the assumption of purely monolayer, or a reproducible sub-monolayer/multilayer of probe) and (c) measurements of the differential capacitance in the double-layer charging potential region/s (i.e. non-faradaic processes) (Jarząbek and Borkowska, 1996). One or more of these processes may be applicable for surface area determination, based on the electrode composition and electrolyte/probe system under consideration. Whereas Jarząbek and Borkowska (1996) have stated that the determination of the capacitance of the electrical double-layer is the main method for the determination of the surface area.

Potentiostatic or voltammetric analysis of the mass-transfer of redox probes under rigorously controlled conditions is commonly applied for the evaluation of real electrode surface area and has often been used in published research articles centred on the fabrication of biosensors. As such, the deliberate absence of such a technique in this Chapter (and proceeding Chapters) needs to be briefly justified. Trasatti and Petrii (1992), in their comprehensive review of the nature of analytical *in situ* methods of determining surface areas of electrodes, have outlined several limitations to this method of determining surface area that are relevant to the research described further onwards:

(1) This technique ultimately measures the cross-sectional area of the diffusion layer possessed by the electrode, which is relatively insensitive to microscopic surface roughnesses. The extracted value is time-dependent (Trasatti and Petrii, 1991), and tends towards unity with the geometrical area with increasing time-of-assessment. For example, within an analytical time frame of 10 ms to 10 s, the diffusion layer thickness is 2 – 70 μm, which necessitates that surface asperities < 1 μm will not be accounted for (McCreery and Cline, 1996). This analytical system, hence, fails to accurately measure microscopic surface roughnesses at time-frames greater than 1 ms (which are common in the low-sweep rate voltammetric techniques employed herein) (McCreery and Cline, 1996; Bard and Faulkner, 2001a). Decreasing the analytical time-frame possesses its own inherent problems:

   a. The surface area as determined by this technique is only influenced by surface roughness at time-frames less than 100 ns i.e. with a diffusion layer of approximately 10 nm away from the electrode surface (Bard and Fualkner, 2001 a).

   b. At these time-frames, time-dependent non-Faradaic currents (e.g. double-layer charging currents) would form a significant bulk of the transduced current (Miaw and Perone, 1979), necessitating that a lot of corrective calculations and control experimentation must be performed in order to account for this and decreasing the applicability of this technique.

(2) Convection alters the produced diffusion layer, affecting the effectiveness of determining surface area in a hydrodynamic system. (Trasatti and Petrii, 1991) such as was routinely employed to assess biosensor functionality.

(3) Typically, reversibly-redox probes e.g. ferricyanide, $(Fe(CN)_6^{3-/4-})$ and ruthenium tetrahydraborate $(Ru(BH_4)^{3+/2+})$ are employed for this technique. In order for this technique to have analytical relevance, the current yields ($I_{p,a}/I_{p,c}$) would have to be unity (Trasatii and Petrii, 1992), which requires rigorously-controlled electrode/electrolyte parameters (e.g. pH, electrode surface state and ionic strength). Neither of these factors can be guaranteed when considering the use of the biosensor in an *in situ* analytical matrix and taking into account the surface reaction kinetics of carbonaceous electrodes (see: Section 3.2.3 of this Chapter).

(4) Trace amounts of redox probes may be adsorbed onto the surface of the electrode and/or biorecognition layer following surface area determinations. Acting as adsorbed contaminants, they may then affect subsequent electrode kinetics inconsistently (McCreery and Cline, 1996) as well as producing redox signals upon voltammetric/chronaomperometric analyses. Given that biomolecule modification of the electrode surface is thereafter intended to take place, this precludes the harsh treatment of the electrode (e.g. organic solvent rinsing or sonication) required to remove the adsorbed redox probes prior to biosensor use. Mechanical cleaning is precluded for the same reasons. The adsorption and interactions of biomolecules with the electrode surface would also alter the surface area, rendering the value of determining surface areas pre-modification questionable. Additionally, interactions arising between the redox probes and the redox active site of laccases (see Chapter 5.1) may alter the kinetics of the biosensor inconsistently.

For the above reasons, redox probes, either diffusionally-controlled, or adsorbed, were not considered a suitable analytical method for determining surface areas in glassy carbon electrodes. Monitoring the formation of the oxide layer of gold during acid-medium electrochemical cleaning was undertaken in order to determine the surface area (Trasatti and Petrii, 1991) for gold electrodes reported on in Chapters 6 and 8 of this Thesis. Non-faradaic electrochemical profiles of individual sensors were used as a basis of determining surface area/composition of glassy carbon electrodes.

1. Capacitance measurements and non-Faradaic electrode processes:

The measured capacitance of an electrode is dependent on a variety of analytical parameters: the composition of the working electrode, the electrolytic solvent used (both the concentration (Jarząbek and Borkowska, 1996), chemical composition (Jarząbek and Borkowska, 1996) and the pH of the selected solvent), the selected potential that capacitance determinations are performed at (Moulton et al., 2004),

While it is implied by stating that the capacitance is dependent on the electrode surface, it should be stressed at this juncture that subsequent modifications to the electrode surface (or indeed, the electrode /

bulk solution interface) will result in an alteration of the capacitance that is measured. The adsorption of protein onto a gold electrode performed by Moulton et al., 2004 exploited this phenomenon, by tracking alterations to the capacitance upon the exposure of the electrode to proteinaceous solutions.

The other aspects which are important to standardise the functioning of a working electrode surface are: surface topography (represented in part by the recognition that real surface area is dependent on the microscopic / macroscopic roughness of the electrode), lateral chemical / physical homogeneity of the surface (of especial relevance when considering of carbon-based materials as electrode surfaces, given their heterogeneous chemical natures).

3.2.3 Carbonaceous electrodes – structure and kinetics

1. Carbonaceous electrodes: general overview

Carbonaceous electrodes have the advantages of a very low cost of manufacture and ease-of-fabrication (Kamau, 1988; Rice et al., 1989; Bowers et al., 1990). This, coupled with their large potential window (Rice et al., 1989; Zhao et al., 2008) and relative inertness with electrolytes (Rice et al., 1989; Bowers et al., 1990) (mainly in terms of corrosion-resistance) are important properties governing the deployment of this technology within an industrial paradigm, while the variability occurring between electrodes is important from an analytical perspective, both qualitatively and quantitatively.

Glassy Carbon Electrodes (GCEs) are widely used carbonaceous electrode surfaces, and are considered to be the most widely-employed electrodes of carbonaceous composition (McCreery and Cline, 1996). They are impermeable to liquids and gases, easily polishable and installable (in a variety of configurations) and are compatible/inert with most common solvents. They also have a large potential window in which they provide electroanalytical information (approximately between 1.2 Vand -0.8 V vs. SCE) without themselves being greatly affected (McCreery and Cline, 1996). This electrode is formed through the high-temperature partial degradation of high-weight carbonaceous polymers (e.g. phenol/formaldehyde resin). The resultant chemical structure is predominantly sp^2-hybridised hexagonal

carbon rings bonded onto the original backbone of the polymer used – essentially forming "a tangled mass of graphitic ribbons" (McCreery and Cline, 1996). This structure produces an increased level of crystalline disorder, relative to Highly-Ordered Pyrolic Graphite Electrodes (HOPGE), but improves the hardness and removes the porosity experienced by the former. Surface roughness of this electrode material type is highly dependent on the polishing/cleaning procedures undertaken, but typically ranges from σ = 1.3 to 3.5 and the observed capacitance between 10 - 20 $\mu F.cm^{-2}$ for microscopically-smooth, heat-treated electrodes to between 30 – 70 $\mu F.cm^{-2}$ for the majority of polished electrodes (McCreery and Cline, 1996).

2. Heterogeneity of response of carbon electrodes and electrode surface studies

The heterogeneous nature of carbonaceous electrodes has a vast effect on the electrochemical transfer kinetics of the electrodes (Mcreery and Cline, 1996), and is thus an important consideration when contemplating their usage for biosensor technology. Of subsequent importance governing electrode reactions are the carbon-oxygen groups found along the electrode surface (Kamau, 1988; Bowers et al, 1990; Ray and McCreery, 1999). These can be broadly classified as hydroxyl, carboxyl, carbonyl and aromatic (mainly phenolic/quinone) groups present on the electrode surface (Kamau, 1988). Concomitant with, and perhaps due to, increasing the oxygen content of a carbon electrode's surface displays an enhanced electrochemical response (Bowers et al., 1990), both in terms of signal and in the redox reversibility of analytes and redox probes (Shi et al., 2007). Of the aforementioned surface groups, the quinone/hydroquinone groups have especially been proposed to function as an electron-transfer mediator for certain redox systems, enhancing the electrodes' reactivity towards their reduction/oxidation (Kamau, 1988). Hence a great deal of research has been performed to achieve reproducible enhancements of the signal through modulation of the presence of these oxygenated species, either electrochemically (Kamau, 1988; Bowers et al., 1990; Shi et al., 2007) or via chemical (Kamau, 1988) means. A wide variety of electrochemical pretreatment strategies already exist, with different applications guiding the extent, type and selected electrolyte used in such pretreatments (McCreery and Cline, 1996).

The proportions, concentrations and lateral distributions of these surface groups differ between the different states of carbon comprising the electrodes; furthermore, surface group density is affected (often increased) by the cleaning (Ray and McCreery, 1999, Kiema et al., 2003; Swain, 2007) and pre-analysis treatments (Bowers et al., 1990; McCreery and Cline, 1996; Swain, 2007) used, as well as exposure of electrode surfaces to electrolyte solutions or air (Ray and McCreery, 1999).

The attachment of contaminants to the electrode surface produces similar alterations in the reproducibility and strength of electrochemical signals. A pertinent sub-set of this is that of polishing debris. Contaminants formed during polishing produce a film that is mechanically and chemically resistant to removal, but has a pronounced effect on the functioning of the electrode (McCreery and Cline, 1996; Kiema et al., 2003). Several methods have been advanced in an attempt to remove this fabricated film including: ultrasonication (in both aqueous solutions and a variety of organic solvents, Kamau, 1988); and electrochemical pretreatment (both electrooxidation and oxidation/reduction cycles, Kamau, 1988). SEM studies performed by Kiema et al. (2003) demonstrated that brief electrooxidation of polished GCEs in an alkaline solution (0.1 M NaOH) adequately removed the layer of debris formed during mechanical polishing of the electrode, improving both the magnitude and reproducibility of electrochemical response between cleanings.

The choice of cleaning and electrode pretreatment strategies has a profound effect on the functioning of electrodes, particularly on the glassy carbon electrodes employed in this study (Engstrom, 1982; Rice et al., 1989; Jürgen and Steckhan, 1992; Kiema et al., 2003). Increases in both the reproducibility and magnitude of electrochemical signals can be achieved through the selection of an appropriate pre-analytical treatment strategy (Engstrom, 1982; Wang and Lin, 1998). Cleaning and pretreatment protocols vary on a study-to-study, and a lab-to-lab basis, having a substantial effect on the reproducibility of results reported using this electrode material (McCreery and Cline, 1996; Kiema et al., 2003). This factor is further complicated by the physical and chemical effects of cleaning strategies on the electrode surface.

The selection of a given cleaning or pretreatment strategy may simultaneously affect both the physical roughness (Smyrl et al., 1989), surface chemical composition (Kamau, 1988; Smyr et al., 1989) and influences the presence/absence of contaminants. These factors hinder attempts at resolving the complex interplay that results in such variability of response (Rice et al., 1989). In addition, the selection of an optimum intersection of treatment/s is considered to be dependent on the analyte (McCreery and Cline, 1996; Hoogvliet et al., 1989) and detection matrix in question (Hoogvliet et al., 1989). Hence, optimisation of electrode response for one analyte does not itself guarantee improved electrode kinetics for others. This has been extensively researched, and in many cases, exploited, in order to improve both the response and selectivity of electrodes towards certain analytes.

3. Laccase assaying

The fabrication and application of enzymatic biosensors at a commercial level is, to a large extent, dependent on the availability and quality of commercially-available enzyme acting as the biorecognition element. For this section, much of the discussion given over to already-commercialised biosensors is relevant for consideration for laccase.

Commerically-available enzyme preparations commonly have > 25% active enzyme by weight and may contain non-protein additives, such as salts and sugars (Roy and Abraham, 2004). This is counterbalanced to a large extent by the typically-low stability of highly-pure enzymes, as well as the time-consuming and expensive processes required to purify enzymes to near-homogeneity (Roy and Abraham, 2004). Hence, there exist both advantages and disadvantages to the fabrication of biosensors using either high or low degrees of enzyme purity.

However, when considering the manufacture of enzymatic biosensors at a commercial i.e. mass-production level, the addition of costly pre-modification purification stages, with their concomitant loss of both active enzyme molecules and subsequent enzyme activity (e.g. Garret and Grisham, 2001b; Uthandi et al., 2010), and enzyme stability (Roy and Abraham, 2004) once purified, makes the preparative steps of purification undesirable from a manufacturing perspective.

The direct application of commercially-sourced enzymes is somewhat problematized by variations in the amount and purity of enzyme obtainable between batches. A common method of assessing both of these factors is the straightforward assaying of total enzyme activity per unit mass of the sourced enzyme. This provides the biosensor manufacturer with an indication of both the total activity of the enzyme and the degree of purity (in the form of specific activity i.e. activity per unit mass) (Garret and Grisham, 2001b). Comparisons between activity and specific activity allows adjustments to be made between different batches, based on the relative performance of the specific batch, in order to provide consistency between biosensors fabricated using different batches of sourced enzyme.

Hence, it was of analytical interest to assess the conditions under which the assaying of laccase activity would provide consistent results regarding both the total, and specific, activity of different batches. In particular, the effects of the amount of enzyme present during an activity assay on the determined activity of the enzyme is explored in this Chapter. Assaying of solubilised laccase is commonly performed through the spectrophotometric detection of the rate of product formation during the oxidation of a specific substrate under pre-specified conditions e.g. standardised pH. A common substrate for this method is catechol, which is used by the supplier of the laccase in question to determine the relative activity of batches (Internet Reference 1).

3.3 Aims and Objectives:

The following aims and objective were set for this phase of research:

(1) Determination of a pre-analytical treatment method for GCEs that provides an adequately clean electrode surface and minimises inter-electrode variance in electrochemical response. Both of these criterion were assessed by non-Faradaic assessments of the electrode surface and with respect to the oxidation / reduction of catechol present in the main electrolyte used for the majority of the research, SLB adjusted to a pH of 4.5.

(2) Validate the selected non-Faradaic method of assessment against a more conventional method of determining electrode surface area. As stated in the Introduction section of this Chapter, the validative technique must also be non-Faradaic, owing to considerations centred around the use of redox probes as means to assess electrode surface areas.

(3) Evaluate certain criterion by which laccase activity is assayed under the conventional paradigm of spectroscopy. These include the relative activity in the presence of other proteins (BSA, for the purposes of this research), as well as the effects of laccase content on the rate of oxidation.

3.4 Methods and Materials:

3.4.1 Apparatus and Reagents

The electroanalytical apparatus used was the same as described in Chapter 2 of this thesis (Section 2.1.1.1), as was the quality of solvents and reagents (Section 2.2)

0.1 M KCl solution was used as the main electrolyte when assessing the effect of cleaning protocols on the double-layer effect of glassy carbon electrodes, diluted from 3 M KCl stock.

0.1 M succinic-lactic acid buffer (SLB) was employed as the main electrolyte and buffer throughout this section. Unless otherwise stated, the pH of this electrolyte was maintained at 4.50. All analyses took place at room temperature, and all electrolytes and cleaning agents were prepared and used once equilibrated to this temperature. Storage of electrolytes was at 4 °C.

All catechol (phenolic) substrate stocks used were prepared to a concentration of 100 mM in water daily and stored in the dark until used.

3.4.2 Methodology for transducer surface studies:

3.4.2.1 Effect of cleaning protocol on charging currents

Several cleaning protocols were used in order to determine the cyclic voltammetric charging current/s arising from the different exposed surfaces. The cleaning procedures investigated in this study are outlined below:

1. Paper-cleaning (negative control):

Electrodes were polished using tissue paper, rinsed with water and stored in water until electroanalysis.

2. Polishing

Electrodes were polished in a slurry of alumina oxide (Al_2O_3) microparticles (> 10 μm) and water for at least 2 minutes. Following polishing, electrodes were rinsed with water and stored in same prior to electroanalysis.

3. Ultrasonication (ethanol)

Electrodes were polished (Section 3.4.2.1.2) before being rinsed with ethanol and ultrasonicated in ethanol for 2 minutes, followed by rinsing and ultrasonication in water for 2 minutes. After ultrasonication, electrodes were stored in water until used

4. Ultrasonication (base)

Electrodes were prepared as in Section 3.4.2.1.2 before being ultrasonicated in 0.1 M aqueous NaOH solution for 2 minutes, followed by ultrasonication in water for the same length of time. Prior to analysis, electrodes were stored in water.

5. Anodic pretreatment (base)

Following polishing, electrodes were electrooxidised in 0.1M NaOH (+ 1.45 V vs. Ag/AgCl) for 5 s before being successively ultrasonicated in ethanol and water, before being stored in water.

Electrodes cleaned in this manner were subsequently cycled repeatedly between 0 and +1.0 V in 0.1 M KCl until a stable CV response was recorded. Voltammetric shapes and current responses at certain potentials were recorded and analysed to assess both reproducibility and alterations to same resulting from the cleaning protocol used. In addition, the effect of the cleaning procedures upon the reduction/oxidation of 0.1 mM catechol within 0.1 M KCl was performed.

In order to assess differences in the double-layer capacitance due to alterations in the electrolyte, as well as to assess the reproducibility of the reduction/oxidation of phenolic compounds at the electrodes' surface, polished electrodes and electrodes that were anodically pretreated were also analysed in SLB, pH 4.5.

3.4.2.2 Validation of dI as an indication of electrode surface area: Non-Faradaic Chronoamperometry

Electrodes, prepared as outlined in 3.4.2, were subjected to two-step chronoamperometry, following cyclic voltammetry. Electrodes were cycled repeatedly between 0 and +1.0 V in electrolyte until a stable response was recorded. Voltammetric shapes and charging currents at +0.5 V (dI) were recorded.

Following cyclic voltammetry, double-step chronoamperometry was performed. Electrode potential was poised at +0.45 V for 5 seconds, to equilibrate the system. Following equilibration, electrodes were subjected to two-step chronoamperometry (E_1 = +0.45 V and E_2 = +0.5 V) for 10 ms each, sampling current at 100 µs intervals. Both cyclic voltammetry and double-step chronoamperometry were performed either in 0.1 M KCl or in SLB, pH 4.5.

Datapoints corresponding to the first 2 ms of the second voltammetric step were imported into Excel spreadsheets and the C_{DL} was calculated using the following equation (Eq. 3.1) using χ^2 as the goodness-of-fit indicator (Appendix A1.4):

$$i_{DL} = \frac{\Delta E}{R_S} e^{\frac{-t}{(C_{DL})(R_S)}} \qquad \text{Eq. 3.1}$$

Where i_{DL} is the double-layer charging current (assumed to be the sole current response in the absence of Faradaic reactions), ΔE is the change in potential (0.05 V) and R_S is the solution resistivity (in Ω) (Miaw and Peronne, 1979; Bard and Faulkner, 2001a).

The capacitance derived from dI was related to the apparent total capacitance of the system, as outlined by Trasatti and Petrii, 1991. In brief, dI values at + 0.5 V are related to the scan rate of voltammetric sweeps through the following formalism:

$$i_{ch} = A_{surf} C_{dl} v \qquad \text{Eq. 3.2}$$

Where i_{ch} is the non-Faradaic i.e. double-layer charging current (A), A_{surf} is the electrode's surface area (cm^2) and C_{dl} is the capacitance of the electrode ($F.cm^{-2}$) (Bard and Faulkner, 2001a). Since dI is the sum of anodic and cathodic sweeps, it is equivalent to 2 x i_{ch} (Bard and Faulkner, 2001a). Assuming that double-layer charging is the only contributor to the current, dI would therefore be equivalent to 2 x 0.1 x ($C_{DL}.A_{surf}$) (Bard and Faulkner, 2001a; Trasatti and Petrri, 1991).

3.4.2.3. Faradaic Voltammetry:

The reproducibility of electrochemical signals for the oxidation / reduction profile of 0.2 mM catechol was assessed by cyclic voltammetry for electrodes subjected to various cleaning protocols as outlined in 3.4.2. Cyclic voltammetry was performed between -0.3 V and + 0.8 V at a scan rate of 0.1 $V.s^{-1}$ and performed in both 0.1 M KCl and 0.1 M SLB.

3.4.3: Methodology for spectrophotometric assay of laccase activity:

The apparatus used for this is described in Chapter 2 of this Thesis, Section 2.1.2. For the determination of laccase activity, catechol (λ_{max} = 450 nm, ε = 2211 $M^{-1}.cm^{-1}$) was selected as the laccase substrate.

1. Initial spectroscopic characterisation of free laccase

Laccase activity determinations were performed in at least quadruplicate replicants and reported on as such henceforth. Spectroscopic assaying occurred at a set temperature of 20 °C, in 0.09 M SLB, pH 4.5 containing 0.05 M catechol. The rate of catechol oxidation was measured at an absorbance wavelength of λ = 450 nm at 4 s intervals, for at least 15 consecutive intervals (i.e. at least 1 minute). All absorbance data was blanked relative to a laccase-free negative control containing 0.05 M catechol. Fresh laccase solution was prepared for each assay

Table 3.1: Volumes, formulations and final concentrations of reagents used during spectroscopic analysis of laccase stock solutions.

Assay Reagent	Volume (µl)	Final concentration
0.1M SLB, pH 4.5	267	0.09 M
Laccase (dissolved in SLB)	3	10^{-2} [a]
SLB (for negative controls)	3	-
Catechol (0.5 M, in water)	30	0.05 M (15 µmol total)

[a] – i.e. a 100-fold dilution, relative to the stock concentration employed for each experiment

Immediately following the addition of catechol to the spectrophotometry well, the solution was rapidly mixed and the change in absorbance at 450 nm was read, as outlined above. From the rate of change of absorbance, the total laccase activity within the stock used was calculated using the following equation (Eq. 3.3):

$$v = \frac{\Delta A}{\Delta t.\varepsilon.[C].L.dl} \qquad \text{Eq. 3.3}$$

Where v is the enzyme activity of the stock solution (units.min^{-1} = µmol.min^{-1}), $\Delta A/\Delta t$ is the gradient of the initial absorbance change (OD.min^{-1}), ε is the molar extinction co-efficient for catechol at λ = 450nm (2211 M^{-1}.cm^{-1}, as cited in Jung et al., 2002; Roy and Abraham, 2006), $[C]$ is the concentration of catechol in the solution (0.05 M), L is the path length (1 cm for the 300 µl volume used) and dl is the

dilution factor (100-fold). 1 unit of enzyme activity was defined as the catalysed degradation of 1 μmol of catechol.min^{-1}.

Specific activity was calculated from the total activity by dividing the total activity by the concentration of laccase used in the formulation of the stocks (mg.ml^{-1}) and applying a corrective factor of 10x (since manufacturers' specifications were that ~10% of the supplied lyophilised mass was active enzyme, Sigma-Aldrich, 2010 – cf. Internet References 1.1 and 1.2 following the Reference section of this Thesis).

2. Spectroscopic determination of laccase activity with increasing laccase concentrations

The initial laccase concentrations were calculated by the manufacturer's specifications provided (typically > 20 U.mg^{-1} protein, reported activities differed according to batch). Laccase activity was assayed at: 1, 2, 5, 10, 20 and 32.6 mg of lyophilised mass.ml^{-1} concentrations, all of which were derived from a single sourced batch of laccase. Laccase, and all other reagents for spectroscopy, were prepared as in Table 3.1, Section 3.4.3.1.

3. Addition of BSA to laccase assays

The same laccase assays outlined above (Section 3.4.3.2) were performed, in the presence and absence of BSA. To the laccase stock solution, BSA was added to a final concentration of 10 mg.ml^{-1} BSA before addition of protein to the spectroscopic wells (final concentration of BSA during assaying: 0.1 mg.ml^{-1}).

4. Laccase activity assays between batches

For each batch of laccase used henceforth in this Thesis, laccase activity was first assayed at 1 mg.ml^{-1} stock laccase concentration as outlined above in Section 3.4.3.1. Activity was adjusted accordingly between batches to correspond to the activity of the first batch (clarified below) used in research in order to maintain the same activity in biosensor and spectroscopic studies conducted.

For reasons discussed in the Results of this section, the activity of the first batch was set to be the activity of laccase at a concentration of 36.2 mg.ml^{-1} laccase. This activity was extrapolated from the laccase assayed spectroscopically at a concentration of 1 mg.ml^{-1}.

3.5 Results:

3.5.1 Effects of cleaning on non-Faradaic indicators of electrode performance

For this phase of study, only 3 different glassy carbon electrodes were used, in order to maintain parity between the effects of different cleaning techniques. Henceforth, the indicated electrodes are separately referred to as GCE 1, GCE 2 and GCE 3, respectively. 0.1 M KCl was selected as the main electrolyte due to its absence of tendency to form adsorptive or ionic bonds with carbon substrates (Müller and Kastening, 1994).

Figure 3.1 displays the typical behaviour of GCEs during the successive scanning of electrodes in 0.1M KCl. Similar behaviour is noted in SLB, pH 4.5 (data not shown). This example is a representative CV recorded at a GCE which was polished and subsequently sonicated in ethanol. The first and tenth scans are included and indicated.

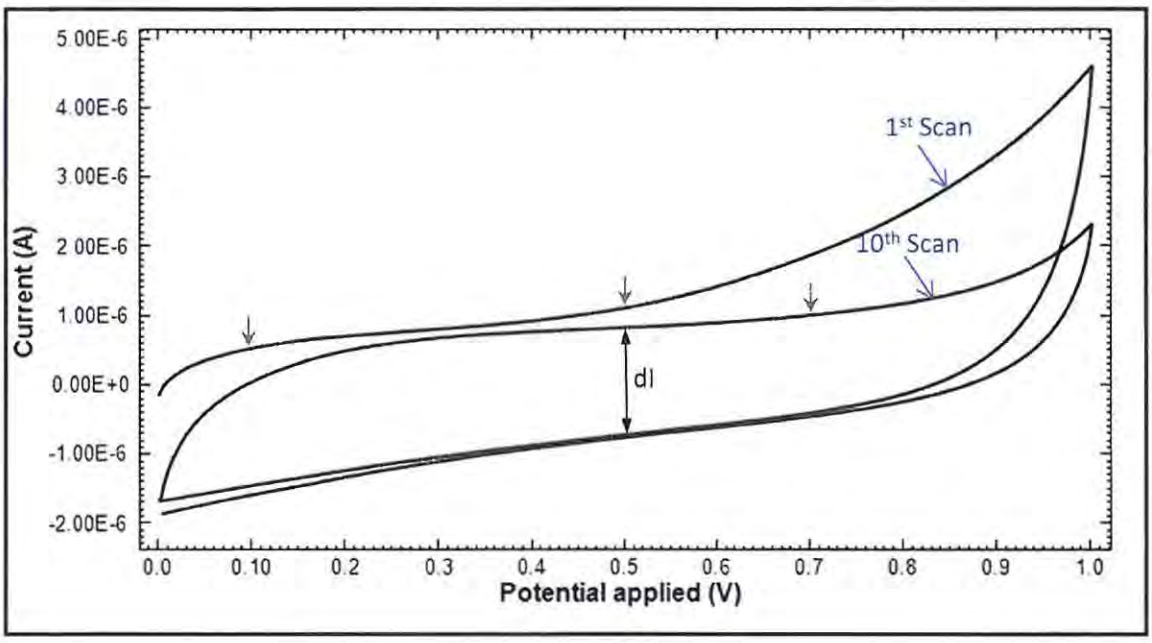

Figure 3.1: Cyclic voltammograms depicting apparent differences in the current-potential curves at the 1st and 10th scan recorded in 0.1M KCl.

The electrode used in this depiction was polished, then ethanol-sonicated. Grey arrows show potentials at which currents were sampled to calculate dI values (double-headed arrow)

For the purposes of estimating surface area of GCEs, electrodes were cycled in electrolyte for a successive series of a minimum of 5, and typically 10, cycles until a stable baseline was achieved (as in Figure 3.1). At selected points along the voltammogram, indicated in Figure 3.1 (i.e + 0.1 V, 0.5 V and 0.7V vs. Ag/AgCl) both the anodic and cathodic currents were recorded and the current separating them (dI) was calculated. These points corresponded to the first plateau of current after the onset of the anodic sweep; the midpoint of the voltammogram and the first current plateau after the onset of the cathodic sweep, respectively.

Figure 3.2 displays the average dI initially calculated for all three electrodes when using different cleaning strategies. It is divided into a summary of the dI values calculated across all 3 selected electrodes i.e. inter-electrode consistenty when current is sampled at the aforementioned potentials of 0.1 V; 0.5 V and 0.7 V (Figure 3.2**A**); and when assessing intra-electrode consistency when dI calculated at E = +0.7 V was used (Figure 3.2**B**).

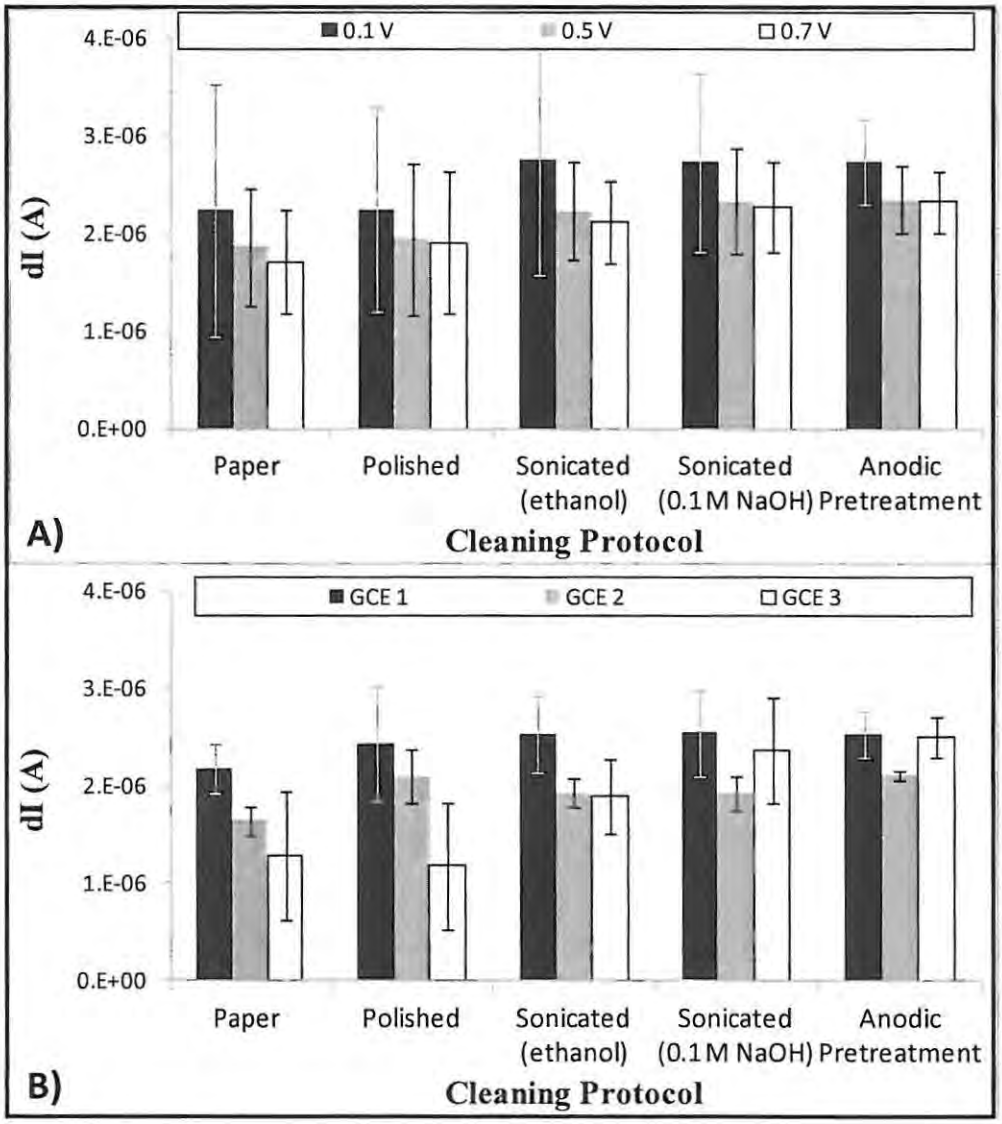

Figure 3.2: Influence of cleaning protocol on dI at selected potentials and between electrodes.

A) Effect of potential selection on calculated dI on total population of analyses, n > 9, across 3 electrodes

B) dI values at E = + 0.7 V vs. Ag/AgCl determined for individual electrodes cycled in 0.1M KCl with different cleaning protocols.

Error bars indicate standard deviation from the mean, n = 3, for each electrode (3).

From the lower degree of deviation observable at the selected potentials using different surface pretreatments (Figure 3.2**A**) dI, as determined at + 0.7 V was used to evaluate the differences in dI between electrode cleanings (Figure 3.2**B**). In order to generate information regarding both inter- and intra-electrode variability with different cleaning techniques, cleaning protocols were repeatedly performed on the same electrodes and the dI evaluated (Figure 3.2**B**). The variance in most cases appears

to be stable and dependent on the electrode, rather than on the global population, evidenced by the lower degree of deviation for individual electrodes (Figure 3.2**B**).

Little discernible difference in dI variability is noted at this stage when electrodes are cleaned with paper or polished and rinsed, from both inter- and intra-electrode perspectives (Figures 3.2**A** and Figures 3.2**B**). Anodic pretreatment, followed by ultrasonication of the electrode in successive solutions of ethanol and water provided the highest noted degree of consistency in the determined dI values, as evidenced by the significant reduction in standard deviation from the mean (error bars in Figure 3.2). This occurs, both between electrodes (Figure 3.2**A**) and between pretreatments performed on the same electrode (Figure 3.2**B**). From this, it can be inferred that anodic pretreatment in alkaline solution results in a more reproducible electrode surface, in both physical and chemical characteristics of the electrode surface, relative to the other pretreatment methods.

Anodic electrochemical pretreatment of electrodes prior to analysis has been employed as means to: enhance surface reproducibility after polishing, enhance response and as a further cleaning measure to remove electrooxidised fouling products (Wang and Lin, 1988). Reproducibility of response was found to be related to the reproducibility of both cleaning and electroanalytical pretreatment (Wang and Lin, 1988). Anodic pretreatment of electrodes in this study resulted in the formation of reddish-yellow films on the electrode surface that were subsequently removed during sonication. These films are assumed to be composed of graphite oxide layers, a by-product of electrode anodisation (Majer et al., 1973; Jürgen and Steckhan, 1992).

The same trends between surface reproducibility as assessed by dI in 0.1M KCl using different cleaning methods (Figure 3.2**A**) are found when determining dI in SLB, for the various electrode pretreatments (Figure 3.3, below). Figure 3.3 displays the mean dI, and the respective variations thereof, when comparing electrodes cleaned via: polishing (negative control), ethanol ultrasonication (which gave a high degree of inter-electrode variation in 0.1M KCl, Figure 3.2**A**) and anodic pretreatment (most reproducible dI between electrodes, 3.2**A**)

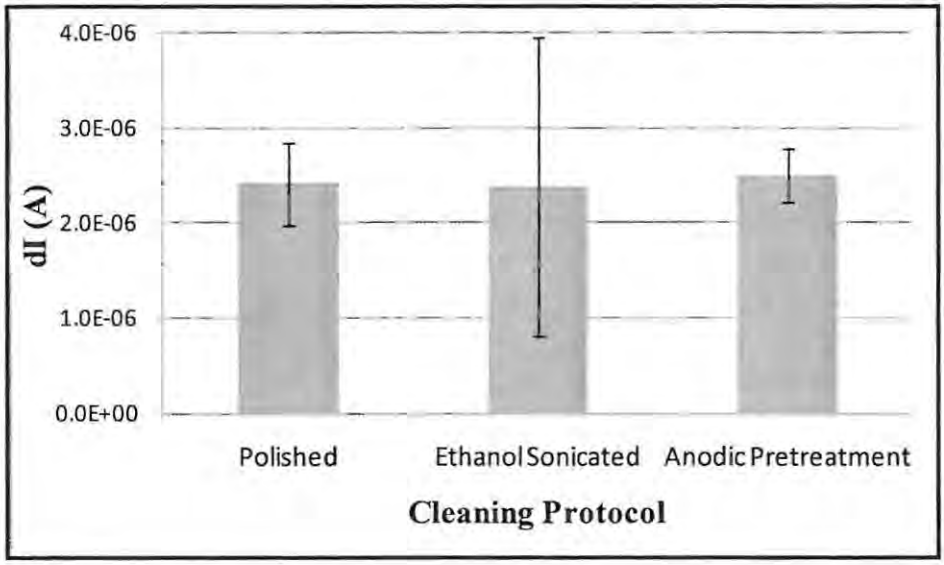

Figure 3.3: dI values determined for different cleaning protocols for GCEs in SLB buffer, pH 4.5 dI determined at +0.6 V vs. Ag/AgCl.

Error bars indicates standard deviation from the mean with number of observations, $9 < n < 15$, using 3 different electrodes.

The calculation of dI in SLB at a potential of + 0.6 V was selected due to the onset of electrolyte oxidation at + 0.7 V (data not shown). A comparison of Figures 3.3 and 3.2 display the same trends in reproducibility of dI calculations observed when applying the different cleaning protocols, irrespective of whether 0.1 M KCl or SLB was the electrolyte used in the determination of dI. This indicates that the state of cleanliness and the inter-electrode surface roughnesses determinable by dI with the various cleaning strategies appear equivalent despite alterations in the electrolyte.

Even though anodic pretreatment resulted in the most reproducible electrode characteristics assessed by dI, the coefficient of variation noted within the group still ranged within 19 % and 16 % of the mean value (Figure 3.2**A**). This indicates that variability between the prepared electrode surfaces remains quite high, reiterating the need for surface area determinations as part of biosensor measurements. This becomes increasingly important when implementing many separate surfaces as both biomolecule immobilisation scaffolds and for multiple analyses to be conducted simultaneously – the homogeneity of electrodes either during the fabrication stage (manufacture, distribution) or at the end-user stage (as typified in the above study) cannot be guaranteed.

3.5.2: Validation of dI as a measure of surface area through non-Faradaic electroanalysis

From the investigations on the effect of electrode pretreatments on the calculated dI, it is apparent that the cleaning procedure selected has a large effect on the apparent non-Faradaic characteristics of the electrode. In an effort to address some of the analytical shortcomings of using dI in order to determine relevant electrode-state analyses, a further validative technique was applied to this method. The determination of C_{DL} via non-Faradaic chronoamperometry was performed and related to dI, for electrodes immersed both in 0.1M KCl and SLB.

Initially, KCl was used as the main electrolyte, not just for the reasons of inertness with the electrode stated in Section 3.4.1, but because it has been previously characterised as an electrolyte (Bobacka et al., 2000) in the literature, while SLB has not. In addition, the interaction of the surface electrode layer with proton concentration was avoided by selecting this electrolyte.

The model used for chronoamperometric determination of the C_{DL} predicted a solution resistivity , R_S, for 0.1M KCl of 114.2 $\pm$ 12.8 Ω before electrode cycling and 115.4 $\pm$ 15.7 Ω after electrode cycling when electrodes were prepared with anodic pretreatment in 0.1M NaOH. Either of these values show excellent agreement with previously-published solution resistivities of the same electrolyte; previous values of R_S for this electrolyte is reported to be 122 $\pm$ 1 Ω (Bobacka et al., 2000, obtained by electrochemical impedance spectroscopy (EIS) at an organic polymer film attached to a planar platinum electrode of comparable geometric area, 0.07cm^2). As this value varies with cell geometry, the nature of the electrolyte and electrode geometry (Yu and Liu, 2010), the value reported in Bobacka et al., 2000 was selected to represent this value with comparable geometries.

Appendix 2, section A2.1 details the modelling system used in order to extract the C_{DL} and the R_S of the electrodes examined using non-Faradaic chronoamperometry, as well as showing examples of the data obtained through the double-step chronoamperometry. Figure 3.4 (below) displays the linear comparison between electrodes treated either through anodic pretreatment in 0.1M KCl and those treated via

polishing when comparing C_{DL} calculated through chronoamperometry (Eq. 3.1) and through dI (Eq. 3.2).

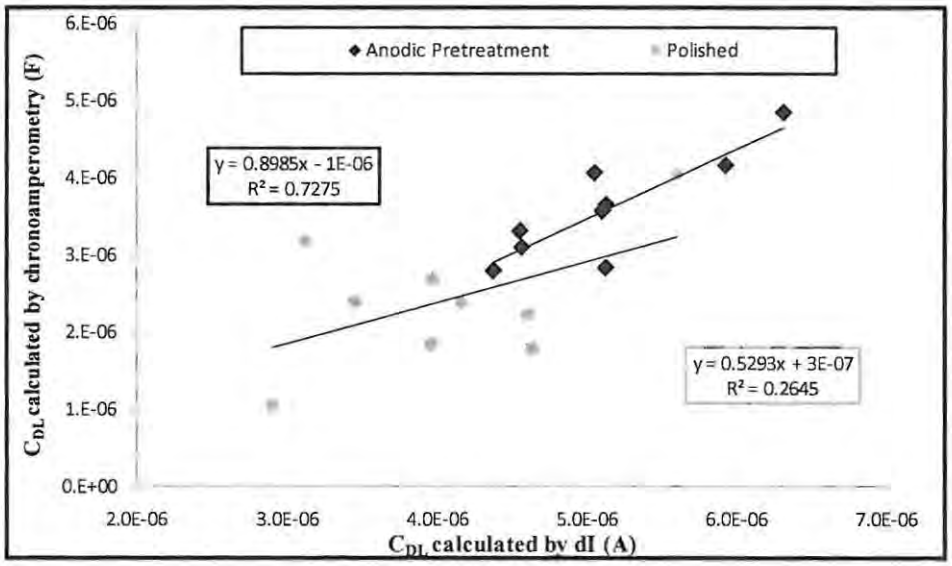

Figure 3.4: Correlations between C_{DL} as calculated by chronoamperomtric determinations of charging current (after voltammetric determination) vs. C_{DL} as calculated by sweep separation current, dI in 0.1 M KCl.

Electrodes cleaned through polishing (circles) and electrodes cleaned through anodic pretreatment (diamonds) are included. Inset boxes in the respective colours of the data-sets indicate linear regressional parameters evaluated from the global population.

Number of measurements per cleaning procedure, n = 9, using 3 different electrodes.

As Figure 3.4 displays, there is a positive linear trend occurring between the C_{DL} values calculated by dI and those determined through chronoamperometry. The degree of linearity is much higher for anodically-pretreated electrodes ($R^2 = 0.725$) than it is for electrodes cleaned via polishing ($R^2 = 0.53$). In addition, while the determined slope for anodically-pretreated electrodes approaches that of unity (~0.90), the slope determined for polished electrodes is much lower (~0.53). This disparity in slope and linearity may be caused by the aforementioned differences in surface composition outlined above. The presence of charged groups on the electrode (such as carboxyl groups) would increase the capacitance of the electrode in neutral pHs, through the concentration of charged groups and the equivalent charge-neutralisation of the electrolyte solution.

In order to account for these differences in surface composition, these experiments were repeated in SLB, pH 4.50. The increased concentration of protons in the electrolyte was anticipated to reduce the

differences arising due to the presence of charged groups at the electrode surface. Due to the shift in electrolyte, and corresponding alteration of cyclic-voltammographic traces, a different potential window and point at which dI (+ 0.6 V) was measured. Figure 3.5 shows the trends occurring between amperometrically-calculated C_{DL} and that calculated by dI.

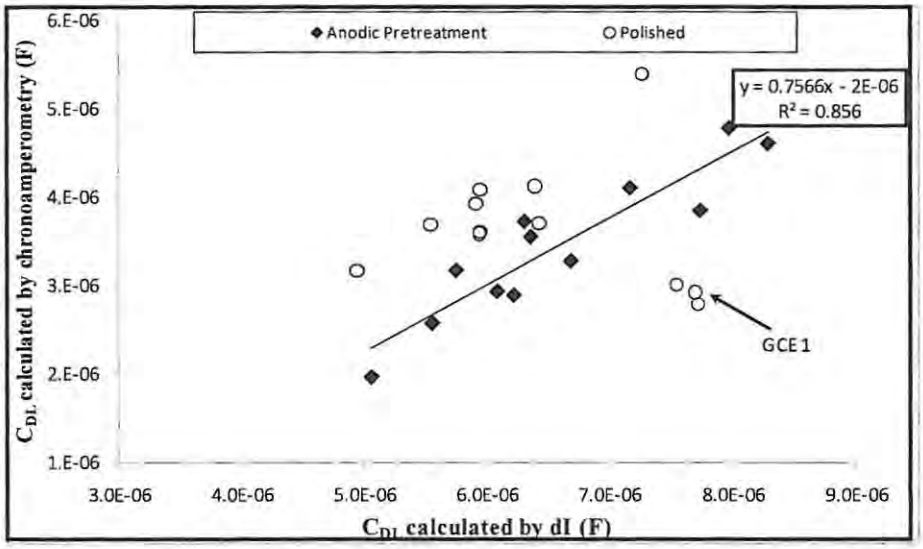

Figure 3.5: Correlations between C_{DL} as calculated by chronoamperomtrically-determined, vs. that calculated by sweep separation current, dI, in SLB buffer, pH 4.50.

Number of observations, n = 12, using 3 separate electrodes.

Electrodes cleaned through polishing (circles) and electrodes cleaned through anodic pretreatment (diamonds) are included

The nature of the electrolyte appears to have a dramatic influence on the current, as determined by amperometric data, while the dI values appear to be less sensitive to electrolyte composition. A much higher degree of linearity is noted when comparing Figures 3.5 (SLB) and Figure 3.4 (KCl). dI values in 0.1 M KCl average 2.14 $\pm$ 0.25 μA, while in SLB, the average dI was calculated to be 2.64 $\pm$ 0.39 μA, an increase of 23%. However, C_{DL} values determined from amperometry ranged from an average of 3.33 μF to 4.69 μF when considering 0.1M KCl or SLB, pH 4.5 as electrolytes. This corresponds to a 41% difference in average C_{DL} values determined amperometrically.

It is also noted that the act of cycling the electrode repeatedly prior to the recording of dI values is itself a cleaning protocol. However, in this instance, as all electrodes were treated identically following the execution of the various cleaning protocols, this should not greatly affect the data retrieved from the studies undergone. As further validation of this assumption, Appendix 2, Section A2.1 and A2.2 contains

the data analysis performed on short-time non-Faradaic chronoamperometry performed on electrodes before and after electrode cycling for both anodically-pretreated electrodes and polished electrodes.

3.5.3: Faradaic responses to selected pretreatment protocols: catechol

The responses of electrodes cleaned by the outlined pretreatment techniques to the oxidation/reduction behaviour of 0.4 mM catechol (in 0.1M KCl) was investigated. Table 3.2 displays a summary of the relevant peak parameters elucidated.

Table 3.2: Examination of electrochemical reversibility exhibited by 0.4 mM catechol using GCEs cleaned via different protocols:

Cleaning procedure	$E_{p,a}$ (V)[1]	$E_{p,c}$ (V)[1]	ΔE (V)	$I_{p,a}$ (A x 10^{-6})	$I_{p,c}$ (A x 10^{-6})	$I_{p,a}/I_{p,c}$
0.1 M KCl						
Paper-cleaned	0.519	0.214	0.305	2.12 ± 0.78	1.63 ± 0.54	0.849
Polished	0.432	0.293	0.139	2.74 ± 1.15	2.52 ± 0.78	0.989
Sonicated (Ethanol)	0.429	0.283	0.144	3.61 ± 0.84	3.30 ± 0.51	0.932
Sonicated (base)	0.444	0.272	0.172	3.13 ± 0.49	3.05 ± 0.28	0.988
Anodic pretreatment	0.331	0.275	0.055	1.66 ± 0.54	3.09 ± 0.69	1.861
0.1 M SLB, pH 4.5						
Anodic pretreatment (SLB, pH 4.5)[2]	0.371	0.313	0.058	8.1 ± 0.91	6.92 ± 0.91	0.853
Polished (SLB, pH 4.5)[2]	0.340	0.274	0.067	4.25 ± 0.91	3.99 ± 0.87	0.935

Number of replicants, n = 6, across 6 different electrodes.

[1] – vs. Ag/AgCl reference electrode. Averaged values are reported ± 15 mV standard deviation from the mean.

[2] – Averaged values reported ± 5 mV standard deviation.

The reversibility of catechol at the electrode is assessed by the difference in the reduction/oxidation of catechol (ΔE of the above table) and the relative differences in the peak currents ($I_{p,c}/I_{p,a}$) (Heineman and Kissinger, 1996).

As can be seen in Table 3.2, the addition of even a modest cleaning stage above that of paper-cleaning greatly improved the ΔE responses of the electrodes. The highest degree of reversibility occurred through the use of anodic pretreatment of the electrode. This alteration in reversibility seems to primarily arise from a modification of the oxidation peak potential ($E_{p,c}$), rather than a difference in that of the cathodic sweep ($E_{p,a}$). Table 3.2 indicates that the cathodic peak potential, after polishing, does not alter greatly with the cleaning procedure undergone after polishing has occurred, while the anodic peak potential is affected to a greater extent.

Studies conducted on glassy carbon electrodes using catechol as a reporter molecule have shown that the extent of pretreatment, as choice of supporting electrolyte (and pH) for anodic pretreatment has a substantial effect on both peak current, and peak potentials for the redox couples of catechol oxidation/reduction (Jürgen and Steckhan, 1992). In general, a decrease in anodic potential and an increase in peak current of phenolic oxidation/reduction electrochemistry (Jürgen and Steckhan,1992), as well as an improvement in peak reproducibility (Engstrom, 1982; Wang and Lin, 1998) is noted with anodic pretreatment of GCEs such as was found with this study using catechol.

The current detected through the different cleaning procedures show a high degree of standard deviation. Current responses could not be related to the dI values extracted from the solutions prior to the addition of catechol when assessed in 0.1 M KCl, as is expected when considering a diffusion-controlled process. This is most likely due to the nature of the electrolyte used and the pH at which the electrochemical reaction proceeds in this instance, rather than an indication of great deviation in the electrode surfaces. As reported in Table 3.2, when the electrolyte was altered to SLB, pH 4.5, the degree of reproducibility, both in current and potential significantly increased, as did the generated current for both polished and anodically pretreated GCEs. From the cleaning procedures investigated, anodic pretreatment produced exhibited both the highest degree of electrochemical reversibility for catechol oxidation/reduction, as well as some of the highest current response (in SLB) combined with a high degree of inter-electrode reproducibility.

3.5.4 Spectroscopic characterisation of laccase activity

Due to the high molar extinction coefficient of their oxidation products, syringaldehydes and 2,2'-Azino-bis(3-ethylbenzothiazoline-6-sulfonic acid) (often abbreviated as ABTS) are the most commonly-reported substrates for determining phenol oxidase (including laccase) activities (e.gs Bourbainnais et al., 1995; d'Acunzo et al., 2002; Jung et al., 2002; Roy and Abraham, 2006; Svobodová et al., 2008). However, catechol was selected as the substrate for spectroscopic assaying of the enzyme activity, in order to provide comparable results between the spectroscopic estimations of laccase activity, and the fabricated biosensor properties determined electrochemically that are reported in this Chapter.

Given the broad substrate range of laccases, it is unsurprising that laccases are reported exhibit rates of oxidation that differ on both the laccase and the substrate under investigation (Jung et al., 2002), and that individual substrate oxidation rates have their own characteristic pH optima (Jung et al., 2002) that themselves differ between laccases. This is discussed in greater detail in Chapter 5 of this Thesis. The activity of the commercially-obtained laccase used in this study was assayed using catechol as a substrate, at pH 4.5 (Sigma-Aldrich, 2010 – See Internet Reference 1.1). The lack of generalisability between substrates is the main reason that the model substrate and pH was maintained as catechol and pH 4.5, respectively, throughout the studies outlined in this Chapter. Modulation of biosensor signal through the exploitation of the phenomenon of preferential substrate-pH intersections for enhancing biosensor response selectivity is discussed in greater detail in the following Chapter (Chapter 5 of this thesis).

Figure 3.6 shows typical spectrophotometric data from the determination of free laccase activity, with catechol as a substrate.

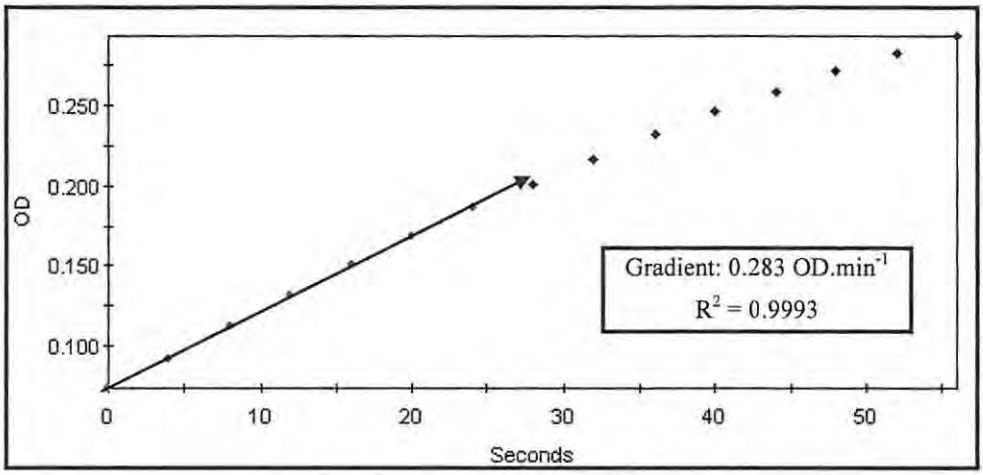

Figure 3.6: Change in spectrophotometric Optical Density units (OD) vs. time for a solution of 0.36 mg.ml^{-1} laccase solution (i.e. from 36.2 mg.ml^{-1} stock solution) during the oxidation of catechol.

Absorbance values are in Optical Density (OD) dimensionless unites. λ_{abs} = 450nm. Linear portion used in activity calculations indicated by arrow. Data is presented 'as-is' from the data-acquisition software used (KCJunior 4.1)

Inset: gradient co-efficient and degree of linearity extracted from data-acquisition software.

As is visible in Figure 3.6, the initial tangential slope of the spectroscopic rate of formation of oxidised catechol (product) was used in the determinations of the velocity of the enzyme-catalysed reaction (Miller and Tanner, 2008).

Initially, laccase activity assays were performed with a high concentration of laccase (20 – 30 mg.ml^{-1}), resulting in very low specific laccase activities as calculated from the spectrophotometric measurement of catechol oxidation. Due to concerns regarding the solubility, and the possibility of irreversible precipitation of laccase following catalysis occurring, this concentration was then adjusted downwards. In an attempt to improve both dispersal and stability of the laccase protein, laccase was additionally solubilised in SLB containing dissolved BSA (final BSA concentration: 10mg.ml^{-1}). Table 3.3 displays the calculated activities from the assays with varying laccase and BSA concentrations. Fresh laccase solution was prepared for each assay outlined in Table 3.3.

Table 3.3: Results of spectroscopic assay of laccase for catechol in SLB buffer, pH 4.5

[Laccase] ($mg.ml^{-1}$)[a]	[BSA] ($mg.ml^{-1}$)[a]	$\Delta A/\Delta t$ ($OD.min^{-1}$)[b]	Activity ($U.ml^{-1} \times 10^{-2}$)	Stock laccase activity ($U.ml^{-1}$)	Specific activity ($U.mg^{-1}$)
36.2	0	0.2963 ± 0.0247	4.02 ± 0.33	13.4 ± 1.1	3.72 ± 0.31
36.2	10	0.2862 ± 0.0089	3.88 ± 0.12	12.9 +0.4	3.60+ 0.11
20	0	0.2880 ± 0.0226	3.91 ± 0.31	13.0 ± 1.0	6.51 ± 0.51
20	10	0.3027 ± 0.0094	4.11 + 0.13	13.7 ± 0.4	6.85 ± 0.21
10	0	0.1985 ± 0.0105	2.69 ± 0.14	9.00 ± 0.5	8.98 ± 0.48
10	10	0.2314 ± 0.0047	3.14 ± 0.07	10.5 ± 0.2	10.5 ± 0.22
5	0	0.1306 ± 0.0173	1.77 ± 0.23	5.91 ± 0.78	11.8 ± 1.6
5	10	0.1101 ± 0.0061	1.49 ± 0.08	4.98 ± 0.28	9.96 ± 0.5
2.0	0	0.0594 ± 0.0041	0.806 ± 0.06	2.69 ± 0.19	13.4 ± 0.9
2.0	10	0.0699 ± 0.0076	0.949 ± 0.05	3.16 ± 0.17	15.8 ± 0.9
1.0	0	0.0358 ± 0.001[c]	0.485 ± 0.01	1.62 ± 0.04	16.2 ± 0.04
1.0	10	0.0379 ± 0.0023	0.515 ± 0.03	1.72 ± 0.11	17.2 ± 0.1

Grey rows indicate assays performed when BSA was added to laccase stocks

[a] – Stock laccase concentration. Concentrations in spectroscopic wells are 100-fold less, as in Table 3.1.

[b] – Number of replicants, n, ≥ 3, uncertainty values represent standard deviation from the mean and are the basis for resultant calculated uncertainties.

[c] – single data point eliminated to decrease standard deviation from the mean – i.e. results are in duplicate

As is readily viewable from Table 3.3, there is a consistently non-linear, albeit positive, trend between enzyme concentration and the resultant enzyme activity determinable from spectroscopic assaying of catechol oxidation rate. The maximal enzyme activity (~13 ± 1 $U.ml^{-1}$) is attained at a stock solution concentration of 20 $mg.ml^{-1}$ and a statistically-insignificant increase occurs thereafter when nearly double the laccase concentration is used (~13.4 ± 1 $U.ml^{-1}$ for 36.2 $mg.ml^{-1}$ stock laccase concentration). Even prior to the plateauing of activity, a significant decrease in specific activity is noted with an increase in the amount of dissolved laccase, both in the presence and absence of BSA. While lower concentrations show a fair agreement with the specific activity provided by the manufacturer (17.19 $U.mg^{-1}$ protein assayed at 1 $mg.ml^{-1}$ stock laccase concentration, compared to the manufacturer's reported 22.1 $U.mg^{-1}$ protein for this batch), the specific activity rapidly decreases upon the use of higher concentrations of laccase, to a specific activity of 3.7 $U.mg^{-1}$ laccase at a concentration of 36.2 $mg.ml^{-1}$ stock laccase)

The addition of BSA to laccase prior to assaying increases the activity of a laccase solution, but not consistently (Table 3.3). However, the addition of BSA did decrease the variability of response between replicants, evident as a decrease in the margin of uncertainty between assays using BSA and laccase and those using only laccase. The enzyme concentration of 36.2 $mg.ml^{-1}$ concentration was included in this study, as it was often used in the fabrication of thick-film sensors reported later in this chapter. Figure 3.7 displays a graphical representation of the information recorded in Table 3.3, comparing the determined laccase stock activity and the specific activity vs. the concentration of dissolved laccase, both in the presence and absence of 10$mg.ml^{-1}$ BSA.

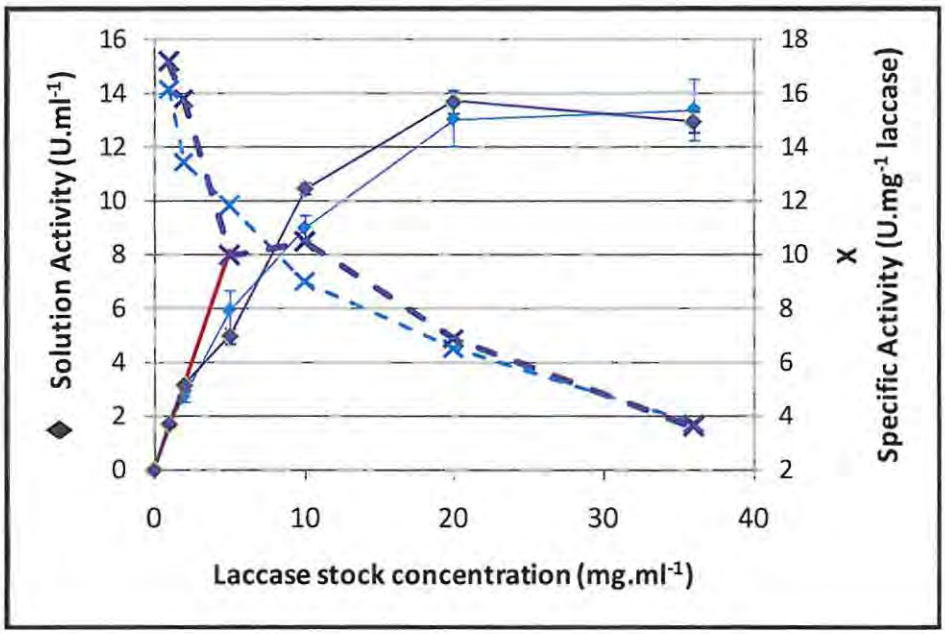

Figure 3.7: Laccase stock activity and specific activity vs. stock concentration of laccase.

Data presented in blue refers to activity calculations of laccase stock solutions in the absence of 10 $mg.ml^{-1}$ BSA solution, while purple depicts activity deduced from laccase stock solutions dissolved in 10 $mg.ml^{-1}$ BSA solution. The red line is a linear equation generated under the assumption that specific activity remains constant between laccase stock concentrations and is merely present to guide the reader.

Substrate depletion was not considered to be the reason behind the non-linear behaviour of the activity vs. enzyme concentration trend observed in Figure 3.7. Since the maximal activity calculated during spectroscopy, that of the 36.2 $mg.ml^{-1}$ laccase stock concentration, in the absence of BSA, averaged only an *in-situ* activity of 4.02 x 10^{-8} mol of catechol oxidised.min^{-1} (4.02 x 10^{-2} U, see Table 3.3) and the total amount of substrate per assay was maintained at 1.5 x 10^{-5} mol (Table 3.3), the initial substrate

concentration was far in excess of the oxidation rate of even the most active laccase concentration used. While constraints in oxygen (co-substrate) availability was also considered to be a possible reason behind this non-linear behaviour, the relative abundance of dissolved oxygen in water at equilibrium at 20 °C (~0.5 to ~0.6 mM, therefore ~$1{,}67 \times 10^{-7}$ mol present) coupled with the assumed stoichiometry of catechol oxidised: oxygen consumed of 4:1 also precludes oxygen depletion. Hence, the reaction was assumed to proceed at maximal velocity throughout the laccase concentration range assayed and that the velocity of reaction as assayed through this method is equivalent to the v_{max} parameter of the Michaelis-Menten enzyme-rate formalism (Eq. 2.3). From this it was inferred that steady-state kinetics were assumed to dominate the reaction at the time-frames that assaying was conducted in (Miller and Tanner, 2008).

The data contained in Table 3.3 and Figure 3.7 contradicts the apparent mathematic formalisms embodied in classical Michaelis-Menton enzyme kinetics (Eq. 2.3). A linear increase in the velocity of the enzyme-catalysed reaction was anticipated with an increase in the concentration of enzyme used in the assay. The non-linearity of expected versus experimental data at higher concentrations is readily observed in Figure 4.5. Two primary mechanisms are thought to be behind this degree of non-linearity and the pronounced decrease in specific activity with increasing laccase concentration. These can be separately classified as the formation of a resting oxidative state of the laccase and the concomitant complexation and aggregation of the laccase (which may, or may not, be dependent on the first mechanism).

There are several other phenomena of soluble enzyme solutions that pertain to concentrated solutions "blue multi-copper" oxidases in general, which include other enzymes such as biluribin oxidase and ascorbate oxidases, and to laccases in particular. These phenomena are not expected to occur in nature, due to the typically low concentration of enzyme (Shleev et al., 2006b). The oxidised/reduced state of the copper ions bound within the active site is critical to the catalytic process (as depicted in Figure 1.4) and the presence of "active" and "resting" states of the enzyme have been postulated (Shleev et al., 2006b). The catalytic function of these proteins is thus strongly influenced by the rate of intraprotein electron transfer from the T1 (oxidative catalyst) to the trinuclear cluster and the co-ordination state of these ions.

Several distinct phases of the enzyme's catalytic state have been postulated, based on kinetic studies (as diagrammatised by Shleev et al., 2006b): ① native intermediate (4 Cu^{2+}, T2/T3 sites co-ordinated with oxygen bridge). Upon oxidation of substrate occurring, with 3 intraprotein electron transfer to T2/T3 sites, this leads to ② fully reduced state (4 Cu^{+}, no co-ordination between T2/T3). Following the reduction of $O_2 \rightarrow H_2O$ the ③ peroxy-intermediate state is reached ($4Cu^{2+}$, T3 sites co-ordinated with T2 sites via epoxy bond), which decays to form the native intermediate state. The alternative development of a 'resting' oxidised state of laccase ④ (4 Cu^{+}, no co-ordination between T2/T3) from the native intermediate state was postulated. In this state, while T1 sites are still oxidised i.e. active, intraprotein electron transfer is very slow, greatly diminishing participation in the catalytic cycle.

In a study conducted by Zopallero et al., 2000, it was found that pH-dependent autoreduction of the T1 site of biluribin oxidase through solvent-protein interactions can take place, decreasing experimentally-determined enzyme activity. Laccases were also implicated to possess a similar phenomenon (Shleev et al., 2006b).

Shleev et al., 2006b, found a complex time-dependance on the activity of stored, solvated highly-pure laccase solutions, which was also influenced by oxygen availability and the source (i.e. structure) of the laccase under investigation. Shleev et al., 2006b, also determined that the generation of laccases in the resting state was also strongly linked with their polymerisation and aggregation, up to and beyond the formation of octameric enzyme complexes. However, due to the reversible nature of this interaction may not be represented in conventional aggregation analyses, such as poly-acrylamide gel electrophoresis (Zopallero et al., 2004).

Overall, the addition of a small amount (10 $mg.ml^{-1}$) of BSA to the stock solution (final concentration in well: 0.01 $mg.ml^{-1}$) was found to slightly improve the activity noted through spectroscopic assaying of catechol oxidation, while decreasing the variability in calculated activity between replicants (Table 3.3). BSA has been used before as a dispersant and stabiliser of enzymes, including laccase. The presence of BSA may cause better dispersion, decreasing the degree of auto-aggregation occurring to the enzyme and retaining the enzyme in a more optimal conformation than occurs in its absence. BSA was included at this stage of research due to the inclusion of it as a co-immobilant in thick-film sensors i.e. as a stabiliser

protein to decrease denaturation undergone by laccase during glutaraldehyde cross-linking (Chapter 4 of this Thesis).

In most biotechnological processes in which high levels of proteins are solubilised (either used as-is or with an anticipated immobilisation application), there is a tacit acceptance of the trade-off between a decrease in the specific activity of a given biocatalyst and the total activity of the resultant solution. Table 3.3 shows that, even though there is a significant decrease in the specific activity between the highest and lowest laccase concentrations assayed (100-fold decrease between 1 and 36.2 $mg.ml^{-2}$ laccase solutions), the overall activity is still much higher (a 9-fold increase between the same). Especially relevant in biomolecular immobilisation is the use of high-activity solutions, which usually entails the preparation of high concentrations of biocatalyst. An increased concentration of proteins means that protein-protein interactions become more important in dictating the final properties of the solution. Protein-protein interactions may improve solubility of other proteins, but may also cause precipitation initiated by aggregation reactions between proteins. Precipitation of the catalyst(s), while important for applications that require soluble forms of enzyme, become less important for applications in which the biomolecule under investigation is immobilised. Rather, it is the conformational changes between the soluble catalyst and the precipitated catalyst that affect the suitability of the biomolecule state during immobilisation strategies.

3.6 Conclusion:

A method of inferring the reproducibility of surface area via the capacitance of a glassy-carbon electrode was investigated and validated for solutions in 0.1M KCl and 0.1M succinic-lactic acid buffer, pH 4.5. The difference between anodic and cathodic sweep currents when the electrode was immersed in an analyte-free electrolyte, dI, was calculated, and the effect of cleaning procedures on the measured dI assessed. Anodic pretreatment in 0.1M NaOH was found to provide a consistent surface with dI higher than those cleaned via polishing and more consistent than surfaces polished, then cleaned via ultrasonication in both organic and alkaline solutions, as well as a flatter baseline. Electrode cleanliness

was related to catechol oxidation/reduction and found to greatly influence the oxidation potential, and to influence the reduction potential to a much lesser degree. The highest degrees of electrochemical reversibility of catechol was found to be present when using electrodes cleaned via anodic pretreatment, both in 0.1M KCl and in SLB.

The use of dI as a measurement procedure was found to be less sensitive to alterations of the electrolyte composition than the validative techniques of determining C_{DL} from chronoamperometric measurements and, therefore, less dependent on the density or presence of charged groups on the electrode surface. Modelling of the charging current showed good agreement with previously-published electrolyte resistivity values of the initial electrolyte, 0.1M KCl, indicating an accurate comparison is achieved between the modelled values to the charging phenomenon occurring at the electrode. A greater degree of linearity and a greater degree of unity with expected results was achieved when using SLB as the electrolyte, as opposed to the ionic solution of 0.1M KCl, indicating that charge-counterbalancing with protons provides a higher degree of unity between C_{DL} values calculated by dI and those calculated through modelling of the short-time charging current. The selection of cleaning protocol substantially affected these results – both in terms of linearity and when considering the unity of results when comparing C_{DL} calculated by dI and that calculated through double-step chronoamperometry.

Assaying of dissolved laccase via monitoring of catechol oxidation spectrophotometrically was found to have a non-linear dependence on the concentration of laccase that couldn't easily be linked to the experimental conditions (namely the concentration of substrate or co-substrate) used during assaying. This non-linear dependence was considered to be due to a combination of aggregation and auto-reduction processes cited in literature to occur at high concentrations of dissolved laccases and other oxidoreductases. On the basis of the findings of this research, laccase activity assays between batches of sourced assays and during storage of laccase were performed using a 1 $mg.ml^{-1}$ concentration of dissolved laccase and activity calculations henceforth performed by extrapolating the concentration of dissolved laccase used with the specific activity calculated for catechol at pH 4.5 at 1 $mg.ml^{-1}$ concentrations. Laccase activities reported in future Chapters are calculated by this method.

Chapter 4: Fabrication and optimisation of laccase biosensors

4.1 Abstract

Fundamental to the fabrication of a biosensor is the selection of an immobilisation strategy in order to concentrate the biorecognition element constituents near the signal transducer. The selection of an immobilisation strategy not only dictates the conformation (and hence, function) of the biorecognition element, but also influences other key aspects of the biosensor's function, such as tolerance to adverse analysis conditions (e.g. pH) and retention of activity during storage. In the research reported on in this Chapter, three separate immobilisation methods: physical adsorption, covalent attachment and cross-linking of the laccase molecules were performed on the surface of glassy carbon electrodes and the resultant biosensors assessed for further development through the detection of catechol. Of the three selected strategies, cross-linking of laccase proteins using glutaraldehyde produced biosensors with the best operational parameters and was selected for further optimisation.

Optimisation of the cross-linking process was performed through the co-immobilisation of bovine serum albumin (BSA) during laccase cross-linking. Parallel to optimisation, biosensors were assessed for their re-usability, an important consideration for the applicability of biosensors. BSA is a common reagent during cross-linking, serving to better retain enzyme function during the denaturative immobilisation process. In this instance, the inclusion of BSA produced biosensors with sigmoidal current responses. Re-use of biosensors resulted in sensors with improved biosensor operational parameters, relative to their pristine (i.e. unused) counterparts. The degree of improvement in these parameters was found to be related to the amount of BSA immobilised in conjunction with the laccase.

In an effort to investigate the reasons behind this behaviour, both the BSA content and the BSA-laccase proportions were varied and the resultant biosensor responses assessed. Sigmoidality was found to increase both with the amount of BSA co-immobilised with laccase and with the proportion of laccase co-immobilised at higher BSA biosensor loadings. Electrochemical studies conducted on cross-linked BSA films indicate that the reason behind this behaviour is due to the binding of catechol oxidation

products by BSA, which gives rise to the apparent sigmoidal current response. Upon exposure to catechol oxidation products, further interaction between BSA and the oxidation products is limited, allowing enhanced mass transport through the film and improving the sensor function upon re-use. In conjunction with this, the attachment of oxidation products to the electrode surface further improve sensor function, although in this study, this is restricted to GCE surfaces.

4.2 Introduction:

4.2.1 Enzyme immobilisation:

As stated in Chapter 1 (Section 1.2.4.3), immobilisation is typically performed in order to concentrate signal-generating biomolecules near, or within, the signal transducer.

The act of immobilisation yields several properties beneficial to the fabrication of biosensors, the most apparent of which is the localised concentration of the signalling biomolecules to generate a detectable signal. Through localisation, it decreases the amount of catalyst required to produce the signal in question, decreasing process costs; it improves the re-usability of the biomolecules in question (Salis et al., 2009); furthermore, by controlling the architecture of immobilisation it allows for heterogenous biomolecules to be co-immobilised, either in discrete areas (as required) or in a mixed fashion. Most importantly to the purposes of biosensor technology, it alters the conformational parameters of the biomolecules, relative to the soluble form of the biomolecule. The latter property is vital to the development of biosensor technologies: since the conformation dictates the functioning of the molecules under investigation.

1. Protein immobilization methods - overview

When immobilising protein molecules, two things are desired: a localisation of functional proteins at a given locus, and a higher degree of stability, relative to the non-immobilised, soluble, 'free' protein. The extent of denaturation undergone by proteins is influenced by both the immobilisation strategy used and the nature of the support onto which protein immobilisation occurs (Freire et al., 2001; Durán et al., 2002; Mateo et al., 2007). Due to the great diversity of proteins' physical and chemical properties coupled with the breadth of application envisaged for the immobilized proteins, there is no generic, or universal, method of immobilization that can be reliably applied to even a small range of different proteins (Freire et al., 2001; Cao, 2005; Mateo et al., 2007) with consistent immobilized properties.

Four broad categories of protein immobilisation may be drawn. These are: physical adsorption of the protein to the solid support, cross-linking (either protein-protein, protein-support, or a mixture of the two), entrapment/encapsulation of the biomolecule and covalent attachment of the biomolecule to the support (Sadeghi et al., 2002). Figure 4.1 depicts the various states and visually summarises the differences occurring between the different immobilisation categories.

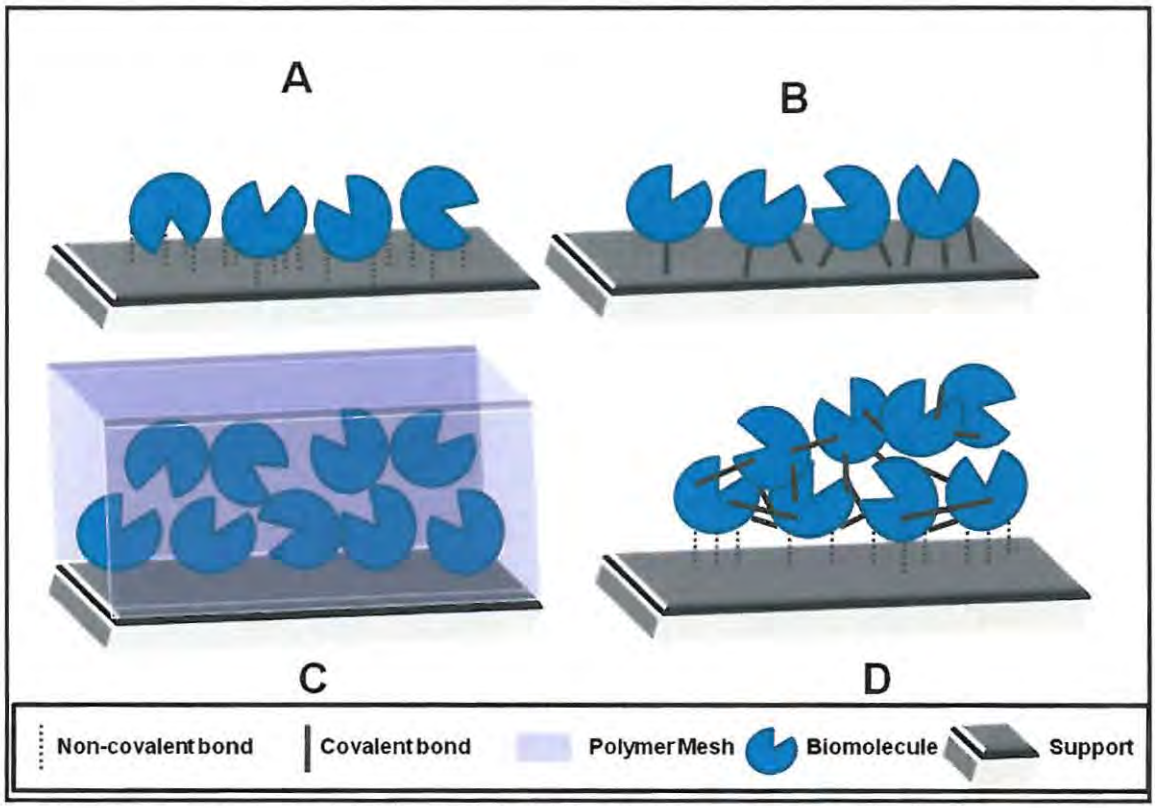

Figure 4.1: Schematic depiction of the major forces involved in immobilization of proteins onto solid supports for different immobilization strategies.

Legend: A - Physical immobilization, B - Covalent immobilization, C - Entrapment/Encapsulation, D - Cross-linking.

Physical adsorption (Figure 4.1**A**) relies on the attachment, and retention, of the protein to the support by means of non-covalent forces (Durán et al., 2002). These forces include: hydrogen bonds (both occurring from the protein backbone and amino acid residues), hydrophobic bonds (hydrophic amino acid residues), ionic bonds (ioniseable amino acid residues) and other van Der Waal forces (Scouten et al., 1995). While these forces are weak, possessing less than 5% of the attractive strength of covalent bonds (Alberts et al., 2002), they occur naturally and in profusion when proteins contact solid surfaces. Due to the weakness of the bonds, attachment via this method does not greatly disrupt the secondary, tertiary, or quarternary structure of the protein in question, minimizing the degree of denaturation undergone by biomolecules during the attachment process (Scouten et al., 1995) and allowing a great degree of activity to be retained, in the case of enzymes.

A natural extension of the principles behind physical adsorption attachment is the entrapment and encapsulation of the protein, behind a semi-permeable membrane for the former and within a semi-permeable polymeric gel for the latter (Figure 4.1**B**). The physical barrier imposed by these structures is the attachment force for this immobilization category (Scouten et al., 1995; Durán et al., 2002). Like physical adsorption, the method generally occurs under mild conditions and the enzyme's structure is not greatly perturbed during immobilisation.

The covalent attachment between the protein and the support (Figure 4.1**C**) produces a very stable protein-support complex, due to the strength of covalent bonds. (Scouten at al., 1995; Durán et al., 2002). In most instances, the major limiting factor in this method of attachment is the nature and chemistry of the support under investigation. A wide variety of moieties naturally occuring on proteins are readily utilizable for the formation of support-protein covalent bonds: carboxyl groups (side-chains of aspartic and glutamic acid residues), amine groups (lysine, histidine, arginine residues), thiol groups (cysteine residues) and some non-protein groups on heteroproteins e.g. carbohydrate moieties. The selection of specific protein groups for attachment has certain drawbacks, such as the loss of activity upon immobilization of areas of the protein strongly influencing the conformation/catalytic activity of a given enzyme. The formation of covalent bonds itself has a denaturing effect on the enzyme, as both the covalent bond and the close proximity of the enzyme to the support constrains the available conformations that can be adopted, decreasing the apparent sensitivity and the protein-substrate/antigen complexes' binding affinities. In addition, the orientation of the biomolecule at the support surface may be of great importance when considering the diffusion of larger analyte molecules, such as other macromolecules, to the active/binding site of the biorecognition layer.

The final category, cross-linking (Figure 4.1**D**), is an extension of covalent modification techniques. Rather than rely on the covalent attachment occurring between enzyme and support, this technique primarily relies on the formation of covalent inter-protein bonds forming a cross-linked network of protein molecules at the surface of the transducer, with the formation of support-protein bonds as a secondary reaction (Durán et al., 2002). A combination of non-covalent support-protein forces and the insolubility of the cross-linked protein complex (Roessl et al., 2010) helps retain the immobilized

molecules at the support surface. Glutaraldehyde is a common homobifunctional cross-linking agent (Roessl et al., 2010)

The suitability of applying a particular immobilization strategy to a given protein is dictated by several factors. Notably: the support in mind, the presence and density of specific groups amenable to a given strategy, their location on the protein of interest and the desired function of the immobilized surface are key factors in the selection of a given category, or specific immobilization strategy, for a specific protein. The following section outlines the broad advantages and disadvantages of the application of strategies that have been outlined above.

4.2.2. Effects, advantages and disadvantages of protein immobilisation techniques

The method used to achieve protein immobilisation has a great impact on the conformation and the conformational mobility of the immobilized protein. Due to the correlation existing between the conformation of an enzyme and its catalytic function, immobilization affects the kinetic operation of the enzyme, relative to the soluble, 'free', enzyme (Royer, 1982; Mateo et al., 2007). Due to the aforementioned link between the tertiary/quarternary structure of an enzyme and its kinetic parameters (Byfield and Abuknesha, 1994) it is of critical importance to minimize perturbation of protein conformation from the optimal structure when immobilizing enzymes.

Due to the aforementioned changes adopted in protein conformation during immobilization, alterations in the enzyme kinetics, reported as changes in both activity and Michaelis-Menten constant (when compared to free enzyme), are frequently exhibited upon following immobilisation of the enzyme to the solid support. In addition, other operational parameters, such as pH optima or substrate specificity, are also affected by immobilisation (Durán et al., 2002). The extent of change reported is uniquely dependent on the selection of support (Durán et al., 2002; Klis et al., 2007b; Kim et al., 2007; Forde et al., 2010), the enzyme in question (Durán et al., 2002; Forde et al., 2010) and method of immobilization

used (Royer, 1982; Freire et al., 2001; Durán et al., 2002; Bayramoğlu et al., 2003; Klis et al., 2007b; Bayramoğlu and Arica, 2008; Forde et al., 2010) to conjoin the protein to the support.

In general, immobilisation has been both cited and demonstrated to improve the stability of enzyme activities, relative to the solubilised (i.e. 'free') enzyme (Cao, 2005). Protein thermostability; (Durán et al., 2002; Roy and Abraham, 2006; Wang et al., 1997; Qiu et al., 2008; Forde et al., 2010), pH-stability (Durán et al., 2002; Forde et al., 2010), resistance to denaturation via exposure to organic solvents (Durán et al., 2002; Roy and Abraham, 2006) and storage lifetimes (Wang et al., 1997; Durán et al., 2002; Quan et al., 2004) are enhanced through the immobilisation of biomolecules, relative to the free enzyme. In addition, inter-substrate selectivity and modulation of protein sites associated with the binding of enzyme inhibitors/effectors are also altered during immobilisation (Mateo et al., 2007), allowing for tuning of the enzyme's functional parameters to be undertaken to produce an immobilised protein with the desired properties for the application under development.

Considerable research has been expended into the minimization of deleterious properties while enhancing those properties deemed desirable during immobilisation (Lowe, 1977; Bayramoğlu G. et al., 2003; Forde et al., 2010). This is often achieved by modulating certain aspects of selected immobilisation procedures (Bayramoğlu et al., 2003; Forde et al., 2010). In principle, the alterations in protein conformation between the immobilized and free enzyme influences the alterations in enzyme kinetics, while the enhancement of stability is due to the constraints imposed in enzyme conformation by the immobilization process.

The formation of covalent bonds, either between proteins (i.e. cross-linking) or between proteins and the support (i.e. covalent attachment), is generally acknowledged to produce a more stable immobilised protein than physical adsorption (Scouten et al., 1995; Durán et al., 2002; Salis et al., 2009). This is due to the strength of covalent bonds, and is generally accompanied by a decrease in the activity of the enzyme, due to the strong alteration of the conformation of the protein caused by bond formation (Durán et al., 2002). For the aforementioned reason, enzyme specificities may also be altered through the use of this technique, sometimes usefully (Durán et al., 2002). Proteins immobilised through cross-linking

possess the same advantages/disadvantages, due to the similarity in the principle governing immobilisation (Scouten et al., 1995; Durán et al., 2002). A drawback to the ease-of-use of employing cross-linking is the difficulty experienced in fine control of the immobilisation process (Scouten et al., 1995).

4.2.3. Select examples of protein immobilisation strategies applied to laccase for electrochemical biosensor construction

Laccase has been immobilised through the use of all the aforementioned immobilisation techniques. The adsorption of laccase has been studied for the purposes of facilitating direct electron transfer between protein and transducer (Qiu et al., 2008) and for biosensing purposes (Jarosz-Wilkołazka et al., 2004). Covalent immobilisation has been studied, both for the purposes of producing monolayer (Vianello et al., 2004) and multilayers of immobilised laccase as well as membrane entrapment and physical adsorption.

Table 4.1 displays select references showing some biosensor parameters reported for fabricated biosensors. These biosensors differ in both quantity, laccase origin (i.e. structure), detection matrix and immobilisation method used, and are reported herein for the purposes of displaying the large disparities between sensitivities within the same class of immobilisation strategy and also as a rough guide to the anticipated "good" and "poor" biosensor kinetics of the biosensors reported on in this Chapter. This list is by no means either definitive or exhaustive, and numerous other operational factors that do affect biosensor parameters have been excluded from the table in the interests of brevity, hence this is to be considered as a very brief overview only.

Table 4.1: Biosensor fabrication techniques and salient parameters found in selected literature examples:

Laccase source	Immobilisation (transducer)	Analyte [a] (matrix)	Sensitivity ($nA.\mu M.cm^{-2}$)[b]	Linear range (μM)[a]	Reference
		Adsorption			
Cerrena unicolor	Adsorption (graphite)	Plant flavinoids	58	1-10	Jarosz-Wilkołazka et al., 2004
Trametes versicolor	Adsorption (carbon fibres)	Catechol	76.4	-	Freire et al., 2001
T. versicolor	(MWCNT-Chit)[1]	catechol	~1400	0 – 30	Liu et al., 2006
T. versicolor	Graphite rods	catechol	77.2	0 – 2000	Portaccio et al., 2006
T. versicolor	Graphite rods	catechol	1321	1 – 10	Haghighi et al., 2003
		Entrapment			
Coriolus versicolor	Membrane entrapment	Catechin (red wine)	0.432	2 – 14	Gomes et al., 2004
T. hirsute	Nafion entrapment (GCE)	hydroquinone	2546	0.1 – 3	Yaropolov et al., 2005
T. versicolor	Polyaniline entrapment (platinum)	catechol	0.022	0.2 – 1	Timur et al., 2004
T. versicolor	Sol-gel entrapment	caffeic acid (wine)	96.92	< 6	Montereali et al., 2009
T. versicolor	(MWCNT-Chit)	caffeic acid	650	0.7 - 10.5	Diaconu et al., 2010
		Covalent attachment			
Denilite ®	Covalent immobilisation (platinum)	*p*-phenylenediamine	2062	0 - 29	Quan et al., 2004
T. versicolor	(MWCNT-Chit)	catechol	3.22	1 – 190	Tan et al., 2009
T. versicolor	Carbon fibre	catechol	469.8	-	Freire et al., 2001
Rigidoporus lignosus	ECH-Sepharose®*	catechol hydroquinone	1287 1471	0 – 500 0 – 500	Vianello at al., 2006
		Cross-linking			
Trametes hirsuta	Glutaraldehyde cross-linking (glass)	lignin	Not reported	10 – 500 $\mu g.ml^{-1}$	Shleev et al., 2006c
Recombinant	Glutaraldehyde (graphite-BSA)	catechol	21.58	0 – 13	Kulys and Vidziunaite, 2003
T. versicolor	Magnetic nanoparticles	hydroquinone	1076.7	0.015 - 1	Zhang et al., 2006
T. versicolor	CLEAs	catechol	489	0 – 100	Portaccio et al., 2006
T. versicolor	Glutaraldehyde	caffeic acid	7.07	0.5 – 83	Gamella et al., 2006

[a] – In cases where multiple analytes were reported on, the substrate detected with the highest sensitivity was selected for these categories. In cases where linear range is not explicitly reported, the LOD is recorded.

[b] – calculated relative to electrode surface area of the transducer employed where not explicitly reported in-text.

[1] – Multi-Walled Carbon Nanotubes, dispersed in Chitosan

* – substrates pre-oxidised in a reactor containing immobilised laccase prior to analysis

Table 4.1 highlights the extreme variability in reported biosensor parameters using different immobilisation techniques. Given a lack of consensus regarding the optimal source/structure of laccase for biomolecular immobilisation, a variety of different sources of laccases have been investigated. However, even considering the same producing organism and similar immobilisation techniques, there is still a large breadth in the reported sensitivity and linear range of biosensors fabricated using laccase as the biorecognition element.

Despite the high level of denaturation reported through its use, the advantages conferred through cross-linking ensure that it remains a valid current method of protein immobilisation. Roy and Abraham (2006) reported a method of producing cross-linking laccase monomers in such a manner that greatly improved the thermostability, with a concomitant decrease in the activity (approximately 78% activity loss). Cross-linked laccase films were investigated as a biorecognition immobilisation technique using glutaraldehyde. Both physical adsorption and covalent immobilisations were selected as alternative immobilisation strategies for this stage of research. Biomolecule immobilisation techniques were selected for their enhanced robustness over the signal-decreasing effects of denaturation, due to the fact that the envisaged end-user application needs will favour stability over sensitivity, and that thick-film sensors (as outlined below) may help to address the need for sensitivity without affecting the stability of the fabricated biosensor overmuch.

4.2.2. Bovine serum albumin – application to laccase biosensors

Bovine Serum Albumin (BSA) is a transport protein extracted from the serum fraction of blood. Serum albumins are principally involved in the maintenance of pH in the blood fraction and are present as the most abundant serum proteins (Huang and Kim, 2004). Serum albumins also function as carrier proteins, being the principal method of distribution and delivery of fatty acids and lipid-associated compounds e.g. steroids, drugs (Demant, 1996; Huang and Kim, 2004; Tian et al., 2005), as well as other proteins, metal ions, co-factors and metabolites present in the bloodstream (Huang and Kim, 2004; Tian et al., 2005; Kun et al., 2010).

Bovine serum albumin (BSA) has been extensively studied and remains a co-reagent in many biochemical studies, due to the breadth of extant knowledge of the protein and its wide commercial availability of this protein in a purified form from a historical perspective (Anderegg, 1955). BSA has been extensively applied in the immobilisation of biomolecules, from blocking of active sites on immobilisation substrates to preclude non-specific binding (Bollag et al., 1996c; Suzuki et al., 1997) to protecting the biomolecule of interest from surface-based denaturation.

When added in high concentrations to dilute i.e. 'free' enzyme solutions, BSA has a stabilising effect on conformational denaturation of the biomolecule of interest (Chang and Mahoney, 1995), preventing loss of activity of the enzyme (Bollag et al., 1996a) with relative protein-protein inertness (RCSB, 2010). BSA, in particular, is cited as a common additive for protein stabilisation for these purposes (Bollag et al., 1996a), due to the high degree of aqueous solubility possessed (Kun et al., 2010). For this application, it is used to prevent both solvent-denaturation and denaturation caused by interfacial interactions (e.g. adsorption onto solid surfaces contacting the solution). BSA is often used as a standard component in protein-content assays (Bollag et al., 1996b) and as a model protein for several research applications and techniques (e.g. Delgado et al., 2002).

Due to its stabilising properties, BSA is frequently applied as an 'inert' protein in the preparation of cross-linked films and particles comprising enzymes (Dong et al., 2010). Within the context of laccase immobilisation, BSA is commonly co-immobilised with laccase during glutaraldehyde cross-linking immobilisations (Freire et al., 2002; Freire et al., 2003; Kulys and Vidziunaite, 2003; Solńa et al., 2005; Cabana et al., 2007; Cabana et al., 2009; Roessl et al., 2010), often added at very high relative concentrations, forming an "inert" backbone to which the laccase proteins are covalently attached and adding a degree of protection from the denaturative effects of glutaraldehyde. The inclusion of BSA as a co-immobilant has been shown to not only improve the retention of activity following immobilisation (Cabana et al., 2009; Roessl et al., 2010), but also to improve the stability of laccase once immobilised (Cabana et al., 2007; Cabana et al., 2009; Roessl et al., 2010), to both solvent-based and thermal denaturations. The use of BSA as a stabiliser is also applied to other enzymes for biosensor fabrication

purposes (Lei and Deng, 1996; Dzyadevich et al., 1998; Yang et al., 1998; Solńa et al., 2005; Aytar and Bakir, 2008; Roessl et al., 2010).

The claim of inertness with regard to the research presented in this Thesis must be investigated i.e. with regard to phenolic compounds and their oxidation products. Given the wide range of substrates BSA binds to in its role as transport protein, it is unsurprising to note that BSA has been found to associate with and to bind phenolic compounds. Albumins have been implicated in the binding of many phenolic compounds. Ellagic acid has been found to associate with albumins (Léger et al., 2009), as have flavinoid compounds (Tian et al., 2005). Other polyphenols found to bind to BSA include: curcumin and resveratrol (Bourassa et al., 2010). This binding is thought to be due to hydrophobic interactions occurring between the polyphenols and hydrophobic amino acid residues of BSA (McManus et al., 1985; Bourassa et al., 2010), specifically, tryptophan residues (Bourassa et al., 2010; Sahoo et al., 2008) within at least one of 2 hydrophobic pockets present on the protein that are associated with lipid binding reactions (Tian et al., 2005; Sahoo et al., 2008; Zhang et al., 2009). Calculated binding affinities between phenolics and BSA range between $10^4 M^{-1}$ (Bourassa et al., 2010) and $10^5 M^{-1}$ (Tian et al., 2005; Sahoo et al., 2008). These are relatively low binding affinities – for comparative purposes, antibody-antigen interactions are typically $10^6 M^{-1}$ and for avidin-biotin binding (one of the strongest known non-covalent biochemical interactions) are typically $10^{15} M^{-1}$, but the affinities suffice to show that binding appears to be via specific and not non-specific methods.

Alterations to the conformation of BSA are noted with high concentrations (~0.5mM in ~μM concentrations of BSA, or stoichiometries exceeding 5 : 1 phenolics : BSA) of polyphenols, consistent with unfolding of the proteins' secondary structure (Tian et al., 2005; Bourassa et al., 2010). These alterations also occur in the presence of other aromatic compounds (Zhang et al., 2009), and some uncertainty exists as to whether they are caused by the adoption of specific ligand-binding conformations or due to microenvironmental changes in the areas surrounding protein molecules caused by the addition of the aromatic compounds.

During the *in-vitro* peroxidase-catalysed oxidation of phenolics in the presence of albumins (Bratkovskaja et al., 2004), it was found that, in high ratios of BSA: peroxidase increased the overall efficiency of conversion, while not affecting the initial velocity of reaction. It was postulated that albumins react with the products of phenolic oxidation, through hydrophobic bonding, forming BSA-phenolic polymer complexes, acting as a trap for the products of oxidation, which typically cause fouling. The presence of BSA has the effect of minimising the inactivation of the enzyme that would otherwise occur through the formation of peroxidase-phenolic polymer complexes (Bratkovskaja et al., 2004).

Given the commonality of the use of BSA in laccase biosensor, it was of analytical interest to investigate the extent and manner with which the inclusion of BSA in biosensor fabrication alters the properties of the biosensor by assessing the effect that varied concentrations of BSA possesses as a co-immobilant in glutaraldehyde-cross-linked sensors.

4.3 Aims and Objectives

Given the amount and varied effects that the selection of an immobilisation strategy possesses on the resultant biosensor, it is imperative to select, and further optimise, an immobilisation strategy that will produce a biosensor of sufficient detection sensitivity to warrant further studies, such as those reported on in Chapters 5 and 6 of this Thesis. The utility of biosensors developed during this phase of research were tested against a single model phenolic substrate, catechol, in order to generate current-concentration functions that provide comparisons between the different biosensor configurations reported on in this Chapter. In addition to assessing biosensor functionality on the basis of graphical analyses of current-concentration curves (e.g. measuring relative detection sensitivities between configurations), this was also an opportunity to test the sigmoidal model described in Chapter 2, in order to assess its modelling robustness and its facility to distinguish between the gradations existing between highly-sigmoidal and non-sigmoidal current-concentration functions. From a fundamental aspect of this research, the potential

reasons behind sigmoidal current-concentration biosensor response should also be examined, in order to provide adequate explanation for this previously-unreported behaviour in laccase-based biosensors.

From the above aims, the following objectives for the research reported on in this Chapter were set:

(1) To assess which of the selected immobilisation procedures selected (physically-adsorbed, covalent attachment and cross-linking) produced a biosensor of sufficient phenolic-detection sensitivity to provide comparable results to those already present in literature regarding this subject. The selected immobilisation procedure would then be subjected to optimisation studies in order to enhance the sensitivity of detection.

(2) Model assessment.

(3) Investigate the effects that the inclusion of BSA as a co-immobilant produces on cross-linked laccase films used as biorecognition elements for a phenolic-monitoring biosensor. While a common co-reagent in laccase immobilisation, to date, no known research has assessed the effects that varying BSA concentration has on biosensors, with most reports regarding this having between 1-2 optimisation stages. This aim also includes the optimisation of the amount of BSA to be co-immobilised in biosensors fabricated for research in later Chapters (Chapters 5 and 6 of this Thesis), as well as assessing the relative alterations to biosensor response with altering relative laccase-BSA proportions.

(4) Examine the mechanism that BSA co-immobilisation has in producing sensors with sigmoidal current-concentration functions.

4.4. Methodology:

4.4.1 Apparatus:

Electroanalytical equipment was used as outlined in Chapter 2, as was the spectrophotometric apparatus. Both electroanalysis and spectrophotometry took place at 21 °C and all reagents were warmed to this temperature prior to the onset of analysis.

4.4.2 Reagents:

Unless otherwise stated, all reagents were of analytical grade, or higher, and sourced from Sigma-Aldrich.

Lyophilised powder containing > 20 $U.mg^{-1}$ laccase, purified from *Trametes versicolor* culture was sourced from the supplier (Sigma-Aldrich), as was crystalline Bovine Serum Albumin. Crystalline bovine serum albumin was stored at 4 °C and laccases were stored dry as stocks at -20°C until solubilised.

Glutaraldehyde solution (15% $^{v}/_{v}$) was diluted from stock solutions (25% $^{v}/_{v}$ concentration, Grade 1 purity, Sigma-Aldrich) using milliQ water.

Protein solutions were dissolved in SLB, pH 4.5. The formulation of SLB took place as described in Chapter 2. BSA stock solution (100 $mg.ml^{-1}$) was stored at 4 °C for up to a week before being discarded.

Solutions of laccase were formulated fresh for each triplicate modification on each lot received from the suppliers. Owing to concerns of solvated protein instability, the exact specific activity of each batch received was assessed spectrophotometrically, as the activity of a 1 $mg.ml^{-1}$ solution of laccase. For the rationale behind this, see Sections 3.5.4 and 3.6 of the preceding Chapter. In order to maintain a constant laccase activity between different batches, laccase solutions were formulated on the basis of their respective activities towards catechol oxidation at pH 4.5, not on the dissolved mass.

Catechol (99+ % pure) was used as the main laccase substrate used in optimisation studies reported in this Chapter. Stock solutions, ranging from 0.08 - 0.1 M were prepared fresh in water just prior to triplicant investigation of modified biosensors. For spectroscopic studies, a 0.5 M stock was prepared prior to activity assaying of the laccase.

UV/VIS spectroscopy was performed using a UV-transmissible 96 well ELISA Microplate, sourced from Greiner Bio-One.

4.4.3 Methodologies:

4.4.3.1. Pre-modification treatment of electrodes

Glassy Carbon Electrodes (GCEs) were cleaned via anodic pretreatment and subsequent ultrasonication, perfomed as outlined in Chapter 3, Section 3.4.2.1.5.

4.4.3.2. Biosensor fabrication:

a) Physical adsorption:

To the surface of cleaned electrodes was added 10 µl of a solution corresponding to a 800 $U.ml^{-1}$ solution of laccase. Adsorption of protein to the electrode surface was allowed to occur for an hour at RT. Following the adsorption stage, electrodes were rinsed with water and equilibrated in 5 ml of SLB for 15 minutes prior to use.

b) Covalent immobilisation:

For activation of carboxyl groups on electrodes for thin-film protein immobilisation, 0.1 M 2-[N-Morpholino]ethanesulfonic acid (MES) buffer, adjusted to a pH of 4.5, was used as the buffer for carboxyl activation. MES (>99.5% pure, catalogue number: M-8250) was sourced from Sigma-Aldrich and titrated with 0.2 M NaOH to pH 4.5 for use in EDC/NHS activation of the glassy carbon surface (Nam et al., 2007).

Activation of the carboxyl groups was performed in a similar manner as has been previously described (Klis et al., 2007b). Into MES buffer was dissolved 15 mM of EDC and 15 mM NHS to form the carboxyl activation solution. EDC/NHS solutions were prepared freshly for each electrode activation in 1ml aliquots and immediately used after dissolution. 20 µls of EDC/NHS solution was added onto the surface of cleaned electrodes and the activation reaction was allowed to proceed for 2 hours at RT, in the dark. Following activation, the electrodes were briefly rinsed with water, before being subsequently modified with laccase, as has been described for physically-adsorbed laccase electrodes, 4.4.3.2(a).

c) Glutaraldehyde cross-linking:

Cleaned, air-dried GCE surfaces were modified through the addition of successive aliquots of 1 µl of the following solutions: 800 $U.ml^{-1}$ laccase solution and 15 % $^{v}/_{v}$ glutaraldehyde. These were briefly mixed and evenly spread over the surface of the electrode. Cross-linking was allowed to run to completion (~30 minutes) at room temperature. Electrodes modified in this manner were rinsed with water and stored in 5 ml SLB prior to analysis (approx. 30 minutes to an hour).

4.4.3.3 Optimisation of glutaraldehyde cross-linking:

Following selection of cross-linking as the superior immobilisation method from those initially selected, based on criterion established in Section 4.4.3.6 and discussed in Section 4.5.1 below, optimisation of the production of laccase-containing cross-linked films was performed in the following method. While the procedure for electrode modification is the same as outlined in 4.4.3.2(c), a further protein co-immobilant (BSA) is included prior to the addition of glutaraldehyde. Concentrations of BSA and laccase were varied (as in Table 4.3, below), the aliquots for all three solutions was maintained at 1 µl volume.

Table 4.2: Varying concentrations of BSA and laccase used in optimising sensor performance in thick-film sensors

Stock solutions		Mass or Activity at electrode	
[BSA] ($mg.ml^{-1}$)	[laccase] ($U.ml^{-1}$)[a]	[BSA] (µg)	[laccase] (U)[b]
0	40	0	0.04
5	80	5	0.08
10	100	10	0.1
20	200	20	0.2
50	400	50	0.4
100	800	100	0.8

[a] – determined through spectroscopic assaying of catechol oxidation using a 1 $mg.ml^{-1}$ concentration of laccase, as described in Chapter 3.

[b] – assuming no denaturation of laccase during immobilisation occurs i.e. that activity remains comparable before and after immobilisation

4.4.3.3. Electrode 're-use'

Following modification and analysis of the biosensor, certain configurations of biosensor were then re-used, rather than cleaned and re-modified for other experiments. These electrodes were stored in 200 μM solutions of catechol (dissolved in SLB, pH 4.5) and either used within an hour when stored at room temperature, or stored overnight at 4 °C before being re-assessed as outlined below (Section 4.4.3.4).

During the optimisation of glutaraldehyde cross-linked laccase films, alterations to biosensor operational parameters upon re-use are presented and discussed in parallel with parameters reported for the pristine (i.e. previously unused) biosensors, before the effects of sensor re-use are discussed in general (Section 4.5.3.2).

4.4.3.4 Electroanalytical determination of biosensor kinetics

For the electroanalytical determinations of biosensor kinetics, SLB pH 4.5 was the sole electrolyte used at this juncture. The following sections describe the electroanalytical methodologies and data treatments used for the determinations of biosensor kinetics.

a) Buffer cycling:

Electroanalysis of the fabricated biosensors took place within 5 ml of SLB, warmed to room temperature. Cyclic voltammograms were executed before and after chronoamperometry. Prior to chronoamperometric estimation of biosensor parameters, electrodes were cycled between -0.3 V and + 0.8 V for 10 cycles before chronoamperometry, in order to determine dI and to ensure the cleanliness of the solution and electrode prior to chronoamperometry.

b) Chronoamperometry:

Chronoamperometry was performed by poising the working electrode at -0.17 V (vs. Ag/AgCl). Stirring was achieved through the use of a Teflon® coated stirring bar set at 2000 rpm. The stirrer bar was placed 0.5 cm away from the surface of the working electrode during stirring. Sequential aliquots of substrate were only added once a steady current response was noted by the biosensor.

Following chronoamperometry, electrodes were cycled between -0.3 V and +0.8 V for 3 cycles. CVs comparing electrode response to catechol substrate in stirred and unstirred solutions were performed i.e. a total of 6 cycles.

4.4.3.5 Electroanalytical investigations of catechol oxidation/reduction at GCEs modified with BSA films.

Cleaned GCEs were modified with sequential aliquots of 1µl BSA and 1 µl 15% glutaraldehyde. Electrodes were modified using the same BSA concentrations outlined in Table 4.2 and allowed to crosslink under the same conditions, with the same post-modification treatment, outlined in 4.4.3.2(c).

Following cross-linking of the film, electrodes were successively scanned in 2 ml SLB, under the same electroanalytical conditions as in 4.4.3.4(a). Catechol was then added to the electrochemical vessel to a final concentration of 1 mM and the solution briefly homogeneised via stirring.

BSA-modified electrodes were then successively scanned between -0.3V and + 0.8V while varying the scan rate at: 10, 33.3, 56.7, 80, 100, 103, 126.6 and 150 $mV.s^{-1}$. Peak characteristics of potential (E) and current (I) were recorded for both the anodic (p,a) and cathodic (p,c) peaks generated by the presence of catechol. The apparent diffusion coefficients of catechol and its oxidation product, *o*-benzoquinone, were calculated from Eq 4.1, as described in Bard and Faulkner, 2001c:

$$I_p = 0.4463 \left(\frac{F^3}{RT}\right)^{1/2} n^{3/2} A D_O^{1/2} C_O^* \nu^{1/2} \qquad \text{Eq. 4.1}$$

Where Ip is the peak current (A), F is Faraday's constant (96 485.3 $C.mol^{-1}$), R is the molar gas constant (8.315 $J.mol^{-1}.K^{-1}$), T is the temperature under which investigations were undertaken (293 °K), n is the number of electrons transferred (n = 2), A is the cross-sectional diffusion area of the electrode (~0.071 cm^2 for all GCEs used), C_O^* is the bulk concentration of catechol (1 x 10^{-6} $mol.cm^{-3}$) and D_O is the diffusion coefficient ($cm^2.s^{-1}$) (Bard and Faulkner, 2001c). All experiments were performed in triplicate and discussed relative to electrodes that were merely cleaned, but not modified with BSA.

Exposure of BSA films to catechol oxidation products was performed by incubating fabricated BSA films in a solution of 200 μM catechol in the presence of 3 U of laccase in SLB for 5 minutes. Thereafter, electrodes were rinsed thoroughly with water and immersed in SLB for half an hour to allow the diffusion of unreacted product away from the electrode before being assessed by CV as outlined above.

4.4.3.6 Data Treatment

Data acquisition of current-concentration response for the biosensor was performed using linear regressional data, using χ^2 minima as the determinant for regressional parameters as outlined in Appendix 1 (Section A1.2).

The modelling of biosensor responses was performed using the model described in Chapter 2 (Section 2.4.1). Goodness-of-fit was for the modelling process was determined in parallel for each sensor investigated, and parameters fitted using either the Sum-of-Square Difference (SSD) or Chi-Squared (χ^2) minima, respectively (Appendix 1, Section A1.4). This was executed as outlined in Section 2.3.3.3 of this Thesis. Parameter *a* was set to zero and all other parameters were varied in order to produce the final modelled parameters. In brief, the pertinent parameters governing biosensor response and relative efficacy was estimated from the following parameters:

(1) Biosensor sensitivity was determined from the gradient of the linear range of sensor response.

(2) Maximal current, I_{max} was reported as analogous to the model parameter *d* of the sigmoidal model response.

(3) The degree of sigmoidality was estimated from the model parameter, *b*.

(4) The K_m was determined from *c*.

(5) Sensor responses were normalised with respect to electrode surface area, in order to accurately compare results with those obtained from literature. For thin-film GCE sensors (physically adsorbed, covalent modification), the capacitance calculated from dI in SLB pH 5.5 (performed prior to surface activation) was used to calculate surface area. For glutaraldehyde cross-linked sensors, the geometric

surface area (~0.071 cm^2 for a 3mm diameter electrode) was taken to be equivalent to the diffusional cross-sectional area necessary for normalisation. Hence the maximal current, I_{max}, is reported as the maximal current density, i_{max}, henceforth. Biosensor sensitivity is also reported relative to the electrode surface area.

The model's robustness was also assessed. The differences in the final modelled parameters when minima-seeking was performed using either SSD or χ^2 as indications of model goodness-of-fit were assessed for their reproducibility, both between sensors and sensor categories. In addition, the ability of the model to produce coherent sensor responses analogous to either the classical (Michaelis-Menten) or non-classical (sigmoidal) biosensor responses was also assessed.

4.5 Results

Sensors fabricated in this Chapter were fabricated using two separate batches of laccase, with specific activities of 21.7 $U.mg^{-1}$ and 32.1 $U.mg^{-1}$, assessed via spectrophotometric assay using catechol at a stock laccase concentration of 1 $mg.ml^{-1}$ (Chapter 3, Section 3.5.4). After adjusting the concentrations of laccase to correspond to 800 $U.ml^{-1}$ solutions, no significant difference was found to be present when laccase from either batch was used in the fabrication of sensors. This indicates that pre-modification adjustments of laccase concentration on the basis of activity is sufficient to produce sensors of consistent enzyme activity, irrespective of the specific activity (and thereby purity) of the batch under examination.

4.5.1: Immobilisation Techniques

The sensitivity of detection, linear range of response and modelled parameters of i_{max}, K_m and the degree of sensor sigmoidality is reported in Table 4.3, below.

Table 4.3: Summary of the properties of sensors fabricated on anodically-pretreated GCE surfaces using different immobilisation methods

Graphical analysis		Modelling Analysis		
Sensitivity ($nA.\mu M^{-1}.cm^{-2}$)	**Linear Range (μM)**	**i_{max} ($\mu A.cm^{-2}$)**	**K_m (μM)**	**Degree of sigmoidality, b**
Physical adsorption:				
6.471 ± 1.064	0- 100	3.5 ± 0.3	246 ± 23	0.9712 ± 0.0422
Covalent Modification:				
6.227 ± 0.349	0 - 127	2.2 ± 0.1	226 ± 22	0.941 ± 0.0135
Cross-linked:				
79.19 ± 5.554	0 - 98	23.3 ± 5.2	152 ± 19	1.08 ± 0.094

Uncertainties represent standard deviations from the means, with number of measurements ≥ 5

While physical adsorptive and covalent attachment methods utilise laccase in the sub-monolayer to thin-multilayer, a larger amount of laccase can be loaded onto the surface of the electrode when employing cross-linking as a means to immobilise laccases. Hence, despite the anticipated denaturation of laccase occurring during cross-linking, a more than 10-fold increase in sensitivity (relative to physical adsorption or covalent attachment of the laccase) is noted when using glutaraldehyde cross-linking as a means of laccase immobilisation.

On the basis of the increases in the catechol detection sensitivity and i_{max} parameter, as well as the lowered K_m values relative to the other immobilisation methods, cross-linked sensors were selected as the primary sensor reported henceforth in this research. Other advantages regarding the stability of the biosensor under adverse conditions (temperature, pH, storage) conferred through the use of cross-linking have been outlined in the Introduction of this Thesis (Section 4.2.2).

4.5.2 Optimisation of glutaraldehyde cross-linked laccase biosensors

In order to examine the effects of varying concentrations of laccase and BSA on the operational parameters of the produced biosensors, the current response of fabricated biosensors calibrated using varying concentrations of catechol was measured.

4.5.2.1 Sigmoidal model parameter extraction under Michaelis-Menten and sigmoidal sensor responses

For the purposes of a visual overview as to the type of data analysed in this section, Figures 4.3 and 4.4 shows typical chronoamperometric raw data and the determined current-concentration relationships for sigmoidal (Fig. 4.3) and hyperbolic (Fig. 4.4) biosensor responses using catechol as a laccase substrate, with the various parameters extracted from modelling of each sensor response presented in both Figures.

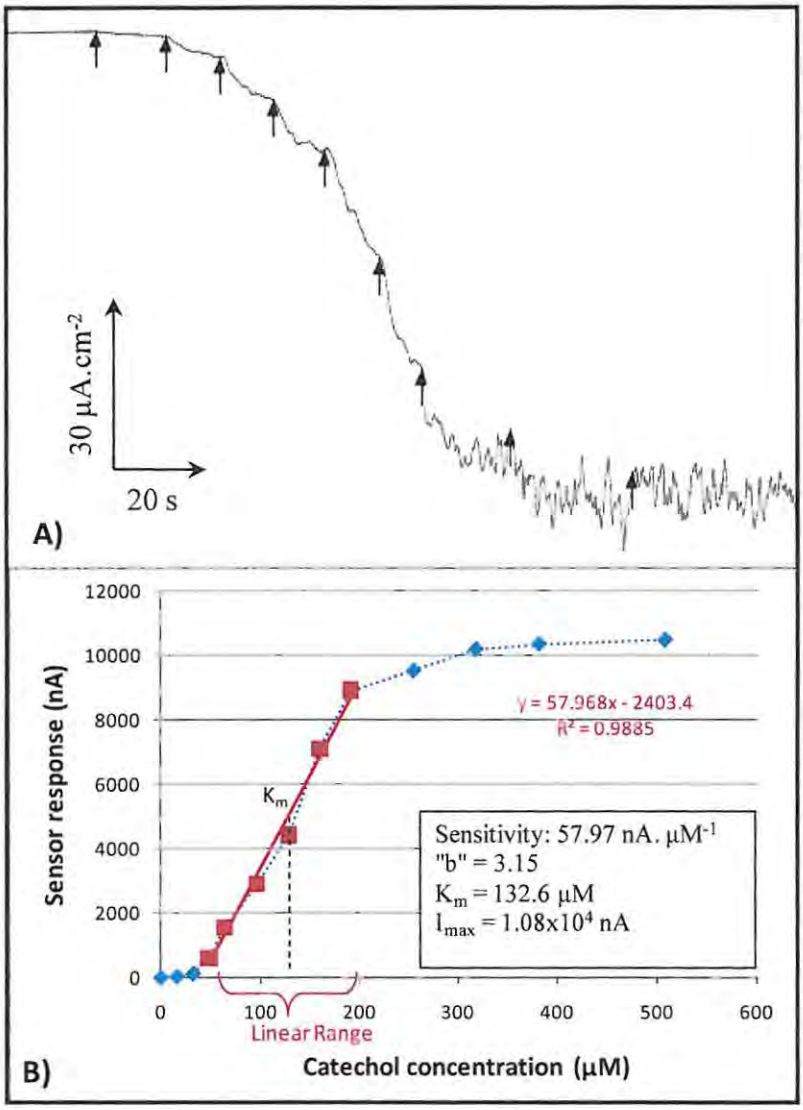

Figure 4.2:

A) Chronoamperometric response of biosensor fabricated with 800 mU laccase and 50 µg BSA to aliquots of catechol.

The addition of catechol is indicated with black arrows.

B) Current-concentration function for the resultant sigmoidal sensor response, as assessed by chronoamperometric determination of response in presence of increasing substrate concentration.

Inset shows biosensor parameters extracted from both graphical and non-linear computer modelling of sensor response. Please note that data used is presented 'as-is' i.e. without normalisation for electrode surface area.

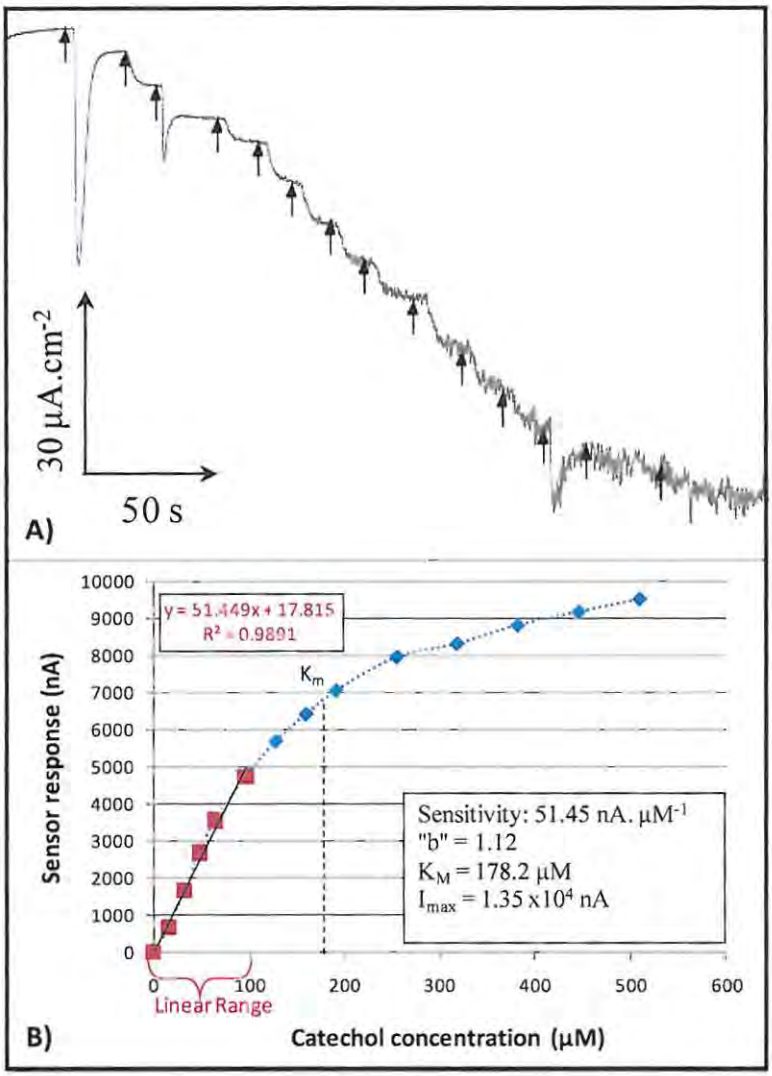

Figure 4.3:

A) Chronoamperometric response of biosensor fabricated with 0.8 U laccase and 10 µg BSA to aliquots of catechol.

The addition of catechol is indicated with black arrows.

B) Current-concentration function for the resultant hyperbolic (i.e. Michaelis-Menten-like) sensor response, as assessed by chronoamperometric determination of response in presence of increasing substrate concentration.

Inset shows biosensor parameters extracted from both graphical and non-linear computer modelling of sensor response. Please note that data used is presented 'as-is' i.e. without normalisation for electrode surface area.

As Figures 4.3 and 4.4 display, a purely-graphical analysis of sensor response often underestimates the I_{max} parameter, due to the hyperbolic nature of the current-concentration i.e. enzyme velocity–substrate concentration response (Garret and Grisham, 2001). This, in turn, leads to an inaccurate determination of K_m values, through Eq. 2.3 (Garret and Grisham, 2001). These inaccuracies would be further

exaggerated by the sigmoidality of the sensor, justifying the use of the non-linear enzyme kinetics modelling techniques used to extract the salient kinetics parameters to describe both sigmoidal and non-sigmoidal (i.e. hyperbolic) sensor responses.

The interpretation for the sigmoidality of the produced current-concentration curves is that sensor response, through reasons that are discussed in further sections, become mechanistically indistinguishable from the empirical Hill Equation for positive co-operativity, as defined in Eq. 2.5 of Chapter 2. Indeed, it is important to note that sensors modelled via either the sigmoidal model (Eq. 2.6) or via the Hill formalism (Eq 2.5) yield the same parameter values.

When comparisons between parameters of sigmoidal biosensor responses elucidated via the sigmoidal response, or by the Hill Equation above were compared, V_{max} was found to be equivalent to 'd', 'n' to 'b' and K' to be equivalent to c^b, with no differences in the SSQ found when comparing either model. The Inset values of Figure 4.5 serve as an example of the congruency. Figure 4.5 depicts the excellent agreement between the extracted parameters fitted using either the Hill Equation or the Sigmoidal Equation sensor response, as well as the equivalency of the aforementioned parameters.

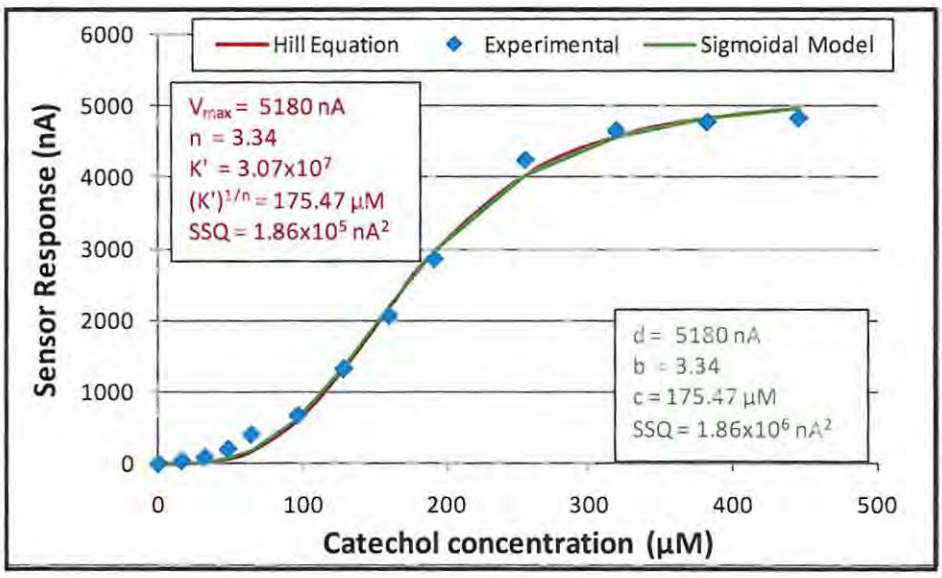

Figure 4.4: Modelling of experimental data vs. functions generated by modelling of parameters using either the Hill Equation or the Sigmoidal Model.

Inset: Parameters extracted through use of either model, Red (upper-left box) = Hill Equation and Green (lower-right) = Sigmoidal Model. Experimental data used: 100mg BSA, 800 $U.ml^{-1}$ laccase, replicant 1, GCE 3 of that set.

This highlights the robustness of the selected sigmoidal model, in that it elucidates parameters that are not only relatable to classic Michaelis-Menten enzyme kinetics, but also to the kinetics governing sigmoidal enzyme kinetics. While the sigmoidal equation has previously been used in order to assess sigmoidal biosensor behaviour (Pauliukaite et al., 2006), the use of this formalism has been rare and, to date, no known correlation between it and established formalisms for determining enzyme kinetics has been published.

For those sensor responses exhibiting a lower degree of sigmoidality ($b \leq 2.5$) and/or a K_m value greater than 250 μM, the model parameters determined from $\chi 2$-minima fitting are henceforth presented, while for other sensor categories, parameters extracted from SSD-minima are presented. Appendix 3 of this section provides supporting evidence for this method of discriminating between highly sigmoidal and less sigmoidal biosensor current response curves.

4.5.2.2 BSA content:

Significant alterations in the performance of the sensor were noted, both assessed graphically and through modelling of the non-linear sensor response with variation of substrate concentration. Figures 4.5 - 4.7 display the relevant alterations to the sensor's performance with an alteration in added BSA, both before and after re-use of the electrode. The various laccase activities and BSA masses reported in this Section are reported in Table 4.2 (Section 4.4.3.3)

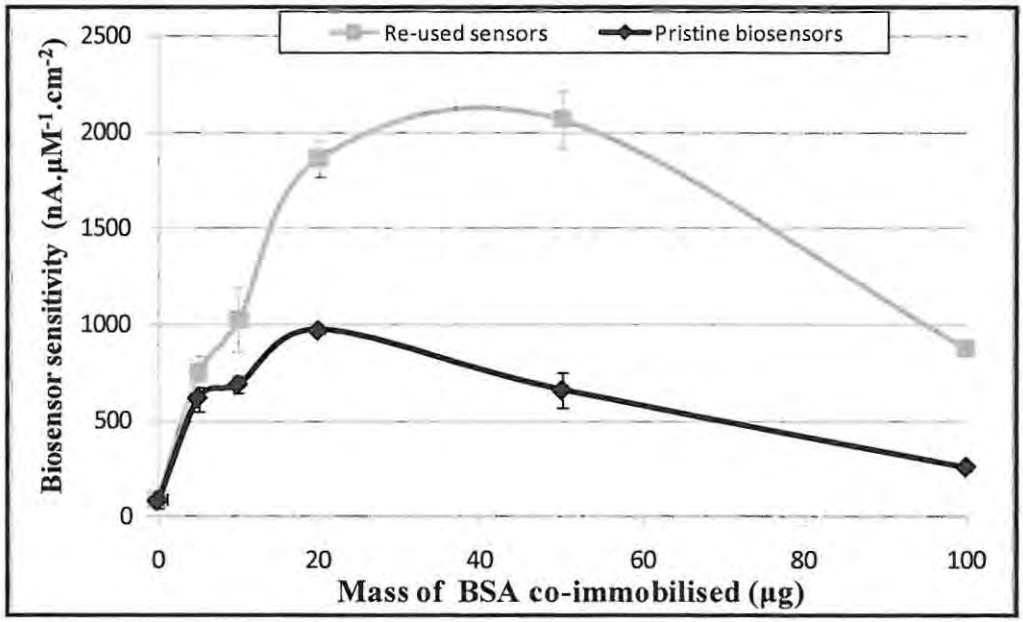

Figure 4.5: Alterations in biosensor sensitivity with addition of BSA.

Laccase activity was set at 0.8 U per biosensor.

Error bars represent standard error from the mean, number of replicants, $n \geq 3$

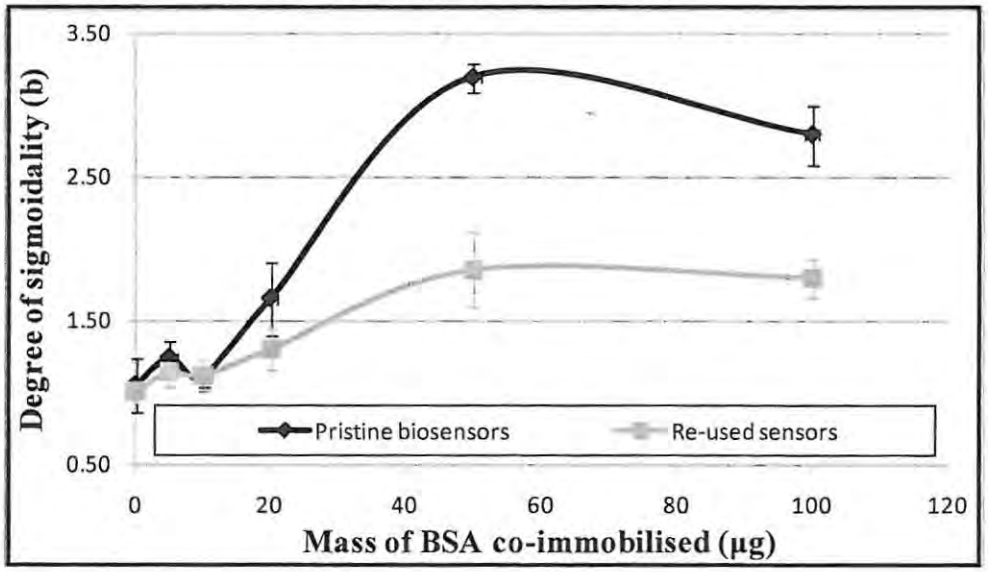

Figure 4.6: Alterations in the degree of sigmoidality, represented as the model parfameter, b with addition of BSA.

Laccase activity was set at 0.8 U per biosensor.

Error bars represent standard deviation from the mean, number of replicants, $n \geq 3$.

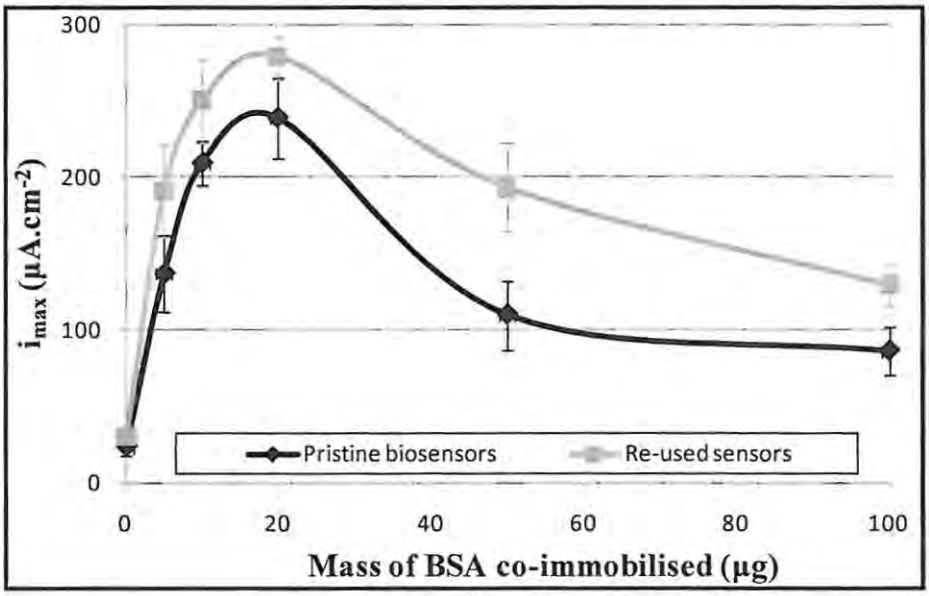

Figure 4.7: Alterations in modelled i_{max} values (parameter *d*), with the varying concentrations of BSA as co-immobilant within the sensor.

Laccase activity was set at 0.8 U per biosensor.

Error bars represent standard error of the mean, number of replicants, n ≥3

As Figures 4.5 – 4.7 display, there is a pronounced effect on the operational parameters of the pristine laccase biosensor with the inclusion of BSA. A significant effect on the sigmoidality of biosensor response is recorded with an increase in BSA content (Figure 4.6). To discuss the various alterations in biosensor responses, the effects of BSA content are categorised into responses that produce non-sigmoidal biosensor kinetics i.e. hyperbolic curves similar to those anticipated with Michaelis-Menten like functioning of the immobilised biomolecules and those that exhibit a higher degree of response sigmoidality.

Laccase biosensors fabricated with low BSA contents (0 – 20 μg) exhibited increased biosensor sensitivity and maximal current with increasing BSA content (Figure 4.5). The absence of BSA results in a biosensor with an averaged sensitivity of 79.1 nA.μM^{-1}.cm^{-2}, a value which, with increasing BSA content, exhibited an almost linear increase to a final value more than 10-fold higher, 967.5 nA.μM^{-1}.cm^{-2}, for sensors fabricated with 20 μg of BSA (Figure 4.4). The modelled i_{max} value also exhibited a nearly ten-fold enhancement in this range, from 23.3 μA.cm^{-2} to 239 μA.cm^{-2} (Figure 4.7).

The degree of sigmoidality (Figure 4.6) remains steady between 0 – 10 μg BSA at (between 1.0 – 1.15) and then increases slightly to ~1.4 at 20 μg BSA co-immobilised, which still produces a sensor response that is visually close to the hyperbolic curve anticipated in Michaelis-Menten enzyme kinetics.

At higher BSA concentrations (20, 50 and 100 μg BSA), the degree of sigmoidality increases rapidly, stabilising at approximately b = 3.2. Simultaneous with the increase in sigmoidality, biosensor sensitivity declines to a value that is still three times larger than that recorded at sensors without BSA included (256 $nA.\mu M^{-1}.cm^{-2}$ for sensors fabricated with 100 μg BSA co-immobilised, vs. 79 $nA.\mu M^{-1}.cm^{-2}$ for those fabricated using laccase alone). Concomitant with the decrease in sensitivity is a decline in the modelled i_{max} parameter (Figure 4.7). Since the laccase content is consistent between biosensors at this juncture, the i_{max} parameter, being analogous to the v_{max} parameter at a fixed enzyme concentration, is itself analogous to the k_2 parameter of the biosensor kinetics.

In addition to the increasing sigmoidal behaviour of sensor response (Figure 4.6) with increasing addition of BSA alters the substrate concentration range through which a linear response is recorded, as well as the apparent K_m of the biosensor assessed during calibration of the biosensors using catechol. Figure 4.8 demonstrates the alteration in both the linear portion of the sensor response and the modelled K_m values (equivalent to the modelled parameter, *c*) that was exhibited by the biosensors when increasing BSA concentrations were utilised in the fabrication of the sensor, prior to re-use.

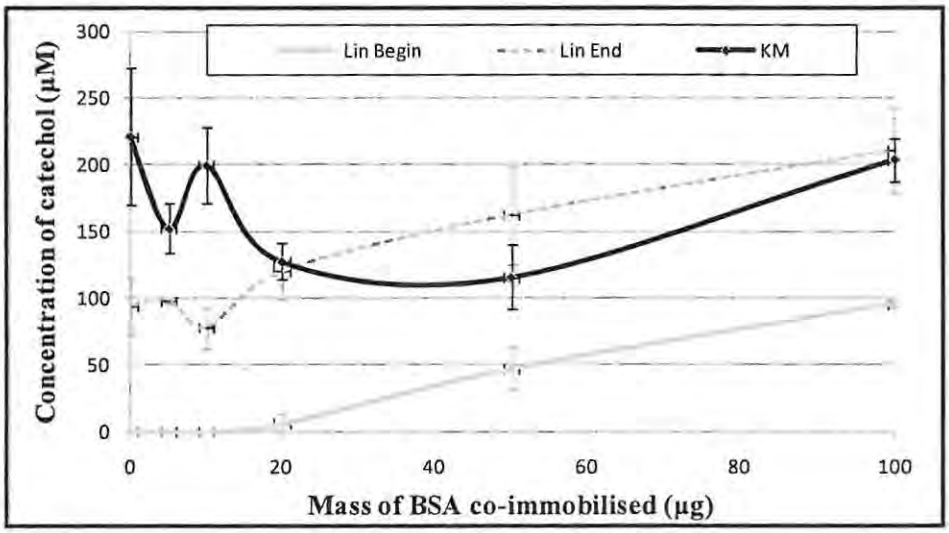

Figure 4.8: Alterations in catechol concentration range exhibiting linear sensor response, and modelled K_m values for pristine sensors fabricated with differing BSA contents, prior to re-use.

Laccase activity was set at 0.8 U per biosensor.

Legend: Onset of linear response (Lin Begin) is solid grey, the end of the linear response (Lin End) is dashed grey, and modelled K_m (KM) values are in depicted in black. Error bars represent standard error from the mean. Number of replicants, $n \geq 3$

In Figure 4.8, the area occurring between the end of linear response and onset of linear response indicates the area in which linear current-substrate concentration response occurs. This area remains fairly constant, with ~100 μM separating the beginning and ends of the linear responses of the sensor. A complex behaviour between the BSA content of the biosensor and the range of linear response is observable, coupled with an equally-complex behaviour of the modelled K_m values (Figure 4.8). Similarly to the i_{max} and sensitivity trends discussed above, these responses can be divided within low-content BSA cross-linked laccase films and high-content laccase films.

When sensors are fabricated with a low BSA content (0 - 10 μg BSA co-immobilised) linear response undergoes deviation that possesses an inverse trend within the modelled K_m values. Since the K_m values are extracted from the entire data-set of response-concentration calibration, while the linear response is obtained from only a portion of the data-set, the trend observed with K_m indicates that this is an intrinsic property of the fabricated sensor, rather than an observational error in the measurement of the linear portion of the biosensors' responses. At higher levels of BSA, concomitant with the increase in sigmoidality, a monotonic increase of the linear range is noted, coupled with a relative decrease in the K_m value.

Electrodes that were re-used, after calibration of 'pristine' sensors with catechol, showed significant alterations in all of the parameters so far reported. Significant increases in both the detection sensitivity (Figure 4.5) and i_{max} values (Figure 4.7) are noted, accompanied by a general decrease in sigmoidality (Figure 4.6), relative to those values obtained at pristine biosensors. The degree of enhancement appears to be linked to the amount of BSA co-immobilised with the laccase, with the largest relative alterations noted with increasing BSA content.

Following re-use, in addition to the alterations in the sensors' sensitivity and i_{max} values, there is a decrease in both the linear response regions and the modelled K_m values. Figure 4.9 displays the linear range and K_m values of sensors fabricated with different BSA contents, for re-used biosensors.

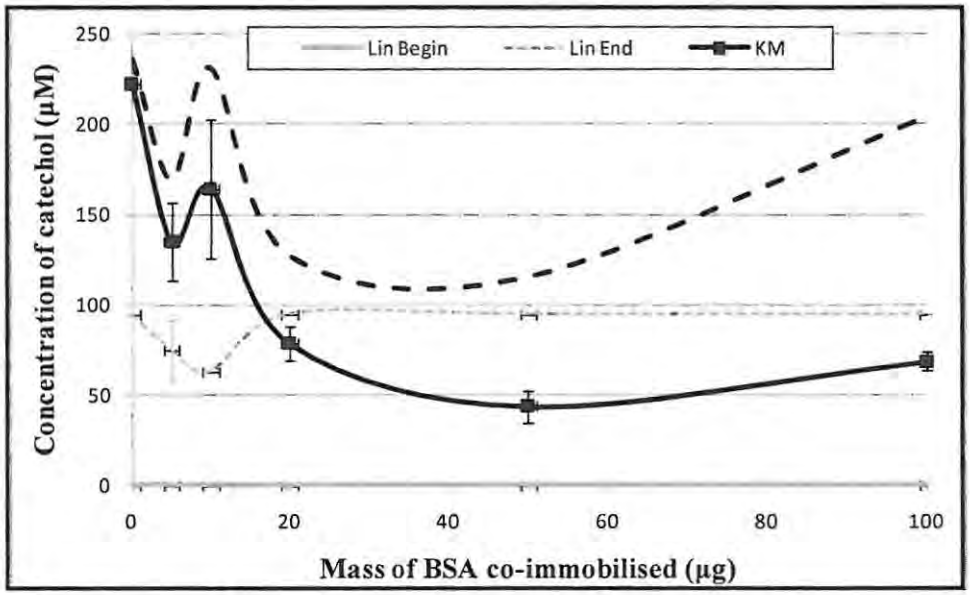

Figure 4.9: Alterations in linear portion of sensor response, and modelled K_m values for re-used biosensors fabricated with differing BSA contents.

Legends and their meanings are the same as in Figure 4.8. The dashed black line indicates trends in the K_m of non-conditioned biosensors (Figure 4.8) and is represented here for comparative purposes

Along with the decline in BSA-dependent sigmoidality upon biosensor re-use (Figure 4.6), both the linear sensor response concentration range and the K_m (Figure 4.9) decline and stabilise, compared to the monotonic increase seen in Figure 4.8. Following a rapid increase, the linear sensor response after re-use occurs between 0 - 100 µM of substrate concentration and becomes independent of the sensor's BSA content.

In order to track the changes in the kinetic parameters governing the biochemical aspect of the biosensor, the V/K value (calculated here as the i_{max}/K_m, or i/K) is presented for biosensors both prior and after re-use in Figure 4.10

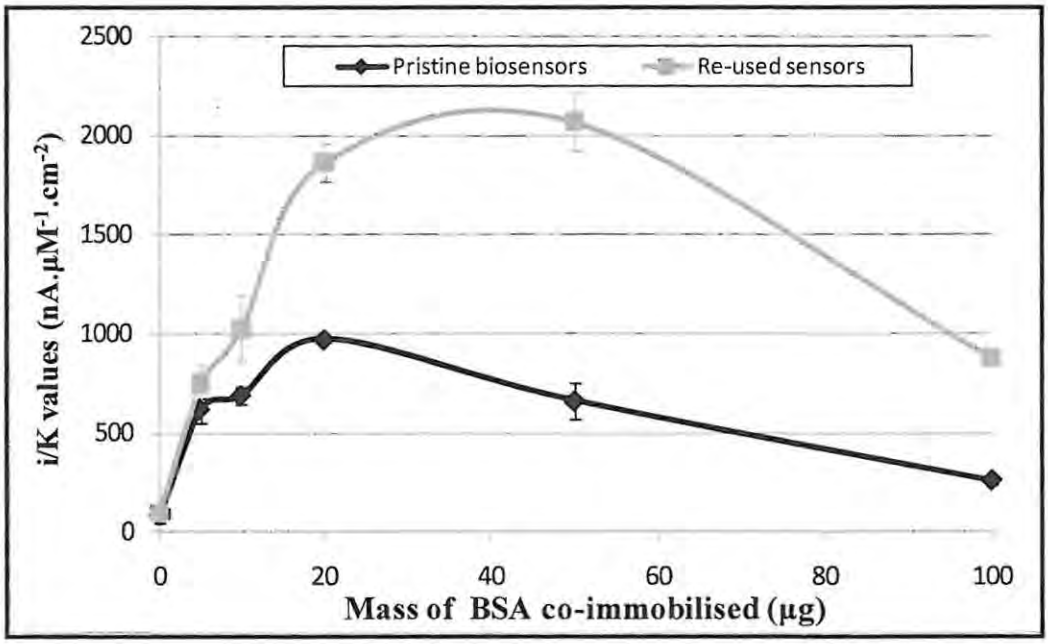

Figure 4.10: i/K values plotted before and after re-use, with differing amounts of BSA co-immobilised with the laccase.

The significant increase in the i/K values between re-used and pristine biosensors can be explained via the large contribution due to the significant decrease in modelled K_m values after re-use has taken place (Figure 4. 10), together with the BSA-dependent increases in i_{max} noted after re-use (Figure 4.7). A comparison between the behaviour of biosensor sensitivity (Figure 4.5) and the i/K values shows very similar trends between these values and their dependence on the BSA loading. Figure 4.11 displays the comparison of i/K values extracted from the modelling process against the sensitivity of the biosensor, both before and after re-use of the sensor.

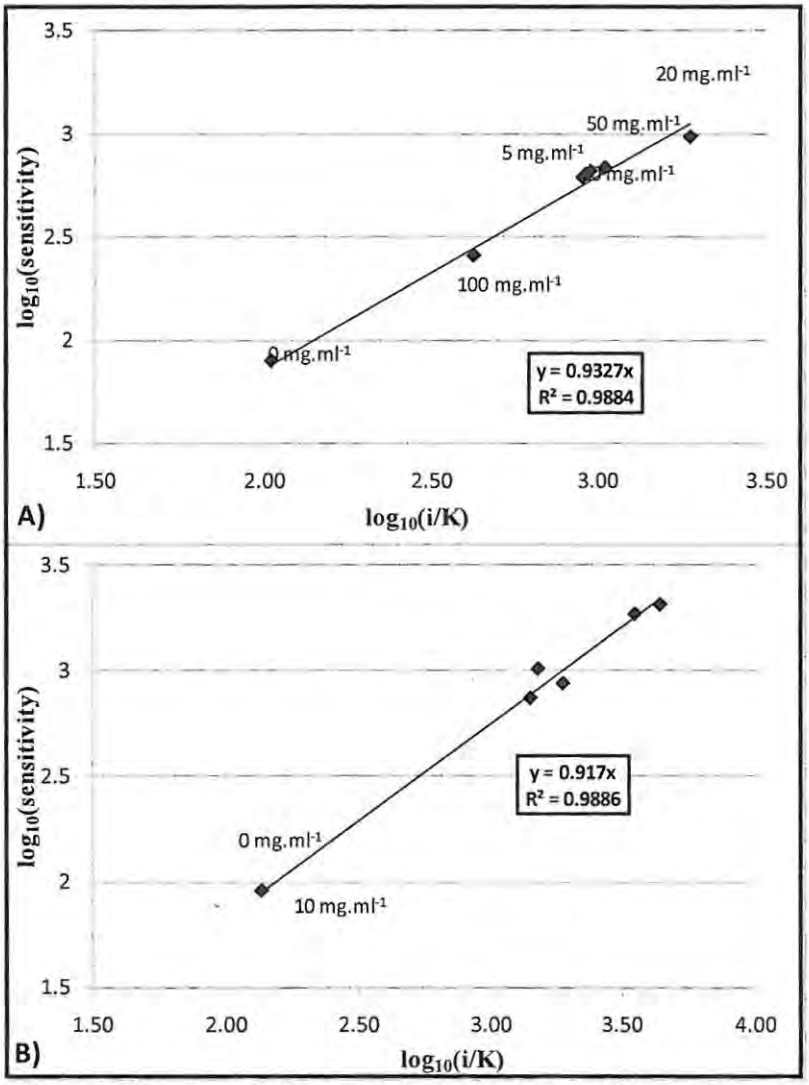

Figure 4.11: logarithm of i/K values plotted against the logarithm of biosensor sensitivity for sensors fabricated with different BSA contents

A: Pristine biosensors

B: Re-used biosensors, following intermediate incubation in SLB containing 50 µM catechol for 1 hour.

Inset text displays the stock BSA concentration used in fabrication of sensors for individual points, Inset boxes display the linear regression function of the data. Green data-points show the i/K values when χ^2 minima-seeking was used for the modelling parameters.

Figure 4.11 demonstrates that a strong linear tendency between the calculated i/K values and the biosensor sensitivities is observable, both before and after re-use of the electrode. While the degree of linearity is stronger after re-use of the electrode ($R^2 \sim 0.98$), the gradient is shallower, with a higher y-intercept, possibly indicating the presence of a further reaction aiding signal generation that is not based solely on enzyme kinetics. For both pristine and re-used biosensors, i/K appears to trend with the detection sensitivity

The empirically-determined linear relationship existing between i/K values and biosensor sensitivities, as shown in Figure 4.11, allow us to postulate that alterations in either the apparent v_{max} (translating to alterations in modelled i_{max} values) or the apparent K_m values alters biosensor sensitivities. This finding is extremely important, not only for unification of the graphical analyses of current responses with the modelling parameters used, but also when consulting the effects that alteration in biosensor parameters (e.g. re-use, BSA content) of the biosensor has on the functional parameters of the produced biosensor, as well as in explaining differences in the different sensor configurations displayed above by tracking changes in the i_{max} and K_m values.

Through the empirical demonstration that i/K correlates with detection sensitivity, alterations in either the i_{max} or K_m upon re-use have a corresponding, positive effect on the biosensor sensitivity. Using alterations in these parameters upon re-use allows a re-interpretation of the effect that re-use has on laccase biosensors fabricated with differing BSA contents. Figure 4.12 displays the relative alterations in biosensor apparent kinetic parameters upon re-use. For ease of representation, the parameters are grouped according to their behaviour (increasing vs. decreasing trends).

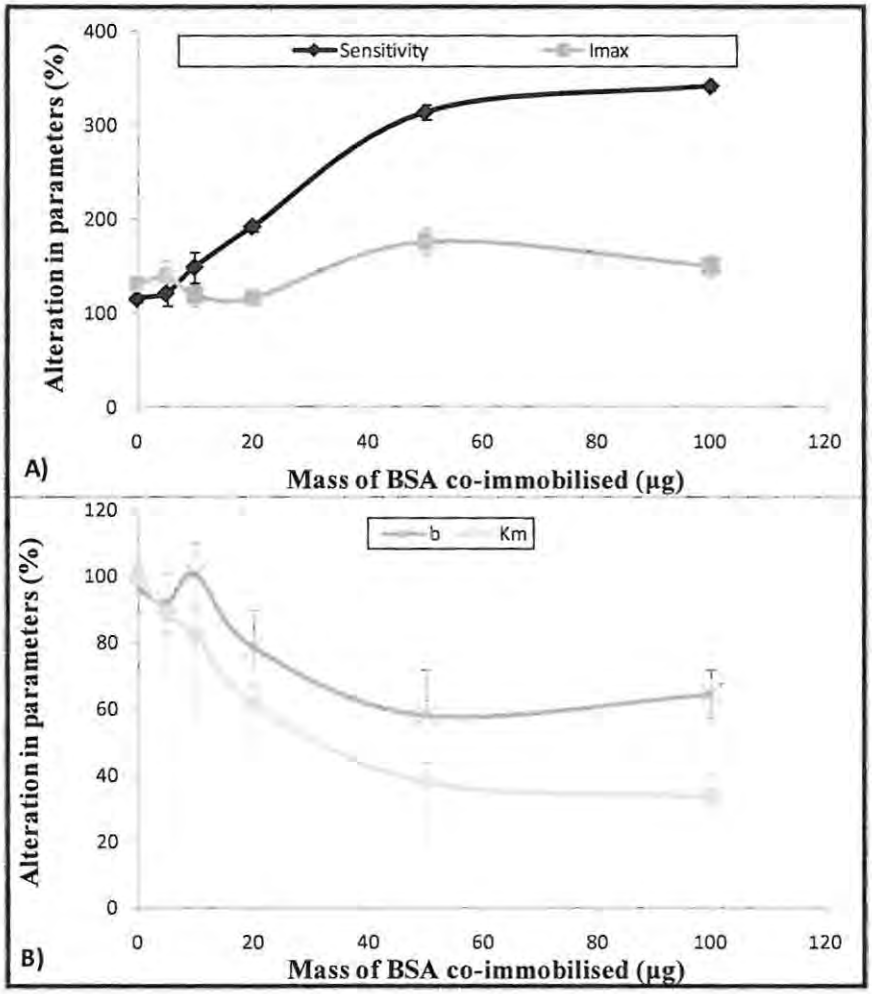

Figure 4.12: Graph depicting change in sensor behaviour with re-use, when different BSA contents are co-immobilised with laccase.

A) Increases in biosensor sensitivity and modelled I_{max} parameters

B) Decrease in sigmoidality and modelled K_m parameters.

Data used is the relative shift in said parameters between conditioned and non-conditioned electrodes and drawn from the same data used for the presentation of Figures 4.8 - 4.15. Error bars indicate standard deviations from the mean with $n \geq 3$

It is evident from the graphical rendering of the data in Figure 4.12 that an increase in BSA content is proportionately (but not linearly) related to an improvement in biosensor parameters following re-use from the non-conditioned counterpart. The relative decrease in the degree of sigmoidality, *b* (Figure 4.12**B**) increases with increasing BSA content following re-use. Proportional increases in both the biosensors' sensitivity and I_{max} values (Figure 4.12**A**) are noted; significant decreases in the modelled K_m values (Figure 4.12**B**) occur with an increase in BSA content. All of these parameters indicate that an

improvement in the operational parameters of the sensors occurs with exposure of the biosensor to substrate. Please note that the very low values of b and the inverse nature of K_m values in the sigmoidal model, and the interrelatedness of b values and the calculated K_m values lead to relatively high uncertainties in the measurement of the relative shift of K_m. Nonetheless, significant alterations in these values are readily observable in the trends present in Figure 4.12**B**.

A comparison of the relative shift in biosensor sensitivity compared to the i_{max} parameters (Figure 4.12**A**) indicates that a major factor in the alteration of the biosensor's sensitivity is the alteration in the modelled K_m response, and the decrease in sigmoidality. While the modelled i_{max} parameters remains relatively stable, being enhanced by approximately 50 $\pm$ 20% increase (relative to pristine biosensors), biosensor sensitivity still shows an impressive 250% increase at the maximal relative difference (100 µg BSA content). This, in turn, can be related to the more than two-fold decrease in the modelled K_m parameter in Figure 4.12**B**, and the simultaneous effect of both on the V/K ratio. The linearity observed between i/K ratios (Figure 4.11) and the biosensor sensitivity indicates that an alteration of the i/K value of a given biosensor has a direct effect on the observable sensitivity of the biosensor.

4.5.2.3. Optimisation of laccase content for BSA-glutaraldehyde-laccase sensors:

As the catalyst for catechol oxidation, laccase is expected to improve sensor response, through the increase in [E] in the Michaelis-Menten equation. If one were to neglect mass transfer constraints that arise from the increased concentration of enzyme (purely for hypothetical reasons, for reasons that are outlined below), the concentration of enzyme in a given solution is related to both the velocity and maximal velocity of the catalytic system. As Eq. 2.3 shows, an increase in the v_{max} of an enzyme system corresponds to an increase in the substrate-dependent velocity. Since v_{max} itself is resolved from:

$$v_{max} = k_2.[E_{tot}] \qquad \text{Eq. 4.2}$$

Where v_{max} is the maximal enzyme velocity for a given concentration of substrate, k_2 is the concentration-independent catalytic co-efficient of a given enzyme and $[E_{tot}]$ is the enzyme concentration

(Miller and Tanner, 2008). There is, hence, a positive correlation between enzyme concentration and the catalytic velocity of a given enzyme-substrate mixture.

However, kinetic functions of 'free' enzyme systems are not necessarily comparable to those dealing with immobilised enzyme kinetics. As mentioned previously (Section 1.3), through immobilisation of the enzyme, a much greater concentration of enzyme near the transducer is achieved, which itself results in increased localised catalysis rates which, in turn, produces the desired high sensitivities of biosensors. Under these conditions, mass transfer kinetics become increasingly significant when describing the overall kinetics of the system, as the transport of substrate to the enzyme and the transport of product to the transducer becomes a rate-determining stage of signal reporting.

Two broad categories of diffusional mass-transport can be made at this junction. The first, being a passive property arising from the diffusional constraints imposed on a molecular diffusion into the electrode through the porous cross-linked protein structure is likely to be impose

Ultimately, it is an interplay of the factors of enzyme loading and mass-transfer restrictions arising from enzyme loading that primarily affect biosensor response.

In addition, the presence of BSA as a stabiliser has been shown in the previous section to have a significant effect on the apparent enzyme kinetics of the sensor, and hence, the final linear range and sensitivity of the biosensor. Given the low sensitivity of the enzyme fabricated in the absence of BSA (see preceding section), the effect of laccase content on the final sensor was assayed at two separate mass-loading of co-immobilised BSA: 10 μg and 100 μg. These BSA loadings were selected on the basis of the sigmoidalities of the biosensors fabricated using when using these amounts of co-immobilised BSA. Although a BSA addition of 20 μg was considered to produce a sensor with optimal parameters, the increase in sigmoidality > b = 1.0 indicated that a lower amount of BSA was preferable for this stage of experimentation, in order to contrast biosensors that appear to obey idealised (i.e. Michaelis-Menten) kinetics and those that do not.

It was of interest to see whether the relative proportion of BSA : laccase would induce significant alteration in the produced catechol calibration curves (as indicated in Section 4.3.3.1), or whether the absolute concentration (i.e. loading) of the laccase or BSA would affect the sensor response, as indicated by the spectrophotometric data in the presence of BSA in Section 4.1 of this Chapter. Since the use of 10 μg of BSA in the preceding section was found to not affect the sensor's anticipated Michaelis-Menten kinetics greatly, this indicated that the intersection of enzyme loading and stabiliser loading did not greatly deviate from the postulated aggregation interaction noted in previous studies.

Issues of protein solubility precluded laccase concentrations larger than 800 $U.ml^{-1}$ (i.e. > 0.8 U laccase loaded per sensor) solutions of laccase being included into this phase of study. As it was, notable precipitation of laccase solution was noted within 5 minutes of solubilisation at this concentration of laccase, necessitating rapid modification of the electrode surface.

Figure 4.13 displays the relative substrate-detection sensitivities of biosensors fabricated using either 10 or 100 μg BSA, both before and after re-use. Figure 4.18 displays the i_{max} as determined through sigmoidal modelling of the current response-substrate concentration curves.

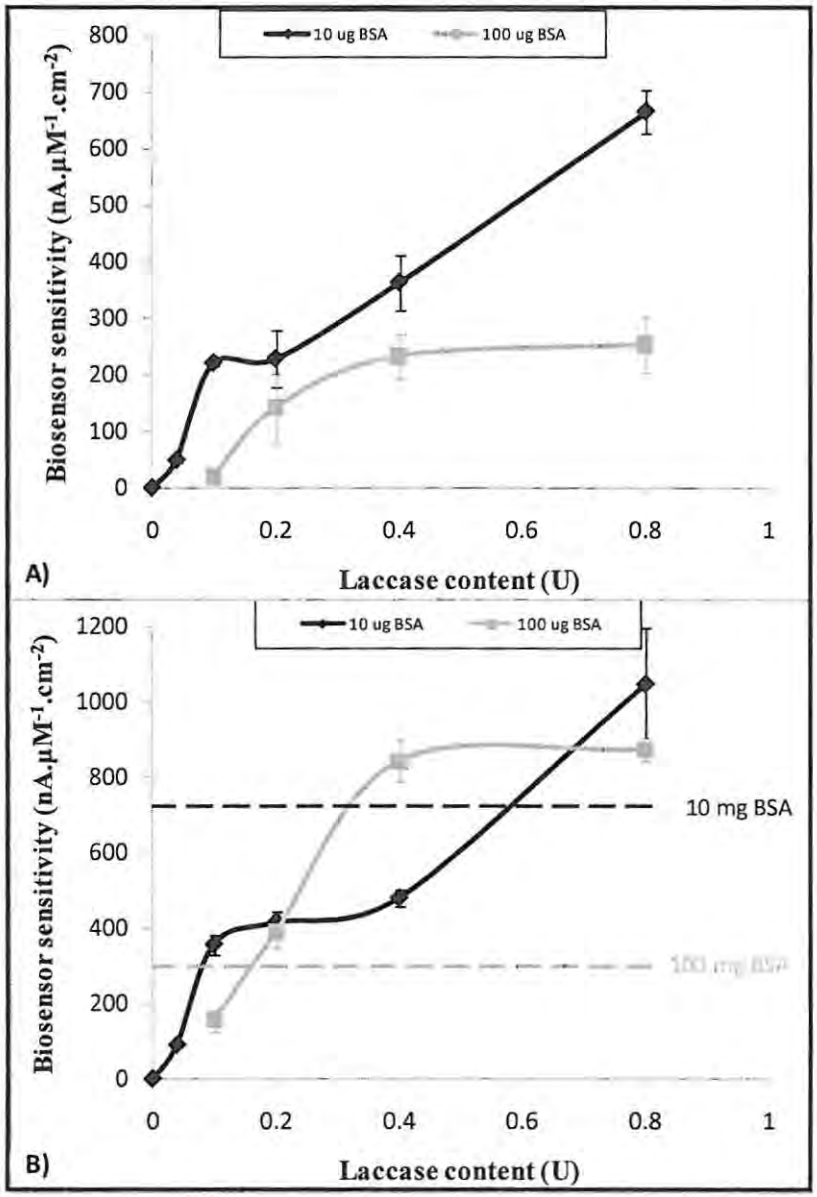

Figure 4.13: Biosensor sensitivities recorded with sensors fabricated with varying concentrations of laccase using BSA co-immobilised at an amount of either 10 or 100 µg per biosensor.

A) Pristine biosensors

B) Re-used biosensors

Dashed lines in Figure 4.13**B** indicate values of maximal sensitivity recorded in Figure 4.13**A**, and are merely for demonstrative purposes.

Error bars indicate standard errors from the mean with the number of observations, $n \geq 3$.

As Figure 4.13**A** depicts, prior to re-use, when 100 µg of BSA is added as the co-immobilant, biosensor sensitivity rapidly levels off, following the addition of 20 µg of laccase, while sensitivity in 10 µg of BSA appears to increase monotonically with an increase in laccase loading. Following re-use (Figure

4.13**B**), similar, albeit more exaggerated, trends are still noted. In addition, the biosensor sensitivities begin to become more comparable, with similar biosensor sensitivities recorded for the same laccase content irrespective of the BSA loading, in addition to a general decrease in the relative error noted for sensitivities. To confirm previous findings underlying electrode re-use in the previous section, the recorded biosensor sensitivities of conditioned electrodes surpass those of biosensors prior to re-use, with the most significant gains in biosensor sensitivity recorded for biosensors fabricated with 100 µg of BSA.

While the increases in sensitivity with increases in laccase concentration may indicate that re-use may help unify sensor response despite the differences in BSA, it is only an apparent unification that is itself due to the effect of alterations in the i_{max} and K_m values (which themselves vary substantially between equal laccase loadings at different BSA loadings) on the biosensor response (Figures 4.14 and 4.15, below). Thus, it is of interest to track changes in these parameters between the sensors, both on the basis of laccase loading, and on that of the BSA loading. Figures 4.14 and 4.15 display the modelled i_{max} parameters and the K_m values, respectively, of both high-BSA and low-BSA biosensor configurations with differing laccase content.

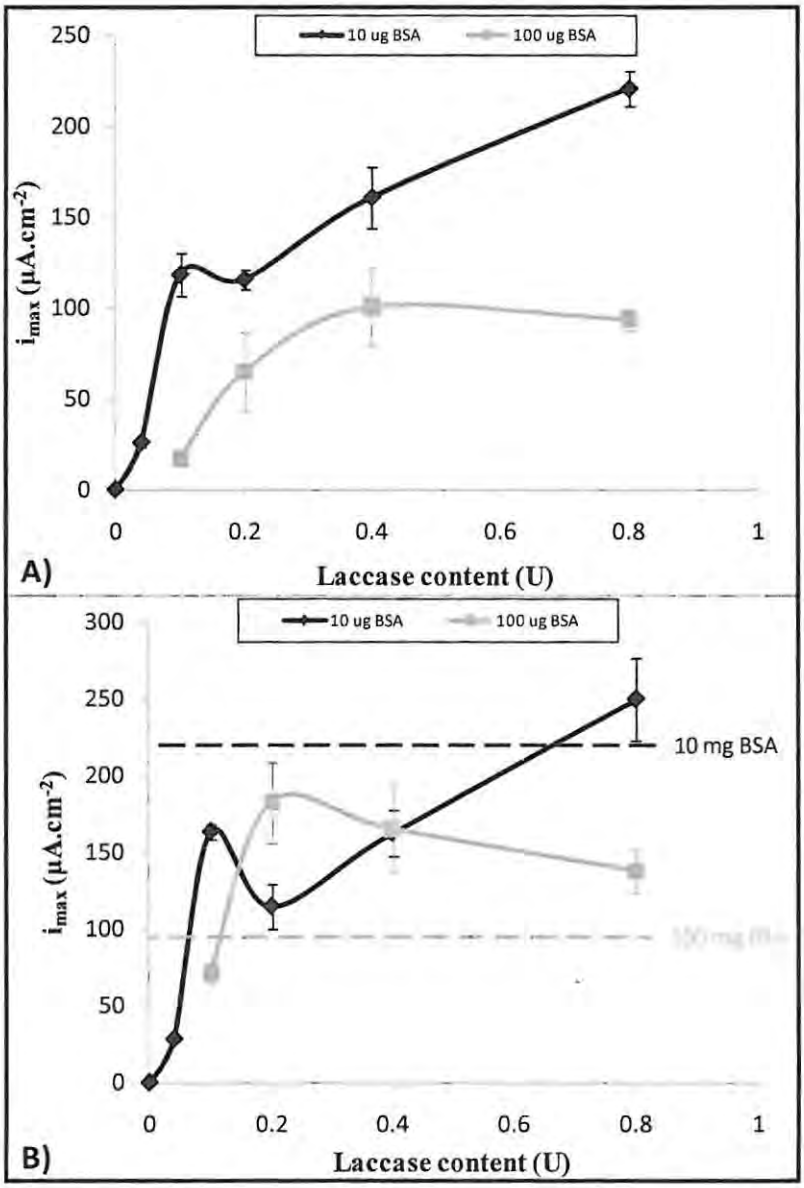

Figure 4.14: i_{max} of biosensors sensitivities recorded with sensors fabricated with varying concentrations of laccase using BSA co-immobilised at an amount of either 10 or 100 µg per biosensor.

A) Pristine biosensors

B) Re-used biosensors

All reported parameters as in Figure 4.3

Dashed lines in Figure 4.18**B** indicate maximal recorded values of i_{max} before re-use for each set. Error bars indicate standard error from the mean, $n \geq 3$.

Consistently, there is a < 50 % gain in the i_{max} parameter value upon re-use (Figure 4.14**B** compared to Figure 4.14**A**), while the biosensor sensitivity has almost doubled in both cases (Figure 4.13**B** vs. Figure

4.13**A**). This can be attributed again to a decrease in the apparent K_m of the biosensor, as Figure 4.15 (below) indicates.

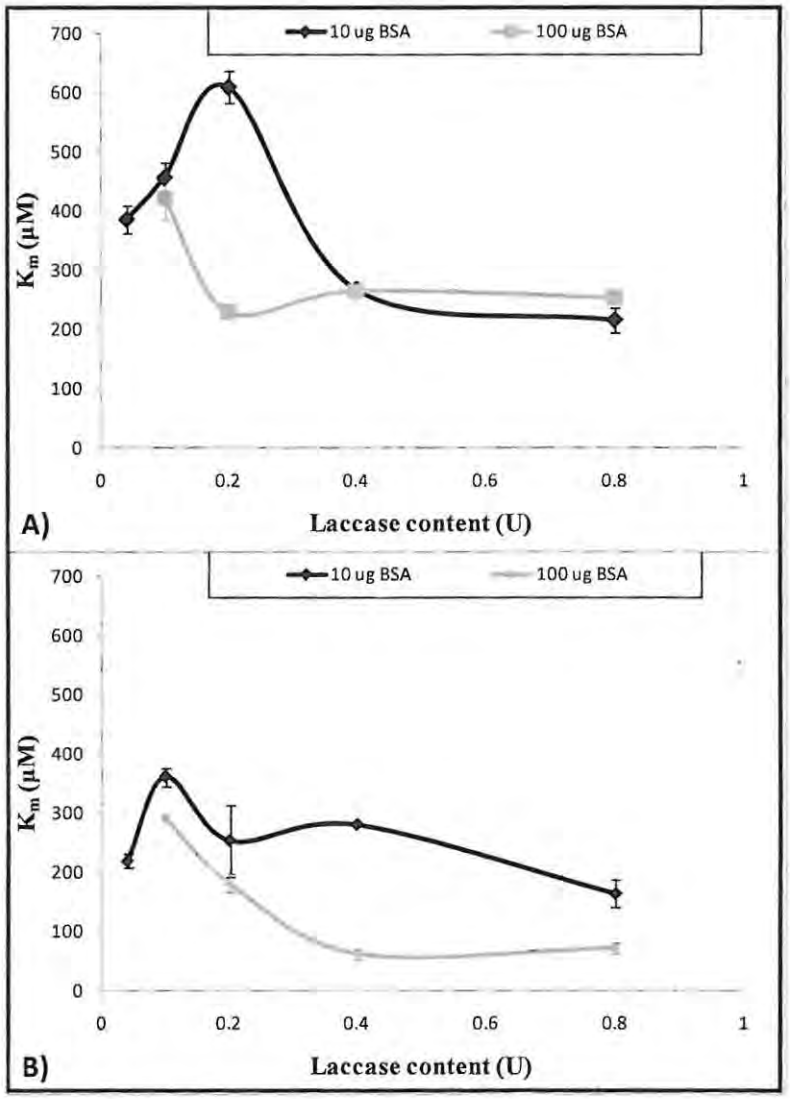

Figure 4.15: K_m values recorded for sensitivities recorded biosensors fabricated with varying concentrations of laccase using BSA co-immobilised at an amount of either 10 or 100 µg per biosensor.

A) Pristine biosensors

B) Re-used biosensors

Y-axes are maintained between Figure 4.15**A** and **B** in order to depict differences occurring during re-use of sensor. Error bars indicate standard error from the mean with $n \geq 3$

Apart from a single aberration in the data (10 µg laccase, 10 µg BSA), the K_m values prior to re-use are relatively close for both categories of BSA content and show a similar decrease with an increase in laccase content. Interestingly, upon re-use, modelled K_m values for sensors fabricated with 100 µg BSA content remain consistently lower when compared to their 10 µg BSA counterparts.

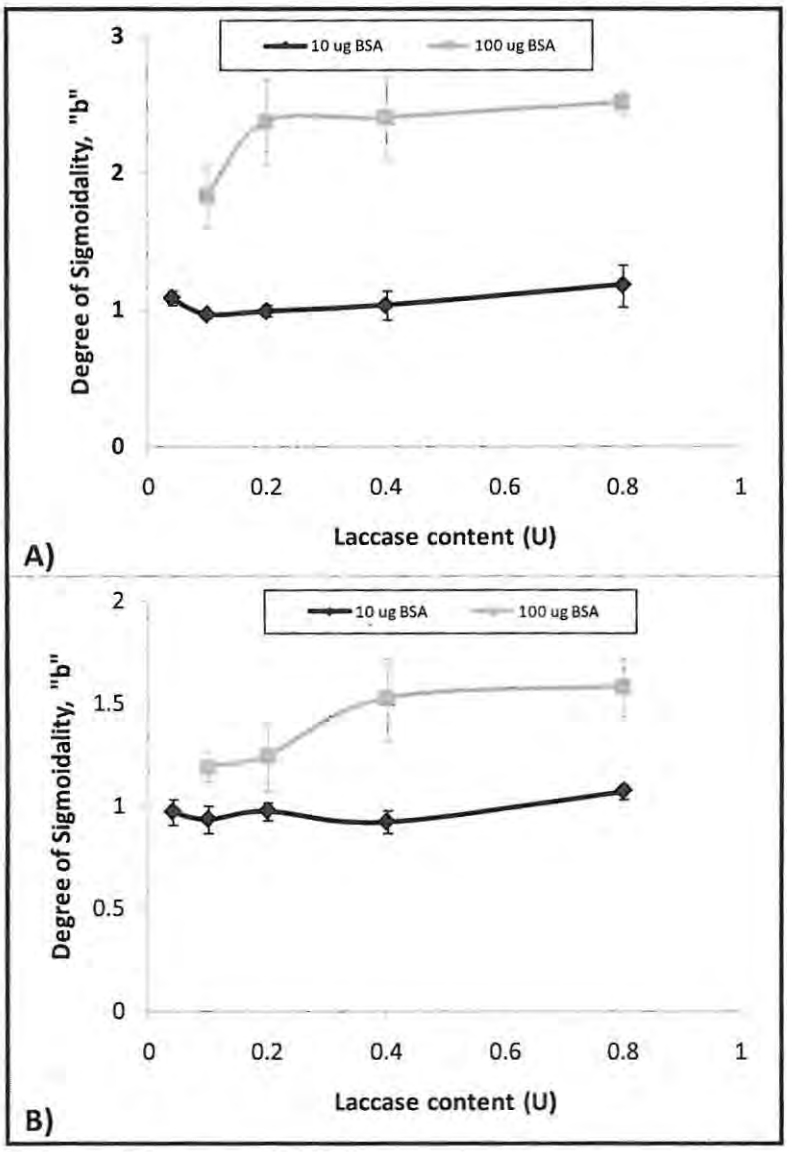

Figure 4.16: Degree of sigmoidality of biosensors at differing laccase contents, co-immobilised with 10 or 100 µg BSA per biosensor.

Error bars indicate standard deviation from the mean, $n \geq 3$.

From inspection of Figure 4.16, it is apparent that the presence of BSA at high concentrations is mainly responsible for the increase in sigmoidality between the two separate categories selected for this study. While an increase in the model's *b* parameter is noted with an increase in laccase content for the sensors fabricated with 100 μg BSA/electrode, no significant increase in b occurs in sensors fabricated with 10 μg BSA/electrode. Hence, the differences between the sigmoidality of the current-concentration functions are more pronounced with increases in BSA, rather than those of laccase.

Following re-use, the degree of the decrease of sigmoidality appears to depend negatively on the content of BSA and positively on the content of laccase. A significant decrease in sigmoidality (from b ~ 2.5 to ~1.25) is noted with high-BSA films following re-use, while no significant decrease in note for films fabricated with a low BSA loading.

Figure 4.17 depicts the relative alteration in the operational parameters of the sensors, following electrode re-use.

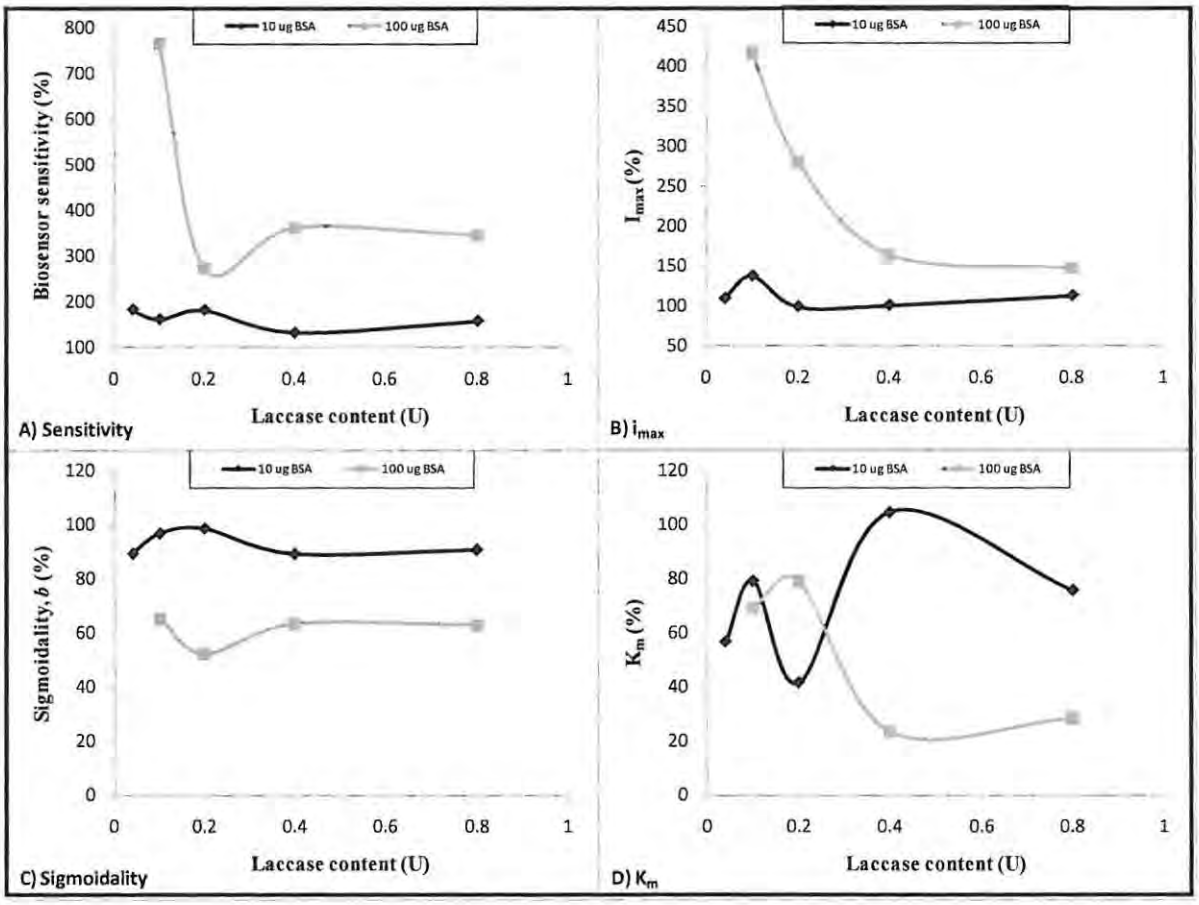

Figure 4.17: Relative alterations in operational parameters of laccase biosensors fabricated with low-BSA (10 µg BSA) and high-BSA (100 µg BSA) loadings, following re-use of the sensor.

Alterations in A) Biosensor detection sensitivity, B) i_{max} parameter C) sigmoidality, represented as the model parameter *b* and D) the modelled K_m were tracked and recorded.

Values were calculated using data previously reported on in this section. Number of observations, $n \geq 3$

Error bars were removed for purposes of clarity.

The improvement in i_{max} parameters following re-use (Figure 4.17**A**) shows an exponential decrease with an increase in laccase loading for biosensors fabricated using 100 µg of BSA. In contrast, sensors fabricated with low BSA content (i.e. 10 µg BSA / sensor) showed almost no improvement in the I_{max} parameters, with only slight improvements noted when laccase loading was less than 10 µg. It is also quite clear that the degree of improvement upon re-use is much higher in the presence of higher loadings of BSA. These two observations combined indicate that increase in I_{max} is apparently governed primarily by the absolute concentration of BSA and, inversely, by the amount of laccase used to fabricate the sensor.

Similar trends are noted for the biosensor sensitivity (Figure 4.17**B**). While it appears to undergo a more complex behaviour than attributed to the i_{max} parameter, this is most likely due to the contribution that the decrease in modelled K_m values (Figure 4.17**C**) provides to the biosensor sensitivity, as discussed when considering differences between sensors fabricated with consistent laccase loadings and varying BSA contents and depicted in Figure 4.14. For all sensors tested in this phase of research, biosensor sensitivity improved – however, the degree of improvement noted was much higher in sensors fabricated with high BSA contents, most likely due to the improvement in I_{max} values recorded in Figure 4.17**A**. The implications for these trends are much the same as those discussed for I_{max} parameters in the paragraph above.

A large, significant decrease in the degree of sigmoidality (Figure 4.17**C**) is noted with sensors fabricated with 100 µg BSA / sensor. The degree of sigmoidality decreased by ~40 % for all electrodes investigated in this category upon re-use and appeared to be more or less consistent despite alterations in the amount of laccase used to fabricate the film, which may indicate that the degree of relative decrease of sigmoidality is governed primarily by the BSA content, and is perhaps weakly influenced by the amount of laccase added to fabricate the biosensor. This behaviour is contrasted against the behaviour of biosensors fabricated using low BSA additions, which showed little to no relative alteration in the sigmoidality of the current-concentration functions. This is most likely due to the Michaelis-Menten-like behaviour of the sensors prior to re-use (i.e. $b \approx 1$, Figure 4.20**A**) in this category, as well as a compliance with the trends noted above.

Of all the trends noted above, the lease consistent is that of the decrease in apparent Km of the sensor response (Figure 4.17**C**). In laccase films cross-linked in the presence of high concentrations of BSA, this response appears to produce a biphasic decreasing trend with an increase in laccase content. A nearly 5-fold decrease in the K_m is noted when laccase contents are larger than 18 µg, which would explain the sudden increase in biosensor sensitivity at higher laccase concentrations for this category of sensor noted in Figure 4.17**B**. The behaviour of the relative K_m decrease is more complex in laccase biosensors comprising of a lower BSA content: while a general decrease in the K_m is noted for most electrodes in this category upon re-use, there appears to be no consistent trend to be found when comparing this

alteration with the laccase content. However, sensors displaying higher than expected K_m alterations i.e. 5 and 18 μg laccase, also consistently display a degree of sigmoidality ($b < 1$) that indicates the presence of negative cooperativity occurring upon re-use (Figure 4.19**B**). This may increase the apparent K_m values, which in turn, increases the relative K_m alteration upon re-use.

In general, the behaviour of sensors following re-use indicates that enhancements in the operational parameters of the biosensor upon re-use is governed primarily and proportionately by the absolute concentration of BSA used in fabrication and. To a lesser extent, the operational parameters trend inversely by the amount of laccase used to fabricate the sensor, or rather the BSA : laccase ratio.

4.5.3. Investigations on the cause of sensor sigmoidality and effects of re-use in BSA-laccase composite sensors:

Bearing in mind the limitations of the Hill coefficient as an indication of cooperative behaviour (Chapter 2, Section 2.3.1.3: A review of the previous data indicates that the degree of apparent sigmoidality (1) increases with the amount of BSA co-immobilised with the laccase in the final biosensor (Figure 4.6) and (2) increases with an increase in laccase content (Figure 4.16). It is also apparent that the effects of re-use are also mediated by both the laccase and the BSA content (Section 4.5.2.2 and Section 4.5.2.3). The positive effects that re-use of the electrode has on the operational parameters of the biosensor when re-analysed are themselves worthy of further discussion. The following section details some of the possibilities that govern both of these phenomenon.

4.5.3.1. Sigmoidality:

A review of the data presented in Section 4.3.3.3 and 4.3.3.4 reveals that the majority of biosensor sensitivities displaying kinetics more complex than conventional Michaelis-Menten kinetics decreases the operational biosensor parameters deemed desirable (i_{max}, biosensor sensitivity, extension of the linear range), revealing them to be poor candidates for potential sensor applications. Indeed, only the biosensor comprising of 20 μg of BSA and 0.8 U initial activity of laccase is used as the thick-film biosensor in

proceeding Chapters. However, the mechanisms governing these kinetic alterations are still worthy of brief discussion and investigation, as they reveal the extent to which the loading of active enzyme and/or BSA as a co-immobilant dictate the operational parameters of the completed sensor. In this section, a theory regarding the interactions of these proteins is postulated and shown to be viable, from a mechanistic perspective.

The context-dependent increase in biosensor sigmoidality response was shown to be directly relatable to the Hill Equation (Section 4.3.3.1 and Appendix A3.1), with a non-trivial increase in the Hill co-efficient being equivalent to the 'b' parameter. Hence, the Hill coefficient, which is commonly referred to as H and n_H for mechanistic studies is used interchangeably with b for the kinetic estimations for the model used in chronoamperometric current-concentration functions in this research. This increase in the b model value was found to depend primarily on the BSA content of the biosensor under investigation (Figure 4.8), but also less significantly on the laccase content of the cross-linked sensor, under conditions of a high BSA loading (Figure 4.20).

As outlined in Chapter 2 of this Thesis, cooperativity, and allostericity in general, entails an oligomeric organisation of the enzymatic system (Garret and Grisham, 1999b). To date, very few fungal laccases are reported to have quarternary structures more complex than monomers. For fungally-secreted laccase, primarily monomers (Baldrian, 2006), some homodimers (Yaver et al., 1996; Baldrian, 2006) and, more rarely, heterodimers or larger oligomers (Baldrian, 2006; Giardina et al., 2007), of isozymes of laccase are reported to occur. Crystallographic (Piontek et al., 2002) and electrophoretic (e.g. Collins et al., 1996; Freixo et al., 2008; Matijošytė et al., 2008) investigations of laccases secreted by the fungus *Trametes versicolor* (used in this research) overwhelmingly report on the presence of monomeric structures: indeed, this is the case when laccase of the same type sourced from the same supplier was assessed (Matijošytė et al., 2008; Birlhani and Yesilada, 2010; Uthandi et al., 2010).

Positive cooperative effects may arise from separate mechanisms other than a natural tendency to oligomerise. Allosteric biosensors have been fabricated, through protein engineering (conferring of

kinetic-acitivating binding sites or greater binding site flexibility) or through inducing the oligomerisation of protein monomers into subunits (Villaverde, 2003). Very few naturally-occurring allosteric enzymes are used, as their modulators are generally not of importance for analysis (Villaverde, 2003

Given the above information it is thus, unlikely to suggest that a natural tendency towards self-oligomerisation is the cause of this sigmoidal response. The mechanistic evidence suggested by cross-linked enzymes in the absence of BSA, or in the presence of low concentrations of BSA, (Section 4.3.3.1, Figure 4.8) consistently possess sigmoidality values closely approaching that of b = 1 (i.e. with no positive-cooperativity noted).

While cross-linking techniques, including the use of glutaraldehyde, have been previously used as a means of both stabilising naturally-occuring oligomers (Hermann et al., 1981; Jaenicke, 1982; Phizicky and Fields, 1995; Löster and Josíc, 1997) and inducing the formation of artificial oligomers/aggregates (Hermann et al., 1981; Jaenicke, 1982; Löster and Josíc, 1997), it is also unlikely that this is the case. Certainly, no other works that make use of cross-linking laccases has made mention of this phenomenon.

The increase in the degree of (apparent) subunit association as indicated via monitoring of the sigmoidality parameter *b* occurs with an increase in the amount of BSA loaded (Figure 4.6, Figure 4.16) Cooperativity models explicitly state that catalytically subunits must be in very close proximity in order for the binding of a substrate to a subunit to affect another; however, an increase in the BSA content increases the degree of cooperativity noted. Finally, the absence of BSA during sensor fabrication appears to produce a sensor with Michaelis-Menten-like kinetics (Figure 4.8). This evidence reinforces the notion that this apparent oligomerisation is not an intrinsic property of the laccase during the cross-linking process. Rather, it is proposed that the apparent sigmoidality of response is due to the effects of BSA on the products of oxidation.

A search through the literature indicates that BSA is able to bind a variety of phenolic compounds (Section 4.2.2), including catechol (McManus et al., 1985). To investigate whether BSA inclusion has any binding ability towards the oxidation products of catechol, cyclic voltammograms were generated in

the presence of 1 mM catechol using electrodes fabricated only with cross-linked BSA at varying BSA content. These CVs reveals a tendency away from the electrochemical reversibility of catechol oxidation/reduction found at non-modified GCEs with increasing BSA film content. The decline in reversibility appears to occur through a decrease in the cathodic peak associated with the reduction of *o*-benzoquinone (Figure 4.17, below)

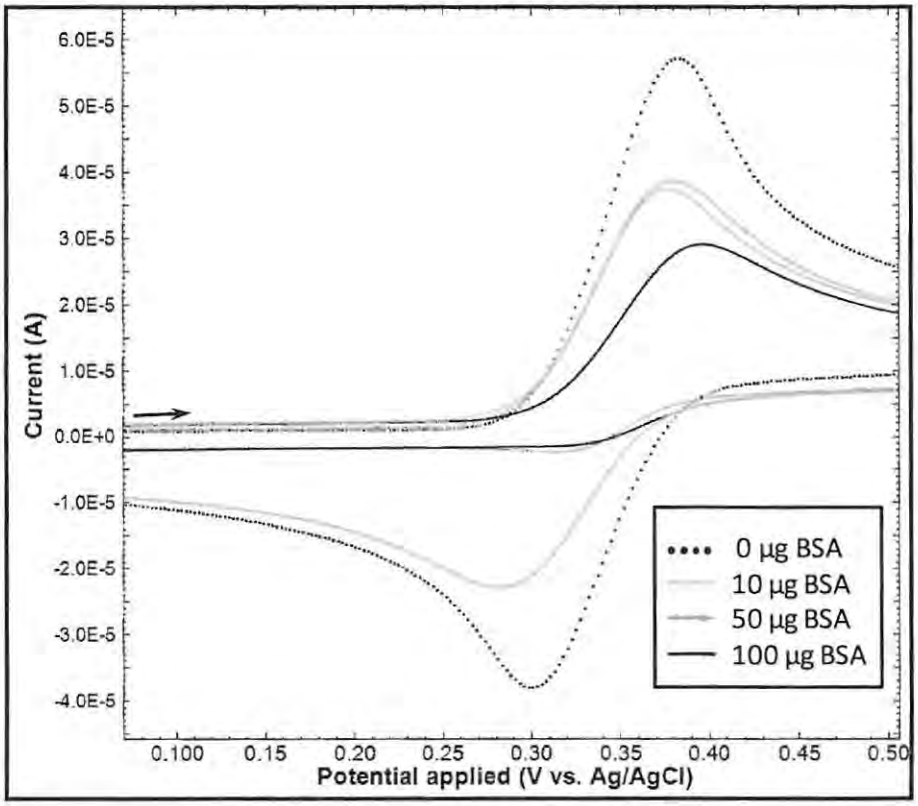

Figure 4.18: Representative Cyclic voltammograms generated showed the oxidation/reduction behaviour of 1 mM catechol in SLB, pH 4.5 when scanned using electrodes coated with cross-linked films of varying BSA content.

Inset legend indicates the amounts of BSA used in fabricating the cross-linked film. Arrow indicates starting direction of scanning, from anodic (oxidation) to cathodic (reduction) sweeps.

Scanning rate = 0.1 $V.s^{-1}$

Even though there is a decrease observable in the oxidation peak current in Figure 4.18 (above) associated with the increased diffusional constraints of catechol through the film, there is a more pronounced decrease occurring in the reductive peak with an increase in BSA. This causes the catechol oxidation/reduction profile to shift from reversible (0 µg BSA) to nearly irreversible (100 µg BSA)

behaviour. BSA thus appears to act as a trap for the oxidation products of catechol following electrooxidation, as indicated in the literature (Kulys et al., 2002). Following exposure of the BSA-film electrodes to oxidised catechol (200 μM in 5 mls of SLB, pH 4.5, for 5 minutes), this apparent trapping effect declines and the electrode response begins to attain degrees of reversibility associated with bare GCEs.

Table 4.4 displays a summary of the effects of the deposition of cross-linked BSA of varying concentration on the resultant catechol oxidation/reduction.

Table 4.4: Electrochemical parameters of catechol and o-benzoquinone through cross-linked films of differing BSA contents.

BSA (μg)	Ep,a (V)[1]	Ep,c (V)[1]	10^6 x D_{Ox}[2] ($cm^2.s^{-1}$)	10^6 x D_{Red}[3] ($cm^2.s^{-1}$)	$I_{p,a}/I_{p,c}$[4]	D_{Ox}/D_{Red}
0	0.375	0.300	3.26	2.92	0.867	0.897
5	0.384	0.272	2.89	2.38	0.777	0.824
10	0.380	0.280	2.37	1.89	0.749	0.798
20	0.393	0.271	1.68	1.19	0.630	0.709
50	0.412	0.310	0.46	0.05	0.213	0.091
100	0.410	0.310	0.38	0.04	0.255	0.110
100 (ox.)[a]	0.406	0.302	0.60	0.49	0.628	0.812

Unless otherwise indicated, values report on averages of 3 independent measurements conducted at a scan rate of 0.1 $V.s^{-1}$

[1] – vs. Ag/AgCl. Mean values of $\geq$ 3 independent measurements reported $\pm$ 10 mV

[2] – i.e. of catechol

[3] – i.e. of *o*-benzoquinone

[a] – following exposure of the film to laccase-oxidised catechol

From Table 4.4: In the regime of BSA of [0] to [20], diffusion coefficients of both unoxidised and oxidised forms of catechol decline slowly and stably and the degree of reversibility declines negligibly. However, after BSA loadings greater than 20 $mg.ml^{-1}$ [stock] BSA concentration, both peak reversibility ($I_{p,a}/I_{p,c}$) and the diffusion coefficient parity (D_{Ox}/D_{Red}) through the film decline significantly. The behaviour of the respective diffusion coefficients is presented in Figure 4.19.

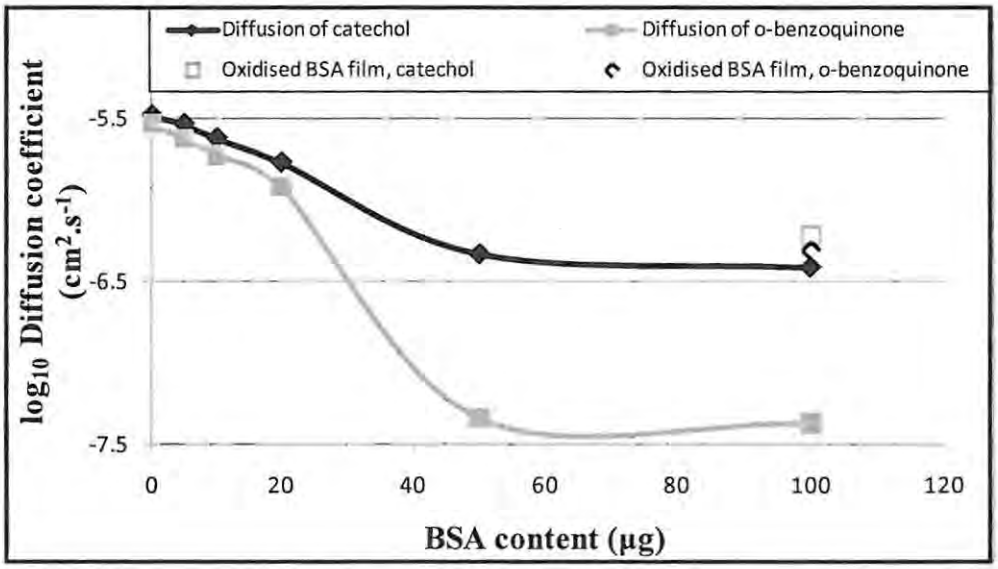

Figure 4.19: Logarithm of diffusional coefficients for both catechol and o-benzoquinone compared to the amount of BSA used in fabricating cross-linked films.

Hence, the apparent sigmoidality is proposed to be caused by a combination of diffusional constraints and oxidation product trapping itself caused by the presence of BSA. During the course of analysis of the biosensor, the interaction between oxidised product (generated by laccase exposed to the substrate) and BSA saturates the BSA film with oxidised products, diminishing the trapping effect of BSA. The increased diffusional coefficients of both catechol and o-benzoquinone are likely due to the relaxing of diffusional constraints placed on the mass transport of substrate to the enzyme and the transport of the product to the electrode. This is most likely due to internal rearrangement of the film caused by the interaction of BSA with the products of laccase-based oxidation of catechol. Only one published article has indicated that serum albumins, both HSA and BSA, interact with the radicalised products of laccase-oxidation (Kulys et al., 2002). From the aforementioned research, it was found that methyl-syringate, following laccase oxidation, resulted in inactivation of laccase *in vitro*, and that the use of BSA/HSA reduced the level of inactivation, through binding of the phenoxy radical in the hydrophobic pockets of BSA/HSA. The inclusion of albumin was also found to decrease the apparent K_m of the reaction and to enhance the velocity of reaction, similar to the findings of this phase of research involving immobilised BSA and laccase.

4.5.3.2 Re-use:

Of further interest from the research detailed in the above sections is the decreasing sigmoidality, and enhanced biosensor parameters, that occur during the re-use of the electrode. While this phenomenon produces a biosensor with more desirable analytical properties, including a significant improvement in the detection limits of catechol, the addition of a further preparative stage could lead to a greater degree of sensor response deviation during transport/storage and application stages of analysis, and demands a greater degree of understanding and explanation.

The behaviour of the biosensor upon re-use, is itself explainable when the recorded biosensor kinetics are analysed using the interaction between BSA and the oxidation products, as outlined above. Mechanistically, the effects of re-use are analogous to the inclusion of the binding of a heterotropic effector (A) to a subunit, as indicated in the M-W-C model of allostericity (Figure 2.3). If substrate-binding and effector-binding only occurs in the R state to form RA, then the equilibrium of T/R is shifted in much the same manner as with the introduction of substrate. This, in turn, leads to an increase of apparent velocity; itself presented as a decrease in the K' (i.e. K_m) value, coupled with a decrease in cooperativity (Garret and Grisham, 1999a). That the effects of re-use are themselves dependent on both the absolute concentration of BSA co-immobilised (Figure 4.12) and less-so on the loading of laccase in films with a low BSA content (Figure 4.17) implies that modification of the BSA occurring during the catalytic function of laccase is necessary for this process and that modification of the laccase molecules themselves are, if occurring, less prevalent for dictating this process.

The apparent decrease in sigmoidality and K_m can be attributed to a decrease in the signal-inhibiting (product-trapping) ability of BSA when re-used, in the same manner by which exposure of the BSA film to oxidised catechol products enhances the rate of reversibility of catechol oxidation/reduction (Table 4.4). As more oxidised product reaches the electrode at low substrate concentrations, the sensor response approaches that of the biochemical kinetics and exhibits the anticipated Michaelis-Menten-like behaviour anticipated for the biosensor, simultaneously decreasing both the degree of sigmoidality and the apparent K_m, through decreasing the initial signal inhibition caused by the presence of BSA. These factors may

also be improved through enhanced mass transport through the film - the increases noted for the diffusion of both catechol and its oxidation product through BSA films previously exposed to catechol oxidation products (Figure 4.19 and Table 4.4) indicate faster mass-transport occurring through the film, which may also improve sensor response. This explains the dependence of the relative decreases in these parameters upon the concentration of BSA (Figures 4.12**B**, 4.17**B**, 4.17**C**). The decline of K_m values of re-used sensors with increasing BSA content (Figures 4.9, Figures 4.15) may be explained through the stabilisation of laccase conformation during immobilisation through the inclusion of BSA, as is expected from the literature.

The increases in i_{max} values upon re-use (Figure 4.7 and Figure 4.14) are considered to have two origins. Similar to the explanation discussing shifts in K_m and sigmoidality, the decrease in BSA-based signal inhibition upon re-use would have the effect of increasing i_{max}. However, a reaction pertinent to GCE surfaces also appears to enhance sensor response. Prior to the re-calibration of re-used sensors using substrate, CVs generated in the absence of substrate revealed the presence of reduction/oxidation couples at more negative potentials than recorded for catechol oxidation/reduction. This phenomenon is not recorded when using gold-surfaced electrodes (AuEs) for the same biosensor configuration (data for AuEs presented and discussed in Chapter 6 of this Thesis). Figure 4.20 displays representative CVs of this phenomenon.

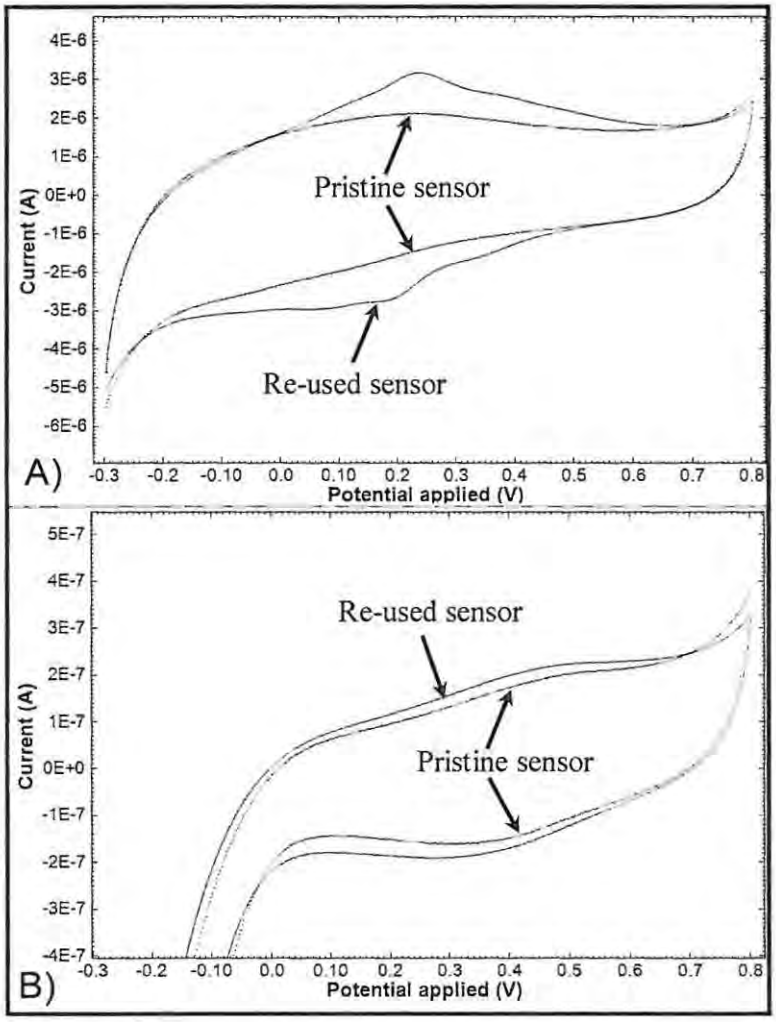

Figure 4.20: CVs generated in SLB performed on pristine and re-used biosensors in the absence of catechol.
A) GCE surfaces
B) AuE surfaces
CVs performed at 0.1 $V.s^{-1}$ in a solution of SLB, pH 4.5

As Figure 4.20 demonstrates, the presence of non-catechol redox peaks on re-used sensors appears to be restricted to GCE surfaces, and do not appear on AuE surfaces. Similarly, significant increases in the i_{max} parameter are not found when considering AuEs as transducer surfaces for laccases biosensors (Chapter 6), indicating that significant increases of i_{max} for re-used sensors fabricated on GCE surfaces is linked to the appearance of these peaks. Furthermore, varying the scan-rate of cyclic voltammetry at re-used GCE sensors indicates that these peaks are attached to the surface of the electrode, rather than being controlled via diffusion (data not shown). This is considered to be due to the attachment of catechol

oxidation products to the electrode surface, a phenomenon known as fouling which is discussed in further detail in Chapter 5 of this Thesis. Fouling, which usually inhibits electrode reactions, appears to be improving the sensor operational parameters in this instance (and when considering certain other substrates, as discussed in Chapter 5) by mechanisms which are not yet clear.

Detection sensitivity, which has been shown to be positively influenced by i_{max} and negatively influenced by K_m (exemplified in the correlation between sensitivity and the i/K values, Figures 4.10 and 4.11) is thereby altered by the alterations in the K_m and i_{max} parameters, for the reasons outlined above.

4.6. Conclusions:

Of the three immobilisation strategies investigated, glutaraldehyde cross-linking of laccase to GCE surfaces yielded the highest sensitivity and was selected for further optimisation.

The sigmoidal model outlined in Chapter 2 was successfully applied to both highly-sigmoidal and hyperbolic graphic functions and extracted parameters from current-curve functions that were consistent between biosensors of the same configuration. This is an important finding, as it demonstrates that, using simple, commercially-ubiquitous software, consistent kinetic parameter estimations can take place, which is a valuable trait when considering the applicability of biosensors.

The inclusion of BSA during glutaraldehyde cross-linking of laccase during biosensor fabrication not only improves operational parameters (K_m, i_{max}, sensitivity) but also has the valuable trait of normalising protein content between batches of laccase. Since the laccases sourced have different specific activities and therefore different degrees of purity, this ensures that only activity needs to be normalised between batches. In addition to this, the use of glutaraldehyde will affect different protein concentrations differently, so this regulates the degree of inactivation between sourced laccases, improving fabrication consistency. This is especially important when considering that this laccase was sourced from a commercial supplier, which normally cannot guarantee purification of laccase to homogeneity.

The studies reported in this Chapter lead us to conclude that the sigmoidal behaviour of the biosensor is related to both the absolute concentration of BSA present as co-immobilant, and is further influenced by the relative laccase-BSA concentration. Electrochemical investigations of BSA cross-linked films in the absence of laccase, but in the presence of catechol, indicates that the oxidation product/s of phenolic substrates bind to BSA, causing a significant decrease in the apparent diffusion coefficient of catechol's oxidised quinone counterpart, o-benzoquinone. Following saturation of the film with oxidised substrate, diffusion coefficients on both unoxidised and oxidised substrates relax, the latter less significantly than the former. In addition to BSA-oxidation product interactions, the attachment of oxidation products to GCE surfaces appears to enhance sensor function, increasing the i_{max} values upon re-use. Neither the presence of oxidation products nor improvement in i_{max} values following re-use are evident when examining re-use at gold electrodes (AuEs, reported on in greater detail in Chapter 6), indicating that this phenomenon pertains only to GCE surfaces, as opposed to a general attachment.

While sigmoidal current-concentration responses are analytically relevant, the concentration thereby being related to the current through the formalism of:

$$[S] = \frac{K_m^{app}}{(I / I_{max} - 1)^{1/n}} \qquad \text{Eq 4.3}$$

Where [S] is the substrate concentration and the other symbols follow from the sigmoidal model used i.e. K_m^{app} is the sigmoidal parameter = c, $I_{max} = d$ and $n = b$ (Kurganov et al., 2001).

Such a determination, however, has a tendency towards greater relative error in the accuracy of the current-concentration, especially in cases where the concentration lies outside the linear response region (Kurganov et al., 2001). The reasons for sigmoidality are discussed, as are their impacts on the other analytical parameters observed. This is considered to be an unnecessary complication of the biosensor (especially from the perspective of the end-user), but still raises some very interesting questions as to what mechanisms are underlying this deviation from the desired behaviour of the sensor.

Due to the interference from sigmoidality and the potential for variability of results upon re-use, the best concession, both in terms of beneficial properties conferred through BSA co-immobilisation, and the detrimental ones associated with the sigmoidality was found to be laccase fabricated via cross-linking at a pre-immobilisation activity of 0.8 U, in the presence of 20 μg BSA. This configuration of sensors were used onwards in the fabrication of sensors reported on in Chapters 5 and 6 of this Thesis.

Table 4.5: Properties reported with respect to catechol for optimised cross-linked biosensors fabricated using 20 μg of BSA and 0.8 U laccase.

Sensor Property	Value (pristine)	Value (re-used)
Sensitivity ($nA.\mu M^{-1}.cm^{-2}$)	970.5 ± 11.15	1864.4 ± 98.73
Linear range (μM)	3.8 – 135	0 – 90
i_{max} ($\mu A.cm^{-2}$)	238.9 ± 26.62	278.6 ± 14.48
Km (μM)	125.6 ± 8.717	78.63 ± 9.24
Degree of sigmoidality, b	1.65 ± 0.250	1.30 ± 0.147

These parameters compare very favourably to other amperometric biosensors reported in the literature (Table 4.1). Sensitivity of detection for catechol exhibits a maximum of ~1300 $nA.\mu M^{-1}.cm^{-2}$ with the examples obtained in literature, which is comparable to the initial sensitivities attained by the optimised laccase sensor and is exceeded during re-use of the sensor (Table 4.1). Those attaining these levels of sensitivity in Table 4.1 also exhibited a much lower linear range of detection than is reported here. Certainly, this sensor exhibits the highest degree of sensitivity of cross-linked biosensors cited from references included in Table 4.1

Prior to re-use, biosensor sensitivity and linear range are favourably comparable to those within its immobilisation class (cross-linking) detecting the same substrate (catechol), from the literature review presented in Table 4.1. After biosensor re-use, this increases to a value only exceeded by Yaropolov et al., 2005 in the detection of hydroquinone (Table 4.1).

Chapter 5: Electrochemical considerations for intra-phenolic substrate detection

5.1 Abstract:

The electroanalysis of phenolic compounds, either through direct electro-oxidation or through the use of biocatalysis, is complicated by the multiple oxidation products that could form as a result of the phenoxy-radical intermediate oxidation stage, some of which are not susceptible to electro-reduction. This complicates the detection of phenolic compounds through the bio-oxidation/electro-reduction mechanism in chronoamperometric laccase biosensors. Herein, we propose a combined approach that seeks to correlate biosensor signal current with both the phenolic-enzyme kinetics (i.e. the suitability of a phenolic species to act as a substrate for oxidation by laccase) and the product-electrode kinetics (i.e. the suitability of the oxidised products to act as analytes for electrochemical detection) during the operation of the biosensor.

In addition, the tendency of analytes to passivate ('foul') the electrode surface by adsorption is also assessed with aims to investigate the feasibility of re-use when considering detection of certain analytes. The tendency of phenolic substrates to foul the electrode surface during electrooxidation was compared to biosensor operational kinetics during the re-use of the electrode following exposure of the sensor to phenolic compounds.

Substrate-enzyme kinetics were monitored through modelling of chronoamperometric data obtained using a crosslinked laccase-bovine serum albumin biosensor, which was optimised in the previous Chapter (Chapter 4) with respect to catechol detection. The K_m value derived from this model was used as a basis for assessing the relative substrate-laccase affinity and was considered to be a property solely derived from biochemical kinetics. i_{max} and biosensor sensitivity, in comparison, were assumed to be governed through a combination of electrochemical and biochemical interactions in the aforementioned substrate/analyte contributions to signal current.

Current yields, through reduction/oxidation of proposed substrates at anodically-pretreated glassy carbon electrodes (Chapter 3), was employed to assess the electroactivity of both the substrate during oxidation and the oxidised product in order to assess the relative signal strength / amount substrate oxidised. While comparisons of substrate-dependant oxidation potentials showed a limited, category-restricted, correlation to the substrate-dependent detection sensitivity, a new parameter comprised of relative current yields with relative enzyme-substrate affinities (K_m) was successfully correlated to substrate-dependent detection sensitivity.

Fouling at the electrode surface was assessed through a decrease in current response during repeated oxidation/reduction of the compound at the electrode surface. In particular, the occurrence of fouling at unmodified GCE surfaces was shown to indicate passivating behaviour of substrates when considering biosensor response upon re-use of the sensor.

5.2 Introduction:

5.2.1: Analyte specificity:

Analyte specificity is a highly desirable property for biosensor technologies. The presence of non-specific signal complicates the analysis, leading to the possibility of false positives (in qualitative analyses) and over/under-estimation of the analyte of interest (quantitative). The routine presence of compounds generating non-specific signals requires laborious sample pre-analysis treatments or post-analysis data treatments in order to disentangle the desired signals from the prepared signals. This has the effect of further increasing the time and complexity of analyte detection, making the application of a biosensor in this context less appealing to potential end-users. These factors combined obviate the main advantages cited for biosensor usage – those of selectivity and rapidity of analysis.

As discussed previously (Chapter 1, Section 1.2.3), biosensors possess an inherent tendency towards specificity due to the specificity of biorecognition events. Since most biorecognition agents bind a very

narrow range of analytes, this greatly decreases the possibility for non-desired reactions to occur, limiting the effects of non-specific signal generation from occurring.

However, a caveat exists in the case of phenolic detection. The variations in structure and exposure effects existing between phenolic compounds (Chapter 1, Section 1.2.1.2) indicates that the detection of phenolics also requires a degree of discrimination, and that it is analytically insufficient to perform assays of the total phenolic content of a given sample. The inability of a given sensor configuration to distinguish between a neutral/beneficial phenolic compound or a detrimental one in a given matrix greatly limits the applicability of this technology from all but absolute quantifications of phenolics in a given sample. Thus, discrimination between phenolic species during detection remains a highly desirable trait when considering the deployment of this technology.

5.2.2: Considerations of substrate ranges for laccase biosensor application

A primary characteristic of laccases are their broad substrate ranges (Claus, 2004). A wide variety of compounds are amenable to oxidation via electron exchange with the T_1 copper ion embedded in the active site of laccases. Apart from *ortho-* and *para*-substituted diphenolic compounds (Couto et al., 2006), polyphenols (Call and Mücke, 1997; Couto et al., 2006), anilines (Claus, 2004; Couto et al., 2006) and polyamines(Call and Mücke, 1997; Couto et al., 2006), nitroaromatics (Claus, 2004), ascorbic acid (Call and Mücke, 1997), aryl diamines(Call and Mücke, 1997; Couto et al., 2006), thiols (Couto et al., 2006); inorganic ions e.g. Mn (Call and Mücke, 1997; Claus, 2004; Couto et al., 2006), chelated metal ions e.g. ferrocyanide (Couto et al., 2006) and other aromatic alcohols (Claus, 2004) are all potential reducing substrates for laccase. In the occurrence of steric hindrance preventing direct substrate-laccase interaction, this is sometimes circumvented through the use of electron-transfer mediators transporting electrons between substrate and laccase (Call and Mücke, 1997; Couto et al., 2006), which further increases the range of potential substrates. These reported compounds that are potentially suitable for laccase oxidation constitute a relatively large array of both natural and xenobiotic compounds. As such,

they must themselves be considered as potential co-analytes/interferents when sample analyses on complex matrices are performed.

Although it is widely accepted that laccases possess very broad substrate ranges, this phenomenon is mitigated by the fact that laccases display preferential binding kinetics to different substrates, which is explored in greater detail below. Preferential substrate-binding kinetics have been assessed as a means of providing a discrimination between co-analytes in a complex matrix.

5.2.2.1 Preferential substrate-binding kinetics within the *o*- and *p*-diphenol classes: substituent effects

Even within the group of compounds classifiable as *o*- and *p*-diphenol compounds, there exist significant differences reported in enzymatic activity towards different phenolics by laccases. The presence and location of substituents on the benzene ring has a great influence on the relative activity of a given laccase (Xu, 1996). In a study conducted by Xu, 1996, the following substituent effects were notable:

- The presence of electron-withdrawing groups ($-NO_2$, $-COCH_3$) increase the oxidation potential of the hydroxyl group, decreasing oxidation rate by increasing K_m and decreasing k_{cat}, evident as a decrease in the logarithm of k_{cat}/K_m. The opposite effect was noted for electron-donating groups (-H, -OH, $-CH_3$, $-OCH_3$,C_2H_5).
- With smaller ortho-substituents (i.e. those listed above), the effect of electron withdrawal/donation is more important than possible steric hindrance. This correlation was not evident for para-substituents for the laccase examined in the study.

The reduction of diooxygen (oxidising substrate) to water is more constant between laccases. Both the variance of K_m between different fungal laccases (20 - 50 μM) and its dependence on pH are much more stable than is reported of the reducing substrate (Xu, 2001).

5.2.2.2 Preferential substrate-binding kinetics within the *o*- and *p*-diphenol classes: enzyme effects

Irrespective of substituent effects, laccases possess varying activities towards different reducing substrates. There is significant research interest in exploring whether variations in interaction affinities between laccases and different substrates could be exploited as a means of promoting catalysis of certain phenolics over others. These differences, while still following certain principles regarding the nature and location of additional substituents (Xu, 1996; Xu, 1997), also vary substantially between the laccase being studied (e.g. Shleev et al., 2004), making generalised characterisation of laccases impossible.

This difference is present when comparing laccases sourced from different strains, or between different isozymes produced by the same culture (e.gs Bourbonnais et al., 1995; Collins et al., 1996). Articles reporting on the biochemical characterisation of a given laccase routinely demonstrate that the recorded laccase activities (Jung et. al., 2002; Robles et al., 2002; Saito et al., 2003; Jordaan et al., 2004; Ibrahim et al., 2010), catalytic rate constant/s and K_m value/s (Robles et al., 2002; Saito et al., 2003; Jordaan et al., 2004; Klis et al., 2007) and pH optima (Jung et. al., 2002; Robles et al., 2002; Quan et al., 2003; Jordaan et al., 2004; Chakroun et al., 2010; Ibrahim et al., 2010) are based on specific substrate-laccase interactions, and differ accordingly. These interactions have been explored using various techniques – while UV/VIS spectroscopic studies of these phenomena are perhaps the most commonly reported (Jung et. al., 2002; Robles et al., 2002; Saito et al., 2003; Jordaan et al., 2004; Klis et al., 2007; Chakroun et al., 2010; Ibrahim et al., 2010), electroanalytical techniques employing both immobilised laccases (e.gs Ahn et al., 2007b; Quan et al., 2003) and solution-phase laccase electroanalytical assays (e.g.s Garzillo et al., 1998; Klis et al., 2007; Frasconi et al., 2010; Ibrahim et al., 2010) form a significant contribution to this ongoing research interest.

Table 5.1 provides a brief quantitative overview of the relative biochemical parameters and kinetics extracted from literature for a selection of substrates' interactions with laccases isolated from *Trametes versicolor* cultures: the fungal source of the laccase used as the biorecognition element of biosensors investigated in this Thesis. Table 5.1 is divided between values extracted from published studies characterising *T. versicolor* laccase-substrate interactions in general (Table 5.1.1), and two further

distinctions that are important – the effects of substrate-specificity interactions before and after immobilisation (Table 5.1.2) and studies comparing substrate preference between isozymes isolated from the same fungal culture (Table 5.1.3).

Table 5.1: Overview of relative substrate affinities for different substrates reported for laccases isolated from *T. versicolor*.

Substrate	pH optima[a]	K_m (μM)	k_2 (s^{-1})	Activity ($U.mg^{-1}$)	Analytical Method	Reference
5.1.1. General overview						
ABTS Hydroquinone	-	455 856	-	-	Voltammetric	Klis et al., 2007
ABTS Dimethoxyphenol Syringaldazine	2.5 3.5 4.0	37 15 -	-	-	Spectroscopy	Baldrian, 2006
Catechol Guaiacol Hydroquinone	4.0 3.5 4.0	-	-	-	Spectroscopy, manometry	Fåhraeus and Ljunggren, 1960
ABTS	4.5	620	-	-	Spectroscopy	Pazarlıoğlu et al., 2005
ABTS 2,4-dichlorophenol	3.5 -	800 350	-	8.000 0.021	HPLC (UV/Vis)	Gianfreda et al., 1998
5.1.2. Free vs. immobilised forms of laccase						
ABTS Catechol Guaiacol Pyrogallol Syringaldazine	5.0	141 539 623 149 741	23.62 6.36 5.6 2.31 9.03	21155 5699 5014 2067 8085	Spectroscopy	Roy and Abraham, 2006 (free) [1]
ABTS Catechol Guaiacol Pyrogallol Syringaldazine	5.0	859 2717 1059 1113 1684	3.21 0.879 0.544 0.081 0.044	2873.2 787.1 487.2 72.7 39.4	Spectroscopy	Roy and Abraham, 2006 (immob.) [2]
Syringaldazine	5.5	9.4	-	21.7	Spectroscopy	Bayramoglu et al., 2010 (free)
Syringaldazine	5.0	19.7	-	15.6	Spectroscopy	Bayramoglu et al., 2010 (immob.)
ABTS Syringaldazine Catechol Dopamine Ferricyanide	5.0	130 66 1110 2100 830	130 77 115 186 215	-	Voltammetry	Frasconi et al., 2010 (free)
ABTS Syringaldazine Catechol Dopamine Ferricyanide	5.0	110 58 740 1200 640	-	-	Voltammetry	Frasconi et al., 2010 (immob.)

(cont. overleaf)

[a] – where underlined, indicates pH at which other reported values were elucidated from, not optimal pH.

[1] – (free): published parameters for the unimmobilised enzyme system reported in this subsection

[2] – (immob.): parameters of immobilised laccase reported herein, for the same reference as in [1]

Substrate	pH optima[a]	K_m (μM)	k_2 (s^{-1})	Activity ($U.mg^{-1}$)	Analytical Method	Reference
5.1.3. Between Isozymes						
ABTS Guaiacol Syringaldazine Vanilyll alcohol	5.0	-	-	1.30 0.15 1.37 0.078	Spectroscopy	Bourbonnais et al., 1995[3]
ABTS Guaiacol Syringaldazine Vanilyll alcohol	5.0	-	-	1.30 0.12 1.00 0.059	Spectroscopy	Bourbonnais et al., 1995[4]
ABTS	1.9 - 3.1	-	-	2.6 – 36.3	Spectroscopy	Koschorreck et al., 2008[5]

Unless otherwise indicated, reported values are obtained from 'free' i.e. dissolved laccases.

[3] – Isozyme I of laccase in Reference. Activity reported in δOD/min.

[4] – Isozyme II of laccase in Reference. Activity reported in δOD/min

[5]– lowest to highest values reported from four recombinant laccase isozymes cloned from *T. versicolor* and expressed in *Pichia pastoris* from this reference

Table 5.1 provides a numerical overview that highlights the degree of variability between reported laccase substrates. As is readily apparent from the tabulated references, any investigation between the biochemical parameters of specific substrate-laccase interactions show marked differences depending on the laccase and the substrate used. The lack of consensus in the reported values of pH optima and K_m values for the most commonly used phenolic substrate (e.gs pH optima of ABTS, Table 5.1.1 and 5.1.2, reported K_m values of catechol at a pH of 5.0, Table 5.1.1 and 5.1.2) strongly indicate a lack of homogeneity of the substrate affinities between laccase enzymes isolated in the articles reported herein. The reported pH optima of the laccase-ABTS interaction, for example, range between 1.9 and 4.5 within the references used in compiling Table 5.1.

Part of the reason behind the disparities in reported biochemical characterisations may also lie in the uncertainty as to which of the number of isozymes present in *T. versicolor* cultures was characterised in the studies from which these values were extracted. The various isozymes of *T. versicolor* laccase show marked distinctions between their substrate affinities as Table 5.1.3 shows. A further plausible reason

may lie in primary/secondary/tertiary structural differences between laccases produced by different strains of the same species.

Critical to the research considerations in this Thesis, the act of immobilisation of the laccase (Table 5.1.2) also alters both the absolute and relative affinities for reducing substrates. An example of alterations in the relative substrate affinities is apparent in the study conducted by Roy and Abraham (2006). Therein, the K_m for ABTS increased 6.1-fold when laccase was immobilised via cross-linking, while the K_m for guaiacol increases by only a factor of 1.7. Similarly, the reported k_{cat} values for catechol and syringaldazine decrease by factors of 7.2 and 205 respectively, upon immobilisation. This indicates that the act of immobilisation, rather than altering the secondary/tertiary protein structure in a manner that affects all subsequent laccase-substrate interactions to the same extent, produces alterations that affect laccase-substrate interactions to differing degrees, in a substrate-specific manner.

This influence on the relative substrate affinities due to the aforementioned conditions (heterogeneity between isozymes, laccase-producing strains and alterations to substrate affinities upon immobilisation) indicates that, in the absence of standardisation of the source and type of laccase under investigation, it would be more meaningful to determine relative substrate affinities on a case-by-case basis, rather than through comparison with published values, or in differences between immobilised/unimmobilised laccases.

Irrespective of a lack of consensus, there is sufficient evidence to posit that there are exploitable differences existing in the biochemical parameters dictating specific substrate-laccase interactions when considering different substrates as analytes for detection using biosensors fabricated using a specified laccase. Control at the level of biorecognition provides a measure of control of intra-phenolic biosensor specificity in order to preferentially detect a desired substrate, or indeed to predict whether the substrate is readily detectable through this analytical technique. Investigations of laccase-dependent substrate specificity, combined with studies examining the relative electrochemical signal response generated through substrate oxidation, is thereby necessary in the successful prediction of a given substrate's ability to be detected through laccase-biosensor technologies.

5.2.3: Electroactivity:

In addition to differences between analytes based on their rate of oxidation, it is also important to consider the relative response each analyte produces upon oxidation by laccase. During electrochemical analysis using a biosensor, it is essential to know whether the potential substrates once oxidised results in product compounds that possess detectable reductive signal when interacting with the transducer i.e. are reducible. In a manner almost analogous to that of the molar extinction coefficient, E, as a measure of the chromophoretic ability of a compound during UV/Vis spectroscopy, the relative electroactivity of a given substrate's oxidised form also requires assessment.

Phenolic oxidation chemistry is a complex research area. The typical oxidation of a phenolic compound yields a phenoxy radical that can undergo electron-transfer reactions, radicalised chemistry and internal re-arrangement reactions with themselves, each other, unreacted phenolic compounds, or unrelated compounds present in the medium. Hence, assessments of this nature are complicated by the multiple end-products that potentially form following the oxidation of phenolics.

Due to the radicalised intermediates that precede the generation of a fully-oxidised product, the production of dimeric, polymeric, or degraded compounds without the formation of a quinone compound necessary for signal generation at the electrode surface can occur. By way of example, the investigation of products formed during the mono-electron oxidation of guaiacol conducted by Hwang et al. in 2008 determined that no less than 6 different monomeric and dimeric products of differing oxidation states (from fully-oxidised quinones to fully-reduced phenolics) are initially formed. Cross-reaction of these products with one-another, or the parent compound yielded still further monomeric/dimeric/polymeric compounds (Hwang et al., 2008). The complexity of oxidation pathways results in uncertainty of the relative proportion and nature of the end-products formed, in turn affecting the proportion of oxidised substrates that can be detected electrochemically.

While simple, hydroxyl-substituted, *para-* and *ortho-* phenolic compounds primarily generate their oxidised (quinone) counterparts, this may not necessarily be the case for other phenolics and non-

phenolics investigated during the course of this phase of research (e.g. amine substituents). To illustrate the scope of possible phenolic-oxidation products that can be produced, Figure 5.1 provides a schematic detailing the possible intermediates formed during the oxidation of unsubstituted phenol and the final products that are detectable via electro-reduction.

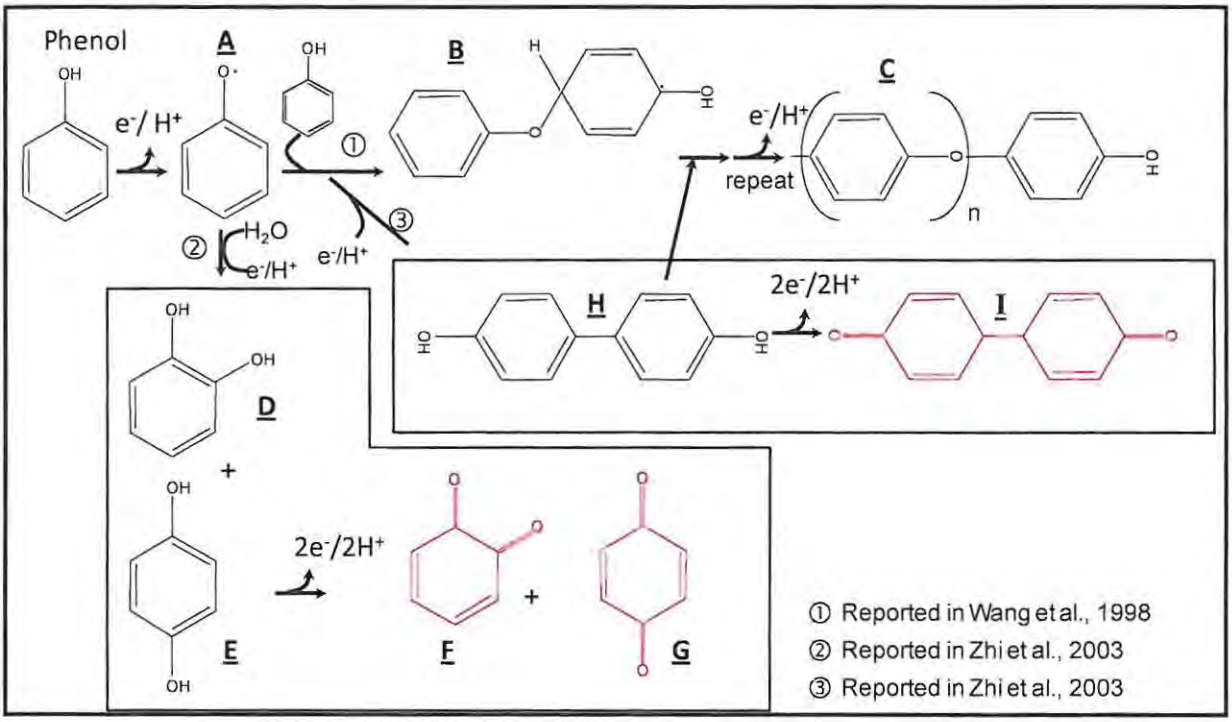

Figure 5.1: Schematic overview of the possible interactions and the resultant end-products of the radicalised intermediate state of phenol during electrooxidation, as obtained from literature.

Structures coloured in red are amenable to electro-reduction under normal conditions; those in black are not. Bolded, underlined letters indicate chemically-distinct phases that are referred in-text, below.

Schemes depicted in this Figure are reproduced from Wang et al., 1998 and Zhi et al., 2003.

An expanded scheme depicting the formation of catechol (D) and hydroquinone (E), and the formation of various dimeric compounds from phenol during electro-oxidation is available (Ferreira et al., 2006)

From Figure 5.1, it is apparent that even for chemically-simple phenolic compounds, a range of end-products are generated during oxidation. The mono-electron oxidation of phenol yields a phenoxy radical intermediate (**A**) which itself forms radical resonance-stabilised structures at carbon atoms located *ortho-* and *para-* to the hydroxyl. If reacted with a reduced phenol parent compound (Scheme ①), this eventually results in the formation of an aromatic polymer (**C**) through the further oxidation of *para-* and

ortho-substituted radicalised intermediates, such as **B**. However, hydroxylation of the phenoxy radical (Scheme ②) yields catechol (**D**) and hydroquinone (**E**), which themselves can oxidise at lower potentials to form their quinone counterparts (**F** and **G**, respectively). Scheme ③ details the possible formation of oligomeric/dimeric structures caused by the reaction of an oxidised phenoxy radical with an unoxidised phenolic compound. This represented here as the para-para conjugate **H**, but can undergo any permutation of *ortho- para-* or oxygen- attachment of one monomer to the other. **H** undergoes oxidation in the manner of **E** and **F** to generate its quinone counterpart, **I**, but can also participate in the formation of the polymeric product, **C**.

Structures outlined in red represent oxidation products that can generate a signal when electro-reduced under normal conditions. Of the 9 represented end-products reported in literature, only 3 of those compounds are reducible under the electrochemical regimen used in this research. While structures **A**, **B** and **C** are technically reducible, their rapid reactivity indicates that they will be precluded from being represented as reduction current at the electrode.

For the above example, the possible formation of redox-active oligomers (**I**), polymers (**D**) or the formation of intermediate phenolics (**E**,**F**) during the oxidation of phenols indicates that the oxidation of a phenolic does not, in itself, necessarily guarantee the generation of significant amounts of reductive current obtainable from the reduction of oxidation products.This heterogeneity of products entails that the signal derived from a laccase biosensor may not be strictly representative of only the laccase-substrate interactions, but also is affected by the differing end-products. The generation of the polymeric end-product/s (represents as **D** in Figure 5.1) itself is problematic to the electroanalysis of phenols, and is discussed in the following section below.

5.2.4: Fouling

1. Electroanalytical: Transducer passivation

As outlined in the previous section, the radicalised intermediate of phenols during oxidation introduces the possibility of the production of oligomeric or polymeric end-products, in addition to the numerous side-reactions outlined in Chapter 1 (Section 1.2.4.3). During the electro-oxidation of phenolic compounds, these products tend to attach to the electrode surface, forming an adherent, passivating film that decreases the electrode's response to subsequent analyses (Wang and Martinez, 1991). This occurrence is termed "fouling" of the electrode surface.

The extent of a given phenolic compound's ability to foul an electrode surface is dependent on several factors, which are listed in decreasing order of importance:

1) The species of phenolic compound(s) undergoing oxidation (Wang et al., 1998; Ureta-Zañartu et al., 2001; Ferreira et al., 2006). As Figure 1.6 of this Thesis (Chapter 1) indicates, phenoxy radical intermediates favour substituent localisation in the order of *para-* > *ortho-* >> *meta-* positioning (Ureta-Zañartu, 2001; Ferreira et al., 2006). Blocking of a favourable locus on the benzene ring by another substituent decreases the possible free radical intermediates, which in turn, restricts the range of potential end-products (Ureta-Zañartu, 2001). The occurrence of other side-reactions, as outlined both in Chapter 1 and depicted by the example provided in Figure 5.1, will also have an effect on the primary end-product, and hence, the structure and proportion of oligomers/polymers film produced during oxidation of the phenolic substrate.

2) The bulk concentration of phenol (Wang and Martinez, 1991). The extent and rate of fouling is positively correlated to the concentration of phenolic compound proximate to the electrode.

3) The materials employed as the working electrode (Ureta-Zañartu et al., 2001) and electroanalytical parameters. Differences in extent of fouling occur between electrodes, not only based on their bulk compositional differences (e.g. Au vs. GCE), but also vary between pre-analytical treatments of the electrode surface and other surface modifications (e.gs Wheeler et al., 1990; Mafatle and Nyokong,

1997). Electroanalytical parameters also influence fouling e.g. scan rate in voltammetry (Wang and Martinez, 1991), applied potentials and oxidation time during chronoamperometry. (Wang and Martinez, 1991)

4) Other operational considerations (chiefly pH (Ureta-Zañartu et al., 2001) and electrolyte specie/s and concentration/s) also influence fouling.

Variations on the parameters listed above produce a wide variety of polymers that are distinct from both the perspective of chemical/electrochemical properties and film architecture (e.g. porous to non-porous, rough to smooth) (Wang and Martinez, 1991; Ferreira et al., 2006). Importantly for the purposes of the research reported on in this Chapter, distinct differences in the degree with which oxidation products passivate electrode surfaces are noted (Ferreira et al., 2006).

Some of these oxidation products find application in research and industry e.g. as electro-conductive polymer molecules (Pałys et al., 2010); as a rule, though, the presence of fouling products is considered to be a hindrance in the electroanalysis of a given phenolic species, requiring a fresh transducer surface be prepared for each analysis. Numerous studies dealing with the modification of electrode surfaces in order to minimise the presence and extent of fouling have been performed.

Biorecognition layer inactivation:

The formation of multiple oxidation products through phenolic oxidation is not only a concern pertaining to the electro-oxidation of phenolics, but also to the application of laccase biosensors, where it is sometimes referred to as "product inactivation". Similar to electro-oxidative techniques, laccases catalyse the abstraction of a single electron from the phenolic moiety, causing the generation of phenoxy intermediate radical species. These can participate in the same oligomerisation/polymerisation reactions depicted for phenol in Figure 5.1, affecting the biocatalysts in the same manner as electrode surfaces. In addition, the products and product intermediates can re-participate in laccase oxidation, increasing the complexity of a given reaction. Numerous studies report on the formation of oligomeric/diimeric

products following laccase-catalysed phenolic oxidation – in some cases, this is an intended effect e.g. in the biosynthesis of polymers (e.g. Karamyshev et al., 2003).

Two potential mechanisms can affect the biorecognition layer: passive or active transformation of the laccase by the oxidation end-products. From a passive sense, entrapment of the catalytic portions of the biorecognition layer can occur by the polymeric/oligomeric end-products of the laccase catalysis (Canfora et al., 2008), imposing diffusional and conformational restrictions on the biocatalysts.

Actively, it is known that oxidation of, and conjugation to, amino acid residues of proteins can occur; principally tryptophan, tyrosine, histidine and cystine/cysteine residues can interact with the intermediates and products of phenolic oxidation (Call and Mücke, 1997), altering laccase activity. In laccases, product inactivation is minimised by the relative absence of these residues along surface-facing tertiary structures (Call and Mücke, 1997), but still occurs as a time-dependant decrease in laccase activity (Canfora et al., 2008). The rate of inactivation is noted to differ according to the substrate undergoing oxidation (Shuttleworth and Bollag, 1986; Canfora et al., 2008).

Conceivably therefore, the oxidation of phenolic substrates during the operation of the biosensor can result in an attenuation of biosensor signal. This could occur either via passivation of the electrode and/or of the biorecognition layer during the normal operation of the biosensor. When considering different substrates, therefore, their inherent capability to generate passivating end-products should also be taken into consideration for a more complete characterisation of the operational applicability of the biosensor.

Due to the potentially-numerous side reactions that can occur in the time between the substrate-laccase interaction/s and product-electrode interaction, a given phenolic compound may demonstrate a high substrate affinity to laccase, but the oxidation of the parent compound may be under-represented through measurement of reductive current during the operation of the biosensor. This, in turn, demonstrates that a method of determining the relative electroactivity of the products of laccase-oxidised phenolic compounds remains an important consideration when exploring the potential effects of different substrates on the biosensor system optimised in Chapter 4.

5.3 Aims:

The overall aim of the research reported on in this Chapter was thus to assess the differences in responses when the biosensor (optimised in the previous Chapter of this Thesis) was employed in the detection of differing phenolic compounds. This was performed with an aim to disentangle the electrochemical properties of a given phenolic compound's oxidation products (i.e. fitness as an analyte) from the same phenol's biochemical properties when considered as a substrate for the immobilised laccase comprising the biosensor used herein (i.e. fitness as a substrate).

Due to the aforementioned considerations of steric hindrance, as well as a desire to restrict the selected substrate range to that of simple electrochemical/biochemical interactions, relatively simple substrates have been tested and compared as to their suitability in this regard.

A key research question addressed in this chapter was to assess whether the electrochemical behaviour of a substrate in the absence of laccase oxidation could be used to predict the efficacy of detection within the biosensor configuration optimised in Chapter 4. While the biochemical reaction rates and kinetic properties of potential laccase substrates have been previously correlated (e.g. Xu, 1996) with their oxidation potential, and studies conducted on the effects of substituent presence and location on the sensitivity of detection via amperometric laccase biosensors Jarosz-Wilkołazka et al., 2006, to date no study has yet been performed on whether electrochemical investigations of different substrates can be of aid in predicting biosensor response to those substrates. Hence, it was of interest to consider if other electrochemical parameters would be of aid in predicting the response of a biosensor to various substrates.

If successful, this research would find application in fields requiring the monitoring of a single phenolic compound, or a small closely-related range of industrial monitoring of a few, known and well-characterised phenolic streams (such as azo dyes, pharmaceutical monitoring, etc.) The extent to which fouling behaviour influences the biorecognition layer and transducer surface, as it is anticipated to affect future analyses using the same sensor was also a key question to be addressed.

The sub-aims of this Chapter are, hence:

(1) The selection of 10 suitable phenolic substrates, with simple, relatable differences in their chemical structures for voltammetric assessment and calibration using the biosensor configuration optimised in Chapter 4 of this thesis.

(2) A brief electrochemical characterisation of the oxidation/reduction reactions of the selected substrates via CV in the absence of laccase, but under the same operational conditions used in biosensor assessment (Aim 3). This was performed in order to determine the basic electrochemical properties, in an attempt to assess the extent of potential side-reactions occurring following oxidation, and to obtain information regarding the relative electroactivities of the substrates.

(3) An investigation of the biosensor's operational parameters while using these substrates. The characteristics, both purely biochemical (K_m, degree of cooperativity) and those arising from both the electrochemical and biochemical properties of the phenolic substrate (i_{max}, biosensor sensitivity). Assessments via CV were performed to determine major differences occurring between electro-oxidation and biochemical oxidation of the selected substrates.

(4) To ascertain which electrochemical parameters have an effect on the operational parameters of the biosensor when deployed against a specific substrate. From the information on the biosensor's operational kinetics (3), substrates were initially categorised based on structural differences and then contrasted against the electrochemical parameters obtained achieving Aim (2) of this section.

(5) To assess the occurrence of biosensor attenuation upon re-use of the biosensor and to relate it to the electrochemical behaviour of the substrate.

(6) Modulation of the biochemical properties of the laccase-substrate kinetics and electrochemical properties of the analyte using small alterations in electrolyte pH to further expand on Aims (3) and (4).

5.4 Methods and Materials:

5.4.1 Apparatus

Electroanalytical equipment was used as outlined in Chapter 2.

Electroanalysis and biosensor modification took place at 21 °C and all reagents were warmed to this temperature prior to use

5.4.2 Reagents

Unless otherwise stated, the main buffer and electrolyte used throughout this research was SLB, which was adjusted to pH 4.5 using 2 M NaOH. In studies requiring different pH values, SLB, adjusted to a pH of either 3.5, or 5.5 was used and is indicated as such in-text.

5.4.2.1 Substrate selection, solubilisation and sourcing:

All substrates used in this Chapter were sourced from Sigma-Aldrich and were of analytical grade purity ($\geq$ 98%), or higher.

Substrates were dissolved in water immediately prior to analysis. In cases of poor solubility (especially prevalent at high concentrations of stock substrate), substrates were induced to dissolve by the addition of a few microliters of 2 M NaOH.

Table 5.2 lists the phenolic substrates used in this phase of research and the acronyms used henceforth in this Chapter, as well as other properties useful in contextualising their harmful/beneficial properties. Figure 5.2 displays the chemical structures of the test substrates used in the subsequent investigations.

Table 5.2: Selected substrate overview:

Substrate	Acronym	Hazard Classification[1]	L_{D50} (mg/kg)[1,2]	Substituent	Ancillary properties[3]	References[4]
2-aminophenol	2-AP	Harmful	951	2-NH_2	Electroactive polymer precursor, synthesis precursor	Pałys et al., 2010
1,2,4-Benzenetriol	BZT	Harmful	Not established	2,4-OH	-	-
Catechol	CAT	Toxic	260	2-OH	Industrial antioxidant and precursor	Antonyraj et al., 2010[a]
Gallic acid	GA	Irritant	5000	2,5-OH 4-COO^-	Phytochemical, antioxidant and antibacterial properties	Max et al., 2010
Guaiacol	GOL	Harmful	520	2-$COCH_3$	Phytochemical, organoleptic properties	Dorfner et al., 2003
3-Methylcatechol	3-MC	Irritant	Not established	2-OH 3-CH_3	Model product for bioproduction of 3-catechols	Hüsken et al., 2001
Hydroquinone	HQ	Harmful	302	4-OH	Ecotoxic (aquatic), industrial antioxidant and precursor	Antonyraj et al., 2010[a]
p-Cresol	PCL	Toxic	207	4-CH_3	Petrochemical industry byproduct	Tallon and Hepner, 1958
Phenol	PHE	Harmful	317	-	Polymer, plastics and resin precursor	Busca et al., 2008
ABTS	ABTS	Irritant	Not established	Non-phenolic 4-COOH	Widely-used laccase activity assay substrate	-

[1] – as reported by MSDS provided by supplier (Sigma-Aldrich)

[2] – as assessed by oral ingestion in mammalian model organism, usually rodent.

[3] – excluding those found in MSDS

[4] – reported relative to the primary hydroxyl common to most substrates (See Figure 5.2)

[a] – Ancillary properties cited in this reference.

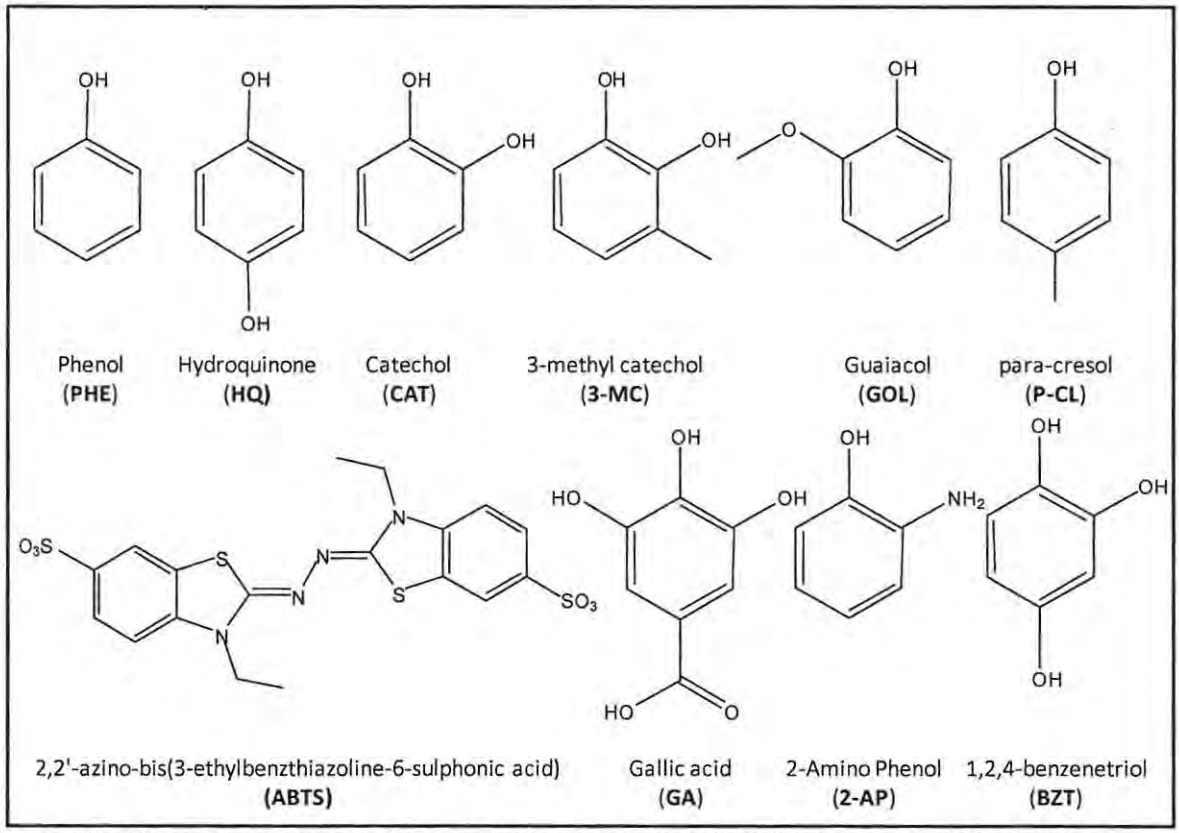

Figure 5.2: Chemical structures and abbreviations of compounds investigated as potential substrates.

5.3.3: Methodology

Throughout this phase of research, all experiments were performed in at least triplicate independent measurements. In general, independent observations were performed in quadruplicate, unless stated otherwise.

All cyclic voltammetry was conducted at a scan rate of 0.1 $V.s^{-1}$, unless otherwise stated. All chronoamperometry was conducted with the working electrode poised at a potential of -0.17 V vs. Ag/AgCl, unless otherwise stated.

5.3.3.1 Electroanalytical substrate characterisation (bare GCEs)

Electrodes were polished, anodically pretreated at +1.45 V for 5 s in 0.1 M NaOH and then sonicated in successive solutions of ethanol and water (as per findings in Chapter 3) and stored in water prior to analysis.

Prior to analyte characterisation, electrodes were cycled in SLB, pH 4.5, between the potentials of -0.3 V and + 1.1 V for 10 cycles, or until a stable baseline was achieved. Following cycling, the phenol under investigation was added to a final concentration of 1 mM and briefly homogenised by stirring. The electrode was then cycled under the above conditions for a further 5 scans.

The resultant peak characteristics: Peak potential (E); Peak Current (A); Peak charge (Q_p) and Wave Charge (Q_w) were noted and used for the proceeding criterion of electroactivity outlined below. In the occurrence of multiple reduction/oxidation peaks present during the assessment of a given substrate, electroactivity was assessed primarily on the characteristics of the most prominent reduction/oxidation peaks.

a) Categorisation of substrate reversibility:

The degree of reversibility of each substrate was determined using the following guidelines. In order to categorise a substrate as either reversible, quasi-reversible, or irreversible, at least 2 of the tabulated criterion had to be fulfilled.

The distance between oxidation/reduction peaks (dE) was assessed by the following formula:

$$dE = E_{p,a} - E_{p,c} \qquad \text{Eq. 5.1}$$

Where $E_{p,a}$ is the apex potential of the anodic peak and $E_{p,c}$ is the apex potential of the cathodic peak. In the occurrence of multiple reductive waves, the distance between $E_{p,a}$ and the closest significant reductive peak was used to determine dE.

The current yield ($\%I$) and the charge yields were determined according to the following formalism:

$$\%I = \frac{I_{p,a}}{I_{p,c}} \qquad \text{Eq. 5.2}$$

Where $I_{p,a}$ and $I_{p,c}$ denote the apex currents of the anodic and cathodic peaks, respectively. Substituting the integrated current for the whole peak to determine the charge passed during the formation of the oxidation/reduction peak, Q_p, for I in Eq. 5.2 provides the charge ($\%Q$) ratio (Eq. 5.3).

$$\%Q = \frac{Q_{p,a}}{Q_{p,c}} \qquad \text{Eq. 5.3}$$

For certain substrates that lacked a distinctive reductive peak, or produced multiple reductive peaks upon oxidation, the charge passed during the cathodic wave at potentials more negative than the primary oxidation peak was calculated to produce $Q_{w,c}$, using Eq. 5.4

$$Q_{w,c} = \Delta Q_{w,red} - \Delta Q_b \qquad \text{Eq. 5.4}$$

Where the charge passed for the reduction of phenolic oxidation products ($\Delta Q_{w,red}$) was corrected for the charge passed by the electrode/electrolyte system in the absence of the phenolic species (ΔQ_b).

To provide a pictorial overview of the above measurements, a typical cyclic voltammogram of the oxidative/reductive profile obtained using unsubstituted phenol (PHE) is presented below (Figure 5.3).

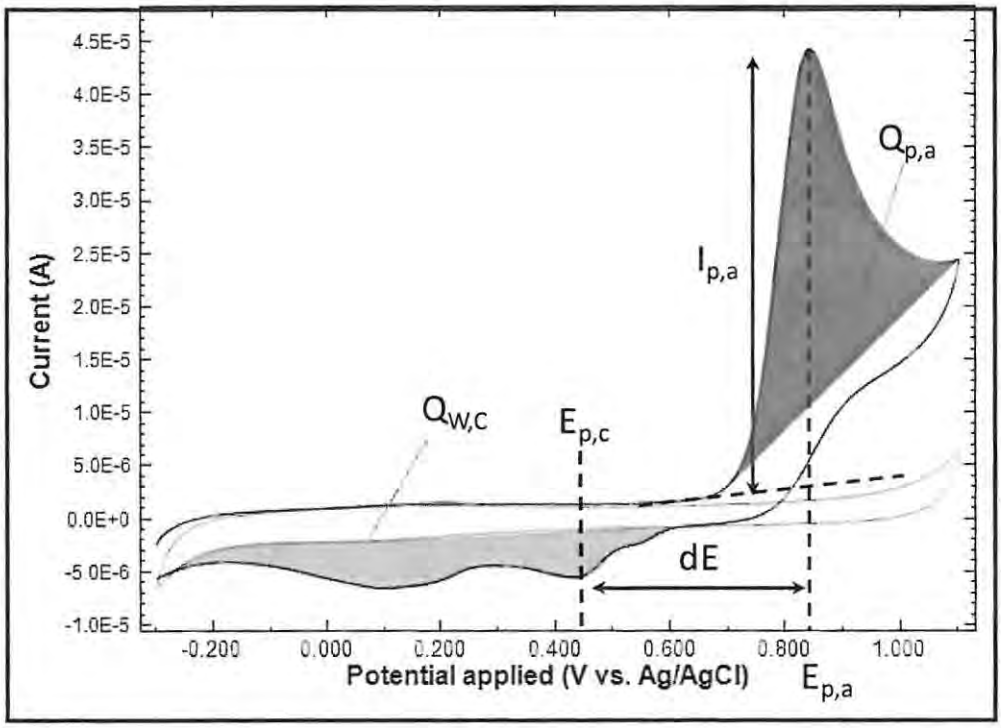

Figure 5.3: Typical oxidation/reduction profile of phenol (PHE) in SLB, pH 4.5.

Annotations depict typical parameters extracted from cyclic voltammograms.

Legend: $I_{p,a}$ – Peak oxidation current; $E_{p,a}$ – Peak oxidation potential; $E_{p,c}$ – Peak reduction potential closest to $E_{p,a}$; $Q_{p,a}$ (Dark grey area) – Peak oxidation charge; $Q_{w,c}$ (Light Grey areas) – total integrated charge for the reductive wave (blank-subtracted).

Grey cyclic voltammogram overlaid shows the cyclic voltammogram generated prior to the introduction of phenol into the electrolyte

From the criterion of dE, %I and %Q, substrates were assigned categories indicating their respective degrees of electrochemical reversibility, using the conventional system i.e. reversible, quasi-reversible and irreversible. Table 5.3 shows the various criterion used in assessing a given substrate's reversibility.

Table 5.3: Criterion for classification of analytes with respect to electrochemical reversibility during oxidation/reduction at bare GCEs:

Degree of reversibility	dE (V)	%I	%Q	Fouling rate
Readily reversible (reversible)	$\leq$ 75 mV	80%-100%	> 70%	Negligible
Quasi-reversible	> 75 mV	20%-80%	> 50%	Moderate
Irreversible	> 150 mV	< 20%	< 10%	Severe

In order for an analyte to strictly qualify as a reversible i.e. Nernstian system, dE values should range between 60.5 and 57.0 mV (depending on the relative distance between the peak potential and the onset of the cathodic sweep), and the ratio of cathodic to anodic peak current should approach unity (i.e. %I ~ 100%) (Bard and Faulkner, 2001). However, given the imprecise measurements of peak currents via CV (Bard and Faulkner, 2001), the complexity of phenolic oxidation/reduction chemistry outlined in the Section 5.2.4 of this Chapter, as well as the non-optimal conditions that analytes were anticipated to find themselves in with regard to pH and electrode effects caused by the heterogeneity of glassy carbon surfaces (Chapter 3), criterions for classification of reversible analytes/substrates presented in Table 5.1 were broadened beyond the strict definition outlined by Bard and Faulkner, 2001.

Similarly, the boundaries between categorisation of quasi-reversible and irreversible substrates were given similar considerations. dE values for quasi-reversible systems range between 61 and 212 mV, depending on the dimensionless CV rate parameter, ψ, for systems exhibiting transfer co-efficient values of $0.3 > \alpha > 0.7$ (Bard and Faulkner, 2001). Hence, while analytes classified as irreversible were not, in the strictest sense, totally irreversible (%I < 20%; dE > 150 mV in Table 5.1, as opposed to the strict definition wherein both parameters would have values of 0% and indeterminable, respectively), classifications of these substrates were performed on the basis that these quasi-reversible substrates tended towards mainly quasi-reversible or irreversible behaviour.

For the purposes of this research, at least three of the properties indicated in Table 5.3 had to be met for a substrate to qualify as a reversible, quasi-reversible or irreversible analyte during this phase of research. The fourth criterion for reversibility was the absence of, or negligible presence of, fouling at a bare GCE surface, in order to distinguish a substrate as either reversible, or quasi-reversible. This was used in cases where uncertainty in categorisation existed for a given substrate. The methodology for ascertaining the extent of fouling is outlined in the proceeding section.

b. Electrochemical fouling rate:

The extent of fouling is assessed electroanalytically by measuring the decrease in voltammetric current as a function of successive scans (Mafatle and Nyokong, 1997), or of oxidation time (Wheeler et al., 1990). Hence, the peak characteristics of 5 successive scans were assessed in order to investigate the extent of fouling that a given substrate produces at a bare electrode during oxidation/reduction. In cases where additional redox products accumulated at the electrode within the potential window used to assess fouling rate, the increase and position of reductive peaks was also tracked.

In order to meaningfully quantify and compare results from different phenolic species, these values were linearised by graphing against the inverse of the scan number used, and the resulting gradients of the $I_{oxidation}$/ scan number^{-1} were presented herein.

c. Assessment of unity between electrooxidation and laccase-catalysed oxidation

Following chronoamperometric analysis of the substrate-biosensor kinetics (Section 5.3.3.2, below), cyclic voltammograms generated between -0.3 V and +0.8 V using the laccase-modified GCE electrode in the presence of the substrate were performed. The presence or absence of peaks arising from the oxidation/reduction of the main phenolic species was recorded in order to deduce whether the same mechanism dictating the electro-oxidation of a given phenolic species governed its laccase-catalysed oxidation.

5.3.3.2. Biosensor responses:

Biosensor performance and the elucidation of operational kinetics was achieved via sigmoidal modelling of the current-concentration profiles of each substrate. This was performed as discussed in Chapter 4, using the biosensor operational kinetics model and data-gathering and processing methodologies outlined in Chapter 2 of this Thesis.

Biosensors were fabricated using sequential 1 µl aliquots of the following: 20 $mg.ml^{-1}$ BSA stock solution; a concentration of laccase corresponding to a total of 800 $U.ml^{-1}$; 15% glutaraldehyde. These were then briefly mixed and allowed to cross-link at room temperature until dry (~30 minutes). Thereafter, fabricated biosensors were stored in SLB, pH 4.5, at room temperature until used, within 0 - 2 hours of fabrication. The relevant optimisation studies and rationales detailing the reasons behind these concentrations of proteins have been reported in Chapter 4 of this thesis.

The electroanalytical procedure for the application of the biosensor to the differing substrates is the same as described in Chapter 4 of this Thesis, as were the conditions for sensor re-use.

Data analysis and extraction of modelled parameters took place as described in Chapter 2, using the modelling system and goodness-of-fit indicators outlined in Chapter 2 (Section 2.4 and Appendix 1, respectively). Values of parameters were interpreted as outlined in Section 2.3 and Section 2.4 of this Thesis.

5.5 Results and Discussion

5.5.1 Electroactivity assessment at bare GCEs:

For the purposes of visual comparison, Figure 5.4 displays typical CV results for: irreversible (gallic acid); quasi-reversible (guaiacol) and reversible (catechol) phenolic electrochemical behaviour as investigated at bare GCE surfaces. Screening downstream of the main peak was performed on biosensors after incubation with substrate in order to determine whether electrooxidation resulted in the same products as that catalysed by laccase.

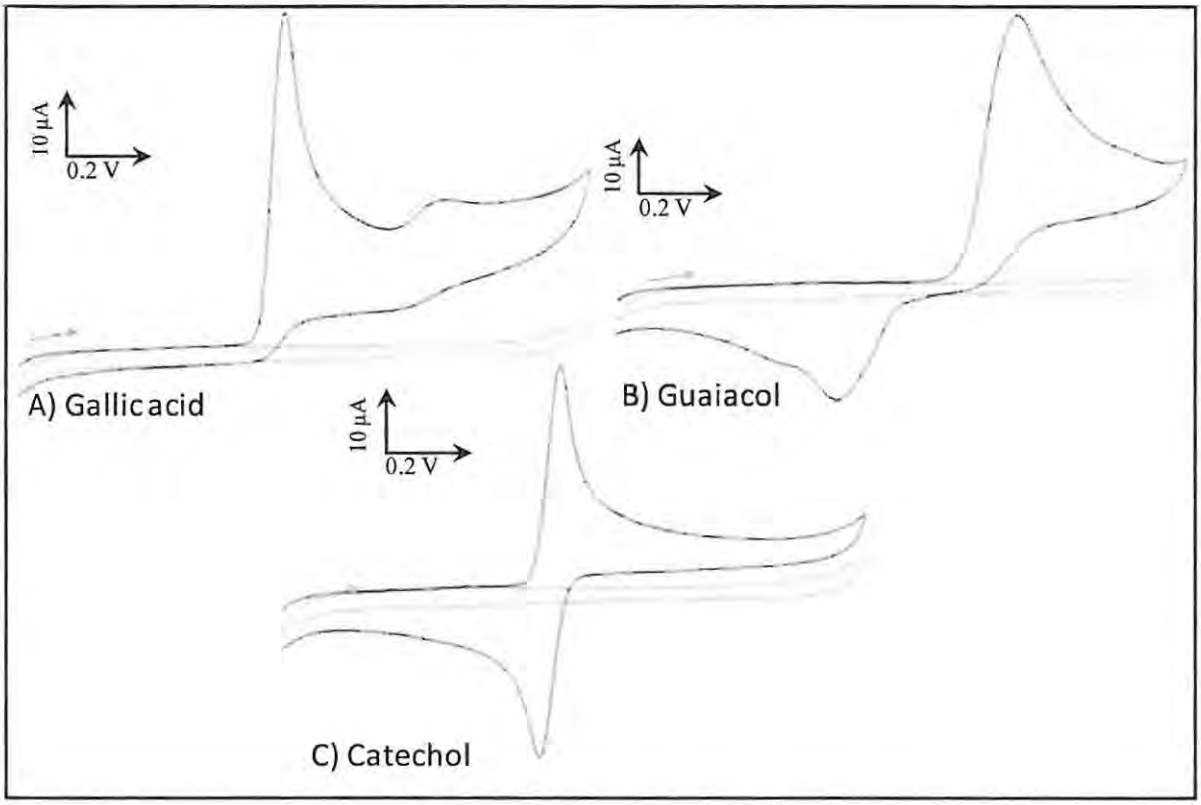

Figure 5.4 : Examples of: A) Irreversible, B) quasi-reversible and C) readily reversible phenolic compounds, as assessed at bare (unmodified) GCEs in SLB, pH 4.5.

Black arrows indicate current and potential scales.

Grey arrows indicate the direction of potential application, from anodic to cathodic sweeps.

Grey cyclic voltammograms inset into each sub-Figure show cyclic voltammograms generated prior to the introduction of said substrate to the electrolyte solution. Scan rates for all represented voltammograms was maintained at 0.1 $V.s^{-1}$.

As evidenced in Figure 5.4, distinct changes in the number, morphology and position of peaks were observed when different analytes were electro-oxidised and then reduced at bare GCEs. This information, together with the fouling analyses was collated, and the averaged values for each substrate are presented below (Table 5.4). Figure 5.5 shows demonstrative data collected from the oxidation-reduction of guaiacol and its oxidation products, together with the data-processing techniques used to assign relative rates of fouling (either oxidative or reductive peaks).

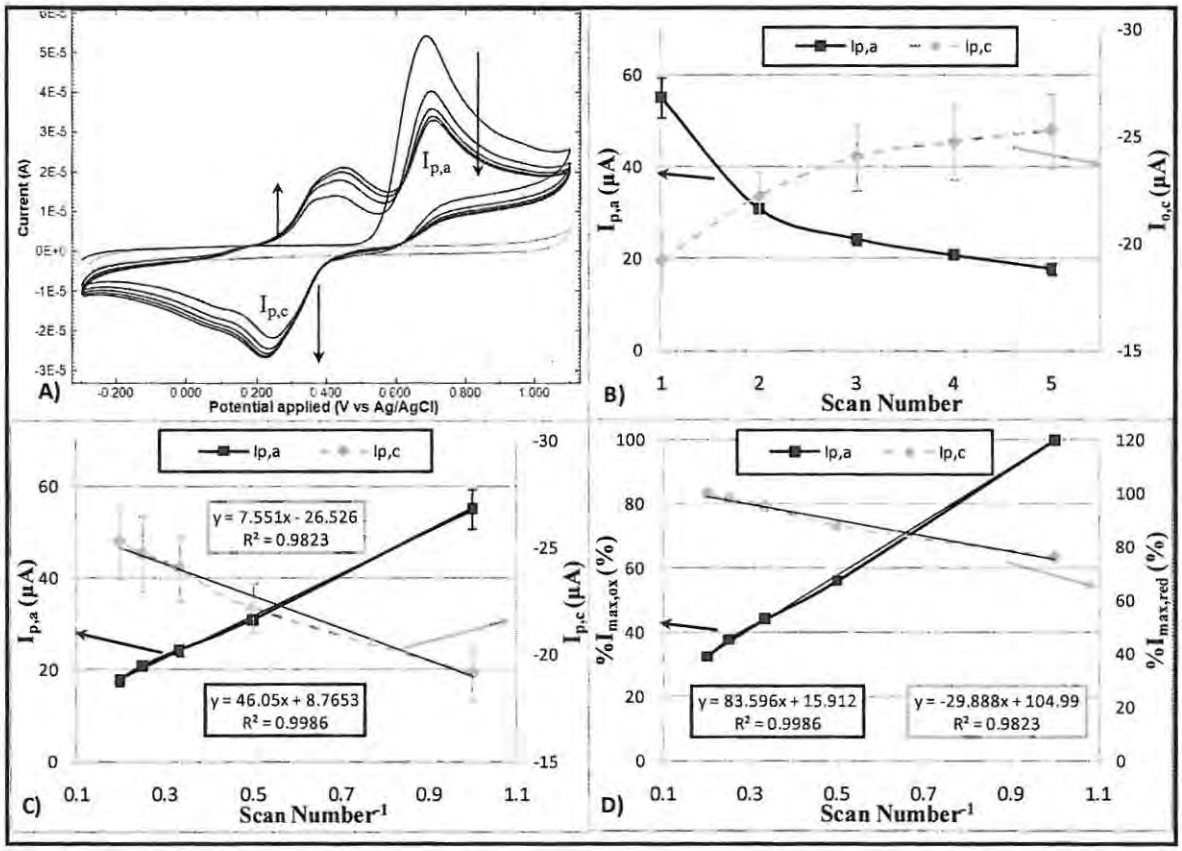

Figure 5.5: Fouling extent of guaiacol (GOL) at a concentration of 1 mM, as assessed at a bare GCE in SLB, pH 4.5.

Both the main oxidative peak (black) and the main reductive peak (grey) are presented here.

Error bars indicate standard deviation from the mean, n = 3.

This figure depicts the transformation of data from:

A) Successive scans showing fouling behaviour of guaiacol (GOL). Grey scan shows cyclic voltammogram in the absence of guaiacol.

B) Averaged peak data tracked against scan number

C) Averaged peak data plotted against the inverse of the scan number.

D) Normalisation of peak data to maximal current observed in the study.

As Figure 5.5 displays, graphing of the oxidative and reductive currents against the inverse of the scan rate provides a satisfactory means of linearising the data (Fig 5.5 **C**), while assessment of the gradients obtained (Fig. 5.5 **D**) provides a rapid method of comparing the relative extents of fouling of the electrode upon oxidation/reduction of the specified phenol/oxidation product(s). Larger gradients are interpreted as an increased rate of fouling at the bare GCE. Table 5.4 displays a summary of the results obtained from the electrochemical characterisation of the laccase substrates, as assessed at bare GCEs.

Table 5.4, below, records the categories that substrates were placed in, and the pertinent electrochemical parameters for the initial oxidative peak and the closest reductive peak.

Table 5.4: Findings of peak reversibility and fouling of the oxidative currents for potential laccase substrates:

	Initial scans					Successive scans	
Substrate	**$E_{p,a}$ (V)[1]**	**$E_{p,c}$ (V)[1]**	**dE (mV)**	**%I (%)**	**%Q (%)**	**Fouling rate[2] ($\Delta I_{p,a}$.scan) %**	**Fouling rate[2] ($\Delta I_{p,c}$.scan) %**
Reversible							
BZT	0.149	0.081	68.4	90.4 ± 1.28	66.9 ± 2.0	3.90	3.88
HQ	0.287	0.211	76.5	94.3 ± 0.94	78.0 ± 1.1	-1.77	-0.97
3-MC	0.348	0.262	85.5	83.9 ± 0.55	91.3 ± 0.5	0.35	0.12
CAT	0.371	0.313	57.8	85.3 ± 0.86	90.6 ± 2.5	-0.85	3.29
Quasi-reversible							
2-AP	0.363	0.061	303	13.9 ± 1.78	26.2 ± 12.5	65.8	-6.87
ABTS	0.548	0.462	85.5	67.1 ± 2.10	107 ± 3	-3.68	-6.76
GOL	0.681	0.244	436	34.8 ± 0.76	49.1 ± 1.1	83.6	-29.7
Irreversible							
GA	0.358	-0.151	509	1.16 ± 0.01	0.033±0.002	84.7	0
P-CL	0.745	0.145	612	1.35 ± 0.03	1.89 ± 0.11	129	0
PHE	0.841	0.438	403	14.7 ± 1.0	37.9 ± 2.9	75.8	-30.4

[1] – reported herein vs. Ag/AgCl reference electrode.

[2] – Negative values of fouling scans are indicative of electrodeposition onto bare GCEs.

Reported values have a standard deviation from the mean ≤ 5 mV or < 1% unless otherwise stated. Number of observations, n ≥ 3.

Substrates classified as reversible (Table 5.4) uniformly showed the lowest dE values (> 77 mV), while possessing very high %I and %Q values accompanied by minimal fouling. In some cases (HQ and CAT), fouling studies indicated an increase in peak current (represented as a negative value for fouling rate measured by $I_{p,a}$) with successive scans. Substrates classed as irreversible possessed opposite characteristics - significantly higher dE values (>400 mV), accompanied by low %I and %Q values and significant relative fouling rates. Those categorised as quasi-reversible exhibited properties that were a mixture of both reversible and irreversible properties, with significant variances in dE, %I and fouling rates that were a mixture of characteristics of either of the other classes of substrates.

$E_{p,a}$ is by itself an important parameter to measure and record, in that it is an indication of the relative thermodynamic ease at which an analyte undergoes oxidation (Section 2.3.2 of this Thesis), which is relevant to both electrochemistry and laccase-catalysed oxidation. Laccases catalyse reactions by shuttling electrons between the reducing substrate (phenolics) and the oxidising substrate/s (O_2 under natural conditions). The copper T_1 atom embedded in the active sites of laccases are often characterised by their oxidation potential obtained through redox titrations; hence, the differences extant between the oxidation potentials of T_1 sites and the oxidation potential of substrates are indicative of the relative ease by which the laccase can oxidise the substrates and are thereby related to the rate of substrate oxidation (Xu, 1997; Hong et al., 2006). Hence, the larger the difference between the oxidation potentials of laccase and the substrate become (Xu, 1997) and the more thermodynamically favourable oxidation of the substrate is.

The oxidation potentials of T_1 sites differ between the laccases under consideration (e.g. Xu, 1997) and (in the case of immobilised laccases) by the conformational alterations occurring due to the immobilisation process. Both the characteristic potentials for substrate and the active site of laccase are influenced by operating conditions (temperature, pH (Xu, 1997), ionic strength, etc). However, while the oxidative potential for substrates decreases at a rate of ~58 mV/decade with increasing alkalinity, T_1 sites exhibit a much lesser negative dependence on pH (Xu, 1997). As alkalinity increases, the difference between these potentials widens, indicating an increased rate of substrate oxidation. Reaction rate increase under increasing alkalinity, however, is counterbalanced through inhibition of the laccase at the copper T_2/T_3 site (involved in diooxygen binding and reduction) caused by increasing OH^- concentration (Xu, 1997).

A cautionary note is warranted at this juncture. The %I values, as they were quantified via electro-oxidation of the substrate, are not to be taken as being strictly representative of the oxidation/reduction behaviour of substrates undergoing oxidation via the immobilised laccases in the biosensors. Heterogeneity between the mechanisms of oxidation through biochemical or electrochemical mechanisms may result in the formation of different compounds. Table 5.5 (below) displays presence/absence of electro-active compounds when comparing the oxidation of laccase substrates

through electrochemical, or biochemical means, indicating the formation of differing end-products. It must be emphasised that the electrochemical investigations were performed to create relative comparisons between the electrochemical behaviour of substrates/products, rather than to produce accurate depictions of oxidation end-products expected to be produced by the immobilised laccase. The ongoing oxidation of substrate during deployment of the biosensor would make determination of the calculated %I values very difficult; added to which was the concern that the CVs performed at biosensor surfaces themselves would result in products arising from both electro- and biochemical-oxidation. Hence, the values reported for the %I in Table 5.4 are not expected *per se* to be an accurate indication of the actual ratio of charge conveyed through the oxidation of substrate by laccase.

Table 5.5: Summary of the peaks found to be present during oxidation-reduction of phenolic substrates at bare GCEs and comparison with anticipated laccase-catalysed oxidation products

	Number of redox Peak(s) (a/c)[1]			Literature	
Substrate	**Bare GCE 1st scan**	**Bare GCE 5th scan**	**Laccase-modified GCE[3]**	**Anticipated laccase-catalysed oxidation product/s[3]**	**References**
Reversible					
BZT	1 / 1	1 / 1	1 / 1	2-hydroxy p-benzoquinone	
HQ	1 / 1	1 / 1	1 / 1	p-benzoquinone	Zhi et al., 2003
3-MC	1 / 1	1 / 1	1 (2) / 1 (2)	3-methyl-o-benzoquinone	Nematollahi and Goodrazi, 2001
CAT	1 / 1	1 / 1	1 / 1	o-benzoquinone	Zhi et al., 2003
Quasi-reversible					
2-AP	2 / 4	4 / 4	2 / 1 (3)	Polymers, dimers, o-benzoquinone, benzoquinone monoiimine	Gonçalves et al., 2000
ABTS	2 / 2	2 / 2	2 (3) / 2 (3)	Stable monocation radical, Stable dication	Munteanu et al., 2006
GOL	1 / 3	3 / 3	3 / 2	Monomers, dimers, oligomers	Hwang et al., 2008
Irreversible					
GA	2 / 2	2 / 2	1 / 0 (1)	-	-
P-CL	1 / 2	2 / 1	1(2) / 0 (1)	Dimers, polymers, Pummerer's ketone	Benfield et al., 1964 Navarra et al., 2010
PHE	1 / 3	3 / 2	4 / 4	CAT, HQ, dimers, polymers	Wang et al., 1998; Zhi et al., 2003

1 – Represented by number of peaks on anodic wave / peaks on cathodic wave of the first scan

2 – Numbers indicated in brackets represent the number of peaks present on the CV that include minor peaks i.e. < 10% current of the main peaks reported in unbracketed terms.

3 – Where published articles based on laccase-substrate oxidation products were not available, those reporting on the electrochemical oxidation of substrates under acidic aqueous conditions at glassy carbon electrodes were used.

The differences in the number and distribution of peaks present between the biosensor-generated CV and the unmodified electrodes (Table 5.5) reinforces the above view that electro-oxidation and biochemical oxidation most likely result in the formation of different end-products. However, the purpose of assessing Table 5.5 displays that those compounds categorised as reversible display only a single oxidation/reduction couple, indicating that a single product is generated during electro-oxidation which is conserved between laccase- and electrode-oxidation pathways, a view bolstered by literature regarding laccase-oxidation products. The sole exception to this, 3-MC, is discussed at a later stage in this Chapter.

As mentioned previously, these compounds exhibit either very little fouling, or exhibit electrodeposition at the bare GCE, perhaps indicating that only very small proportions of the oxidation products are produced in more complex states than the anticipated oxidation products described in literature.

Furthermore, Table 5.5 indicates that those compounds indicated in literature to possess numerous oxidation-products themselves have numerous peaks present in the reductive wave. The sole exception of this is P-CL, which was noted to deposit a strongly-coloured yellow-gold film on the electrode surface following electro-oxidation. In addition, Table 5.4 indicates that both P-CL and GA analytes exhibited two of the highest relative fouling rates when bare GCEs were successively scanned in solutions where they were present. This infers that the products of both these substrates, while themselves being negligibly electroactive (possessing very low *%I* and *%Q* values), are formed during its oxidation and have a pronounced passivating effect on the transducer surface. Fouling of the electrodes during GA oxidation was found to be unaffected by narrowing the potential window to just after the main oxidation peak seen in Figure 5.4**A** (data not shown), indicating that the least-positive oxidation event is the source of the production of passivating compounds.

In all other assessments of the quasi-reversible and irreversible substrates, the oxidation of the parent compound is accompanied by the production of numerous peaks at potentials significantly more negative than the main oxidation peak. This is evidenced by the significantly large dE values (Table 5.4) in these categories, relative to reversible substrates. This is considered to be due to the formation of electroactive compounds that are not structurally identical to the parent compound and, as such, do not regenerate back to the parent compound upon reduction. Secondary reduction/oxidation peaks exhibited an increasing current with increasing scan numbers, concomitant to the decrease of the current associated with the oxidation of the parent compound. As stated previously, these substrates also exhibited significant declines of the main oxidative peak current with successive scans.

As cyclic voltammetry at the laccase biosensor surfaces were performed after chronoamperometry (i.e. at conditions of substrate saturation, or near-saturation within the biorecognition layer), significant amounts of the parent substrate were assumed to be present at the electrode surface during cyclic voltammetry. As

expected, peaks corresponding to the oxidation of the parent compound were present for all the substrates analysed. While it was potentially true that, in the case of reversible substrates, their reduction at the electrode at potentials more negative than the oxidation peak may cause the localised formation of the parent compound (giving rise to an oxidation peak), the presence of these peaks in both quasi-reversible and irreversible compounds indicated the presence of significant amounts of parent substrate within the biorecognition layer following saturation of the immobilised enzymes.

5.5.2 Biosensor response to different substrates:

Detection sensitivity and i_{max} were considered to be governed by both substrate-enzyme kinetics and analyte-electrode kinetics. Through their inclusion of electrochemical signals (current), their determination arises from a mixture of electrochemical and biochemical effects. Conversely, K_m and the degree of sigmoidality, b, were considered to be wholly biochemically controlled, due to their mathematical exclusions of any electrochemical considerations (Eq. 2.3).

A high degree of variability in the sensitivity of detection was apparent between selected substrates. Figure 5.6 shows representative current-concentration curves generated by the biosensors when calibrated using different candidate substrates, HQ and GA.

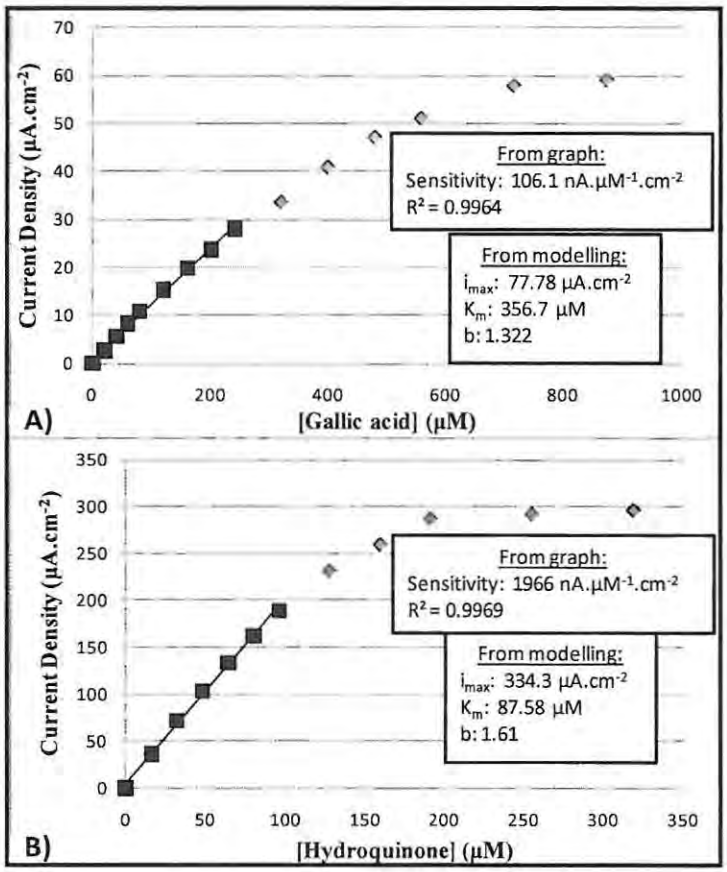

Figure 5.6: Current-concentration responses of laccase biosensors to two separate substrates. A) Gallic acid (GA) and B) Hydroquinone (HQ).

Points on the graphs displayed as black squares joined by a line correspond to the areas of the current-concentration range at which detection sensitivity and linear response range were calculated.

Inset boxes show operational parameters drawn from the regression of the linear portion of the graph and those obtained from modelling of the data

A comparison between the two current-concentration curves provided in Figure 5.7 **A)** and **B)** readily shows that substantial differences occur between substrates with regard to their individual detection sensitivities, linear response ranges, and modelled parameters i_{max}, K_m and a lesser variation of the degree of sigmoidality, b, when concentration of substrates was varied using laccase biosensors. Figure 5.8 provides a graphical depiction of the differences obtained in detection sensitivity when different substrates were assessed using laccase biosensors.

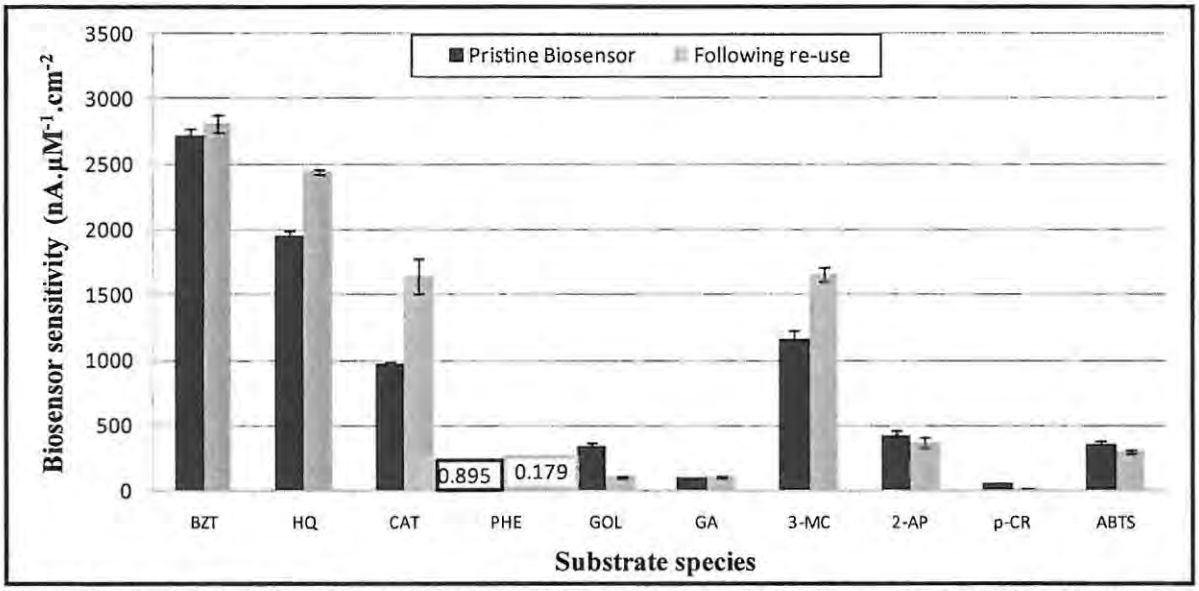

Figure 5.7: Overview of the substrate-detection sensitivities from the linear range obtained from the current-concentration functions of different substrates by the laccase biosensors.

Where not visible, biosensor sensitivities are recorded by their average value, in boxes coloured respectively black and grey, indicating pristine biosensor values and those that were generated using re-used biosensors.

Error bars indicate the standard error from the mean. Number of observations, $n > 3$.

Due to the high degree of variability in detection sensitivity and other parameters between substrates (as evidenced in Figure 5.7) and the associated difficulties in meaningfully presenting this data graphically, the operational parameters obtained from this phase of research are presented in tabulated form, below. Tables 5.6 and 5.7 outline the main parameters elucidated from the analysis of the laccase biosensors when exposed to different substrates, both in the pristine state (i.e. immediately after modification) and following analysis of the same substrate ("Following re-use"). Table 5.6 displays the relevant operational parameters of the biosensor obtained graphically (detection sensitivity and linear response range), while Table 5.7 specifically displays the operational parameters of the biosensor-substrate interactions obtained from the modelling process (i_{max}, K_m and b value). The effects of biosensor re-use, while reported in this section, are discussed in greater detail in Section 5.4.4.4

Table 5.6: Substrate sensitivity and linear ranges, as assessed from the graphical current-concentration curves

	Before re-use			After re-use			
Substrate	**Sensitivity ($nA.\mu M.^{-1}cm^{-2}$)**	**Linear onset (μM)[a]**	**Linear endpoint (μM)[b]**	**Sensitivity ($nA.\mu M.^{-1}cm^{-2}$)**	**Linear onset (μM)**	**Linear endpoint (μM)**	**$\frac{Sens_{before}}{Sens_{after}}$**
Reversible:							
BZT	2713 ± 58.02	0	100.0 ± 5.0	2813 ± 72	0	74.33 ± 4.91	103.7%
HQ	1947 ± 47.59	0	120	2443 ± 23	0	103.3 ± 8.3	125.5%
3-MC	1154 ± 71.60	5.3 ± 2.3	93.33 ± 5.77	1662 ± 53	0	90.00 ± 5.00	143.9%
CAT	970.5 ± 9.7	3.8±3.8	135.0 ± 8.66	1639 ± 135	0	88.60 ± 5.84	168.9%
Quasi-reversible:							
2-AP	424.9 ± 39.5	0	166.7 ± 16.67	366.7 ± 43.6	0	150.0	86.30%
ABTS	358.3 ± 18.8	0	220 ± 10	302.7 ± 12.3	0	240.0	84.49%
GOL	340.5 ± 29.7	0	264.7 ± 47.67	110.7 ± 5.7	0	345.4 ± 37.3	32.50%
Irreversible:							
GA	95.85 ± 4.78	0	166.7 ± 16.67	110.2 ± 8.1	0	300.0 ± 61.2	115.0%
P-CL	59.18 ± 5.07	0	380 ± 11.55	14.18 ± 3.04	0	200.0	23.96%
PHE	0.8952 ± 0.0385	2518 ± 496.71	13398 ± 3377	0.1786 ± 0.0140	3874 ± 595.6	37626 ± 3625	19.95%

Uncertainties represented as standard error from the mean. Number of replicants, $n \geq 3$

Values highlighted in grey do not have a co-efficient of variation < 10% from the mean value.

[a] – Start of linear response range for current-concentration functions of the biosensor

[b] – End of linear response range for current-concentration functions of the biosensor

As Table 5.6 indicates, there exist considerable variations between substrates tested, both in detection sensitivities and linear response concentration ranges. This highlights the concern surrounding electrochemical detection of phenolic compounds through the application of laccase biosensors, as substrates of varying toxicity (Table 5.2) are not equally detectable by this method. For example GA and GOL which are both phytochemicals (and might therefore be present in the same sample matrices), vary 10-fold in their estimated lethal doses and vary 3-fold in their detection sensitivities. Similarly, PHE, HQ and CAT, which possess similar L_{D50} values (~300 mg/kg, Table 5.2) and are likely to be present in the same analyte matrix that PHE is present in (through the scheme outlined in Figure 5.1) possess significantly different average detection sensitivities of ~<1, ~1950 and ~970 $nA.\mu M.cm^{-2}$ respectively for the laccase biosensors used in substrate calibration studies, producing a range of sensitivity of

approximately 2000-fold. These significant, consistent, variances in detection sensitivities between these substrates would conceivably lead to the over/under-estimation of a given phenolic substrate of analytical relevance (for example, detection of CAT in a mixed sample containing GA) during the analysis of samples.

A comparison between Table 5.4 and Table 5.6 shows that biosensor sensitivity decreases in the same order in which the E_{ox} increases. However, this negative trend was not found to be consistent with the global data including all substrates, but to be consistent within the groups classified according to electrochemical reversibility in Section 5.5.1. This is discussed further in Section 5.5.4 below, where findings from the electrochemical and biochemical parameters are compared.

With the exception of phenol, all substrates tested exhibited an onset of linear current-concentration behaviour at approximately 0 μM of substrate. The end-point of the linear response region appears to decrease logarithmically with the logarithm of the sensitivity, as Figure 5.9 indicates. Trends established here do not include datapoints obtained for PHE, as the values obtained from PHE were quite displaced from the grouping of the other substrates. This, in turn, was found to be linked to the positive trend existing between $\log(K_m)$ and the logarithm of the end-point concentration (data not shown).

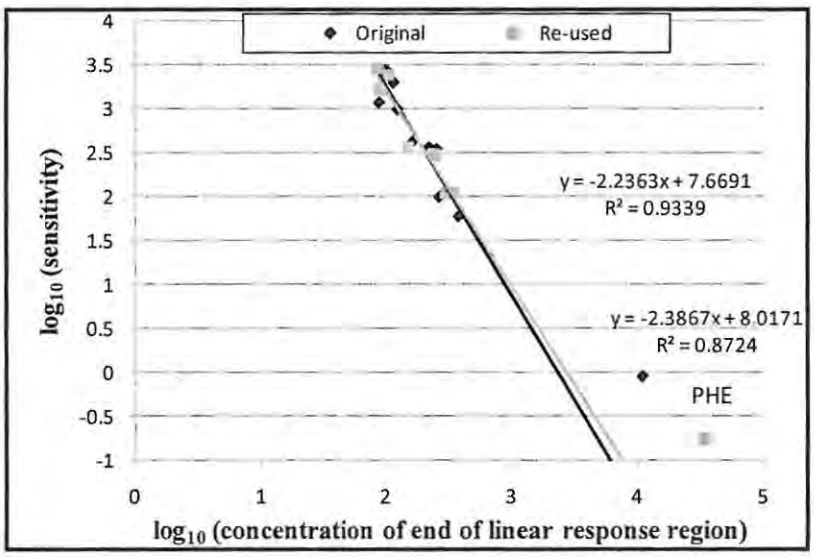

Figure 5.8: Plot of the logarithm of biosensor sensitivity for each substrate against the logarithmic concentration at which the linear response region ended for each substrates.

Averaged data used (n ≥ 3). Trends depicted herein exclude the data-points found for PHE substrate (datapoints labelled PHE indicate their position). Inset boxes display the regressional parameters for the trends found.

Legend: Black – pristine sensors used; Grey – re-used sensors.

Table 5.7 presents the data obtained through sigmoidal modelling of the current-concentration functions generated through calibration of the laccase biosensors with the selected substrates.

Table 5.7: Data obtained from modelling of the biosensor kinetics, taking into account sigmoidal current-concentration behaviour

	Before re-use			After re-use		
Substrate	**i_{max} ($\mu A.cm^{-2}$)**	**K_m (μM)**	**b**	**i_{max} ($\mu A.cm^{-2}$)**	**K_m (μM)**	**b**
Reversible:						
BZT	410.4 ± 16.9	79.79 ± 3.38	1.31 ± 0.02	347.1 ± 33.8	57.81 ± 6.04	1.42 ± 0.05
HQ	342.8 ± 7.5	87.04 ± 2.53	1.40 ± 0.02	366.1 ± 20.1	71.29 ± 2.29	1.39 ± 0.04
3-MC	221.6 ± 19.2	110.1 ± 3.0	1.42 + 0.02	344.6 ± 8.2	105.5 ± 9.1	1.23 ± 0.11
CAT	236.9 ± 11.0	125.6 ± 4.4	1.66 ± 0.12	286.1 ± 12.7	77.87 ± 5.66	1.25 ± 0.08
Quasi-reversible:						
2-AP	149.5 ± 8.6	176.7 ± 26.8	1.61 ± 0.03	168.5 ± 4.9	245.8 ± 29.1	1.24 ± 0.06
ABTS	235.3 ± 7.6	445.7 ± 0.2	1.09 ± 0.02	301.6 ± 13.0	759.9 ± 10.1	0.95 + 0.01
GOL	175.6 + 16.6	248.9 ± 32.8	1.22 ± 0.13	99.34 ± 12.22	489.1 ± 38.1	1.13 ± 0.04
Irreversible:						
GA	75.38 ± 5.28	373.4 ± 22.1	1.26 + 0.03	120.5 ± 7.8	554.5 ± 4.8	1.06 ± 0.06
P-CL	22.31 ± 1.96	216.5 + 29.3	1.17 ± 0.12	18.54 ± 1.47	918.6 ± 91.6	0.98 ± 0.03
PHE	43.97 ± 6.93	29 056 ± 2 963	1.50 ± 0.06	16.66 ± 0.91	44 093 ± 2 165	1.27 ± 0.11

Uncertainties presented as ± standard error from the mean. Number of replicants, n ≥ 3.

Values highlighted in light grey do not have a co-efficient of variation (C.V.) < 10% from the mean value.

An excellent degree of reproducibility (C.V. < 10%) was found for most substrates calibrated using the biosensor. Even those values above the critical threshold of 10% relative uncertainty were not much more than 10%. From this, it can be concluded that reproducible and consistent differences arise from the calibration of the biosensor with different substrates. Those substrates categorised as reversible demonstrated the highest I_{max} values, coupled with the consistently lowest K_m parameters of all of the categories (Table 5.7). Irreversibly-oxidised substrates exhibited the opposite characteristics; while

quasi-reversible substrates exhibited a compromise of these characteristics (high i_{max} coupled with high K_m, and vice versa).

Biosensor sensitivity was compared to the i/K values calculated from the averages of the modelled i_{max} and K_m parameters presented in Table 5.7 Figure 5.10 below displays the correlation existing between biosensor sensitivity and the calculated i/K values for the substrates assessed in this Section.

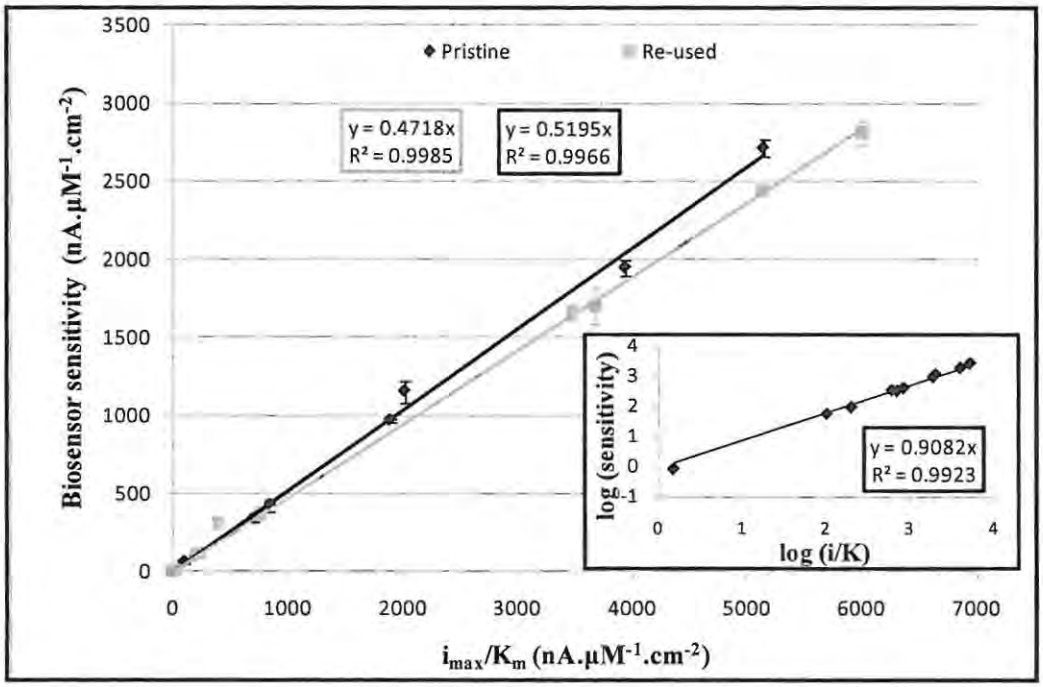

Figure 5.9: Correlation existing between biosensor sensitivity and i/K values, obtained for the substrates analysed using the optimised laccase biosensor.

Both the values obtained from the use of the pristine biosensor (black) and the biosensor after re-use (grey) are presented here. Inset boxes in the respective colours indicate the linear-regressional parameters obtained when y-intercepts are forced through the origin of the graph.

Inset box depicts a $\log_{10}$-$\log_{10}$ plot of the sensitivity plotted against the i/K values for the pristine biosensors.

Error bars indicate standard error from the mean. $n \geq 3$

The logarithmic relationships between the sensitivity and the i/K values (Figure 5.9, inset) are presented to confirm that the degree of linearity observed was consistent throughout the data-set, not merely artificially caused by those substrates possessing higher sensitivity (or i/K) values. The degree of

linearities measured through log-log plots of sensitivity vs. i/K values also possessed strong linearity (R^2 values > 0.99) for both pristine and re-used biosensors (data not shown for re-used biosensors).

The excellent linear compliance between the biosensor sensitivity and i/K values (Figure 5.9, $R^2 > 0.995$) strongly indicates a correlation between the detection sensitivity and those parameters extracted from the model. Thus, differences between the various biosensor sensitivities achieved between substrates can be discussed in terms of their contributions from the aforementioned modelled parameters: positive influences on biosensor sensitivity from the i_{max} and negative influences from the K_m values, respectively.

It is at this point that the contributions arising from the relative electrochemical properties of the oxidation products can be discussed. While CAT, 2-AP and P-CL have K_m values that differ by only a factor of 2 (means of 126, 176 and 217 μM, respectively), indicating similar substrate-binding affinities and binding/release rates (Chapter 2, Section 2.3.1.1 and Eq. 2.4), their relative detection sensitivities range more than 15-fold (970, 425, 59.2 $nA.\mu M^{-1}.cm^{-2}$, respectively). This is most likely due to the disparities between their i_{max} values, with the oxidation of GOL resulting in a nearly 7-fold higher i_{max} value than P-CL, while CAT exhibited a 10-fold increase (Table 5.7). This, in turn, can be related to the differences in electroanalytical behaviour of their respective oxidation products: P-CL, being irreversibly oxidised, exhibits a very low return current (Table 5.4) and subsequent charge yielded, GOL exhibits approximately 50% and 35% for the charge and current yields, respectively; of these examples, CAT possesses the highest %I and %Q values of 85% and 91%. This indicates that the proportion of electro-reductive oxidation products (analytes) formed during oxidation of the substrates trend with CAT>GOL>>P-CL, thus representative currents are ranked in a similar way during the operation of the biosensor. This example, in conjunction with the rest of the data presented in this section serves to indicates that knowledge of the electroanalytical properties of the oxidised products (%I, i_{max}) is required in order to equate the biochemical properties of the laccase-substrate interaction (K_m) estimated through modelling of the current-concentration functions to that of the biosensor during operation. Figure 5.10,

below, demonstrates the substrate-dependence of detection sensitivity on their respective values of i_{max} or K_m, determined from the modelled parameters.

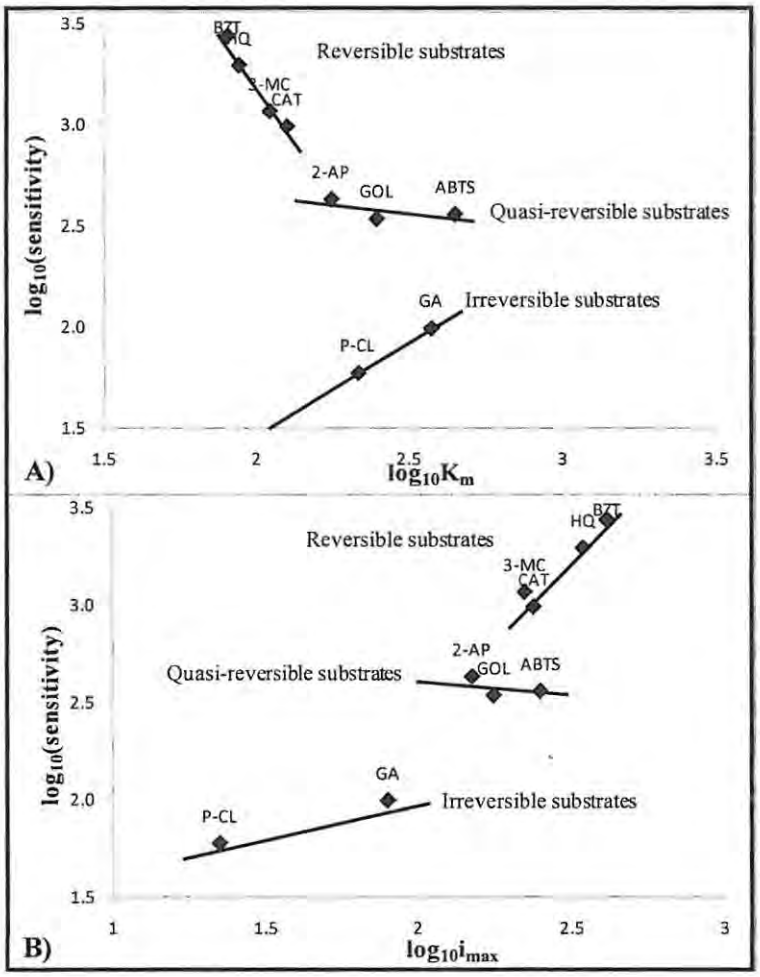

Figure 5.10: Substrate-dependence of detection sensitivity on modelled parameters

A) K_m

B) i_{max}

Data is presented in a logarithmic format for the ease-of-representation of disparate values of i_{max} and K_m across reported substrates (Tables 5.6 and 5.7)

Lines indicate linear trends existing between substrates that are grouped together on the basis of their respective reversibility categories (Table 5.4). The above graphs do not show PHE, due to the large difference in x-axis values.

When substrate-dependence of detection sensitivities is compared to K_m or i_{max} (Figure 5.10**A** and **B**, respectively), rather than the i/K values (Figure 5.9), separate trends between the substrates emerge, when grouped by their degree of reversibility as reported in Table 5.4. The detection sensitivity of

reversible substrates shows a linear positive dependence on i_{max} and a negative dependence on their K_m values. A lesser negative dependence on K_m (Figure 5.10**A**) is noted for quasi-reversible substrates, while a very slight negative dependence on i_{max} (Figure 5.10**B**) is also noted for this class of substrates. Irreversible substrates possess a positive detection-sensitivity dependence on K_m accompanied by a strong positive dependence on i_{max}. These respective trends indicate the degree to which sensitivity is affected by the modelled parameters: irreversible substrates appear to have detection sensitivities largely influenced by i_{max}, rather than K_m, since the correlation between sensitivity and i/K would indicate that increasing K_m values would decrease the sensitivity of detection. Similarly, detection of quasi-reversible substrates is influenced by K_m, rather than i_{max}, while reversible substrates show dependence on both factors. Apart from reversible substrates, K_m does not decrease sequentially with an increase in detection sensitivity (Figure 5.10**A**) – overlaps in K_m values between quasi- and irreversible substrates exist, despite significant differences in detection sensitivities. Similar behaviour in the comparison of i_{max} vs. detection sensitivity is also evident (Figure 5.10**B**). The above serves to indicate that, combined with the above shows that i_{max} (taken in this study to contain a non-negligible contribution from the proportion of oxidised product resulting in detectable analyte, analogous to the %I values established at bare GCEs) has a profound effect on the functioning of the sensor, causing the categorisation seen in Figure 5.10

5.3.3 pH studies:

An alteration in pH was anticipated to affect the laccase biosensor through 3 separate means, which are divided into their electrochemical and biochemical effects. Electrochemically, the effect of a pH alteration on the electrochemical parameters gathered using bare GCEs was anticipated to affect sensor response through the proportion of oxidised substrate converted into reducible analyte (%I) and affect the thermodynamic ease with which the substrate is oxidised by the laccase (represented by shifts in the $E_{p,a}$). Potential biochemical effect of pH on sensor were the effect of pH on the conformation, and hence, activity of the immobilised laccase, to which is conjoined the effect of pH on the active sites of the laccase, through ionisation of the Cu active atoms, or the other amino acids, as outlined by Xu, 1996.

The pH studies were performed with two main purposes in mind: (1) Modulation of the oxidation potential of the parent substrate, in order to further explore the putative $E_{p,a}$ – sensitivity correlation in the case of reversible substrates and to provide the basis for further studies in modulating sensor signal in the presence of multiple laccase substrates, which is presented in Chapter 6 of this Thesis.

For the aforementioned purposes, substrates classified as electrochemically reversible (i.e. BZT, 3-MC, HQ and CAT) were selected as model substrates for this study. These were selected on the basis of their uncomplicated oxidation/reduction mechanisms (i.e. their implied high oxidation to signal yield), both when electro-oxidised (Section 5.3.1) and during analysis by laccase (Section 5.3.2). From these sections, it was assumed that differences in sensitivity caused by change in pH and substrate species would be primarily dictated by biochemical kinetics, not electrochemical kinetics. Examples of a quasi-reversible substrate (GOL) and an irreversible substrate (GA) were additionally analysed. The inclusion of reversible and irreversible substrates was done in order to explore the relative contribution arising from analyte-electrode kinetics and their effects on biosensor kinetics. Selection of these substrates were justified on the basis of the relatively strong signal produced during analysis at pH 4.5 (Section 5.3.2).

In addition to the studies conducted at pH 4.5 (Section 5.3.2), two additional, closely-grouped pHs (3.5, 5.5) were included for substrate analysis, using both biosensors electro-oxidation, as outlined above. The narrow pH range used was selected to produce very small modulations in both the electrochemical and biochemical kinetics of the substrates, rather than to provide a complete characterisation of the biosensor under vastly different pHs. Summaries of the pertinent parameters investigated in this section are tabulated and summarised in Table 1 of Appendix 4, with select examples of the findings of the substrates used to illustrate points and the trends observed throughout discussed in general.

Increases in electrolyte alkalinity were observed to decrease the oxidation potentials and the reduction potentials of the selected substrates, both at bare GCEs and when CV was performed at the surface of biosensors exposed to saturating concentrations of substrates (Appendix 4, Tables A4.1 and A4.2),. This effect was expected (Costentin et al., 2010) due to the nature of phenolic oxidation / reduction, which undergoes a $1e^-/H^+$ or a $2e^-/2H^+$ reduction/oxidation process, and supported by Xu, 1996. As examples,

Figure 5.14**A** displays the pH-dependant behaviour observed during the electro-oxidation of HQ and Figure 5.14**B** displays the same behaviour for the voltammetric biosensor response for BZT. Summaries of the relevant 3-point peak potential vs. pH shifts are available in Table A4.2 of Appendix 4.

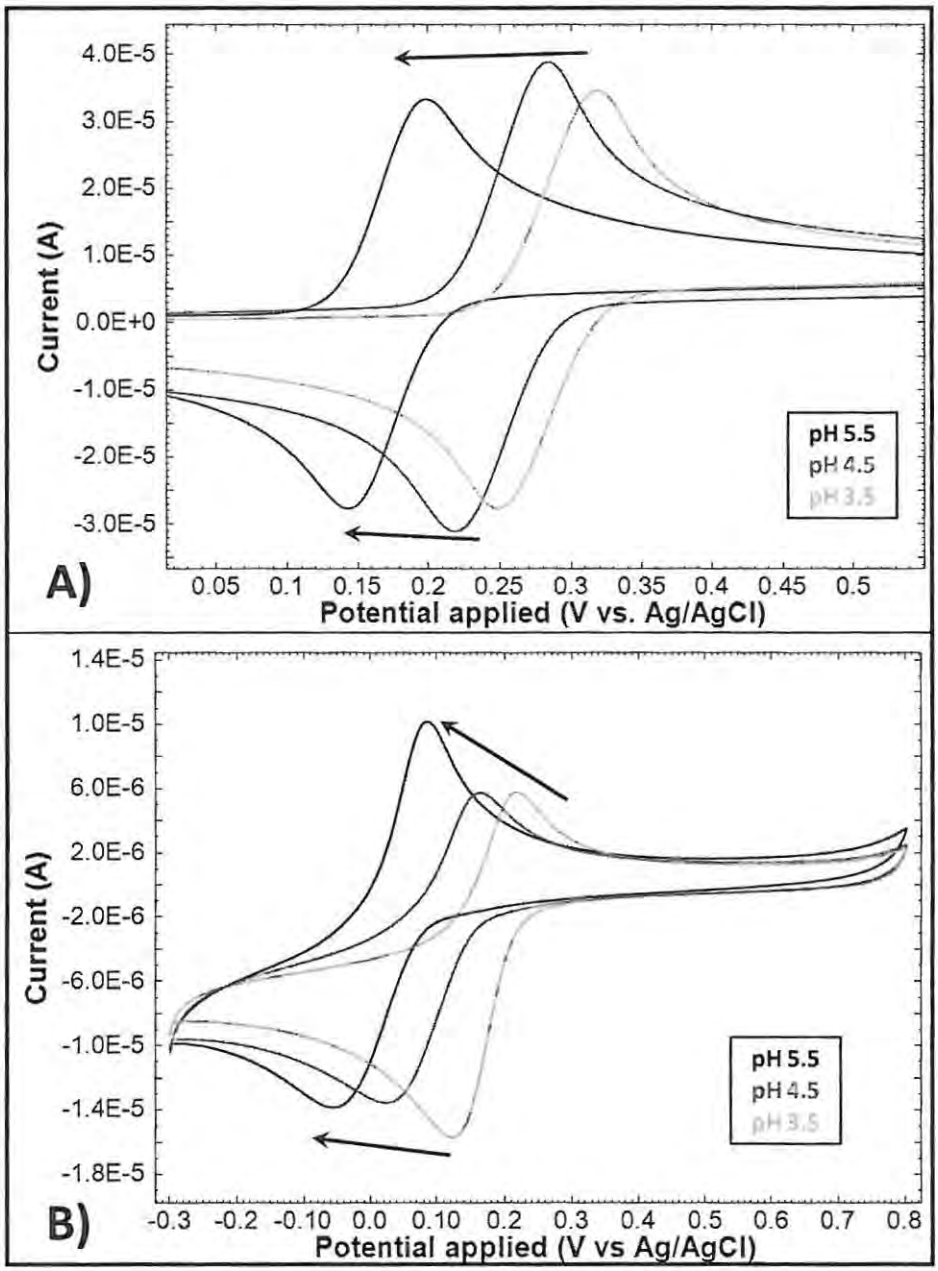

Figure 5.11: Representational CVs of the pH-dependant behaviour of oxidation/reduction cycles of: A) HQ at bare GCEs and B) BZT at laccase biosensors in SLB with pH values ranging between 3.5 and 5.5. Arrows indicate trends in oxidation peak currents with an increase in alkalinity.

Disparities between the currents present between A) and B) are due to the differing concentrations of substrates used for bare-GCE assessments (1 mM) and those used for biosensor assessments (~300 μM).

Biosensors exposed to substrates exhibited, in general, higher averaged i_{max} values (Figure 5.12**A**) with an increase in electrolyte acidity while K_m also tended to increase with an increase in acidity (Figure 5.12**B**). The sole exception to these trends in i_{max} are 3-MC and GA, for reasons that are discussed further on in-text. Tabulated summaries of the biosensor kinetic parameters are available in Table A4.2 of Appendix 4.

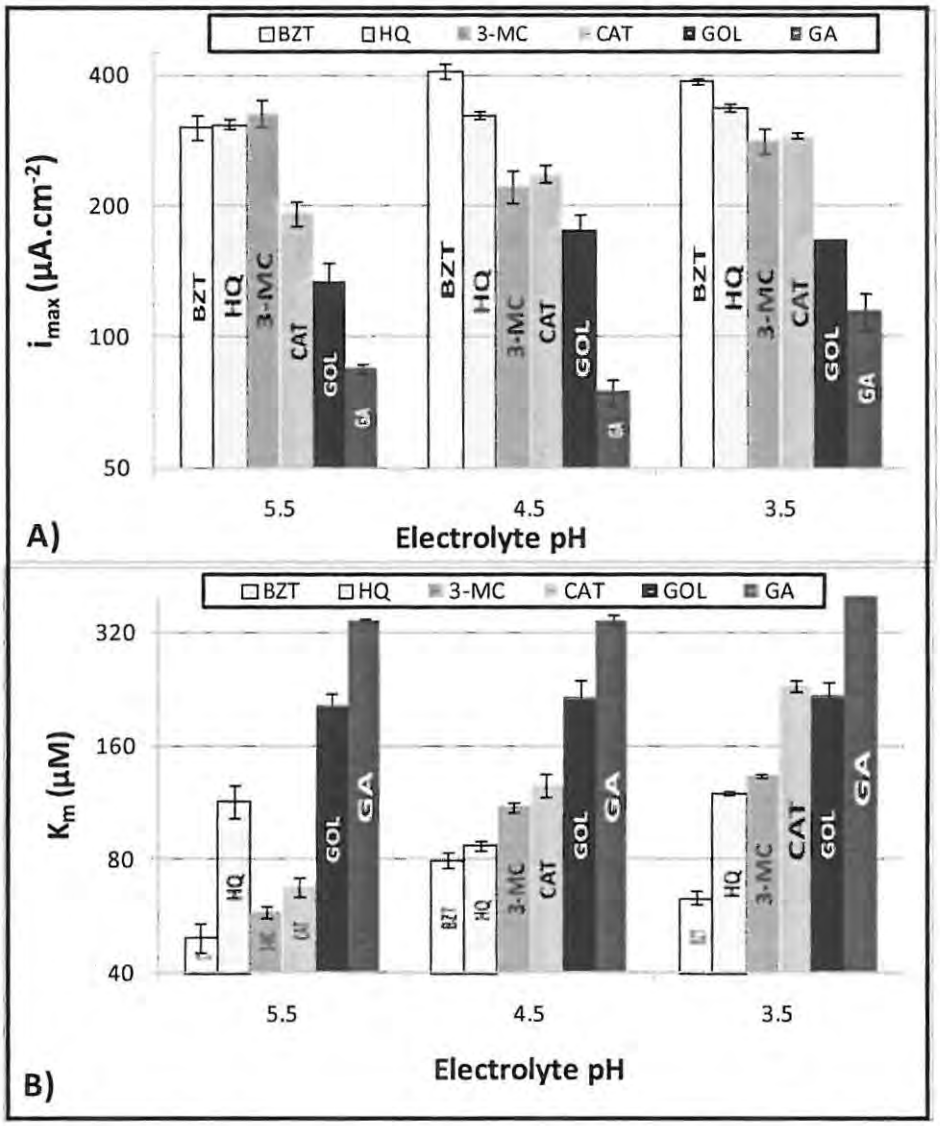

Figure 5.12: pH-dependence of imax and Km parameters for laccase biosensors calibrated using different substrates

A) pH dependence of the i_{max} parameters.

B) pH dependence of the K_m parameters.

Data in Fig. 5.12 is presented in $\log_2$ format in order to satisfactorily resolve the differences between substrates. Error bars indicate standard error from the mean, $n \geq 3$.

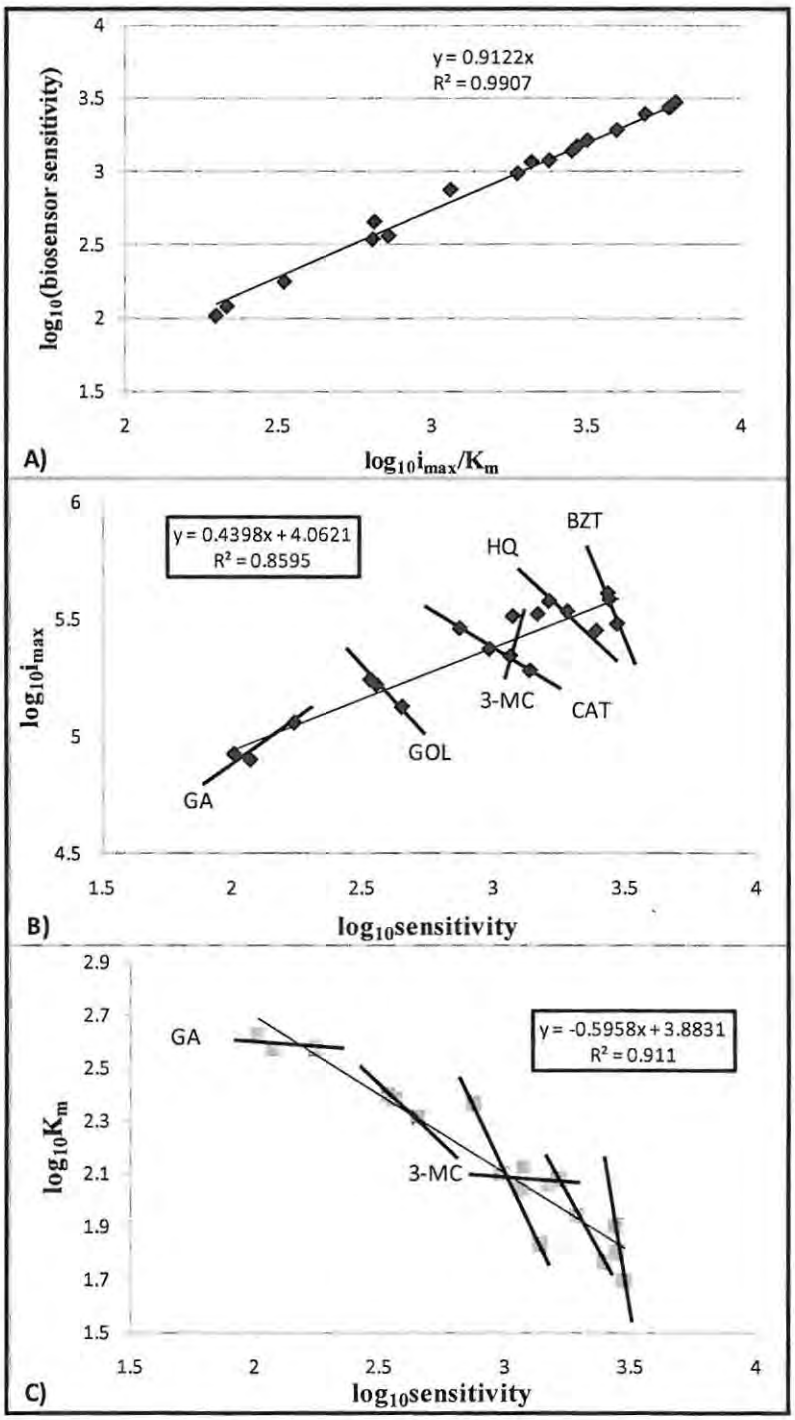

Figure 5.13: Dependence of detection sensitivities on modelled biosensor properties of selected substrates under varying pH:

A) i/K (i_{max}/K_m)

B) i_{max} parameter

C) K_m parameter

Lines present in Figures 5.13**B** and **C** indicate pH-dependent alterations in these values for individual substrates.

Figure 5.13**A** demonstrates the correlation between substrate-dependent biosensor detection sensitivities and the i/K values for the selected substrates examined under varying pH. Figure 5.13**B** demonstrates that, in the case of most substrates exhibiting reversible electrochemistry (BZT,HQ,CAT, but not 3-MC) that an increase in the i_{max} parameter (itself increasing with increasing acidity) predicts a *decrease* in the sensitivity (itself analogous to i/K values, 5.13**A**), rather than an increase. Both 3-MC and GA show a reversal of this trend, with an increase in i_{max} trending positively with the sensitivity. When comparing K_m to detection sensitivity, both GA and 3-MC show limited effect from the K_m on the produced sensitivity. This is in strong contrast to the degree of apparent dependence exhibited by the other substrates' detection sensitivity on the K_m (Figure 5.13**C**) This indicates that the detection sensitivities (i.e. i/K values) of substrates BZT, HQ, CAT and GOL are positively affected by decreases in K_m and negatively affected by declines in i_{max} occurring with a increase in electrolyte acidity. The increase in sensitivity with an increase in alkalinity indicates that the dependence on i_{max} for these substrates' detection is less than the effect on K_m. The detection of these substrates are thus controlled primarily through the biochemical kinetics occurring in the immobilised laccase film, rather than the electrochemical properties of their oxidation products. The converse is true for substrates GA and 3-MC, which record both increases in sensitivities with increasing i_{max} and no apparent dependence on K_m. (as indicated in Figure 5.13**C**). Sensitivity of detection of these substrates are thus primarily controlled through a combination of electrochemical/biochemical kinetics, rather than just through biochemical kinetics.

The i_{max} of biosensors was itself found to possess a positive linear dependence with reference to the oxidation potential of substrates at the selected pHs, as assessed at bare GCEs (Figure 5.14). This indicates that a decrease in the ease-of-oxidation of a substrate (with increasing alkalinity) increases the i_{max} value of biosensors detecting said substrate.

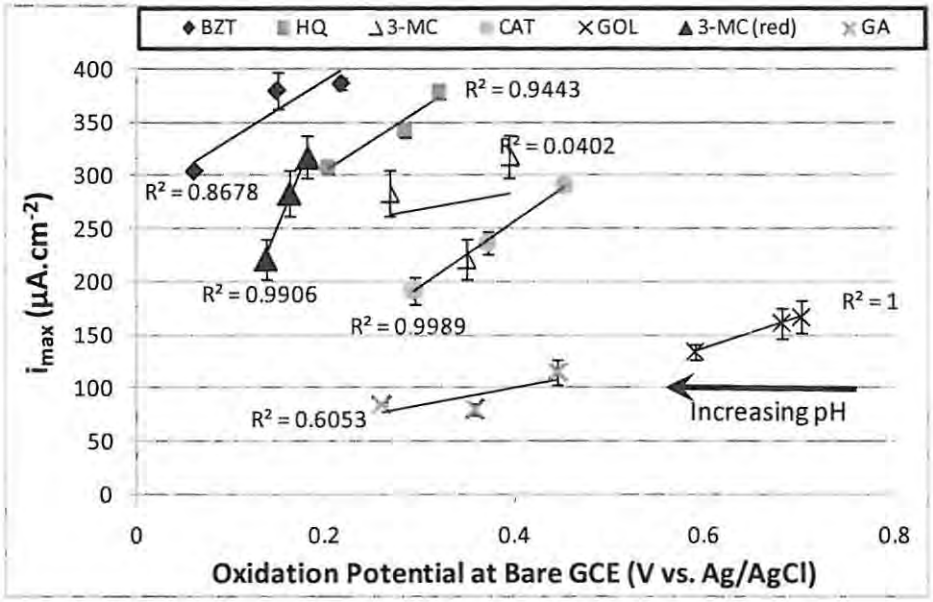

Figure 5.14: Correlation between oxidation potential ($E_{p,a}$) of substrates at bare electrodes with the modelled i_{max} parameter of the selected substrates at varying pH.

Arrow indicates the behaviour of $E_{p,a}$ with increasing pH.

As Figure 5.14 demonstrates, a positive linear trend was noted for all the substrates when the i_{max} parameter of the biosensor was plotted against the oxidation potential of the substrate established using unmodified GCEs, with an average Pearson's correlation coefficient of $R^2 = 0.900$ between the sets. The sole, partial, exception to this was 3-MC. 3-MC exhibited the formation of a pH-dependant additional redox couple situated at more positive potentials than the parent compound, when CV was performed at the surface of the biosensors (Figure 5.15, below), indicating the presence of a side-reaction which diminishes the proportion of oxidised substrate converted to analyte. This additional reaction, which is either masked or not occurring at the bare GCE, was considered to be the source of the aberration between the oxidation potential of the substrate and the i_{max} values extracted from the biosensor's calibration with 3-MC. However, taking the reductive potential of these oxidation products as being equidistant from the oxidation potential (as was the case for all other substrates, Appendix 4) and therefore indicative of the oxidative behaviour of the parent compound (Appendix 4) (3-MC (reduction) in Figure 5.14 above) produces the same linear positive dependence of i_{max} on potential.

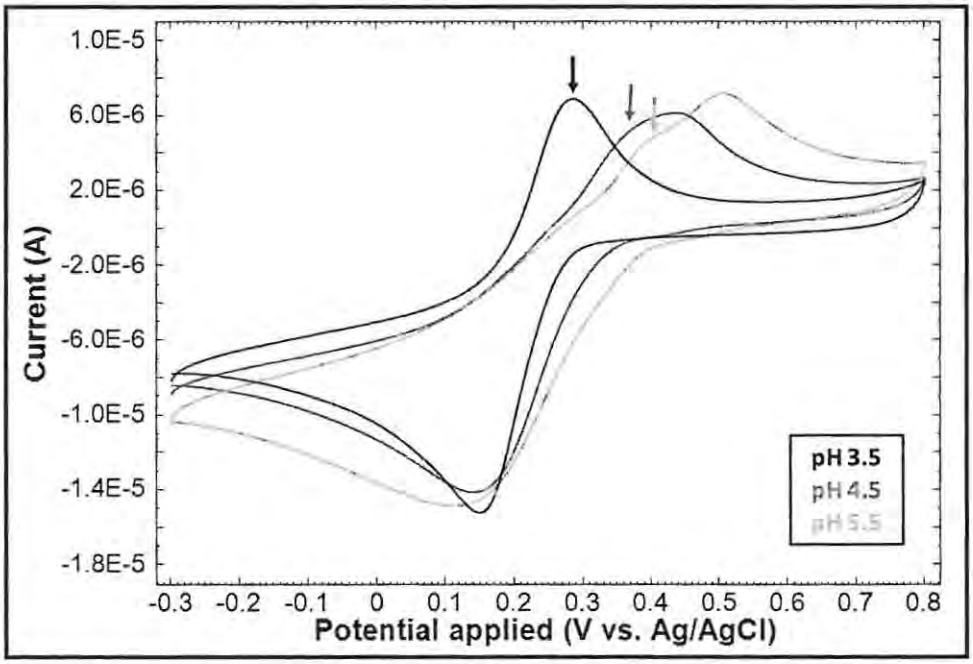

Figure 5.15: Cyclic voltammograms generated by biosensors in the presence of 200 µM of 3-MC dissolved in 0.1 M SLB adjusted to different pHs.

Arrows indicate the potential of the oxidation of the 3-MC parent compound, to distinguish between the reduction/oxidation couple occurring at more positive potentials at higher electrolyte pH values. This behaviour is not found at a bare GCE (data not shown).

The positive correlation existing between $E_{p,a}$ (oxidation potential) and %I are initially non-intuitive. A decrease in the oxidation potential indicates a more readily-oxidisable substrate, so it is expected that k_2 catalytic rate constant for the biorecognition layer would increase with an increase in the pH (Xu,. 1997), resulting in a larger i_{max}.

However, it is reported that an increase in acidity of the medium enhances the conversion of oxidised phenolics to quinones. Studies conducted on the different end-products of the radicalisation of 2,4,6-Tri-*tert*-butylphenoxyl have demonstrated that a high degree of acidity in the surrounding medium favours the protonation of the phenoxy radical, in turn promoting the formation of quinones over that of diimeric/oligomeric products (Omura, 2008). While this may not be evident when considering the less-complicated phenol-to-quinone formation exhibited by the reversible substrates, the significant increases in %I as assessed at the bare GCE for GA indicate a much higher proportion of oxidised GA is converted into reducible compounds with a decrease in pH. Table A4.1 shows that the recoverable current from GA

oxidation (%I) alters more than 5-fold under the pH range studied. The %I values exhibited by the other analytes selected for this study (Table A6.1) do not vary that substantially: The co-efficient of variation of the reported values of %I in Table A6.1 between ~13% (BZT, GOL) and ~2 % (HQ, 3-MC, CAT) of the mean values, between pHs. GA, however has a coefficient of variation ~ 99% of the mean value between pH ranges. This may indicate that, in the case of GA, rather than signal current being primarily dictated by enzyme-substrate kinetics (as would be predicted through $E_{p,a}$, such as was found for all other analytes, Figure 5.18, below), signal current is strongly influenced by the pH-dependant formation of reducible oxidation products. Hence, in the case of GA, the increase in sensitivity with a decrease in pH / increase in oxidation potential is most likely attributable to the increase in production of detectible (i.e. reducible) analyte within the system. Figure 5.16 displays the biosensor response for saturating conditions of GA under the varying electrolyte pH values profiled in this study:

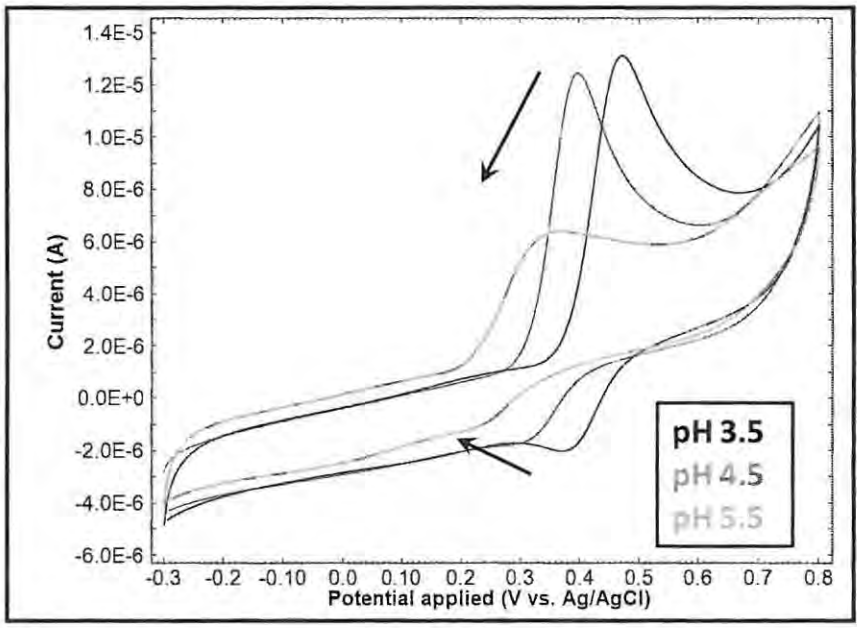

Figure 5.16: Cyclic voltammograms of GA performed at a laccase biosensor under conditions of varying electrolyte pH.

Arrows indicate trends in peak currents and potential with an increase in pH.

In the absence of substantial analyte-pH interactions, such as those exhibited by GA, the above study demonstrates that alterations in $E_{p,a}$ through manipulation of the electrolyte pH can predict sensor response to a given analyte. This is discussed in further detail in Section 5.5.4.2, below.

5.5.4: Comparisons between electrochemical characterisations and biochemical characterisations of the substrates tested.

A relationship between the oxidative potential difference between substrate and laccase and their respective oxidation rates has been found for both phenolic (Xu, 1996; Xu, 1997) and for non-phenolic aromatic compounds (Xu et al., 2000), as well as other compounds classified as laccase substrates (Xu, 1997). K_m, k_{cat} and k_{cat}/K_m values were found to possess logarithmic dependence on the difference in oxidation potential (Xu, 1996; Xu et al., 2000). This difference translates into a more thermodynamically favourable electron transfer between the substrate and the laccase, meaning that faster oxidation rates are realised. Hence, the oxidation potentials measured during this phase of research are also indications of the relative ease that laccase can oxidise the substrates characterised. Similar relationships have been derived for other laccase studies (e.g. Xu, 1996). However, oxidation rates measured in the majority of the cited studies were assessed via spectrophotometry, or oxygen-consumption which, while providing an accurate indication of substrate-enzyme kinetics are of little relevance when predicting sensor response considering opposing analyte-electrode kinetics. This study aimed to understand the principles underpinning the disparity of biosensor sensitivity between substrates, and to assign causal values based on their respective electrochemical or biochemical origins, rather than direct measurement of the biochemical conversion rates. Thus, for the purposes of this study, other electrochemically-determined parameters (%I, in particular) were included when considering how electrochemical characteristics affect biosensor response.

5.5.4.1.Pristine biosensor responses for all tested substrates: pH 4.5

Figure 5.17 displays the comparison of oxidation potential ($E_{p,a}$), of individual substrates as assessed at bare GCEs (Table 5.4) against their sensitivity of detection assessed at laccase biosensors.

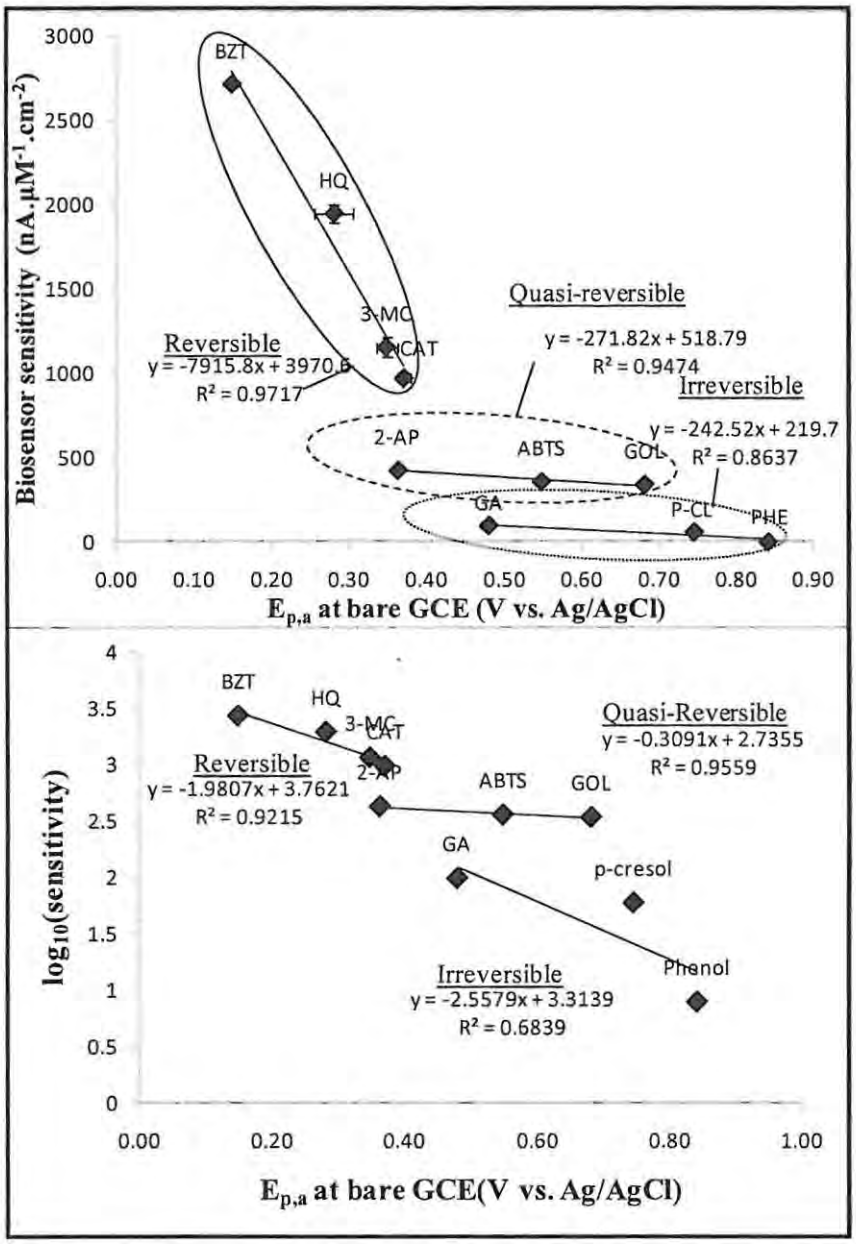

Figure 5.17: Comparisons of the oxidation potential ($E_{p,a}$) of all substrates assessed at GCEs at a pH of 4.5 to their detection sensitivity at laccase biosensors at pH 4.5.

A) Biosensor sensitivity of the tested substrates vs. the oxidative potentials, established at unmodified GCEs.

B) Logarithm of the bisosensor detection sensitivity vs. the oxidation potentials

Error bars indicate standard error from the mean (y-axis) and standard deviations from the mean (x-axis), respectively.

As mentioned previously (Section 5.3.3.2), there is a general tendency for biosensor-assessed detection sensitivity to decline with an increase in substrate-dependent oxidation potential, $E_{p,a}$ (Figure 5.17), although this only holds true within the classes of reversibility established for each substrate. Figure 5.17 shows that, even though there exists several overlaps in $E_{p,a}$ values between the three classes of electrochemical reversibility as established at bare GCE surfaces, biosensor sensitivity displays different linear trends that are consistent only within the groups characterised by their degree of reversibility, and not by the population as a whole.

The logarithm increases the degree of linearity observed for these classes. By excluding BZT, the R^2 coefficient value increases to 0.999 for reversible substrates, while the degree of linearity for quasi-reversible substrates increases from an R^2 of 0.947 to 0.956. Reasons for the exclusion of BZT are discussed in Section 5.4.4.2, for reasons uncovered during the investigation of pH-substrate-biosensor interactions. The decrease in linearity observed for irreversible biosensors is caused by the deviation of PHE from the trend observed. This is considered to be due to the high oxidation potential that, rather than favouring catalysis, may indicate the presence of an thermodynamically-unfavourable oxidation by the laccase biomolecules.

As sensitivity displays a strong linear correlation with the i/K electrochemical catalytic specificity constant (Figure 5.9) obtained through the data-modelling process, this indicates that the oxidation potential possessed the same effects on the i/K constant as it does on the detection sensitivity. In order to remove considerations of the i_{max} (as it is influenced by both electrochemical properties of the oxidation product, as well as biochemical properties from the product-enzyme dissociation kinetics) value from considerations of the enzyme-substrate affinity, the following relationship is postulated and expanded on to produce a new value containing information on both the electrochemical properties of the products of a given phenolic species, and it's relative biochemical affinity, $\%I/K_m$:

The K_m value is an indication of substrate-binding affinity and equivalent to the rate of substrate release / rate of substrate binding ($k_2/k_1+k_{-1}/k_1$, Chapter 2, Section 3.1.1). As %I tracks the proportion of oxidised substrate converted to reducible substrate ($I_{p,c}/I_{p,a}$), the value of $\%I/K_m$ corrects for the conversion proportion as outlined below:

$$\text{Sensitivity} \propto \frac{i_{max}}{K_m} = \left(\frac{v_{max}}{K_m}\right)\left(\frac{\text{Phenol oxidised}}{\text{Quinone produced}}\right) = \left(\frac{k_2(P/Q)}{K_m}\right)[E]_0 \qquad \text{Eq 5.5}$$

Where the symbols take their usual meaning from Eq. 2.2

Since, from Equation 2.2:

$$1/K_m = \frac{k_1}{k_2} + \frac{k_{-1}}{k_1} \qquad \text{Eq. 5.6}$$

Then, in the context of the biosensor:

$$1/K_m^{app} = \frac{k_1}{k_2(P/Q)} + \frac{k_{-1}}{k_1} \qquad \text{Eq. 5.7}$$

Since the rate constants k_1 and k_{-1} do not of themselves result in oxidised phenolic product, corrections in the form of (P/Q) are not necessary.

As stated previously %I is = $I_{p,c}/I_{p,a}$ and therefore is representative of:

$$\%I \sim \left(\frac{\text{Quinone produced}}{\text{Phenol oxidised}}\right) \qquad \text{Eq. 5.8}$$

So, therefore:

$$\frac{\%I}{K_m} \sim 1/K_m \propto \text{Sensitivity} \qquad \text{Eq. 5.9}$$

This formalism neglects three important considerations. Firstly: that the proportion of quinone produced remains invariant with both time of exposure of substrate and the bulk concentration of parent phenolic compound. Secondly: that the k_2 rate constant remains consistent between substrates. Third, that the K_m and i_{max} parameters are apparent, rather than actual, values indicating the rate constants of enzyme-substrate association and enzyme-product dissociation, for reasons indicated in Eq. 5.6 and 5.7 above.

The first is outside the scope of the research and, while of fundamental relevance in understanding the numerous factors comprising signal generation, are of little analytical relevance. For the second, Xu (1996) demonstrated a greater variance exists for K_m values than for k_2 parameters when monitoring the biochemical oxidation rates of different substrates with laccase. Irrespective of the above considerations, an empirical correlation between the substrate-dependent $\%I/K_m$ and the substrate-dependent detection sensitivity exists that was not found when comparing other values obtained from either the modelling process (K_m or i_{max}, Figure 5.10A and B, respectively), or from an evaluation of the electrochemical parameters of the substrates assessed at bare GCEs (Figure 5.17 for $E_{p,a}$, data not shown for %I). Figure 5.18 displays the comparison of $\%I/K_m$ values to the detection sensitivity for this phase of research.

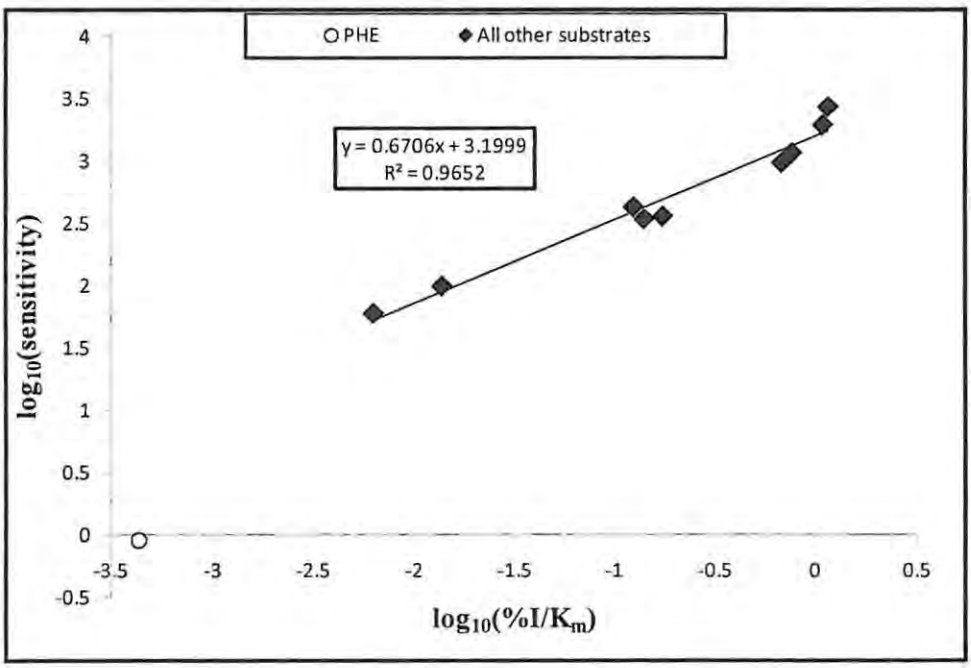

Figure 5.18: Comparison of the empirical %I/K_m value to the detection sensitivity for all tested substrates at pH 4.5

Trend was drawn excluding PHE.

As evident in Figure 5.18, a strong positive linear correlation is obtained when comparing substrate-dependent detection sensitivity to the substrate-dependent %I/K_m value. Due to the previously-discussed difficulties associated in accurately determining the conversion rate of phenolic substrate to reducible product at the biosensor through the use of %I values, %I/K_m acts as a relative indicator of a substrate's suitability to detection, rather than an absolute numerical indicator. However, the linear correlation noted extends through all the substrates tested (excluding PHE), irrespective of their degree of reversibility, in addition to the sequential increase in substrate-dependent detection sensitivity with %I/K_m values (compared to the non-sequential increases noted when comparing K_m or i_{max} alone to the detection sensitivities evident in Figure 5.10). This strongly indicates that the %I/K_m value effectively predicts the relative detection sensitivity of a given substrate on the bases of both the estimated electrode-product and estimated substrate-enzyme kinetics.

5.4.4.2 Selected substrates analysed under varying pH.

Figure 5.19 displays a comparison of the pH-dependent oxidation potential ($E_{p,a}$), of individual substrates as assessed at bare GCEs (Table A3.1) against the pH-dependent sensitivity of detection as assessed at laccase biosensors (Table A3.2).

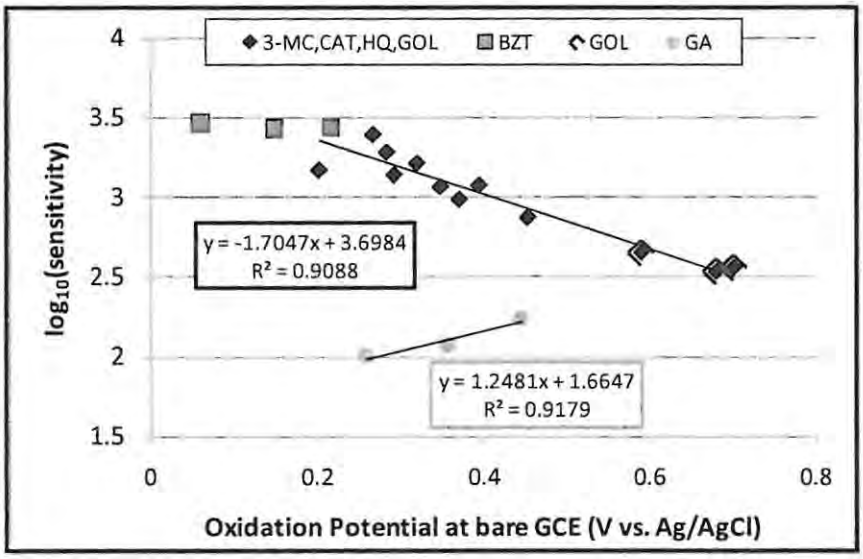

Figure 5.19: Comparison of substrate- and pH-dependent detection sensitivity (assessed with laccase biosensors) to the dependent oxidation potential ($E_{p,a}$) of selected substrates (assessed at bare GCEs)

A biphasic profile when comparing the logarithm of the sensitivity with the oxidation potential is notable (Fig. 5.19) when considering the detection sensitivity of reversible substrates (BZT, CAT, 3-MC, HQ) and GOL. The plateauing of the trend between BZT may indicate the onset of operational limitations of the biosensor sensitivity by factors such as transport limitations affecting the diffusion of dissolved O_2 into the biorecognition layer. Certainly, none of the other substrate-pH interactions produced higher results, which indicates that the biosensor system used during these investigations has an upper limit of ~2800 $nA.\mu M^{-1}.cm^{-2}$, with regard to sensitivity.

As is observable in Figure 5.19, a strongly linear negative trend ($R^2 = 0.909$) between the logarithm of the biosensor sensitivity and the oxidation potential of a substrate at a bare GCE was shown. By eliminating the aberrant data-point (HQ assessed at a pH of 5.5), the degree of linearity rises to $R^2 = 0.951$. A similar trend is noted when the logarithm of the sensitivity is plotted against the oxidation potential of substrates when cyclic voltammetry was performed at the surface of the laccase biosensors, albeit with a slightly lower degree of linearity ($R^2 = 0.9185$, data not shown). This linear behaviour is evident even when GOL is accommodated within the trend, as is the case in Figure 5.19. This indicates that, for the reversible substrates investigated in this phase of research, there is cause to suggest that

determining the oxidation potential of a given substrate in a given system, using a bare GCE, does predict the sensitivity with which the laccase biosensors used herein, can detect it.

The negative linear correlation between $E_{p,a}$ and sensitivity for reversible substrates (Figure 5.19) is anticipated, due to the kinetic considerations between $E_{p,a}$ and substrate oxidation rate (Xu, 1996), coupled with the observation that detection of these substrates shows greater influence from the modelled K_m values than it does for i_{max} values (Figure 5.13). However, in the cases of GA and BZT, for reasons previously discussed, the correlation between $E_{p,a}$ and detection sensitivity is not readily available. For the same reasons outlined in Section 5.4.4.1, the substrate-dependent, pH-dependent alterations in sensitivity was compared to the $\%I/K_m$ value established in this study to study the combined effects of biochemical and electrochemical reactions of substrate oxidation and detection (as in Figure 5.18). Figure 5.20 displays the comparison between detection sensitivity and the %I/Km values calculated for biosensor-based detection of BZT,3-MC,HQ,CAT,GOL and GA under conditions of varying pH.

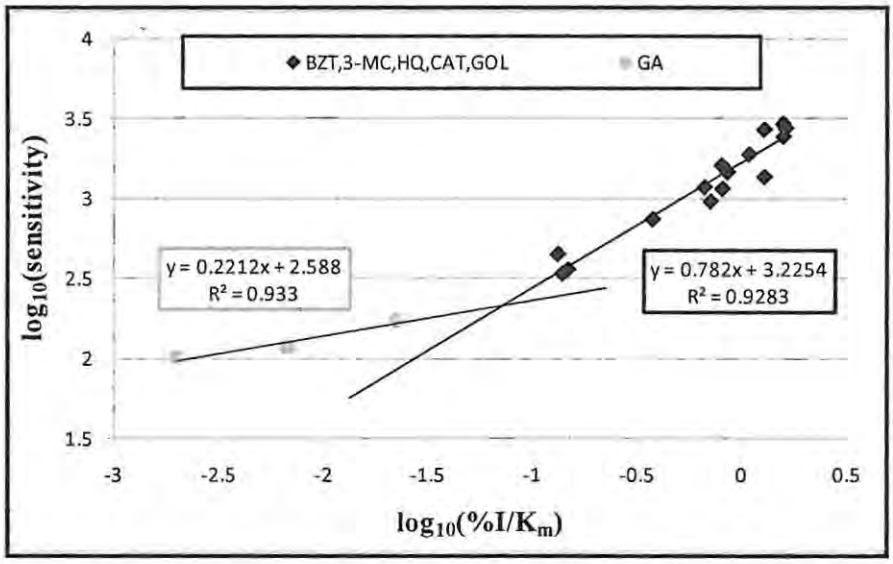

Figure 5.20: Comparison of the substrate- and pH-dependent detection sensitivity to the dependent $\%I/K_m$ values.

The use of $\%I/K_m$ as a predictor of detection sensitivity (Figure 5.20), rather than $E_{p,a}$, (Figure 5.19) has the effect of linearising all biosensor responses, irrespective of their classification of reversibility, as was previously noted for the detection of substrates at pH 4.5 (Figure 5.18). In addition, a higher degree of

correlation is noted for those substrates classified as reversible or quasi-reversible than is found when $E_{p,a}$ is compared to detection sensitivity ($R^2 = 0.928$ in Figure 5.20, compared to $R^2 \sim 0.909$ in Figure 5.19). Similar to the findings represented in Figure 5.18, an increase in the $\%I/K_m$ trends with a sequential increase in the detection sensitivity of a given substrate, under given pH conditions, compared to the non-sequential increases noted for i_{max} or K_m alone as predictors of sensitivity (Figure 5.13**C** and **B**, respectively) or that noted for $E_{p,a}$ (Figure 5.19). Again, this strongly indicates that the $\%I/K_m$ value is a more effective predictor of the relative detection sensitivity of a given substrate than the other parameters reported on in this study.

5.4.4.4 Comparisons of alterations to operational biosensor parameters following re-use for all substrates at pH 4.5

Table 5.8 displays the relative alteration to operational biosensor kinetic parameters (detection sensitivity, i_{max} and K_m) to biosensors re-calibrated with their respective substrates, in addition to pertinent behaviours of the substrates when fouling behaviour at bare GCEs was assessed.

Table 5.8: Alterations to sensor operational kinetics following re-use and correlation with studies found at bare GCEs

	Biosensor operational parameters after re-use (presented as a percentage of values obtained for "pristine" unused biosensors)				**Bare GCE**	
Substrate	**% sensitivity**	**% i_{max}**	**% K_m**	**%Sens|%i_{max}|%K_m**	**Fouling (oxidative current)[1]**	**Electroactive oxidation species[2]**
Electrochemically Reversible						
BZT	105	84.6	72.5	↑↓↑	Yes	No
HQ	126	107	81.1	↑↑↑	No	No
3-MC	144	156	95.8	↑↑↑	No	No
CAT	169	121	62.0	↑↑↑	No	No
Quasi-Reversible						
ABTS	84.5	121	171	↓↑↓	No	No
GOL	32.8	53.4	133	↓↓↓	Yes	Yes
2-AP	86.3	113	139	↓↑↓	Yes	Yes

			Irreversible			
GA	115	181	178	↑↑↓	Yes	No
P-CL	24.0	85.2	252	↓↓↓	Yes	No*
PHE	20.0	37.9	152	↓↓↓	Yes	Yes

[1] – original data presented in Table 5.4

[2] – other than the quinone counterpart of the parent compound, Table 5.4

* presence of pigmented film indicates formation of fouling compounds that were not found to be strongly electroactive under experimental conditions.

Due to the correlation occurring between sensitivity and the modelled parameters of K_m and i_{max} (Figure 5.9), a review of the information in Table 5.8 indicates that alterations in sensitivity upon re-use are primarily governed via alterations in the K_m parameter following re-exposure of the sensor to the selected substrate, rather than alterations in the i_{max}. For example, for electrochemically reversible substrates, the generally-observed decrease in Km following re-use is coupled to an increase in sensitivity, while the reverse is true, for example for quasi-irreversible substrates. The i_{max} parameter appears to vary much less upon re-exposure than do the K_m and sensitivity values.

The fouling behaviour of substrates assessed at bare GCEs does seem to predict biosensor inactivation following exposure to substrates. All those substrates classified as quasi-reversible and irreversible substrates that exhibited fouling behaviour at the GCE (Table 5.4) produced declines in the sensitivity and concomitant increases in the apparent K_m of the biosensor following re-calibration with the selected substrate (Table 5.8), with the exception of GA. Furthermore, the majority of these substrates also produced a decline in the i_{max} modelled parameter.

All non-reversible substrates tested showed an increase in the modelled K_m response following re-use, indicating inactivation of either the transducer, or the biorecognition layer by oxidation products of same. All those substrates showing occurrence of fouling at the electrode surface exhibited a decrease in the i_{max} with exception of 2-AP, most likely through passivation of the electrode surface.

However, all those substrates exhibiting a decrease in sensitivity, concomitantly show a decrease in K_m, while i_{max} doesn't appear to alter significantly. A decline in the i_{max} parameter due to a decrease in the k_2

rate constant would result in a decrease in the apparent K_m of the enzyme system (Equations 2.3 and 2.1 and Scheme 2.1 in Chapter 2), as opposed to the increase observed (Table 5.8). Hence, two reasons may be equally plausible for describing the decrease in i_{max} following re-use of the sensors: destabilisation of the enzyme-substrate complex assembly parameter (resulting in a concomittant decrease of the k_1 parameter, Eq. 2.2) via inactivation of the biorecognition layer by the oxidation products, or electrode passivation, which fouling behaviour indicates. This, combined with the formation of electroactive species found adsorbed onto the surface of re-used GCE biosensors that appear to be linked to an increase in i_{max} during the detection of CAT when deploying re-used sensors (Chapter 4, Section 4.5.3.2), indicates that the alteration of i_{max} is linked to the attachment of oxidation products to the transducer surface i.e. fouling of the electrode, inhibiting current response upon re-use. The opposite holds true for those substrates classified as reversible, for reasons that have been outlined in Chapter 4, Section 4.5.3.2. This indicates that a categorical distinction exists between the fouling behaviour of a given substrate (as assessed at a bare GCE) and the effects of its exposure to the biosensor, which affects the current response of biosensors upon re-use. Quasi-reversible and irreversible substrates passivate biosensor response, while reversible substrates appear to enhance biosensor response when the substrate under investigation is re-analysed using the same biosensor.

5.6 Conclusions:

Chemically-distinct substrates were analysed using both unmodified GCEs and laccase-modified GCE biosensors in order to investigate whether the individual electrochemical behaviour of substrates could aid in predicting variations in biosensor detection sensitivity between substrates. This variation is postulated to exist based on differences between substrates with regard to their individual substrate-laccase kinetics and on their subsequent behaviour prior to electro-reduction at the electrode surface.

Preliminary examinations of the substrates using unmodified GCEs indicated consistent differences existed between studied substrates in terms of their peak oxidation potential ($E_{p,a}$), anodic-to-cathodic peak potential separation (dE), the ratio of oxidation to reduction (%I and %Q) and fouling behaviour.

These parameters allowed the various substrates to be categorised according to the degree of reversibility observable at the electrode. Reversible, quasi-reversible and irreversible behaviour at the electrode surface was found to consistently occur in a substrate-dependent manner when assessed at bare GCEs in SLB, pH 4.5

Substantial variances were noted between substrates when used to calibrate laccase-modified GCE biosensors for all the biosensor operational parameters reported (linear response range, detection sensitivity, K_m, i_{max}). In general, the linear response range was found to decline logarithmically with an increase the logarithm of the sensitivity of detection. Sensitivity declined in the order: of reversible > quasi-reversible > irreversible between the global population of assessed substrate and, within these categories, decreased with increasing oxidation potential. While substrate-dependent detection sensitivity was found to correlate to the substrate-dependant i/K (which combined i_{max} and K_m values), no such correlation could be found for either of these values independently. Differences between substrate-dependent i_{max} values were assigned to arise from a combination electrochemical and biochemical origins, while substrate-dependent K_m values were assigned to arise from biochemical origins, primarily. Reversible (and to a lesser extent, quasi-reversible) substrates were shown to have detection sensitivities with negative dependence on the K_m value, indicating that the detection of these substrates is controlled biochemically. Irreversible substrates were found to have a positive dependence on K_m, while possessing a positive dependence on the i_{max} parameter (taken to have a non-neglible contribution from %I), indicating that the detection of these substrates is controlled through both biochemical and electrochemical considerations. While a general correlation was found, within groups, between substrate-dependent biosensor detection sensitivity and the $E_{p,a}$ assessed at bare GCEs and validated through the literature existing on the subject, this correlation did not provide a linear correlation between the general population of substrates. A further parameter, $\%I/K_m$, combining the electrochemical behaviour of the substrates at bare GCEs with the affinity for the substrate assessed at the biosensor, correlated strongly with the substrate-dependent detection sensitivity across most of the selected substrates, which none of the other parameters assessed (either electrochemical or biosensor-originating) was found to achieve.

In order to explore the relative roles of electrochemical / biochemical control of substrate-dependent detection by the laccase biosensor, 6 substrates corresponding to all the substrates classified as reversible (HQ, BZT, CAT, 3-MC) and substrates selected from the quasi-reversible and irreversible categories (GOL and GA, respectively) were selected for further studies under varying electrolyte pH (pH 3.5 to pH 5.5). This was performed in order to modulate the various electrochemical and biochemical parameters postulated to govern signal generation, in order to further investigate in greater detail the interaction between these parameters. Both electrochemical parameters and biosensor operational parameters were found to alter with pH. In general, an increase in both K_m and i_{max} was noted with an increase in electrolyte acidity, while a significant increase in %I was noted for GA.

A correlation between detection sensitivity and the i/K value was found during the pH studies, allowing sensitivity to be discussed in terms of the relative contributions of each of these parameters. For most of the reversible substrates (HQ, BZT, CAT, GOL), sensitivity was found to depend negatively on both the i_{max} and K_m, indicating that signal generation is primarily governed by the K_m values, and hence, the biochemical substrate-laccase kinetics, rather than electrochemical considerations. For the substrates 3-MC and GA, the opposite was true: while sensitivity was not found to be affected greatly by K_m, positive correlations between i_{max} and detection sensitivity indicated that, for these substrates at least, signal generation is strongly linked to both biochemical and electrochemical considerations. While a strong correlation existed between the pH-dependent detection sensitivity of reversible substrates and their pH-dependent $E_{p,a}$ values under conditions of varying pH than was noted when assessing all of the substrates at pH 4.5, this formalism still does not take into account sensor responses from either BZT or GA. A comparison between the detection sensitivity and the $\%I/K_m$ values under these conditions revealed a stronger correlation than was observed when comparing sensitivity and $E_{p,a}$, as well as a sequential increase of $\%I/K_m$ with an increase in detection sensitivity, which was not evident when assessing detection sensitivity with any other reported parameter. This, combined with the findings of all of the tested substrates at pH 4.5, indicates that $\%I/K_m$ can be successfully used in predicting sensor response to a given substrate, both on the basis of the substrate-dependent, pH-dependent substrate-laccase biochemical kinetics and on the basis of dependent product-electrode kinetics.

The substrates' effects on biosensors during re-use were compared to the electrochemical parameters established at bare GCEs. In general, only reversible substrates resulted in re-used biosensors exhibiting more sensitive substrate detection upon re-analysis, for reasons outlined in Chapter 4 pertaining to alteration to the structure of the BSA-laccase film and GCE surface upon exposure of both to laccase-oxidised phenolic products. A combination of product inactivation of the biorecognition element and electrode passivation (fouling) was indicated to reduce sensor response upon re-use for quasi-reversible and irreversible substrate. A categorical correlation between electrode passivation during electro-oxidation of substrates at unmodified GCEs and a reduction in re-used biosensor operational parameters (relative to the prisine biosensor) was established.

Hence, it is proposed that electroanalytical assessment of individual substrates (performed both at bare GCEs and laccase biosensors) can be used in order to predict the efficacy of a given substrate's detection limits when considering the biosensor used in this research. This is of great application when considering the deployment of this sensor against industrial effluents where characterisation of the substrates and their relative electroactivity can take place, but also helps explain the lack of consensus regarding kinetically-driven parameters obtained for amperometric biosensor devices – vis, that it is not necessarily alterations in the biosensor-substrate kinetics that by itself informs the transduced sensitivity, but non-negligible considerations of the fate of the oxidised product that themselves can be assessed electrochemically. Monitoring of the $E_{p,a}$ alone provides insufficient information regarding the efficacy of detection of a given analyte/substrate. While the actual velocity of the enzyme reaction may be strongly-correlated to the oxidation potential when considering any *o*- or *p*-diphenols (as demonstrated by Xu, 1996), this is not of great concern when considering the biosensing applications – it has been shown in this research that the signal itself can be correlated to parameters that take into account both the electrochemical and biochemical parameters that combine to generate signal at the electrode surface.

Chapter 6: Multiple-Pulse chronoamperometry applied to the real-time, specific detection of phenolics in mixed samples

6.1 Abstract:

This Chapter sought to investigate simultaneous, specific detection of multiple phenolic substrates using the laccase biosensor examined in Chapters 4 and 5 of this Thesis. A proof-of-concept regarding the application of Multiple Pulse Chronoamperometry (MPCA) to address this aim is outlined.

Three separate substrates were selected as case studies for this phase of research, given their uncomplicated oxidation products established in Chapter 5. To further separate the oxidation from the reduction peaks associated with the electrochemistry of catechol (CAT), hydroquinone (HQ), 1,2,4-benzenetriol (BZT), laccase fabricated on gold electrodes (AuEs) were fabricated. AuEs were selected as they are notoriously poor oxidising agents of aromatic compounds. Further separation of the oxidation peak of the parent compound, and the reduction of the laccase-generated quinone is desirable in order to include a 'resting' potential, which allows the system to relax between multiple detection ('sensing') potentials, in order to maintain a constant, representative mixture of all three substrates near the electrode surface.

The kinetics and detection sensitivity of the aforementioned substrates by the laccase biosensors on AuEs was, thus, determined under the different conditions pertinent to this research. Firstly, AuEs were compared to the standard GCEs, in terms of their detection sensitivity and modelled biochemical rate parameters, K_m and i_{max}, for the detection of each substrate under single-potential chronoamperometry, as has been previously reported for GCEs. Secondly, AuEs operating under multiple-pulse chronoamperometric detection of substrates in isolation were compared to the first results. Finally, AuEs operating under MPCA conditions in the presence of all three substrates are reported on.

6.2 Introduction

6.2.1 Multiple-pulse chronoamperometry:

Multiple-pulse chronoamperometry (MPCA, also sometimes referred to as Pulsed Amperometric Detection or "PAD") is an electrochemical waveform concerned with the rapid, sequential switching between selected potentials and monitoring their resulting currents independently. The theory governing the current response to these multiple excitation steps remains similar to that of chronoamperometry. Scheme 6.1 follows to better depict this analytical waveform:

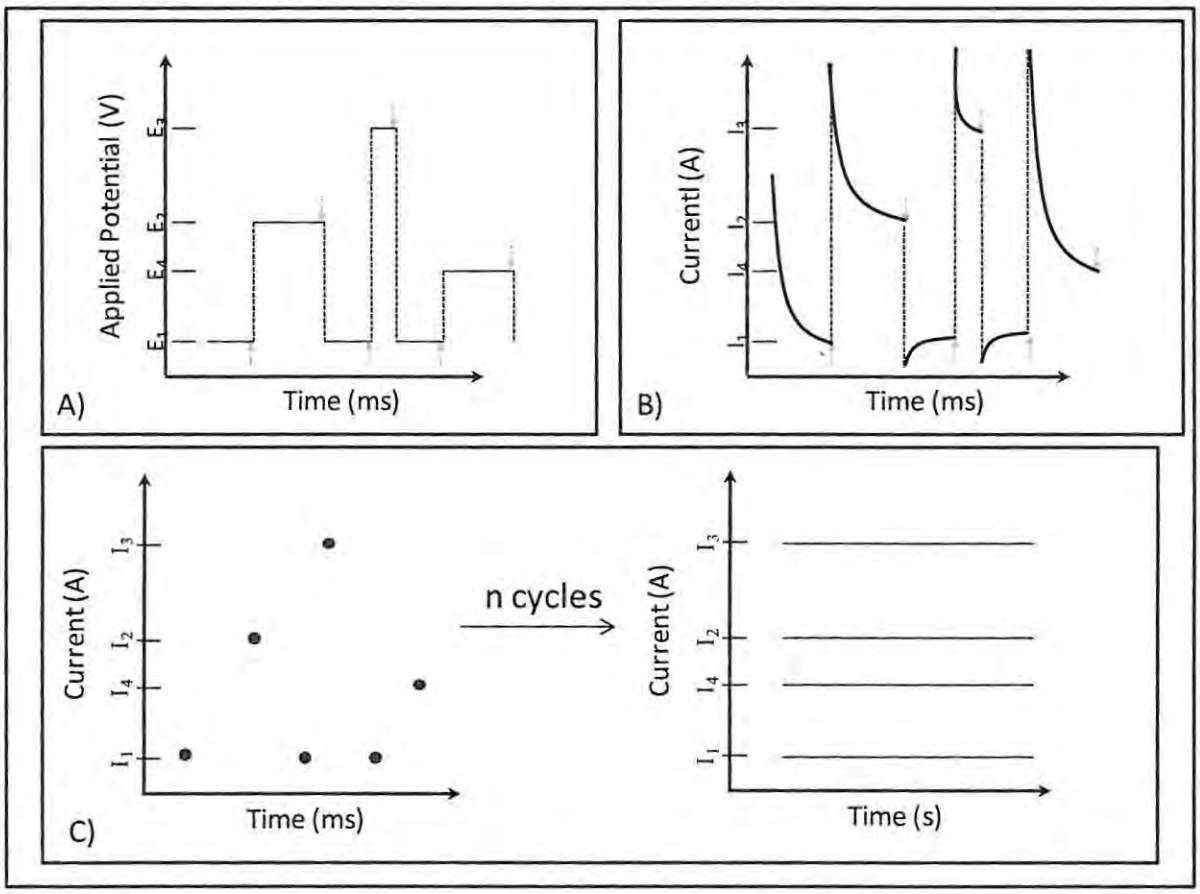

Scheme 6.1: Generic example of multiple pulse chronoamperometry

A) Single scan of a generic potential-time pulse cycle. Grey Arrows indicate times at which current is sampled.

B) Currents transduced from the potential shifts in Scheme 6.1**A**. Grey arrows indicate times at which current is sampled

C) Sampled currents resulting from the potential-time pulse imposed on a given electrochemical system over a single potential-time cycle (left-most graph). In multiple-pulse chronoamperometry, these currents are tracked discretely and, over sufficient potential-time cycles, resolve to provide separate currents-time functions superimposed over the same time axis (right-most graph).

A review of the available literature reveals MPCA, as an electroanalytical waveform, is used for two major applications not pertinent to this research: firstly, in order to clean and reactivate electrode surfaces *in situ*, following, or during, electroanalysis (e.g. to remove phenol-generated anodic fouling products, Ding and Garcia, 2006; Bebeselea et al., 2010) or secondly to enhance stability, or sensitivity, of detection. The second occurs primarily through the inclusion of a pre-concentrative or excitation potential, increasing the analyte's concentration near the electrode during analysis or generating the analyte prior to detection at another potential (e.g. Neuberger and Johnson, 1987). For the second application, the use of MPCA in carbohydrate detection using gold electrodes (as outlined and optimised by Neuberger and Johnson, 1987) is a common method of carbohydrate detection (e.g.s Zook and LaCourse, 1995; Blanco et al., 2004) and is often coupled to HPLC separation of analytes during real-time analysis.

The third application, that of selective simultaneous detection through the control of different potentials, is the most recent and least researched application of this waveform, and is the principal motivation for the use of MPCA in the research reported on in this Chapter. Since, as outlined in Chapter 2, the applied potential of the working electrode dictates which reaction(s) occur(s) at the surface of the working electrode, control of the potential provides a means of specification between competing signals. Thus, the use of MPCA can provide multiple levels of specificity to be imposed on the same analysis. This results, potentially, in a real-time separation of multiple signals which normal i.e. static-potential chronoamperometry cannot provide. The principles of this have similarly been applied to the selective determination of different ions (Küpper and Schultze, 1997).

Recently, several articles dictating signal separation for the *anodic* detection of multiple phenols and phenolic derivatives using MPCA have been published (Ding and Garcia, 2006; Medeiros et al., 2010). However, none of the research to date has yet been performed on the cathodic detection of different oxidation products generated through the laccase-based oxidation in a biosensor configuration.The former (anodic detection) is simplified by the application of appropriate potentials for the measurement of the current following oxidation of the analytes. In the biosensor assembly for cathodic detection, it is the application of the potential for reduction of the oxidation products which is of interest. As research

reported in Chapter 5 indicates, substantial differences exist in the potentials at which these products are reducible at for different substrates. However, the *cathodic* detection of multiple phenols oxidation products is then complicated by the selection of relevant reduction potentials which do not overlap the oxidation potentials of the substrates themselves within a mixture. This concept is conveyed further in Figure 6.1(below) which shows the CVs of substrates BZT, CAT and HQ and the prospect for overlap. In theory therefore, simultaneous detection of a mixture of phenolic compounds through the use of MPCA imposed at a laccase-modified electrode is possible if sufficient separation of the anodic and cathodic waves can be achieved.

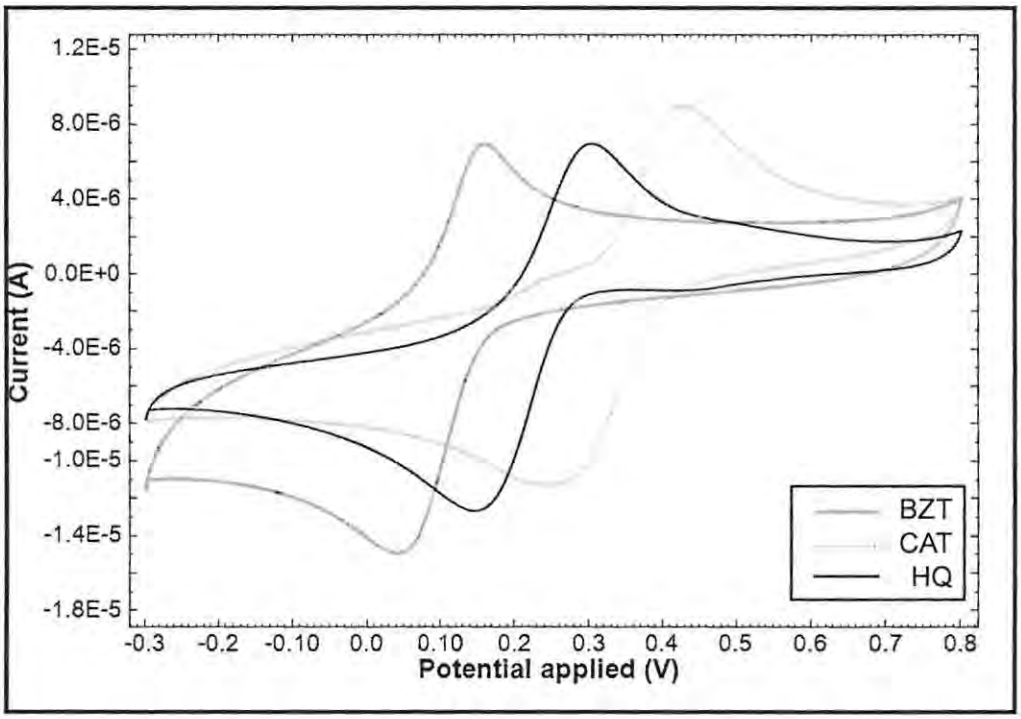

Figure 6.1: Cyclic voltammetry profiles showing the close proximity of anodic and cathodic peaks for the selected substrates (BZT, CAT, HQ) when assessed at laccase biosensor-modified GCE surfaces.

Data from the above is reported in Chapter 5 of this Thesis.

All of the above cyclic voltammograms were generated at a scan rate of 0.1 $V.s^{-1}$, in SLB, pH 4.5

This chapter therefore seeks to examine methods for separating signals resulting from the oxidation of three phenolics possessing simple oxidation/reduction chemistry at laccase-modified electrodes to allow for feasible application of MPCA to achieve simultaneous phenolic detection. To this end, the application of the inclusion of resting potentials and gold electrodes is examined.

6.2.2 Considerations for MPCA – Resting potentials

If one considers the irreversible electrochemical reduction of the system ($\mathbf{O} + ne^- \rightarrow \mathbf{R}$) under which only **O** is initially present and is the sole electroactive element:

Using MPCA with potentials applied both ahead (more positive) and behind (more negative) of the formal redox potential, $E^{0'}$; switching of electrode potential to $E < E^{0'}$ results in the generation of a reductive current from $\mathbf{O} + ne^- \rightarrow \mathbf{R}$. This causes a depletion of **O** located near the electrode surface generating the subsequent imposition of a distant-dependent concentration gradient, $\delta\mathbf{O}/\delta x$, where x is the one-dimensional distance from the electrode surface.Under conditions of semi-infinite linear diffusion, the current (i_t) is then governed by the following equations (derived from Fick's first law of diffusion):

$$i_t = \left(\frac{dQ}{dt}\right) = nF\left(\frac{dN}{dt}\right) = nFAD_O\left(\frac{\delta \mathbf{O}}{\delta x}\right)_{x=0,t} \qquad \text{Eq. 6.1}$$

Where n is the number of electrons, F is Faraday's constant (96458.3 C), A is the cross-sectional diffusional area (cm^2) and D_O is the diffusion coefficient of **O** ($cm^2.s^{-1}$) (Heineman and Kissinger, 1996). In the absence of any other forms of mass transfer other than diffusion, Eq 6.1 becomes the Cottrell equation, which describes an exponential decrease in the sampled current as a function of time:

$$i_t = \frac{nFAD_O^{1/2}C_O^*}{\Pi^{1/2}t^{1/2}} \qquad \text{Eq. 6.2}$$

Where C_O^* is the bulk concentration of **O** ($mol.cm^{-3}$) and the other symbols have their usual meaning as in Eq. 6.1 (Heineman and Kissinger, 1996).

This becomes important when considering the effects of generated currents obtained when trying to separate current between several analytes. To extend the above example, consider the detection of several analytes O_a, O_b and O_c, which reduce at increasingly negative potentials E_a, E_b and E_c, respectively. Thus, E_c generates current from the reduction of all three substrates, E_b from the reduction of O_a and O_b and so on. One cannot simply apply a potential cycle of $(E_a \rightarrow E_b \rightarrow E_c)_n$ in order to detect all three

substrates. Depletion of O_a during the application of E_a will cause the current generated from $E = E_b$ to be under-represented, through the depletion of O_a at $E = E_a$

However, upon altering the potential to $E > E^{0'}$: **O** no longer undergoes reduction and the concentration gradient then decreases as the system relaxes again towards its original state (i.e $\delta O/\delta x$ decreases), increasing the amount of **O** localised near the electrode. Hence, the application of a so-called "resting" potential is necessary between each step in order to ensure that representative proportions of all three analytes be present near the electrode surface throughout all 3 potential steps used for the detection of analyte (designated as "sensing" potentials herein).

For the purposes of biosensor investigated throughout this research, which are deployed under stirred conditions to aid mass transfer, the examination of a hydrodynamic element to describe current-time behaviour is controlled through convection and warrants a brief examination. In the absence of kinetic considerations (i.e. current is limited by mass-transport only) and under the stirred conditions in which the biosensor is applied (presence of convection), current response is no longer limited by the time of applied potential. Rather, it becomes analogous to that of the limiting current defined by the Levich Equation (Bard and Faulkner, 2001):

$$I_{l,c} = \frac{nFAD_O[C_{O*} - C_{O(x=0)}]}{\delta_O} \qquad \text{Eq. 6.3}$$

After sufficient time the diffusion layer (δ_O) of **O** becomes a constant, given sufficient time. δ_O corresponds to a non-time dependent element of:

$$\delta_O = 1.61 D_O^{1/3} \omega^{-1/2} \nu^{1/6} \qquad \text{Eq. 6.4}$$

Where ω is the speed of rotation undergone by the electrode (radians.s^{-1}) and ν is the kinematic viscosity of the analyte matrix (~0.0091 $cm^2.s^{-1}$ for water at 25 °C) (Bard and Faulkner, 2001). While this corresponds to studies normally conducted at a rotating disk electrode (RDE), a similar behaviour is anticipated for electrodes placed near a stirrer-bar during the application of a potential that is not

kinetically-limiting to a particular substrate. Hence, similar principles to those outlined above will apply, with respect to substrate depletion due to potential switching during MPCA analysis.

6.2.3 The selection of Au as an electrode surface:

Gold electrodes are relatively poor oxidisers of organic compounds, including phenolics, which is due in part to the complex basic electrochemistry exhibited by the gold surface itself (Burke et al., 1994). Rather than participating in direct electron exchange, oxidation of phenolics by Au and Pt is postulated to proceed via an ECE mechanism (i.e. a reaction with an intermediate chemical step between charge-transfer stages) involving the formation of hydrous gold-oxide adatoms which mediate electron transfer between the electrode and phenols (Burke et al., 1994; Burke and Nugent, 1998 Iotov and Kalcheva, 1998). Several separate species of such electro-generated mediators that are present under different conditions, primarily electrolyte pH, have been proposed (Burke and Nugent, 1998). The above reaction limitation, coupled with the weak chemisorption behaviour observed at Au surfaces (Burke and Nugent, 1998) combine to make Au particularly difficult to routinely apply to a variety of analytes.

The proposed ECE mechanism however at AuEs possesses a large advantage for the application of MPCA – rather than each substrate possessing individual oxidation potentials, as was observed at GCEs in Chapter 5 (and above), all substrates should in theory possess similar oxidation potentials corresponding to the formation of the surface-bound mediator, such as outlined by (Burke et al., 1994; Burke and Nugent, 1998). Similarly, this restricts the reduction of analytes to potentials at which the mediator is not generated (Burke and Nugent, 1998).

For the purposes of the research reported in this Chapter, this has the advantageous effect of markedly separating the oxidation and reduction potentials of the substrate from one-another. This desirable separation is a property that the GCE cannot provide for the substrates investigated. All of the substrates under investigation are classified as "reversible" phenolic substrates in Chapter 5 of this Thesis, indicating anodic-to-cathodic peak separations of ≤ 75 mV. The effects of individual analytes undergoing oxidation during the application of sensing potentials would severely hamper the detection of the desired reductive current produced through detection of laccase-oxidised substrate products. Hence, while AuEs

may not provide the best transducer surface for the detection of these analytes *per se*, Au surfaces may, through their restrictive surface properties provide an opportunity to generate uncomplicated signal separations that would not be possible with the GCE surface used thusfar in the course of this study.

6.3: Aims and Objectives:

This phase of research was developed as a proof-of-concept in the development of the selective, simultaneous real-time analysis of a mixed sample of phenolics. Research reported on in Chapter 5 indicated that the phenolic substrates: hydroquinone (HQ), 1,2,4-benzenetriol (BZT) and catechol (CAT) all possessed uncomplicated oxidation/reduction profiles, when investigated using both electro-oxidation and through biochemical oxidation by immobilised laccases. In selecting these compounds for investigation in this Chapter, we obviate many of the problems of under-representative signal current and inactivation of the sensor during operation: properties that other the substrates reported on in Chapter 5 possess.

The overall aim of this chapter is to elucidate conditions under which MPCA could be applied to achieve simultaneous phenolic detection. In order to draw meaningful conclusions, comparative studies for substrates was performed at single potential CA as well as at MPCA for both single substrates (eg CAT alone) and in combination with other substrates as described further.

The objectives for this phase of research were as follows:

(1) Assess the feasibility of laccase modified AuE for cathodic detection of phenol oxidation products through comparison with similar studies at GCE (as described in Chapter 5) in order to determine if transducer surface differences affect the biosensor response significantly

(2) Assess the extent to which gold electrodes hinder the oxidation of phenolics for their intended use in MPCA, relative to GCEs. This will be performed by assessing alterations to biosensor kinetics at a laccase AuE when applying multiple potentials during chronoamperometry for each substrate in isolation and compared to the findings outlined in the first stated objective.

(3) Develop a chronoamperometric strategy in order to minimise (or at least, account for) the generation of current through electrooxidation of substrate (through application of resting

potentials and judicious selection of the time of potential application) and subsequent re-reduction at the electrode during sensing potentials. A method to discriminate between electro-generated oxidation of substrate and the laccase-generated oxidation of substrate (normal biosensor function) is of benefit in accurately distinguishing between these two causes of current generation during the application of sensing potentials.

5) Simultaneous, real-time and selective determination of the above-mentioned substrates using MPCA.

6.4 Methods and Materials

6.4.1 Apparatus and Reagents

6.4.1.1. Apparatus

Electroanalytical equipment was used as outlined in Chapter 2, as was the spectrophotometric apparatus.

Both electroanalysis and spectrophotometry took place at 21 °C and all reagents were warmed to this temperature prior to the onset of analysis.

The transducer surface used throughout this phase of research was gold-surfaced electrodes, as described in Chapter 2 of this Thesis. Comparisons in this chapter between AuE and GCEs were made on the basis of data reported on in Chapters 4 and 5 for the relevant substrates under the relevant conditions.

6.4.1.2. Reagents

Piranha solution (cleaning solution for AuEs) was formulated using a 3 : 1 solution of H_2SO_4 (> 95% purity, Saarchem) and H_2O_2 (30% $^{w}/_{v}$, Saarchem). Piranha solution was formulated immediately prior to the chemical etching step employed to clean AuEs (outlined in Section 6.4.2.1 below).

The substrates BZT, CAT and HQ were selected from Chapter 5 of this Thesis and formulated as outlined in Chapter 2 (Section 2.2.5).

SLB, adjusted to a pH of 4.5, was the main electrolyte/buffer used throughout this research.

6.4.2 Methodology:

6.4.2.1. Pre-modification treatment of AuEs

Gold electrodes (AuEs) were polished (Chapter 2) and sonicated in ethanol and rinsed with water. Thereafter, gold electrodes were chemically etched using fresh Piranha solution for 2 minutes before being rinsed with successive solutions of water and ethanol. Electrochemical pretreatment was performed by successively cycling the electrode between potentials of -0.15 V and +1.60 V (vs. Ag/AgCl) at a scan rate of 0.1 $V.s^{-1}$ in a solution of 0.1 M aqueous H_2SO_4 solution. Electrochemical pretreatment occurred until a stable baseline was achieved (~100 cycles, followed by rinsing the surface with water. Following rinsing, the electrodes were dried under N_2 flow and immersed in de-aerated ethanol for an hour, before drying under N_2 flow and used for biosensor fabrication. The above succession of cleaning stages used in preparing AuEs has been shown to reduce surface roughness and decrease surface inconsistency between cleanings (Carvalhal et al., 2005).

6.4.2.2. Biosensor fabrication

After electrode pretreatment (Section 6.3.2.1) biosensors were fabricated on the surface of AuEs using BSA-laccase-glutaraldehyde crosslinked films as outlined in Chapter 4 of this Thesis, Section 4.4.3.2, using 0.8 U laccase and 20 μg of BSA per biosensor (Section 4.4.3.3).

6.4.2.3. Single-substrate, single-potential chronoamperometry

Fabricated AuE biosensors were calibrated against the selected substrates (HQ,BZT,CAT) as described in Chapter 5 for GCE transducers. Potentials applied for chronoamperometry (for single substrate analysis using single potential CA) was set to -0.25 V vs. Ag/AgCl, rather than -0.17 V (as used in previous Chapters). This was performed in order to accommodate the negative shift of the reduction potential of oxidised BZT compound(s) found using AuEs, reported below (Table 6.1). Potentials were

selected in order to accommodate the reduction potential of the quinone form (oxidation product of phenols) of the specific substrate (as outlined in Chapter 6.5.1)

Data analysis and treatment occurred as described in the Methodology sections of Chapters 2 and 4, using the model formulated in Chapter 2, and applied as in Chapters 4 and 5 of this Thesis. Comparisons between biosensors fabricated on GCE surfaces and those performed on Au surfaces were performed in order to ascertain consistency between these sets. Electrodes were stored in SLB after initial calibration and re-used as described in Chapter 4, for each tested substrate, and compared against biosensor counterparts manufactured on GCE surfaces.

CVs generated under the potential window described above (6.3.2.2) were performed before and after substrate calibration in order to determine peak characteristics of substrate oxidation/reduction at the AuE. Potentials corresponding to values more negative than the peak reduction potentials were selected as substrate-dependent sensing potentials for 6.2.4.2, (with the exception of HQ, for reasons outlined in Section 6.4.1) while a resting common to all three substrates was selected on the basis of being more positive than the onset of reduction at AuEs for any of the selected substrates. This was performed under the same electroanalytical waveform described in Chapter 5 of this Thesis.

6.4.2.4. Biosensor characterisation: Single substrate, multiple-pulse-potential chronoamperometry (Effect of resting potential and applied potential time)

Two potentials were selected: a resting potential (+ 0.4 V, as determined with respect to the findings of investigations outlined in Section 6.4.2.3) and a sensing potential, which differed with respect to the substrate under analysis. The selection of the applied sensing potential was performed on the basis of maximising substrate response current, while minimising the response current of substrate(s) which reduced at more negative potentials. Thus, CAT was assessed at + 0.088 V, HQ at -0.055 V and BZT at -0.25 V, vs. Ag/AgCl at AuE electrodes.

Biosensors were calibrated using the relevant substrate under the relevant potentials outlined above. Results obtained from this were compared to results obtained from the previous section in order to

compare sensor performance under normal i.e. single-potential chronoamperometric control and those obtained using MPCA.

In addition to assessing the effects of the selected potentials on the produced biosensor detection sensitivity, the time of application of both resting and sensing potentials were assessed with regard to ensuring that substrate-specific biosensor current responses obtained via MPCA remain representative of the current responses observed for biosensors under normal CA. An example of the relevant optimisation study, for CAT detection, can be found in Table 6.2, in Section 6.5.2 of this Chapter.

6.4.2.5. Biosensor characterisation: Multiple-substrate, multiple-pulse-potential chronoamperometry

Sensing potentials corresponding to a compromise between reductive potentials of the selected substrates and minimising interfering current from substrates reducing at more negative potentials were selected. These were selected on the basis of findings from single-electrode, single-potential studies outlined in Section 6.5.1

Alternating aliquots of select substrates were added during chronoamperometry and the various effects of these single additions tracked on each of the selected potentials.

6.5 Results:

6.5.1 Comparison between AuE and GCE as transducer surfaces for biosensing

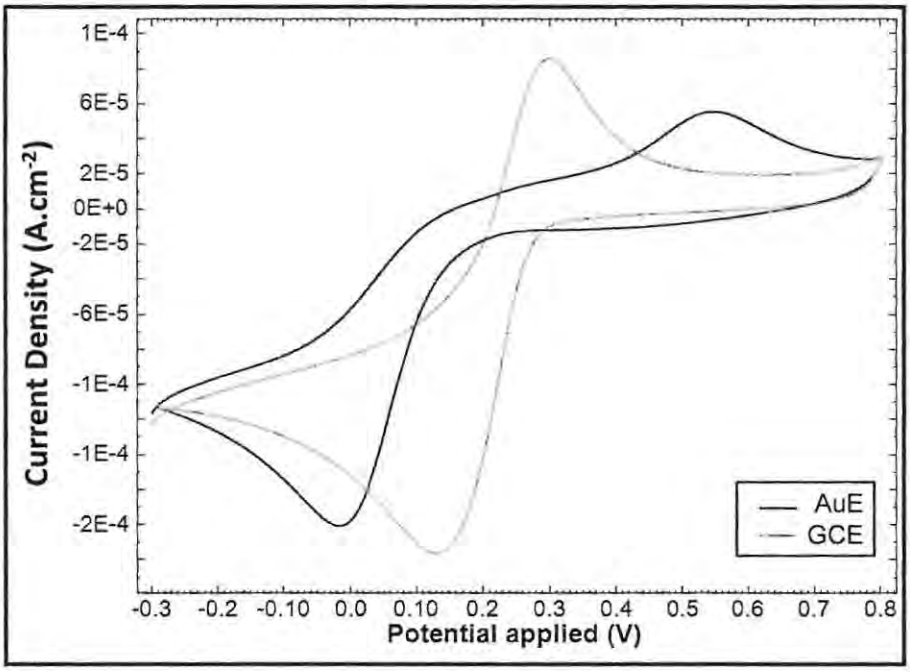

Figure 6.2: Representative CVs comparing the oxidation/reduction profiles of hydroquinone/p-benzoquinone at AuEs (black) and GCEs (grey).

In order to effectively compare differences in currents between electrode, current responses have been normalised relative to surface area and presented as current density.

A comparison between Figures 6.1 and 6.2 Figure 6.2 indicates that significant alterations in both the oxidation potential and the reduction potential of HQ and its oxidation product (p-benzoquinone) occurs when comparing CVs generated using AuEs to those generated using GCEs. This is most likely due to the aforementioned ECE mechanism which dictates the potential of both reduction and oxidation of analytes when considering AuEs (Burke and Nugent, 1998). Similar differences in oxidation/reduction peaks are noted for the other substrates when comparing electrode surface compositions.

Table 6.1 reports on the average values obtained when calibrating laccase-BSA crosslinked biosensor films produced on AuEs against those produced on GCEs (as reported in Chapter 5 of this Thesis). In order to account for the differences in electrode geometry, biosensor parameters relying on surface area

measurements (sensitivity and i_{max}) were calculated using the cross-sectional diffusion area (~0.020 cm^2) for AuEs, as opposed to calculations involving GCE-based biosensor responses (~0.071 cm^2).

Table 6.1: Operational parameters of laccase biosensors fabricated on AuEs compared to those obtained from previous findings on GCE surfaces.

AuE				GCE			
$E_{p,c}$ (V)[a]	Sensitivity ($nA.\mu M^{-1}.cm^{-2}$)[a]	K_m (μM)	i_{max} ($\mu A.cm^{-2}$)	$E_{p,c}$ (V)[a]	Sensitivity ($nA.\mu M^{-1}.cm^{-2}$)	K_m (μM)	i_{max} ($\mu A.cm^{-2}$)
CAT							
0.09 ± 0.01	901 ± 15	134 ± 4	234 ± 4	0.250 ± 0.005	964 ± 14	126 ± 9	237 ± 11
	1323 ± 60	113 ± 4	238 ± 15		1757 ± 127	78.6 ± 5.3	286 ± 18
BZT							
-0.215 ± 0.01	1633 ± 132	124 ± 10	311 ± 2	-0.063 ± 0.005	2713 ± 58	79.8 ± 3.3	410 ± 17
	1308 ± 32	115 ± 11	291 ± 14		2813 ± 72	57.8 ± 6	347 ± 33
HQ							
-0.05 ± 0.01	1867 ± 163	93 ± 10	331 ± 14	0.09 ± 0.01	1947 ± 48	87 ± 2.5	343 ± 7
	1049 ± 130	86 ± 12	299 ± 20		2443 ± 23	71.3 ± 2.3	366 ± 20

Maximal current density (i_{max}) and sensitivity values are calculated taking into account differences in cross-sectional diffusion area of the electrodes, with radii of 0.8 mm for AuE and 1.5 mm for GCEs, respectively.

Uncertainties represent standard error from the mean. Number of independent measurements, $n \geq 3$.

Rows shaded in grey indicate biosensor parameters obtained from re-used electrodes, in each category.

Detection potential for AuE: -0.250 V; Detection potential for GCE: -0.170 V

[a] – As assessed by CV under stirred conditions, following calibration of the sensors with substrate,

[b]– As assessed between the same concentration range as reported for GCEs

As Table 6.1 displays, dissimilar behaviours are observable between the AuEs and the GCEs in terms of the sensitivity of detection for the selected substrates BZT and CAT, with minimal difference observed for HQ. K_m values obtained using AuEs were consistently higher than their GCE counterparts, while comparable i_{max} values were obtained between the substrates. This indicates that the higher K_m values largely influence the lowered detection sensitivities observed between AuEs and GCEs through the relationship proposed in Chapters 4 and 5, between i_{max}/K_m and sensitivity.

The lack of relative alteration in the average i_{max} parameter upon re-use, together with the lowered K_m values for GCE surfaces compared to the same studies at AuE (Table 6.2) supports the supposition (Chapter 4) that the attachments of oxidation products to the surface of GCEs facilitates electron transfer

between the electrode and the oxidised substrates. This is not evident when considering AuEs as surfaces for biosensor fabrication, although a decrease in K_m upon re-use corresponds to the assertion that the interaction between phenolic oxidation products and the BSA co-immobilant enhances the rate of substrate and product diffusion through the cross-linked film.

The findings from this phase of research indicate that AuEs produce consistent biosensor operational parameters, even though they are dissimilar to their GCE counterparts reported on in Chapters 4 and 5 of this Thesis.

Most importantly, from the perspective of this research, the selection of gold as a transducer surface consistently increases the distance occurring between reduction and oxidation potentials (for example, as shown in Fig 6.2) when modified for use as a biosensor (reduction potentials noted in Table 6.1). This was a key consideration in the selection of this surface, as it also allows the selection of a resting potential not associated with the oxidation potential of parent compounds used in this study, as would occur with GCEs. As aforementioned, the inclusion of a resting potential would prove to be problematic when attempting to resolve sensing currents that contain contributions from both oxidation and reduction of substrates. Figure 6.3 displays typical CVs obtained at AuEs modified with laccase in the presence of each substrate in isolation. Peak characteristics from this phase of research were used in the selection of sensing potentials for each substrate.

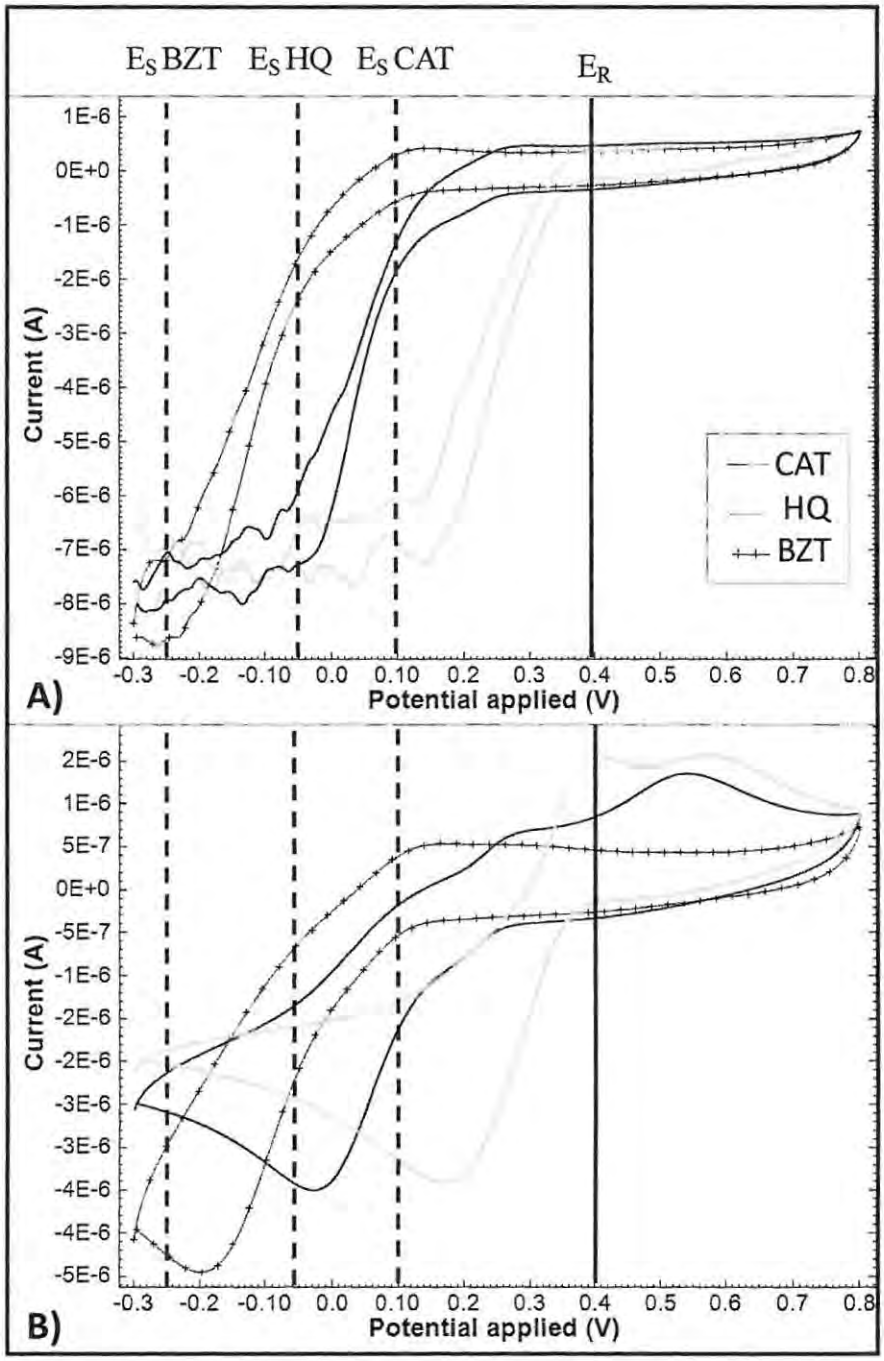

Figure 6.3 CVs of biosensors generated under: A) Stirred and B) Unstirred conditions in the presence of response-saturating concentrations of substrate.

Dotted lines indicate potentials which refer to values hereafter used at laccase modified AuE used in the detection of the various substrates

Cyclic Voltammograms were generated in SLB, pH 4.5, at a scan rate of 0.1 $V.s^{-1}$

A comparison between Figure 6.2**A** and 6.2**B** shows that the act of stirring the solution drives the apparent peak apices to slightly more negative potentials. As MPCA was performed under stirred

conditions, potentials were selected on the basis of peak generation under stirred (Figure 6.2**A**) rather than quiescent (Figure 6.2**B**) conditions. The following selected potentials were designated for the specific detection of the various substrates at a laccase modified AUE. CAT was henceforth detected at + 0.088 V and BZT at -0.250 V, both at potentials more negative than the peak potentials indicated in Figure 6.2 and Table 6.3. HQ, however was selected to be detected at E_S = -0.055V, which is poised slightly too positive for it to be confidently stated that current is purely mass-limited. However, an examination of Figure 6.3 reveals that the onset of BZT reduction at potentials more negative than the selected potential would significantly affect the selectivity of detection. A resting potential corresponding to +0.4 V was selected, as it was more positive than any of the potentials observed to cause reduction of any of the selected substrates (Figure 6.2**A**)

In an effort to further minimise deviations between detection sensitivities obtained under conditions of normal chronoamperometry and those obtained using MPCA, the time of potential(s) application was optimised in order to ensure that current representative only of the biorecognition layers' activity on substrates was included.

6.5.2. Single-substrate, Multiple-pulse chronoamperometry studies

(Effect of resting potential and applied potential time)

The correct application of a resting potential, both in the potential selected (as described in the preceding section) and the time at which it is applied every cycle is critical to producing an optimised current response that is still an accurate depiction of the laccase-generated current, due to the inherent opposition of these factors. Optimised current response of the sensing potential entails a resting potential step sufficiently separated, both in terms of potential and application time, from the onset of quinone reduction potentials. However, the selection of these parameters may cause the oxidation of laccase substrate that occurs both from the reduction occurring at the electrode surface during the sensing phase/s of the potential cycle, and that occurs during saturation of the biorecognition element at higher bulk substrate concentrations.

In order to sample current simultaneously at the two selected potentials (E_S and E_R), electrodes were calibrated with the respective substrates as reported in Section 6.4.1. The following MPCA potential regimen was imposed, as described in Table 6.2:

Table 6.2 MPCA regimen used in optimising potential time application for sensing and resting potentials for the substrate CAT:

Potential Designation (Current designation)	Potential Applied (V)	Current sampling time (s)	Total application time / potential (s)
E_{S1} (I_{S1})	0.088	0.1	0.1
E_{S2} (I_{S2})		0.1	0.2
E_{S3} (I_{S2})		0.1	0.3
E_{R1} (I_{R1})	0.400	0.1	0.1
E_{R2} (I_{R2})		0.1	0.2
E_{R3} (I_{R3})		0.1	0.3
Full cycle			0.6

Similar time optimisation studies were applied to BZT and HQ calibration, using sensing potentials (E_S) of -0.250 V and -0.055 V, respectively and the same resting potential as in Table 6.2. In this manner, simultaneous current-sampling was tracked at several time constants when potentials were sequentially switched between resting and sensing states. Comparisons between the current-concentration functions at the different sampling-times were made in order to ascertain which provided current-concentration curves comparable to those in Table 6.2 (Section 6.4.2)

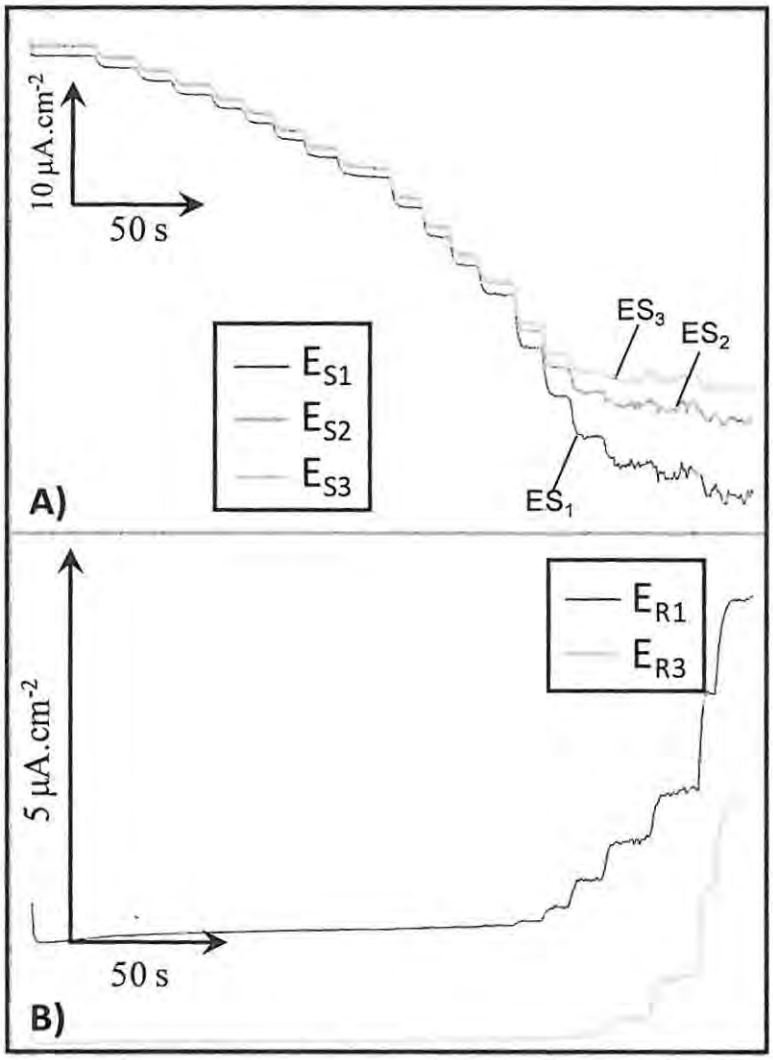

Figure 6.4: Example of effects of optimisation of current sampling time (i.e. potential application times) for the calibration of AuE-surfaced biosensors with the substrate HQ.

A) Effect of increasing HQ concentration on sensing potentials ($E_{S:}$ -0.055V)

B) Effect of increasing HQ concentration on resting potentials ($E_{R:}$ +0.4 V)

Current plateaus indicate current response following addition of HQ aliquots into electrochemical vessel. Inset legends display the potential designations for individual current-time curves, and are the same as in Table 6.3.

Since all time and potential optimisation studies were performed in the timescales > 100 ms, there is negligible non-Faradaic current (from e.g. double-layer charging) anticipated when switching potentials and sampling current as time regimes remained > 10 ms, (Miaw and Perone, 1979). Charging current becomes negligible between 10^{-4} s and 1 s, depending on the system used and the current passing through that electrode (Bagotsky, 2006a). Indeed, the baseline difference between E_{S1} and E_{S2} (0.1 s and 0.3 s

times of potential application, respectively) do not exceed ~ 0.5 $\mu A.cm^{-2}$ for AuEs, as exemplified in Figure 6.4, prior to the addition of the first substrate aliquot.

In the presence of low concentrations of substrate (i.e. when the majority of substrate present near the electrode surface is oxidised by laccase), all three of the selected time-constants correspond very closely (Figure 6.4**A**). This is accompanied by very slight changes to the resting currents upon the introduction of further substrate (HQ in the example, Figure 6.4**B**). However, when concentrations are increased further, IS_1 and IR_1 deviate substantially from IS_3 and IR_3; similar behaviour (albeit of a lesser degree) is noted for the comparison of I_{S2} and I_{S3} and the resting states, respectively.

This behaviour is most likely due to the generation of reductive current through the electro-oxidation of unreacted substrate at the electrode surface under conditions of enzyme saturation. Even at increased bulk substrate concentrations, at higher sensing potential application times (E_{S3}), minimal contribution to the current through this mechanism occurs, due to its exponential decay as a function of time – Eq 6.2). However, the current resulting from the generation of analyte by laccase remains constant and remains the predominant source of current signal at E_{S3}. In order to account for the differences at different time constants caused by anodically-generated re-reduction of analyte, currents from the resting states were subtracted from the respective sensing states. Thus, current for this phase of research is represented as the difference between E_{Sn} and E_{Rn} (where n = 1,2,3). For the sake of brevity, currents from n = 1 and n = 3 are presented for comparative purposes henceforth. Figure 6.5 below displays current-concentration curves obtained when considering the different potential application times for E_S and E_R.

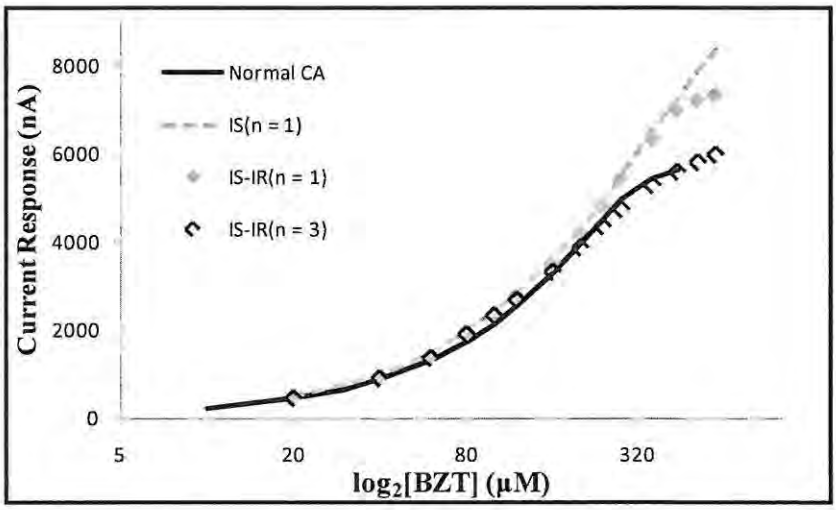

Figure 6.5: Semi-log plot displaying an example of current-concentration response curves obtained at different sensing-to-resting potential switching time constants for the calibration of AuE biosensors using BZT.

Substrate concentration is presented here in a logarithmic format, in order to display sensor responses at both low and high substrate concentrations. Note that this data is presented without normalisation relative to the electrode surface area.

Legend:

Normal CA: response recorded using CA with a single potential, set at -0.25 V (data reported in Section 6.4.1)

IS (n = 1): I_{S1} , as referred to in-text, above.

Similarly, IS-IR(n = 1): I_{S1}-I_{R1}; IS-IR(n = 3): I_{S3}-I_{R3}.

The similarity in current-concentration behaviour when comparing I_{S3}-I_{R3} to the response of a biosensor undergoing normal chronoamperometric calibration with the substrate (exemplified in Figure 6.5) produced detection sensitivity values that were comparable to those presented in Table 6.1, for both BZT and CAT. This indicates that, under the potentials selected, little alteration to the apparent biosensor function (inferred from the current) is caused by the imposition of a pulsed, rather than static, potential during chronoamperometry.

However, the imposition of a less-optimal potential for the detection of HQ, itself selected to minimise current interference on HQ detection by BZT (Figure 6.3), significantly altered the current-concentration function of the biosensor. Detection sensitivity decreased from a mean value of 1867 $nA.\mu M^{-1}.cm^{-2}$ (Table 6.1) to approximately half that: 853 ± 53 $nA.\mu M^{-1}.cm^{-2}$, while the apparent K_m value trebled from 93 ± 10 to 341 ± 7 µM. This is due to the selection of a potential that produced current-concentration functions that were both kinetically-limited and mass-transfer limited. As mentioned above, the selection

of this potential was due to the desire to maximise current resulting from HQ detection, while minimising current derived from the detection of BZT in the next phase of research.

6.5.3. Multiple-substrate, multiple-pulse chronoamperometry studies

Having ascertained the relative effects of the selected potentials on the detection sensitivity of each substrate, the ability of MPCA to separate signal arising from the introduction of all three selected substrates was assessed. The following waveform was imposed on the biosensors during MPCA (Table 6.3)

Table 6.3: Multiple Pulse Chronoamperometry waveform applied for simultaneous detection of specified phenolics BZT, CAT and HQ

Potential Step (#)	Potential Designation	Applied Potential (V)	Time of application (ms)
1	$E_{S,CAT}$	0.088	300
2	E_{R1}	0.400	300
3	$E_{S,HQ}$	-0.050	300
4	E_{R2}	0.400	300
5	$E_{S,BZT}$	-0.250	300
6	E_{R3}	0.400	300
Total time per cycle			1 800

Figure 6.6 displays typical chronoamperometric responses recorded simultaneously for the determined potentials when sequentially introducing the different substrates into the electrochemical cell.

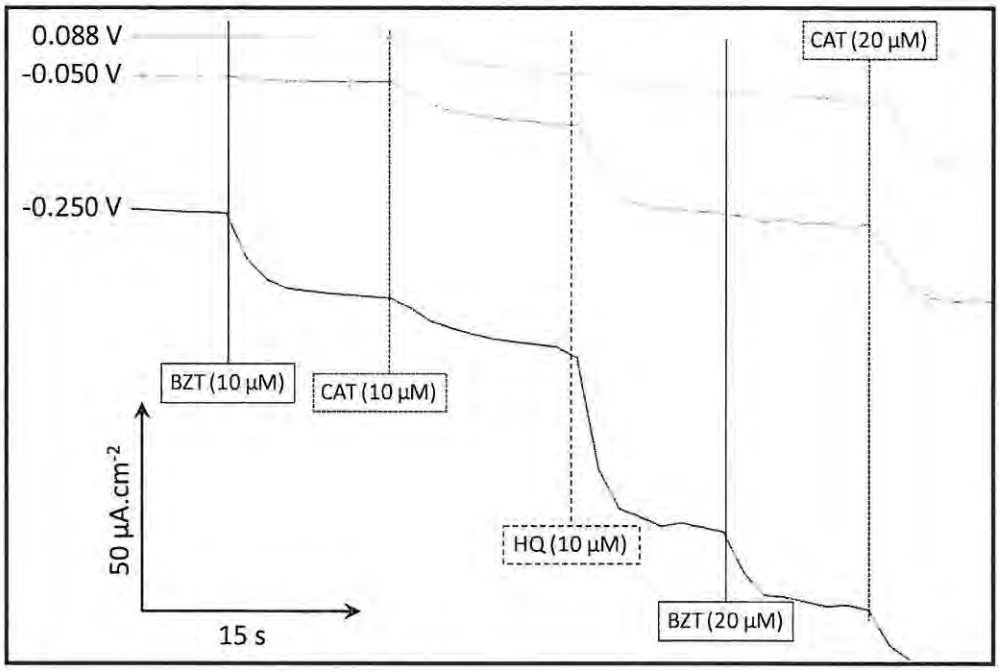

Figure 6.6: Example of chronoamperograms ("raw data") obtained from MPCA analysis of the sequential calibration of AuE biosensors when introducing alternating aliquots of BZT, CAT and HQ to the electrochemical cell.

The respective sensing potentials used herein are recorded at the upper-left of each curve. Points corresponding to the introduction of substrate to the electrochemical reaction vessel are indicated by vertical lines, with final concentrations of each substrate indicated in the appended boxes.

As displayed in Figure 6.6, the applied potentials used in MPCA showed distinct behaviours upon the introduction of different substrates to the electrochemical vessel. The most negative selected potential (-0.25 V) successfully detected the introduction of all 3 substrates visible as an increase in reductive current. The mid-potential (-0.055 V) showed only slight alterations to reductive current upon the introduction of BZT to the detection matrix; however, due to the aforementioned non-optimal positioning of the potential, exhibited a smaller reductive current to HQ introduction relative to the normal CA performed at -0.250 V. In contrast, the most positive sensing potential (+0.1 V) registers a reductive current upon the introduction of CAT comparable to the other two sensing potentials and is influenced very slightly by the introduction of HQ to the matrix. Hence, through the application of MPCA and the careful selection of sensing potentials, selective simultaneous determinations of each substrate can be performed, by subtracting the current response of the preceding sensing potential from the one under examination.

6.5.4 Overall data summary between reported electrochemical conditions

Figure 6.7 summarises the relative detection sensitivities exhibited by the selected sensing potentials for all of the waveforms

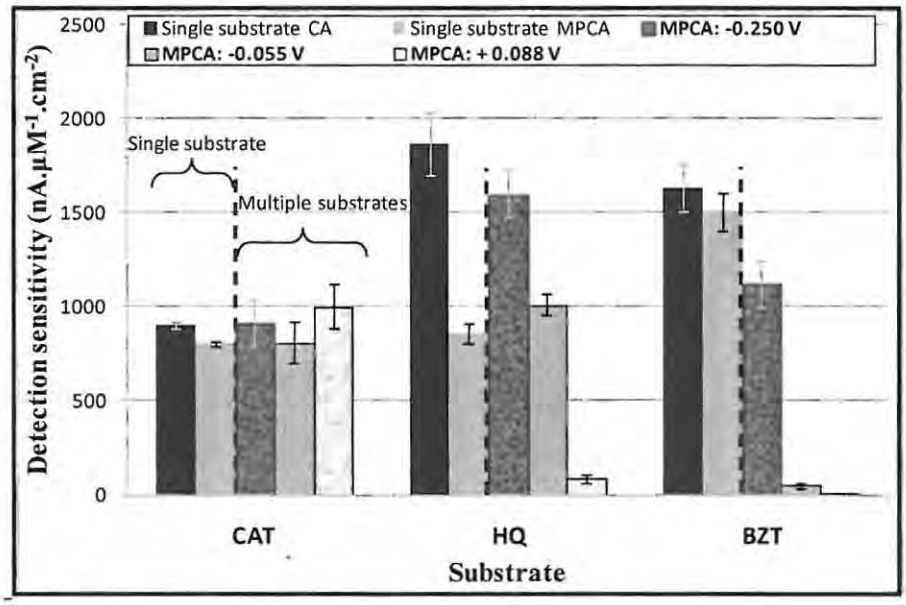

Figure 6.6: Summaries of the detection sensitivities for the substrates under investigation, as assessed at the different stages of AuE detection that are reported on in this Chapter.

Detection sensitivity was determined between 0 and 100 μM bulk concentration of each substrate. Error bars reflect the standard deviation from the mean. Number of independent references, $n \geq 3$

From the detection sensitivities recorded and contrasted in Figure 6.7 above, it can be concluded that MPCA can be successfully used to simultaneously analyse and separate currents arising from the laccase-based oxidation of several phenolic species. The detection of CAT, for example, is negligibly affected, both when comparing its detection using MPCA at all sensing potentials, and when comparing results from MPCA to those obtained from normal chronoamperometry. The detection of HQ, while exhibiting a significant decrease in detection sensitivity due to the imposition of a non-optimal sensing potential, is detectable at the same degree of substrate sensitivity observed both with single-substrate MPCA and multiple-substrate MPCA. BZT, while producing consistent detection sensitivities both

during detection via normal CA and MPCA in isolation from other substrates, produced a significant decrease when detected in the presence of CAT and HQ, for reasons that are unclear at this time.

When viewed from the perspective of the sensing potentials during multiple-substrate MPCA, there is a clear indication of specific detection of substrates using the selected sensing potentials (Figure 6.6). A An applied potential of -0.250 V detected all three substrates satisfactorily (albeit with slightly lowered sensitivities for both BZT and HQ), while the imposition of an applied potential of -0.055 V drastically decreased the detection of BZT by approximately 10-fold while maintaining HQ detection at the sensitivity previously noted at this potential. The selected sensing potential for catechol (+0.088 V) greatly diminished the detection of HQ while producing a negligible response for BZT, even though the detection sensitivity of CAT left practically unchanged. This shows proof of the principles under which this research was conducted – that MPCA can successfully be applied to the selective detection of substrates simultaneously, under-real time conditions.

6.6 Conclusions

AuEs gave relatively poor responses when applied as transducer surfaces for the laccase-based biosensors optimised on GCEs. Both increased modelled K_m values and lower detection sensitivities were recorded for the cathodic detection of selected substrates (CAT, HQ and BZT) using AuE-surfaced biosensors at a static potential of -0.25 V. However, pertinent to the purposes of the research conducted, consistent shifts in peak potentials were noted to occur, for both the anodic and cathodic peaks corresponding to the oxidation of parent compound (substrate) and the reduction of the laccase-catalysed oxidation product (analyte). The repositioning of the anodic potentials, in particular, is desirable for MPCA as it removes considerations of analyte oxidation occurring during the application of sensing potentials.

No substantial differences in detection sensitivity were noted when applying MPCA to the detection of analyte from the substrates BZT and CAT, in isolation from other substrates. However, the application of a non-optimal sensing potential for the detection of HQ showed a markedly decreased detection

sensitivity approximating to half that noted for the detection under static-potential conditions. In this instance, a compromise between enhancing the detection of HQ and minimising the detection of BZT at this potential was made. Detection sensitivities from sensing potentials applied for 300 ms per potential cycle was found to have a good correlation to the sensitivities obtained at static chronoamperometry, once the current response from resting potentials was taken into account.

MPCA performed in the presence of all three of the selected substrates has shown a good degree of simultaneous signal selectivity between these substrates when sensing potentials corresponding to selective potentials for each substrate were applied. CAT was detected equally well at all three potentials selected for MPCA, while the detection of BZT and HQ were severely restricted at potentials more positive than their selected sensing potentials. CAT and HQ responses obtained at this stage were comparable to responses obtained under MPCA conditions in the sole presence of the respective substrates. These findings all indicate that selective, simultaneous assessment of individual substrates present in a detection matrix containing all three selected substrates are possible through the careful application of MPCA. As such further examination and application of this technique is warranted, but is beyond the scope of this study.

Chapter 7: Assessment of the quartz-crystal microbalance as an analytical tool for biosensor development and fundamental studies: case study metallophthalocyanine – glucose oxidase biocomposite sensors.

7.1 Abstract:

As mentioned in Chapter 1 of this Thesis, one of the challenges in biosensor fabrication is the optimization of procedures immobilizing biomolecules onto, or near, the transducer surface. Ideally, this should occur in a manner such that a significant amount of biomolecules is immobilized while maintaining the maximum amount of function. Gaining a fundamental knowledge of the processes underlying immobilisation of the molecules onto the electrode surface is thus, of significant interest in understanding the mechanisms by which molecules are immobilized onto the electrode surface, and how this itself affects the sensor's performance. It is in this light that the following two Chapters are presented, in which piezoelectric QCM-D technology (and the rheological modeling of film responses) is contrasted against the functioning of various sensors. Chapter 7 reports on the initial proof-of-concept, using well-characterised processes and biomolecules (glucose oxidase). Herein QCM-D technology was used to assess the formation of 2 layers comprising a composite sensor fabricated in the same manner as one whose operational parameters have been previously reported (Mashazi et al., 2006)

In this research, we report on the application of the Quartz-Crystal Microbalance with Dissipation as a tool for fundamental analyses of the immobilisation of successive monolayer attachments of tertra-carboxylated cobalt(II) metallophthalocyanine (TCACoPc) and glucose oxidase (GOx) onto a gold electrode for the enhanced detection of glucose.

The data presented in this Chapter forms the basis of the following publication and is not further referenced in this Chapter: "Critical assessment of the quartz-crystal microbalance as an analytical tool for biosensor development and fundamental studies: case study metallophthalocyanine – glucose oxidase biocomposite sensors." Fogel, R., Mashazi, P., Nyokong, T. and Limson, J., 2007. Biosens. Bioelectron. 23, 95-101.

In order to maintain compatibility during piezoelectric analysis, the sensor was constructed in aqueous phase and covalently linked the gold surface to the TCACoPc, and the TCACoPc to the GOx. It was found that the aqueous metallophthalocyanine formed a multilayer over the surface of the electrode, but this multilayer could be removed to leave a fairly rigid monolayer with a mass loading that compared favourably to the theoretical value expected. Analysis of frequency and dissipation plots indicated the covalent attachment of glucose oxidase onto the metallophthalocyanine layer. Furthermore, the amount of GOx bound compared favourably to calculations derived from the amperometric functioning of the sensor, but not to theoretical values derived from the dimensions of GOx as established by crystallography.

The strength of the binding of the GOx film with the TCACoPC layer was tested by using 2% SDS as a denaturant/surfactant, and the bound mass associated with the GOx film was not found to be significantly affected by exposure to this. This indicates the formation of covalent bonds occurring between GOx and the TCACoPC layer; similarly, the removal of adsorbed TCACoPC to form a monolayer indicates the formation of covalent bonds occurring between TCACoPC and the cystamine SAM surface assembled onto the piezoelectric sensor surface which confirms a covalent attachment of GOx to the SAM surface.

7.2. Introduction:

7.2.1 Quartz-Crystal Microbalance with Dissipation: Principles and properties

The Quartz-Crystal Microbalance with Dissipation monitoring (QCM-D) is a piezoelectric sensor that is frequently used to monitor inter-molecule interaction on the surface of a piezoelectric sensor platform. Previous research using this analytical technique has focused on such diverse elements of research as: bio-photovoltaic cell construction (Lam et al., 2006), protein-surface interactions (Höök and Kasemo, 2006; Andersson et al., 2004 and Hemmersam et al., 2005), antibody-antigen interactions (Marx et al., 2006 and Larsson et al., 2005), protein-protein interactions (Limson et al., 2004) and cell adhesion monitoring for implant surface technology (Lord et al., 2006 and Modin et al., 2006)

Data retrieved from QMC-D analysis is two-fold. Firstly, the frequency shift (Δf) upon attachment/detachment of electrode-bound mass is related to the mass by the Sauerbrey equation ,Equation 7.1 (Sauerbrey, 1959). :

$$\Delta m = \Delta f \times C / n \qquad \text{Eq. 7.1}$$

Where Δf is the frequency shift (in Hz), Δm is the mass area change (in $ng.cm^{-2}$), C is the mass sensitivity constant (17.7 $ng.cm^{-2}.Hz^{-1}$ at an oscillation frequency of 5 MHz, as was used here) and n is the overtone number (1, 3 , 5 , 7...). The Sauerbrey equation may also be used to estimate the layer thickness and viscosity of the attached layer. However, the Sauerbrey equation only holds true for thin, homogenously-distributed, light (relative to the electrode mass) and rigid films firmly adsorbed onto the electrode surface that couple to the electrode's oscillation (Höök et al., 1998). The interaction of the piezoelectric sensor with a viscoelastic film (such as protein) that does not satisfy the above criterion, causes frequency dampening to occur, resulting in an overestimation of the mass of the attached layer (Höök et al., 1998). Additionally, the presence of water coupled to the film results in an overestimation of mass (Höök et al., 1998).

The dissipation factor, D (dimensionless units, x 10^{-6}), provides data regarding the viscoelasticity of the attached layer, giving information about the strength of attachment, and the structure of the attaching layer (Höök et al., 1998). This information can be combined with the Δf values to assess whether the Sauerbrey equation holds true (i.e. a rigid film strongly bound to the previous layer would possesses a low dissipation value relative to the frequency shift) (Höök et al., 1998).

Comparison of the dissipation as a function of the frequency shift (f vs. D plots) can often reveal information regarding the strength of film-film interaction and identification of the various phases undergone during the attachment stage/s (Höök et al., 1998). Furthermore, analysis of the Δf and ΔD values at multiple overtones can, in turn, generate information regarding the thickness, shear and viscosity of the attaching layer (Höök and Kasemo., 2001).

7.2.2 Principles and properties of the sensor under examination

During the fabrication of a biosensor, the addition of inorganic components is often performed in order to improve the analyte specificity (Ahuja et al, 2006) enhance the signal strength of the biomolecule-mediated reaction (Ahuja et al, 2006; Chen and Gorski, 2001 and Murphy, 2006) and to improve the stability of the immobilised biomolecule (Ahuja et al., 2006; Chen and Gorski, 2001 and Murphy, 2006).

Glucose Oxidase (GOx), is an enzyme that catalyses the oxidation of glucose with the concomitant formation of hydrogen peroxide from water and is thus used in the fabrication of commercially available sensor technology for monitoring of glucose in the health as well as indsutrial sectors. Research development in this area is targeted at improvements in the sensitivity of the final sensor, and may be afforded by the use of mediators such as the metallophthalocyanines.

Metallophthalocyanines (MPc) are synthetic aromatic compounds that possess catalytic properties towards a wide variety of compounds, and have been shown to have photocatalytic and electrocatalytic effects (Zagal, 1992). Aqueous-soluble derivatives of metallophthalocyanines have exhibited the tendency to aggregate in solution (Iliev and Ileva, 1995 and Kuznetsova et al., 2003), which has been found to decrease their effectiveness as

photocatalysts (Iliev and Ileva, 1995). Cobalt(II) Phthalocyanine is a metalloorganic compund that has been previously shown to mediate the electrooxidation of hydrogen peroxide, and to increase the signal response of a GOx-based amperometric biosensor for the determination of glucose (Mashazi et al., 2006).

One of the major concerns in the fabrication of biocomposite biosensors (i.e. biosensors comprising of both a biological and chemical operative agent) is to assess the interaction existing between the biological and chemical conjugates. While the strength, assembly mechanism and level of interaction between the abiotic component and the electrode surface can be easily assessed (through, e.g. Raman spectroscopy (Zhang et al., 2003) and impedance electroanalysis (Calvo et al., 1996)), little high-quality data can be gathered regarding the interaction of the biomolecule with the chemical component of the composite biosensor. While QCM-D technology seems very suitable for this area of analysis; the challenge is to develop analytical protocols that closely model the desired method of fabrication. Multi-layer, or non-optimal orientations of tightly-packed metallophthalocyanines have been considered undesirable, as it may prevent solvent exposure of the metallic centre of the metallophthalocyanine (Agboola et al., 2007)

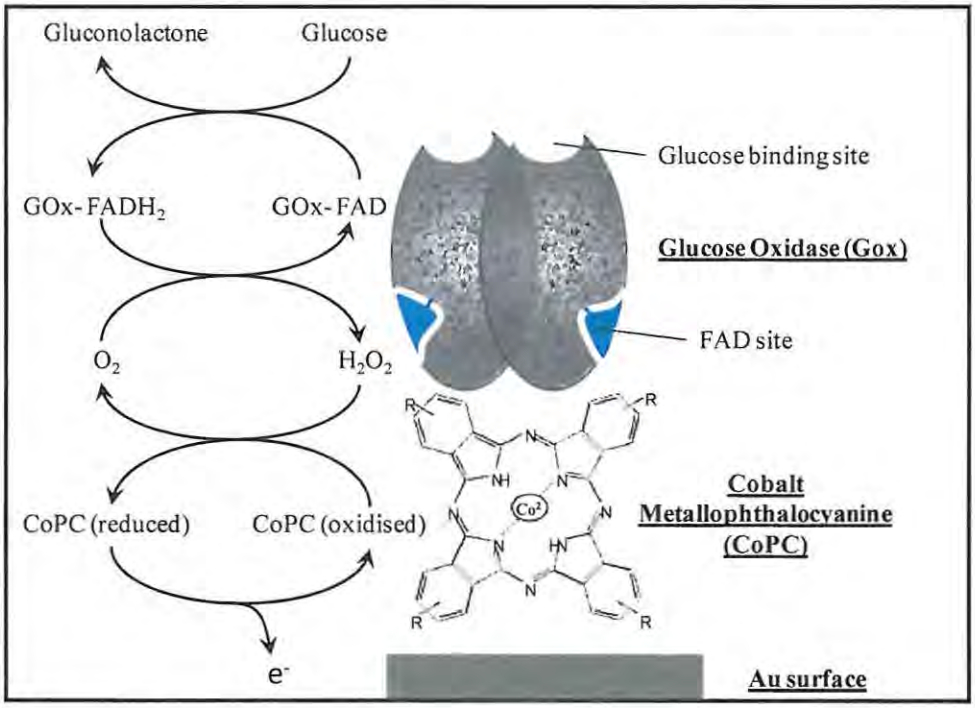

Figure 7.1: Schematic of proposed electron-transfer pathway between substrate (glucose) and transducer surface (Au) for the biocomposite GOx-CoPc biosensor and relevant participants.
Adapted from Mashazi et al., 2006.

In the reported research, previous research conducted by Mashazi et al., 2006 is expanded upon by assessing the fabrication of a glucose-detecting biosensor fabricated by the conjugation of Tetra-carboxy cobalt(II) phthalocyanines (TCACoPc) to the gold surface (as illustrated in Figure 7.1), and glucose oxidase (GOx) to the TCACoPc layer. The QCM-D was used to assess the various parameters and interactions occurring between the various layers built up on the electrode surface, and a comparison was performed between previously published literature on this biosensor configuration, theoretical maxima and those parameters determined by QCM-D technology.

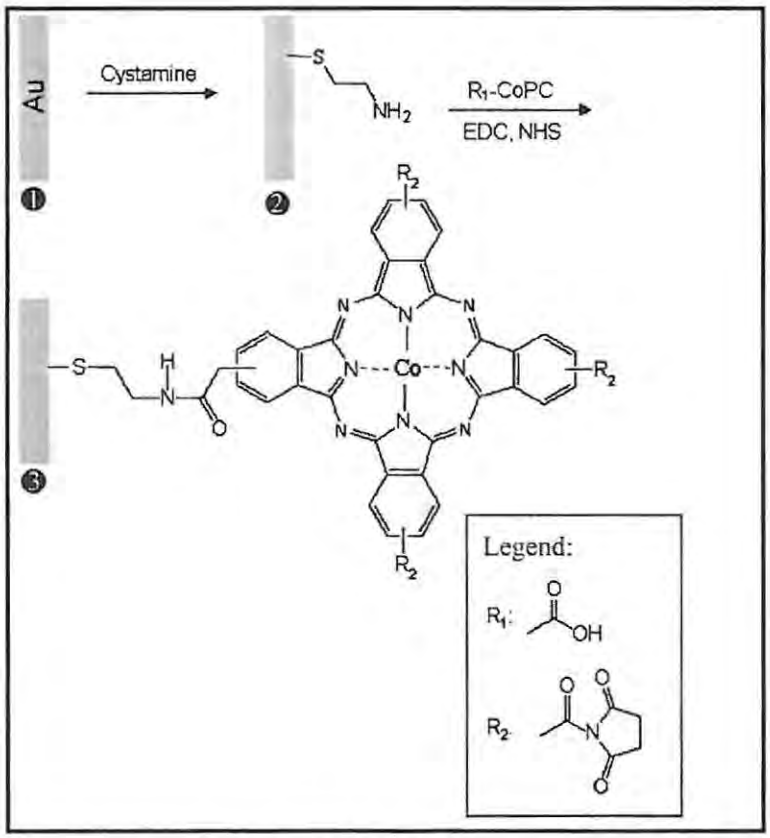

Figure 7.2: Scheme for the formation of an activated TCaCoPc layer over the surface of a gold electrode. The addition of cystamine to a gold surface (1) gives rise to the formation of an NH_2-terminating SAM (2). Incubation of the EDC and NHS to the non-activated TCACoPc carboxyl groups (R_1) results in the production of the activated form (R_2). The activated TCACoPc binds to the SAM layer via covalent linkage of the activated COOH groups of the TCACoPc and the NH_2 groups of the SAM, forming a TCACoPc layer (3). Unreacted activated groups of the TCACoPc then covalently bind to NH_2-terminating amino acid residues on the GOx, forming a biocomposite sensor.

7.3 Methods and Materials:

7.3.1 Reagents:

Tetra-carboxylic acid cobalt(II) phthalocyanine (TCACoPc) was prepared as described previously (Mashazi et al., 2006).

Cystamine dihydrochloride (≥98%), *N*-(3-dimethylaminopropyl)-*N'*-ethylcarbodiimide hydrochloride (EDC); *N*-hydroxy succinimide (NHS), sodium dodecyl sulphate (> 98%) and sodium heptane sulphonate (HS) were all sourced from Sigma-Aldrich. Glucose oxidase (Type VII, from *Aspergillus Niger*, 157 U/mg) was sourced from Sigma-Aldrich.

Phosphate Buffer (0.05M), pH 6.50 (PB) was prepared using equimolar solutions of NaH_2PO_4 and Na_2HPO_4 in water.

All non-proteinaceous solutions were degassed by sonication in a sonicator bath (Elmasonic S 10 H) for 10 minutes prior to experimentation. Proteinaceous solutions were crudely degassed by allowing the solution temperature to equilibrate at 25 °C for 15 minutes prior to use.

7.3.2 Apparatus:

Crystals used were AT-cut quartz crystals, QSX-301, surfaced with gold. These were mounted in titanium QCM-D flow chambers, which were in turn housed in a Q-Sense E4 QCM-D sensor system. All of the above were sourced directly from Q-Sense®, Sweden.

Flow was regulated by an Ismatec® peristaltic pump.

7.3.3 Methodology:

7.3.3.1 Pre-analysis cleaning of crystal

Prior to modification, all crystals used were cleaned by exposure to ozone-producing ultraviolet light (UV-O) for 5 minutes. Following UV-O treatment, the crystals were immersed in a solution of NH_3 : H_2O_2 : H_2O in a ratio of 1 : 1 : 5, heated at 75 °C for 5 minutes. The crystals were then rinsed thoroughly with water, dried under nitrogen gas and then exposed to UV-O for a further 5 minutes prior to use.

QCM-D analysis took place under the following parameters: 20 °C temperature and a flow rate of 25 µl / minute.

7.3.3.2 Formation and confirmation of cystamine self-assembled monolayer (SAM):

Dried and cleaned crystals were immersed in a solution of 25 mM cystamine prepared in an ethanolic solution (1:1 of ethanol : water) that was thoroughly degassed prior to crystal immersion. Chemisorption of the cystamine to the gold surface took place for 16 hours at room temperature, or for 24 hours at 4 °C. Following SAM formation, the crystals were rinsed thoroughly with ethanol and water, successively, and dried under N_2, before being mounted into the titanium chamber. The dried electrodes were then checked (by monitoring resonance peak formation and dissipation values in air at multiple overtones) to ensure that they were satisfactorily cleaned and dried prior to analysis.

Cystamine SAM coverage ($\Gamma_{cystamine}$) was estimated using the charge produced by the reductive desorption of a cystamine SAM in 0.5 M KOH (El-Deab and Ohsaka, 2004), formed as above on a Bioanalytical System gold electrode (1.6 mm geometric diameter) that was cleaned as outlined in 3.3.1

7.3.3.3: Phthalocyanine layering:

Prior to use, a 1.3 mM solution of TCACoPc was prepared in a 0.05M HS solution (pH 5.80 at 20 °C) containing 15 mM EDC and 15 mM NHS for 1.5 hours at 4 °C, in the dark. Insoluble aggregates were removed from the solution by centrifugation (13,000 x *g*, for 30 seconds) prior to analysis. A cystamine-modified crystal was exposed to the activated metallophthalocyanine solution for 40-50 minutes before washing with HS, followed by successive rinses of PB and 2% w/v SDS in PB (SDS-PB) until a steady baseline was once again achieved.

7.3.3.4: GOx layering and binding:

Glucose oxidase (GOx) was dissolved in PB to a final concentration of 1 mg/ml. This was flowed over the immobilised quartz crystal, both modified with TCACoPc and over a cystamine-SAM electrode.

In an attempt to estimate the strength of GOx-TCACoPc interaction, a 2% solution of sodium dodecyl sulphate (SDS) (prepared in PB) which is a denaturant/surfactant, was flowed over the electrode for 5 min, and then the electrode exhaustively rinsed with PB until a steady-state was achieved.

7.3.3.5: Data analysis

f vs. D plots were generated using the 3rd overtone, as were all mass estimations, both theoretical and experimental.

Data analysis was performed using Q-Tools® software from Q-Sense®, whereupon multiple overtones (≥ 4) were used in determining the other salient properties of the various layers built onto the electrode surface (thickness of the layer and layer viscosity).

7.3.3.6: Theoretical data generation:

TCACoPc modelling (both activated and non-activated) was performed using HyperChemLite™. *Aspergillus niger* GOx dimension estimations were performed using Rasmol v2.06 (PDB reference file: 1GPE.pdb).

7.4. Results and Discussion:

7.4.1 Estimation of SAM coverage

The active surface area of the electrode corresponded to a surface roughness factor (σ) of ~1.5. The average charge produced by reductive desorption of cystamine was 0.378 μC, corresponding to a $\Gamma_{cystamine} = 2.58 \times 10^{-10}$ mols.cm^{-2}, or 1.54 molecules.nm^{-2}. This level of coverage is in good agreement of the surface concentration constituting a SAM, and also correlates closely to the surface coverage of 2.8 x 10^{-10} mols.cm^{-2} as found by *Arias et al.*, 1996.

7.4.2 Theoretical coverage permissible by TCACoPC:

As shown above, the average space taken up by a cystamine molecule is 0.644 nm^2, which corresponds to a square area with dimensions of 0.802 (0.806) nm x 0.802 nm (0.806), or a circular area with a diameter of 0.45 (0.413) nm. An unconstrained, activated TCACoPc molecule bonded head-on with a cystamine molecule has a molecular width of approximately 1.43 nm, providing a ratio of 1 TCACoPc molecule covering 2 bound cystamine molecules at the $\Gamma_{cystamine}$ calculated in section 7.4.1. This ratio was used to determine the mass of bound phthalocyanine expected in a monolayer (96.4 ng/cm^2), and substitution into the Sauerbrey equation provided the anticipated frequency shift at the third overtone (Δf_3) of -16.3 Hz. As the bound phthalocyanine is a rigid, linear molecule, very little frequency dampening is expected. However, bound / trapped water in-between the phthalocyanine molecules in the mediator layer was expected to add additional mass.

7.4.3. Analysis of phthalocyanine layering of cystamine SAM:

Figure 7.3 shows an abbreviated Δf and ΔD plot vs. time for the 3rd, 9th and 11th crystal overtone for the addition of an activated TCACoPc layer onto a cystamine SAM (Section A), the removal of multilayers (B) and the attachment of GOx to an activated monolayer (C) .

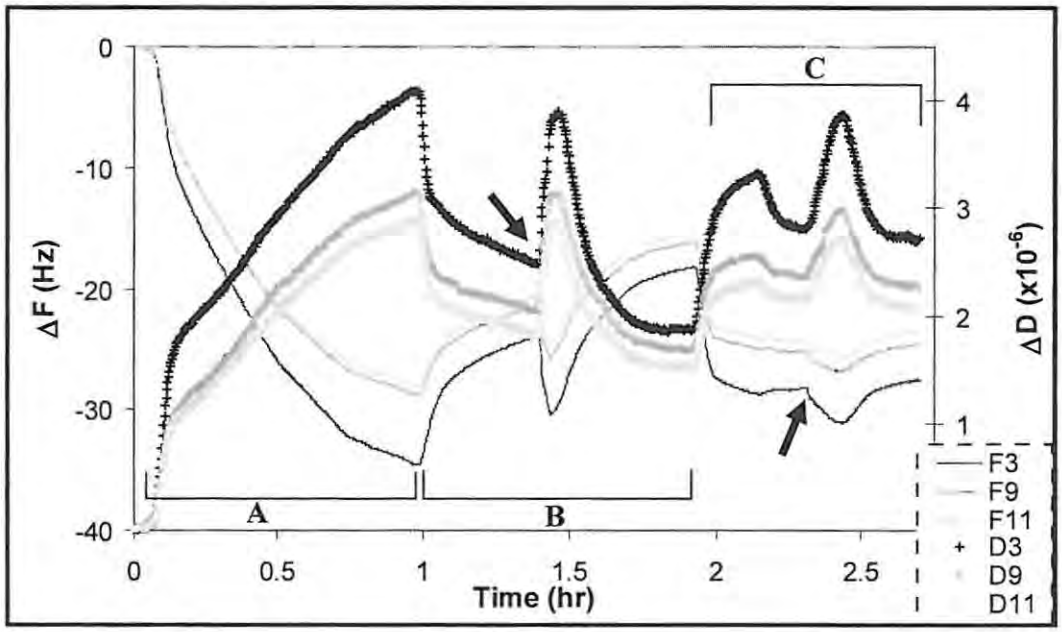

Figure 7.3: Abbreviated QCM-D response on a cystamine-modified, QCM-D electrode.
This figure shows the frequency response (lines) and dissipation shifts (symbols) at the overtones n = 3, 9 , 11. The progression is as follows: (A) the layering of the TCACoPc layer, (B) a PB (phosphate buffer) wash and removal of multilayers, (C) GOx layering and washing. The start of 5-minute SDS washes are indicated with arrows.

As can be observed from Section A in Figure 7.3, the addition of TCACoPc causes a frequency shift many times greater than the expected theoretical Δf_3 of approximately -16 Hz. Extending the layering time further (up to 1.2 hours, data not shown) does not produce steady-state f and D values, with regard to time. This indicates the formation of a multi-layered, loosely adsorbed film over the surface of the electrode, as opposed to the desired monolayer.

Plotting the dissipation as a function of the frequency shift (D vs. f plot) showed that the addition of TCACoPc was a multi-phased process. A typical f vs. D plot for the formation of a mediator-layer is shown in Figure 7.4.

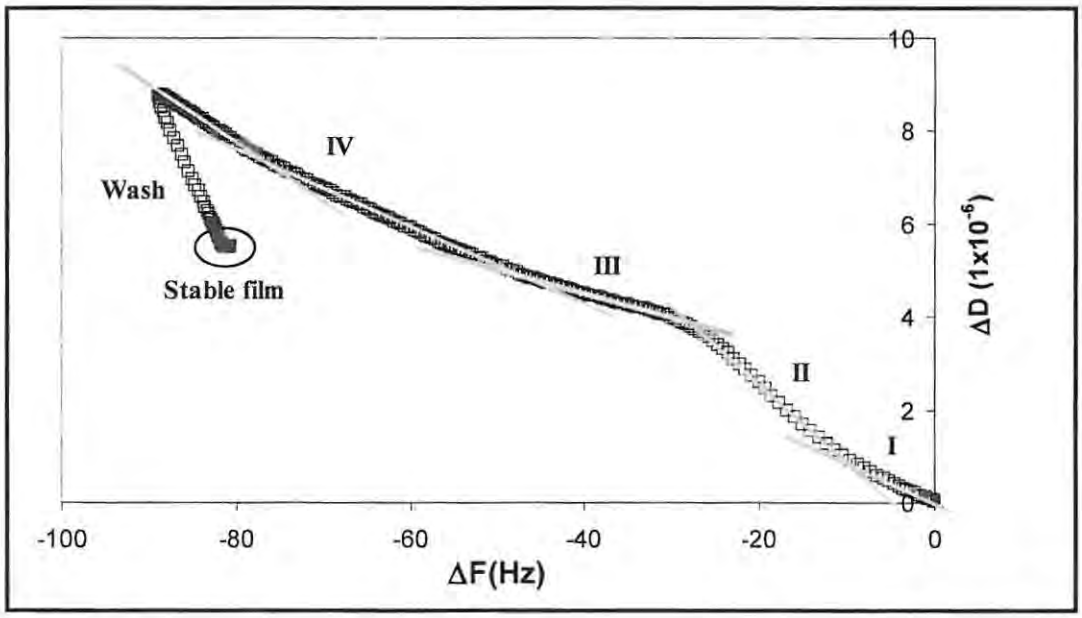

Figure 7.4: ΔD vs Δ*f* plot for the binding of TCACoPc in heptane sulphonate at overtone n=3.

Several distinct phases for the attachment of TCACoPc to the cystamine-primed electrode surface are easily notable (Figure 7.4). Phase I shows a fairly rigid (low dissipation vs. frequency gradient) attachment, probably relating to the covalent attachment of the TCACoPc to the pre-formed cystamine SAM. Phase II shows either the attachment of a viscoelastic stratum onto the first layer, or the loose (i.e. imperfectly coupled) binding of a rigid further layer onto the first. Given the rigidity and the tendency towards aggregation of the TCACoPc molecule, it is more probable that the latter occurs. Phase III shows a further increase in the frequency, with a relatively smaller decrease in the dissipation, relating to film thickening and possibly the removal of water molecules from between the loosely-bound adlayers. Similarly, phase IV shows the possible addition of a further layer on to the electrode surface. During the washing phase, a rapid decrease of D concomitant with a slight *f* decrease was noted. This most likely refers to the removal of the outer (i.e. film-solvent located) loosely-adsorbed TCACoPc molecules by the buffer solution, as well as the removal of EDC and NHS. After the washing stage, the dissipation value falls to within ~5% of the Δf_3 (a frequency shift of ~80 Hz and a dissipation value of ~5 x 10^{-6}), at and below which the Sauerbrey equation is assumed to hold valid. Using the Sauerbrey equation for a crude estimation of the bound mass, one can estimate that approximately 472 ng/cm^2 of mass (including TCACoPc, coupled water and ionic buffer components) has bound, a value nearly five times the

expected theoretical value, strongly indicating the accumulation of a multi-layered TCACoPc film on the electrode surface.

A mediator multi-layer has many disadvantages – primarily in terms of biomolecule attachment and surface irreproducibility. Since the biomolecule would attach to surface TCACoPc molecules, which are in turn loosely-bound to the electrode surface, this would result in a poor attachment of the biomolecule to the electrode surface. Figure 4 shows the instability of the TCACoPc film multilayer when the solvent was altered to phosphate buffer, following the HS rinse.

As is illustrated in Figure 7.5, below, a stable film was formed in HS that was resistant to washing. This film was found to be unstable when PB was flowed over the electrode surface, resulting in a linear-type removal of mass from the electrode surface. Additional washing steps of SDS were included in order to accelerate the removal of loosely-bound TCACoPc aggregates from the electrode surface. An average Δf_3 of -16.30 $\pm$ 1.25 Hz was recorded, corresponding satisfactorily to the expected theoretical frequency shift.

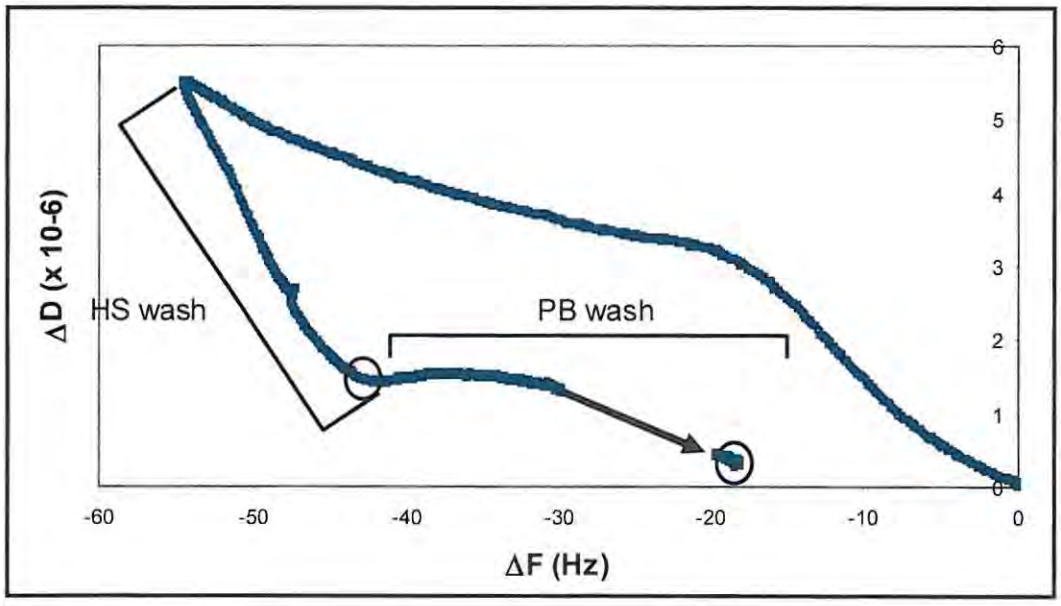

Figure 7.5: ΔD vs. Δf plots for the attachment and detachment of TCACoPc multilayers onto a gold quartz crystal electrode modified with a cystamine SAM.
2% SDS wash steps are indicated by a gap with an arrow, and solvent-stable films are indicated by a circle. HS = Heptane sulphonate, PB = phosphate buffer.

Negative controls using non-activated TCACoPc showed a rapid, logarithmic-like removal pattern of TCACoPc from the electrode surface, with an average of -1.7 Hz obtained prior to an SDS wash and a positive frequency shift (relative to the origin of analysis) after an SDS rinse (Δf_3 = +2.7 Hz). This positive frequency is considered to be caused by baseline drift, which was more pronounced after the extended time of analysis (2 hours).

Figure 7.6 shows the 3 major conformations of GOx binding as predicted from the crystallography data.

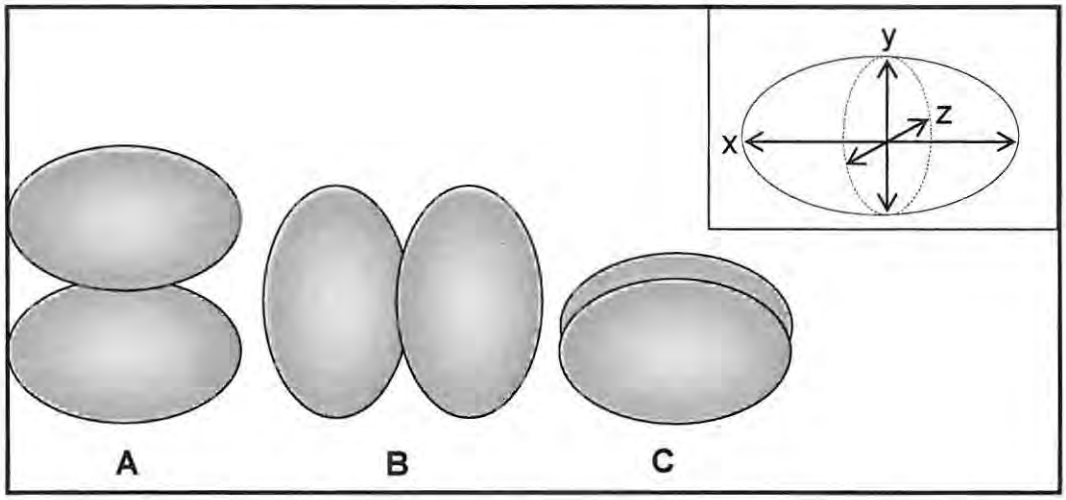

Figure 7.6: Illustration showing the 3 major possible conformations of a GOx dimer binding to the activated electrode surface.
Inset shows the dimensions of a GOx monomer as a geometric ellipsoid.

Crystallography data showed that GOx monomers bind in a configuration that is identical along the x axis, but with both y and z dimensions inverted at the point of binding. This results in the positioning of the FAD co-factor at opposite facings of the completed dimer. Since the FAD co-factor is responsible for the formation of the analyte (hydrogen peroxide) this results in the production of at least 50% of the analyte substrate that remains unavailable to the electrode surface. Additionally, it was found that the subunits associated through non-covalent bonds, without disulphide bonds stabilising the interaction.

The GOx monomer was determined to have the dimensions of 6.4 x 4.7 x 3.8 nm (x;y;z as illustrated in Figure 7.6), which have a good correlation with a non-glycosylated *Aspergillus Niger* GOx diimer previously described (Hecht and Schomburg, 1993). Theoretical surface areas of the three conformations were calculated as a flat ellipsoid with those protein dimensions parallel to the electrode surface. Surface areas for the various electrode-attached conformations were calculated to be 76.78 nm^2, 111.82 nm^2 and 186.31 nm^2 for conformations A, B and C, respectively. This provided final surface masses of: 348.78 $ng.cm^{-2}$ (Δf_3 = -59.1 Hz), 239.49 $ng.cm^{-2}$ (Δf_3 = -40.6 Hz) and 143.74 $ng.cm^{-2}$ (Δf_3 = -24.4 Hz) for the conformations A, B and C, respectively.

An important consideration is that the GOx subunits are not covalently bound together (by the formation of a disulphide bridge). Hence, conformation A would be the least stable towards non-optimal solution conditions, as it is more prone than the other conformations to subunit disassociation. By contrast, conformation "C" would be considered to be the most stable, as it has the largest proportion of protein bound at the electrode-solvent interface.

Binding of the GOx onto the activated electrode layer showed a relatively high viscoelastic response. The addition of SDS caused a slight addition of mass, with a significantly larger increase in dissipation. This is considered to be due to the linearising effect caused by the increase in electrostatic repulsion by the binding of the negatively-charged SDS to the GOx. As the proteins adopt more expanded conformations, this would have the effect of increasing the viscoelasticity of the bound molecules, resulting in an increase in the dissipative force exerted during oscillation. However, upon the removal of SDS, a frequency/dissipation profile similar to that achieved prior to SDS incubation was found, indicative that the GOx film was stable and resistant to denaturation and removal, itself indicative of covalent attachment of the GOx at multiple residues to the TCACoPc layer. Section C of Figure 7.3 illustrates this.

An average of Δf_3 = -12.23 ± 0.69 Hz bound, equating to approximately 72.157 ± 3.7 ng/cm^2, slightly less than half of the projected level of bound protein that was expected to bind when the largest conformation (conformation C).

In previous work (Mashazi et al., 2006), a biosensor created using Au-MPC-GOx was found to provide a maximal current output (at saturated levels of glucose) of 17.13 μA.cm^{-2}, with the signal transduced created by the phthalocyanine-catalysed electrooxidation of hydrogen peroxide. An electron yield of 2 electrons / molecule H_2O_2 oxidised was determined.

Since the current output is related to the charge, and the total charge is related to the amount of participant molecules by equation 3, the total output of H_2O_2 produced by the immobilised GOx per minute was calculated (as in Equation 7.3).

$$Q = n \times F \times N \qquad \text{Eq. 7.3}$$

Where Q is charge (in C), n is the number of electrons transferred in the redox reaction, F is Faraday's constant (9.6485 x 10^4 C/mol) and N is the number of molecules participating in the redox reaction (mols) (Bard and Faulkner, 2001a).

It was determined that the bound GOx possessed a maximal H_2O_2 production of 5.33 x 10^{-9} mol.min^{-1}.cm^{-2}. Since at least 50% of H_2O_2 produced remains unrepresented, due to the non-optimal binding conformations of the diimer subunits, this relates to a total H_2O_2 production of approximately 1.066 x 10^{-8} mol.min^{-1}.cm^{-2}. The diffusion coefficient of hydrogen peroxide was taken to be between 1.6 x 10^{-5} cm^2.s^{-1} and 1.61 x 10^{-5} cm^2.s^{-1} in aqueous solutions between the pH range of 6 to 8 (Prabhu et al., 1981). Given the relatively high diffusion coefficient and that the distance between the phthalocyanine layer and the active site of the electrode-facing monomer of the GOx can be estimated to be not greater than 6 nm (based on crystallography data for the distance between the active site of the enzyme and the outside of the protein for the various conformations of the predicted bound GOx), this means that little substrate destruction is expected to occur during the transport of the hydrogen peroxide to the electrode's surface.

This translates to 1.066 x 10^{-2} U.cm^{-2} of GOx activity bound at the electrode surface. Assuming that no denaturation of the bound GOx has occurred (i.e. GOx is not bound in a catalysis-inhibiting conformation), this translates to a protein loading of 5.33 x 10^{-5} mg.cm^{-2} (or 53.26 ng.cm^{-2}), which results in a frequency shift of Δf_3 = -9.2 Hz. Since this value does not give an indication of coupled water, a film containing an additional 50% mass of water (Δf_3 = -13.8 Hz) still falls within the frequency shift range, indicating a fair correlation with that of the QCM-D data.

7.4 Critical assessment of QCM-D as a fundamental biosensor:

The poor compatibility of some of the QCM-D flow chamber components with select organic solvents may make it difficult to assess the layering of organic-phase biosensor components. In previous work (Mashazi et al., 2006), layering of the phthalocyanine and the removal of a possible multilayer down to a TCACoPc monolayer onto the electrode surface took place using DMF (as a Pc solubilising agent), which shows poor compatibility with certain QCM-D components. Hence, an exact comparison between the previously published methodology and the one described in this paper (Mashazi et al., 2006) could not be performed. Aqueous-soluble substitutes and derivatives for chemical layer components in biocomposite materials may have to be used in order to successfully use this analytical technique. However, a good comparison between the theoretical maxima modelled in both this paper for TCACoPc layering and the experimental data for GOx loading compared to previous work (Mashazi et al., 2006) outlined here has been successfully achieved, showing the relevance and applicability of QCM-D as a analytical technique for probing fundamental interactions between multiple layers in biocomposite materials.

It is important to note that crystallography data may not accurately model the dimensions and conformation of the solubilised protein. Certain procedures crucial to the crystallisation of proteins prior to X-ray crystallography (for example, exposure of the protein to a buffer with a pH value that of the protein's pI value in order to minimise electrostatic repulsion (Bollag et al., 1996a; Bollag et al., 1996b;

Harris, 2001), and the use of precipation agents (Harris, 2001) have the effect of altering the conformation of the protein molecules, typically compacting them in order to adopt an aggregated conformation suitable for precipitation and crystal growth. This results in an underestimation of the volume that protein will adopt in a solvated environment, tending towards an overestimation of the theoretical mass that can be bound. Additionally, the differences extant between crystalline and solvated protein molecule conformations may have the effect of altering the number of available (i.e. surface-exposed) binding sites, further shifting possible binding conformations beyond those projected. A further comparison with the electrochemical output of a biosensor fabricated in a similar manner and making use of the same components shows a fair correlation with that predicted to have occurred via QCM-D.

7.5 Conclusion:

The QCM-D was successfully used to create and assess various layers present in previously published composite GOx-based sensors mediated through the attachment of Cobalt(II) metalophthalocyanine. Although the requirement for aqueous modification of the piezoelectric sensor created an undesirable TCACoPc multilayer, successful removal of the multilayer was achieved, leaving the sensor with a monolayer coverage of TCACoPc that exhibited a frequency shift that correlated satisfactorily with the theoretical value. GOx was then attached onto the surface of the TCACoPc, and the strength of attachment gauged through the use of a protein-denaturating surfactant, SDS. Based on the stable formation of the GOx film, and its minimal interaction with SDS, it was assumed that a strong (i.e. covalent) attachment between the GOx molecules and the underlying TCACoPc layer was achieved. While the experimental values for the mass addition of GOx did not correlate with the theoretical maximum based on crystallography modelling, it did correlate with the theoretical maximal current output of the previously-published sensor, even when the additional factor of coupled water was added. This displays proof-of-principle that the measurements of mass addition as tracked by QCM-D can be successfully applied in biosensors.

Chapter 8: Monitoring fundamental film characteristics of immobilized laccase monolayers: a comparison between QCM-D piezoelectric analysis and immobilized enzyme kinetics in a sensor configuration.

8.1 Abstract

Enzyme immobilization is an ever-growing research-area for both analytical and industrial applications. Of critical importance in this area are the effects of immobilization procedures upon the functionality of the immobilized biomolecules. Both beneficial and detrimental effects can be conferred through the selection and tuning of the immobilization procedure. Quartz-crystal microbalance with Dissipation (QCM-D) has been previously used to great effect in tracking alterations to thin films of biomolecules immobilized onto quartz transducers.

In this study, we investigate the ability of QCM-D to track and monitor film parameters of a monolayer of laccase immobilized on a series of self-assembled monolayers (SAMs), differing in lateral density of binding residues on the SAM and height of the SAM from the quartz surface. Both mass gains and rheological parameters for these varying surfaces were measured and trends compared to the apparent enzyme kinetics of the immobilized laccase films, assessed via chronoamperometry.

For covalent attachment of proteins, both shear and viscosity were increased relative to physically adsorbed proteins. An increase in lateral density of protein-binding surface of the SAM components was shown to increase the shear/viscosity of the resultant film while an increase in distance from the electrode (through incorporation of lysine linkers) was shown to decrease the shear/viscosity while simultaneously increasing the wet mass gain of the films.

The subject matter of this chapter has been submitted for publication as follows:

R. Fogel, J. Limson. Probing fundamental film parameters of immobilized enzymes - towards enhanced biosensor performance. Part I - QCM-D mass and rheological measurements. Enzyme and Microbial Technology.

R. Fogel, J, Limson. Probing fundamental film parameters of immobilized enzymes - towards enhanced biosensor performance. Part II – electroanalytical estimation of immobilized enzyme performance. Enzyme and Microbial Technology.

Shear and viscosity may be indicative of both enzyme denaturation and increased lateral protein packing within the film structure hence it is assumed that less distortion occurs with the inclusion of linkers which allow for more optimal protein immobilization.

The apparent enzyme kinetics of laccase films immobilized on the SAM series were measured through the detection of hydroquinone. Increases in both the maximal enzyme-generated current, i_{max}, and the apparent detection sensitivity of hydroquinone, as well as a decrease in the apparent Michaelis-Menton constant, K_m were noted for most of the surfaces with increasing linker length. Decreasing the lateral density of the spacer-arms brought about a general improvement in these parameters, which is attributed to the decrease in multiple points of immobilization undergone by functional proteins.

Finally, comparisons between rheological data and enzyme kinetics data showed that a dependence in K_m on the measured viscosity of the film between the different surfaces. Due to the contribution of increased viscosity brought about through the method of immobilization, these trends are restricted to the various surface classes used, rather than being a global trend, but a satisfactory trend between these classes indicates similar principles governing the correlation between viscosity and K_m. The relative detection sensitivity of immobilized films was found to be related to the degree of immobilized protein hydration (as estimated through the QCM-D parameters of Sauerbrey-calculated Mass and Voigt-calculated mass), between the different surfaces examined. This trend was found to be opposing when considering rigid films (as indicated by their shear values) with non-rigid films. The findings of this research indicate that viscoelastic measurements of immobilized enzyme thin-films using the QCM-D can produce valuable insight into the mechanisms dictating the kinetics of said films.

8.2 Introduction

The majority of protein immobilisation techniques have two often-conflicting factors to balance, namely finding a means to attach proteins in as firm a manner as desired for the application, while ensuring that the active conformation/s of that protein are retained in the finished product. While many immobilisation techniques have been investigated in biosensor-application research, much of this research is not addressing a key factor in this – an understanding of the interplaying factors that affect the final conformations present in the attached biomolecule, and, further, their effects on the functioning of the attached biomolecule. A greater understanding of the biomolecules participating in biosensing applications is, hence, of high desirability (Göpel and Heiduschka, 1995). Furthermore, a deeper appreciation of the changes undergone by these biomolecules during their immobilisation, and the subsequent effects that these alterations have on the functionality of that biomolecule is of utmost importance in the design and construction of immobilized-biomolecule structures, regardless of their intended use. Due to the alteration in protein conformation upon binding and catalysis of a substrate, an overly-reticulated protein molecule for example, may undergo additional decrease in efficiency based on the lack of protein mobility.

A number of papers have examined the immobilized film-structures of biomolecules using Quartz Crystal Microbalance (QCM), and QCM-D technology (QCM with Dissipation) through measurement of frequency changes (Δf) and in the case of QCM-D, the dissipation of molecules immobilized on quartz crystal surfaces (Höök et al., 1998a; Höök et al., 1998b; Voinova et al., 2002). These provide information on amount of mass bound, film thickness, viscoelasticity and assessment of conformational changes which can occur upon biomolecule immobilization (Voinova et al., 1999). However no such studies have attempted to relate these physical parameters identified to the performance of an amperometric sensor at similarly formed films, nor to the immobilised-enzyme kinetics thereof determined via electroanalytical techniques.

To this end, the studies reported on in this Chapter examine the physical film characteristics observed following the immobilization of laccase onto gold quartz crystal surfaces, either through physical adsorption or through covalent attachment to modified mixed thiol monolayers in different configurations. Parameters of the immobilized enzyme films' physical state are then compared to the observed kinetic functioning of the enzyme when attached to gold electrodes for amperometric detection of hydroquinone

.

8.2.1 Influences of protein immobilization at the molecular scale:

The method of protein immobilisation has a great impact on conformation, and hence, the kinetic operation of the enzyme, relative to the soluble, 'free', enzyme(Royer, 1982). These effects can be broadly categorized as:

(1) Changes occurring due to the non-primary interaction between support and enzyme (hydrostatic, ionic and hydrophobic interactions that occur due to the close proximity of the support to the enzyme) (Royer, 1982) (Bayramoğlu et al., 2003) (Bayramoğlu and Arica, 2007);

(2) Changes due to primary interactions occurring between support and enzyme (e.g. covalent bond formation, orientation(Bayramoğlu and Arica, 2007) and cross-linked reticulation)(Bayramoğlu et al., 2003);

(3) Microenvironmental factors, such as the accumulation of protons in the microenvironment surrounding protein films due to the presence of charged amino acids (Royer, 1982) (Lowe, 1977). An important sub-set of microenvironmental factors is:

(4) increased diffusional constraints arising from the accumulation of enzyme at a selected regions (affecting the rate of substrate interaction with the enzyme and the rate of product release to the transducer / bulk solvent) (Royer, 1982), (Kim et al., 2007). Additionally, immobilisation increases the concentration of biocatalytic protein at the area of attachment, resulting in an increase of protein-protein interactions, altering both microenvironmental and non-primary interactions occurring at the point of immobilisation. Alterations in the activity, kinetic stability and Michaelis-Menten constant (compared to free enzyme) have been

frequently reported upon immobilisation of the enzyme to the solid support, the extent of change being uniquely dependant on the selection of support (Klis et al., 2007b, Kim et al., 2007), the enzyme in question and method of immobilisation (Freire et al., 2001, Klis et al., 2007b), Bayramoğlu et al., 2003, (Bayramoğlu and Arica, 2007,Mateo et al., 2007) used to conjoin the first two elements (Royer, 1982). Considerable research has been expended into the minimization of deleterious properties while enhancing those properties (such as improved thermostability (Lowe, 1977) or pH stability) deemed desirable during immobilisation (Bayramoğlu et al., 2003, Cabaj et al., 2009)). This is often achieved by modulating certain aspects of selected immobilisation procedures (Bayramoğlu et al., 2003), but many of these papers report only on effects evidenced by the functioning of the protein (i.e. alterations in enzyme kinetics), as opposed to any physical changes undergone by them (Bayramoğlu et al., 2003, Bayramoğlu and Arica, 2007).

Direct observation of conformational changes undergone by immobilized proteins is difficult to achieve, primarily due to the low concentrations of proteins found at the immobilisation site and analytical interferences due to the support (Royer, 1982). Atomic Force Microscopy has been previously used to analyse both mono-dispersed and aggregates of proteins attached to supports and used to document attached particles' size and shapes (for example, Mazur et al., 2007), but this method (while very useful in assessing surface coverage of a given surface) gives very little indication of the extent of distortion or denaturation undergone by the protein layer. The research reported in this Chapter thus aims to fuse both data obtained from the determination of physical parameters of monomolecular layer of protein via the QCM-D and the kinetic parameters obtained by electroanalysis of products resulting from the activity of laccase within this film.

8.3 Aims and Objectives

The aim of this work was twofold: to examine i) whether QCM-D could be used to monitor fundamental film parameters that may impact on the operational properties of an amperometric sensor manufactured in the same manner and ii) whether the protein-film characteristics explored through the use of QCM-D as a

fundamental technique show any correlation with the kinetic parameters and functioning of the laccase when used as a biorecognition element in a biosensor for the electrochemical detection of hydroquinone. This study does not aim to construct a desirable biosensor. With reference to this Chapter, the aim is rather to determine if QCM-D can be of use in the fabrication of biorecognition layers by examining the fundamental constraints involved in the immobilisation of biorecognition elements to transducers. While QCM (Mazur et al., 2007; Rahman et al., 2008) and QCM-D (Saarinen et al., 2009) has been used as a gravimetric measurement of immobilized laccases at various surfaces, similar studies have not been reported in the literature for QCM-D analyses.

8.4 Methods and Materials

8.4.1 Apparatus

Apparatus for QCM-D was the same as previously described in Chapter 2 (Section 2.1.3)

8.4.2 Reagents

All reagents used were of analytical purity, (Sigma-Aldrich), and used without further purification. Stated purities of all reagents used in this research follow: 99% succinic acid, >99% cysteamine chloride, 98% β-mercaptoethanol, 99.9% sodium dodecyl sulphate (SDS) and 99+% L-lysine. Lactic acid, 85% $^{w}/_{w,}$ and 25% $^{w}/_{v}$ glutaraldehyde (Grade 1, high purity) were obtained in solution form at the stated concentrations and laccase purified from a culture of *Trametes versicolor*, was obtained as a lyophilized powder.

QCM-D analysis and protein modification of the electrode surface took place using 0.025 M succinic and 0.025 M lactic acid buffer (SLB), adjusted with NaOH to a pH of 4.5. All non-proteinaceous solutions were degassed by ultrasonication to remove bubbles for at least 10 minutes prior to QCM-D analysis.

Laccase solutions were prepared in SLB to a final concentration of 3.67 $mg.ml^{-1}$ (80 $U.ml^{-1}$). These were prepared > 1 hour before use and stored at 4 °C. Laccase solutions were allowed to stabilize at room temperature for 15 min prior to QCM-D analysis.

Electrochemical apparatus was the same as outlined in Chapter 2 of this Thesis (Section 2.1.1). The working electrodes used in this study were gold-surfaced electrodes (AuEs), as described in Chapter 6 of this Thesis.

Hydroquinone stocks were prepared at either 50 mM or 100 mM concentrations, as outlined in Chapter 2 (Section 2.2.5).

8.4.3 Methodology: QCM-D studies

8.4.3.1 Self-assembled monolayer (SAM) formation:

100 mM stock solutions of cysteamine and β-mercaptoethanol were prepared in de-aerated water and stored at 4 °C in the dark until used (within 36 hours of preparation).

Gold-surfaced crystals were cleaned as described in Chapter 7. Following cleaning of the crystals, mixed solutions of cysteamine and β-mercaptoethanol were prepared in de-aerated 20% ethanol, 80% water solution to a final concentration of 0.1 mM and the gold surfaces exposed to this solution for at least 8 hours at 4°C in the dark. Two different deposition solutions of different molar fractions of cysteamine and β-mercaptoethanol were prepared: a solution of 1 : 99 cysteamine : β-mercaptoethanol (henceforth referred to as "SAM 1") and 1 : 4 cysteamine : β-mercaptoethanol ("SAM 2") were used to modify the gold surface.

8.4.3.2 Self-assembled monolayer modification to produce a multi-layered SAM:

1 mM solutions of glutaraldehyde or L-lysine were prepared in either: milliQ water (for ex-vitro crystal modification) or 0.025M SLB (for QCM-D analysis). Surfaces were exposed to alternating solutions of the two for 5-10 min for each solution, followed by an ethanol / water rinse (ex-situ) or a 0.025M SLB rinse for 10 minutes (in-situ). Table 8.1 below tabulates the various completed surfaces formed, prior to the addition of laccase. For example, surface SAM 2.3 would be exposed to sequential alternations of glut-lys-glut-lys-glut.

Table 8.1: Compositions of the various surfaces investigated in this Chapter

SAM Number	Cysteamine content (%)	Cysteamine modification [a]
1	1	none
1.1	1	glut
1.2	1	glut-lys-glut
1.3	1	glut-lys-glut-lys-glut
2.1	25	glut
2.2	25	glut-lys-glut
2.3	25	glut-lys-glut-lys-glut
Au	none	none

[a] – layer-by-layer, starting at the basal SAM. "glut" designates glutaraldehyde and "lys" indicates the addition of a lysine residue

8.4.3.3 Attachment of laccase molecules: QCM-D analysis and biosensor fabrication

For all films that required glutaraldehyde activation prior to the addition of laccase (Table 8.1), the final activation of glutaraldehyde always took place during QCM-D analysis and was followed with a 10-minute SLB rinse, as described above. Glutaraldehyde exposure was required in order to activate the requisite surface residues (cysteamine), as described elsewhere (Lee and Chang, 2005).

Laccase solution was flowed over the QCM-D crystals until such a time as a stable mass response was recorded (typically 10-15 minutes), followed by a 10-minute rinse with SLB, and a short exposure (~2 minutes) of the crystal to 0.3% SDS solution. SDS exposure was followed by a final, extensive, wash phase using SLB.

8.4.3.4 Raw data treatment of QCM-D response curves:

The principles of QCM-D are outlined in the literature (Rohdal et al., 1995; Höök et al., 1998a). Upon attachment/detachment of bound mass at a piezoelectric material, the shift in frequency Δf is related to the mass by the Sauerbrey equation (Sauerbrey, 1959), Eq. 7.1. This relation is only valid for thin, rigid films firmly adsorbed onto the electrode surface that couple to the electrode's oscillation (Höök et al., 1998a; Höök et al., 1998b). Viscoelastic films (such as protein) or those with coupled water generally result in a dampening of the frequency to occur, and an overestimation of the mass of the attached layer (Höök et al., 1998a; Höök et al., 1998b). Data regarding the viscoelasticity and strength of the attached layer, can then be obtained from QCM-D measurements of the so-called D factor, or dissipation factor, D (dimensionless units, $\times 10^{-6}$). D is essentially the ratio of energy dissipated from the surface of the crystal versus that stored during one period of oscillation. During QCM-D measurements of Δf and ΔD are taken at multiple overtones. These essentially refer to multiple integers of the resonant frequency. In so doing these measurements can provide further information of thickness, shear and viscosity of the layer (Höök et al., 2001).

For QCM-D analysis, the same solvent (0.025 M SLB, pH 4.5) was used throughout to minimize the perturbation of the QCM-D response by a large alteration of the solvent composition. For similar reasons, low concentrations of glutaraldehyde and L-lysine were used, additionally to decrease non-specific binding at the electrode surface and the reversible polymerization of the glutaraldehyde (Lee and Chang, 1995). Frequency and dissipation data were normalised to possessing values of 0 after glutaraldehyde activation of the SAM surface prior to the analysis of the protein film, when surfaces requiring glutaraldehyde activation was used. This was performed in order to account for very slight drifts in the Δf and ΔD values following glutaraldehyde exposure.

Two major parameters of the protein binding were used to determine the efficacy thereof. The first is the viscoelasticity index (*V.I.*). The viscoelastic index of the protein determined in these studies is the inverse of the conventional $\Delta D/(\Delta f/n)$ relation (Dutta et al., 2008) and calculated as in Eq. 8.1 in order to display increases in rigidity more intuitively.

$$V.I. = \Delta f_{tot} / \Delta D_{tot} \qquad \text{Eq. 8.1}$$

where Δf_{tot} is the total change in frequency, normalised after the stable frequency of response of the glutaraldehyde activation (Hz), with $\Delta f_{tot} = f - f_o$ being the difference between the recorded frequency value (f) assessed after reaching a stable frequency and the initial frequency recorded at a stable baseline prior to sample adsorption (f_o). Similarly, ΔD_{tot} is the total change in dissipation for the same ($x10^{-6}$ dimensionless units). .

Secondly, from Δf_{tot}, the Sauerbrey equation was used to determine the mass gain on the crystal surface. The Sauerbrey equation was only held to be valid if the V.I. was $\geq$ 10 Hz.10^6. The Sauerbrey equation (Sauerbrey, 1959) was solved as in Eq. 7.1.

The V.I. and the Sauebrey-calculated mass gain were determined at the three major stages of the protein attachment: (1) at the height of protein attachment, (2) at the steady-state of the subsequent rinse of loosely-adsorbed proteins and (3) following a short SDS rinse in order to remove all protein that was not covalently bonded to the electrode surface. Experiments were performed in at least triplicate, and the mean values with standard deviation presented henceforth.

8.4.3.5 Rheological monitoring

Film thickness, elastic shear modulus and viscosity determinations of the attached protein films were performed using Q-Tools viscoelastic determination functions using the raw Δf and ΔD values drawn from a minimum of 3 overtones and a maximum of 5. The Voigt-based model of coupled motion for viscoelastic films attached to a quartz piezoelectric sensor developed by Voinova et al., 1998 was used for the determination of these parameters during the laccase attachment / detachment stages. The film density, fluid viscosity and fluid density were assumed to be 1000 $kg.m^{-3}$, 0.001 kg.ms and 1100 $kg.m^{-3}$ respectively for all protein films examined. An abbreviated summary of the modeling system and relevant calculations used in these determinations is available (Dutta et al., 2008), as is a more detailed investigation into the mathematics and assumptions underlying this system (Johannsmann, 2008), but is excluded from here for the sake of brevity.

The Voigt mass gains of the film at different states of rinsing were determined from the film thickness, and effective film density. In order to maintain parity between replicants, laccase films adsorbed to surfaces (Au and SAM 1) were modeled as possessing low shear ($>10^5 N.m^{-3}$) in order to satisfactorily fit the experimental data of all the replicants to the model data. All other surfaces were modeled under the assumption of a high-shear ($< 10^5 N.m^{-3}$), in order to provide a satisfactory fit to the data and a consistent grouping of rheological parameters between replicants.

8.4.4 Methodology: Immobilised enzyme kinetics monitoring via electroanalysis

8.4.4.1 Electrode Cleaning and surface area estimations

AuEs were cleaned as outlined in Chapter 6, (Section 6.4.2.1). Following cleaning, the final CV was saved and analysed to calculated the surface area of individual electrode surfaces.

Real electrode surface area was estimated through integration of the gold oxide reduction peak of the final cleaning voltammograms of each electrode in order to determine the charge of that peak. Peak charge was then used to determine the real surface area of the electrode using a surface-charge relation of 400 $\mu C.cm^{-2}$ (Trasatti and Petrii, 1991).

8.4.4.2 Modification of gold surfaces and formation of immobilized enzyme layers

Gold electrodes cleaned as in Section 8.4.4.1 were modified with the various SAM layers outlined in Table 8.1 in the same manner as was used to modify gold QCM-D sensors (Section 8.4.3.1)

Following formation of SAM films and subsequent cleaning, electrodes were modified through alternating exposures of the SAM film to glutaraldehyde and lysine, for a period of 10 minutes per modification. After each modification, electrodes were thoroughly rinsed with ethanol, then water. This was performed to produce the SAM amendments outlined in Table 8.1.

Once SAM amendments had taken place, SAMs were activated via a 10-minute exposure to glutaraldehyde, rinsed with ethanol and then water, and 20 µl of an 80 $U.mg^{-1}$ solution of laccase was aliquoted over the surface of the activated SAM.

Electrode surfaces labeled as "SAM 1" received no glutaraldehyde activation prior to addition of laccase. Electrode surfaces designated "Au" were modified with laccase as above, using cleaned electrodes without SAMs.

The SDS wash stage following protein immobilisation (Section 8.) was used exclusively for QCM-D analysis in order to rapidly remove loosely-bound proteins from the film. It should be stressed that this was not considered necessary for the fabrication of the electrochemical biosensor, due to the rapid washing of the modified electrode using comparatively large volumes of water and buffer, neither of which are readily utilizable using QCM-D without causing signal perturbation.

8.4.4.3 Chronoamperometry

Chronoamperometry was performed under stirred conditions (stirrer speed: 15 000 rpm) using 5 ml of 0.1M SLB, pH 4.5. The working electrode was poised at -0.15 V (vs. Ag/AgCl) and the current-sampling time was 0.2 s per reading. Aliquots of either 50 mM or 100 mM HQ stock solution were used to calibrate the immobilized enzyme films

8.4.4.3 Electroanalytical Modelling system

Immobilised enzyme parameters were determined using the sigmoidal model (Eq. 2.6) as outlined in Chapter 2 and Appendix 1 of this Thesis. Measurement of detection sensitivity; K_m; i_{max} and the degree of sigmoidality, b, proceeded as described in Chapter 4 of this Thesis.

From surface area determinations (Section 8.4.4.1), i_{max} and biosensor sensitivity were calculated as an expression of current density (current per cm^2 of surface area, $A.cm^{-2}$), and reported as such henceforth.

8.5 Results and Discussion:

8.5.1 QCM-D Analysis

β-mercaptoethanol was selected as a non-active SAM filler (Bain et al., 1989; Bumm et al, 1999; Smith et al., 2004) i.e. in order to alter the space occurring between protein-binding cysteamine SAM components. Based on the similarities in its chain-length to cysteamine, and the polar head-group, β-mercaptoethanol was expected to have a similar aqueous solubility, allowing for a laterally-homogenous deposition of SAM components onto the electrodes.

8.5.1.1 Characterisation of typical protein film attachment and protein wash-off

Figure 8.1 below shows a typical QCM-D response for the attachment of laccase to a sensor surface, in this instance, SAM 2.2. f and D values are normalised relative to the glutaraldehyde activation of the SAM, with the phase shifts indicated by labeled arrows.

Typically, the attachment process of laccase consisted of the following phases in all surfaces examined: a rapid increase of bound mass to the sensor (concomitant with a rise in dissipation), followed by slow stabilization of that response. Wash-off of the protein occurred in two similar stages, with final phase being that of a very slow and steady loss of mass from the sensor surface. The SDS wash was used to induce a more rapid removal of unbound protein from the electrode surface (Yin et al., 2008) and the post-SDS phase exhibits a more rapidly-stabilized removal of mass from the electrode surface. The differences between the Δf vs. time and ΔD vs. time gradients of the buffer rinse stages before and after exposure to SDS confirm this.

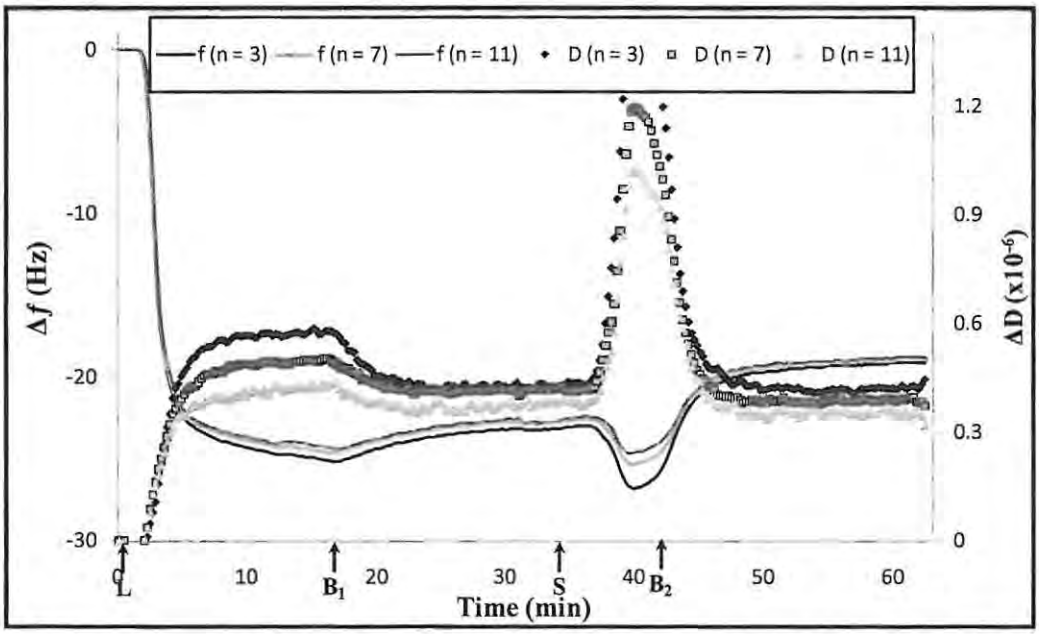

Figure 8.1:($\Delta f/n$) vs. time and ΔD vs. time plots (overtone number, n = 3, 7, 11) of the attachment of laccase to the surface of SAM 2.2.

Values are normalized relative to the QCM-D response following glutaraldehyde activation of the SAM and rinse-off of unbound aldehyde. Arrows indicate alteration of the solvent flowing over the crystal.

Legend: L = 80 U.ml^{-1} laccase solution, B_1 and B_2 = buffer wash, S = 0.3% SDS solution

8.5.1.3 Mass and V.I. variations between laccase-adsorption phases and binding surfaces investigated:

Due to the better resolution of the phases, Δf and ΔD values drawn from overtone n = 9 were used for calculating V.I. and mass gain, as displayed in Figures 8.2**A** and Figure 8.2**B** for the different surfaces outlined in Table 8.1.

In Figure 8.2, mass gain displayed was calculated using the Sauerbrey equation (Eq. 7.1) for all investigated surfaces at different phases of protein attachment/desorbtion, except for analyses following the SDS rinse step where these are reported using both the Sauerbrey equation (after SDS rinse, S) and Voigt viscoelastic modeling (after SDS rinse, V). Of the four categories displayed in Figure 8.2, only the last three ("Buffer Rinse" and "After SDS-Rinse, S" and "After SDS-Rinse V") should be considered important for elucidating the efficacy of any electrochemical biosensor fabricated in the same manner as was modeled on the QCM-D. It must be considered that the initial measurement (that of the protein film after a buffer rinse) is indicative

of an adsorbed protein multilayer, as opposed to the washed enzyme monolayer that was used for electrochemical determination.

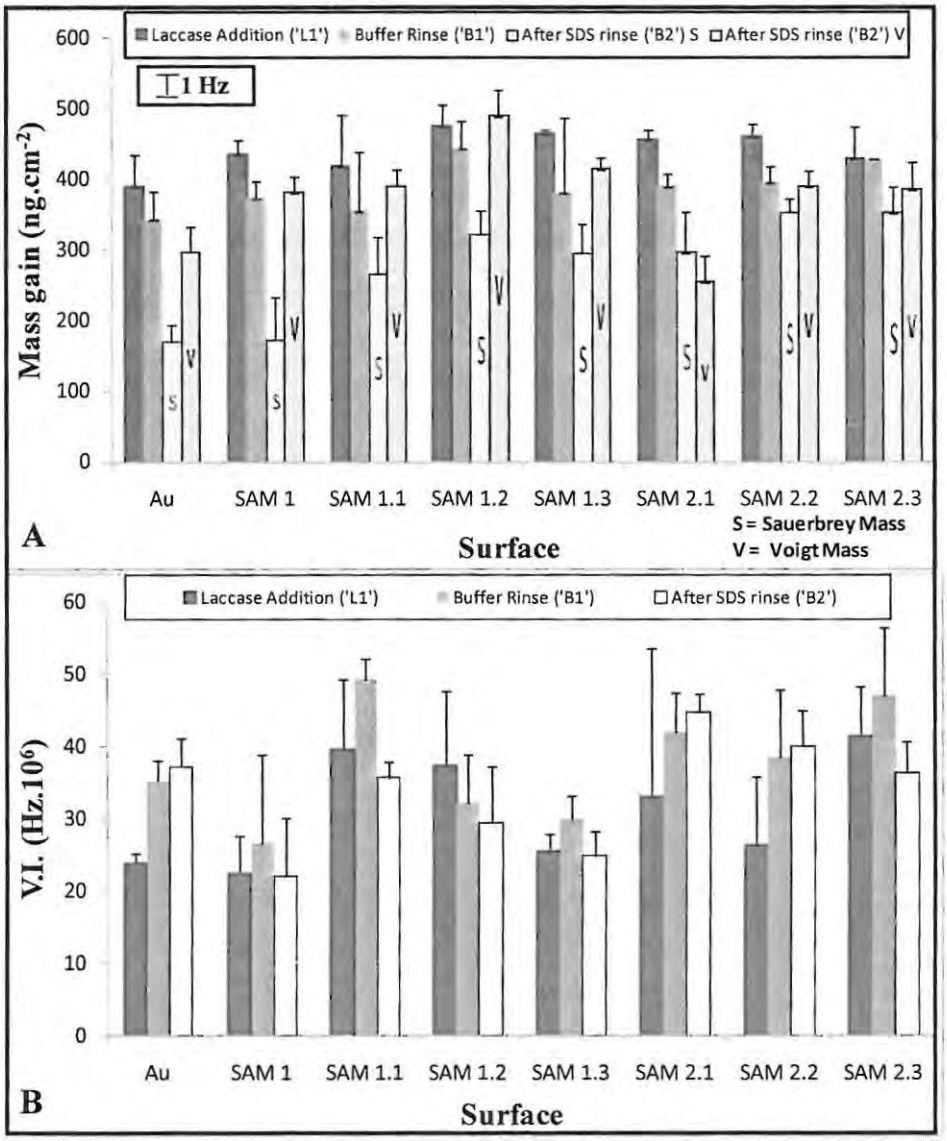

Figure 8.2: Mass and V.I. variations for the different surface configurations at different stages of protein attachment as monitored via QCM-D. Number of independent measurements, n ≥ 3

A) Protein film mass gain (in ng.cm^{-2})

Values are drawn from stable areas of the laccase adsorption-desorption phases indicated in Figure 8.1

Inset box shows effects of + 1 Hz deviation of frequency on the calculated mass

"After SDS rinse – S" refers to mass gains calculated via the Sauerbrey formalism, while "After SDS rinse- V" refers to mass gains calculated via the Voigt film thickness.

B) Viscoelastic Indices (V.I.) of same protein films.

Considering here only the Sauerbrey-determined mass gains in this section (Figure 8.2**A**), comparable amounts of protein was retained after the SDS wash on both basal films and between controls. Taking into account uncertainties, average bound masses of ~280 ng.cm^{-2} were recorded for both SAM 1.1 and SAM 2.1 and ~173 ng.cm^{-2} for Au and SAM 1). This is indicative of a bound monolayer (or sub-monolayer in the cases of controls) with a greater cohesiveness than a multilayer would possess. The use of dilute SDS would ensure that only loosely-bound proteins would be removed from the transducer surface, leaving behind the sub- to full-monolayer of bound protein.

The two controls used for this study, namely, laccase adsorbed onto a plain gold surface (designated Au in Table 8.1) and onto 1:99 cysteamine: B-mercaptoethanol surface (designated SAM 1) show that the addition of dilute SDS removes the majority of the protein film formed by the adsorption of laccase. Laccase adsorbed onto gold displayed a greater averaged V.I. (film rigidity) than SAM 1, probably due to the adoption of a non-optimal surface-bound conformation of the bottom-most layer on contact with the gold electrode. Since SAM 1 possesses both hydrophilic and basic SAM head-groups, this increased hydrophilicity may aid the proteins in retaining a solvated conformation when interacting with this surface. The low V.I. value of SAM 1 (Figure 8.2**B**) and larger proportional mass loss after rinsing (relative to other surfaces) are indicative of a less rigidifying interaction between protein and surface. The low average V.I. value, coupled with the large degree of uncertainty present in the determination of V.I. and bound mass itself may indicate the presence of a sub-monolayer of protein of variable coverage retained after SDS exposure, possessing a substantial mass contribution from coupled water trapped in-between adsorbed protein molecules on the surface contributing to the dissipation of the film.

A comparison between the two basal SAMs (SAM 1.1 and SAM 2.1) layers shows immediate differences in their respective rigidities. Consistently, protein films attached onto SAM 2-based surfaces showed greater rigidity than their SAM 1 counterparts (Figure 8.2**B**). An increased surface concentration of cysteamine provides a greater number of attachment points between the enzyme and the electrode. Increased reticulation

of the enzyme will have the effect of increasing the rigidity of the film, by decreasing the possible conformations and orientations that the enzyme can adopt following attachment. This increase in rigidity with increase in protein concentration conforms with previous studies (Saarinen et al., 2009). This also helps to explain why a consistently higher level of protein binding was also observed for SAM 2 surfaces when compared to their SAM 1 counterparts. The initial surfaces themselves bound a comparable amount (~266 $ng.cm^{-2}$ in SAM 1.1 compared to 296 $ng.cm^{-2}$ for SAM 2.1 Figure 8.2**A**), but a much greater average V.I value was recorded for SAM 2.1 (44.1 $Hz.10^6$ Figure 8.2**B** compared to SAM 1.1 (35.6 $Hz.10^6$). Film rigidity has previously been used as a parameter to investigate inter-protein cross-linking of adsorbed films onto QCM-D crystals (Dutta et al., 2008) and it is logical to assume that a greater degree of surface-protein bonds would increase the degree of rigidity.

An increase in the amount of final bound mass of protein (i.e. following SDS desorption) was found to be the general trend with the addition of lysine linkers connecting the surface to the protein (Figure 8.2**A**). Similar behaviour has been previously observed with the inclusion of ionic spacers between the surface and laccase using QCM, with surface plasmon resonance indicating a significant increase in bound mass (Mazur et al., 2007). With a greater degree of linker length and mobility (Hermanson et al., 1992) the number of protein-binding attachment points was increased, resulting in greater mass binding, as supported by other research (Bayramoğlu and Arica, 2008). Additionally, the presence of carboxyl and amine groups present on lysine, and the carbonyl groups present on glutaraldehyde are expected to increase the hydrophilicity of the attachment surface, decreasing denaturation of the enzyme when interacting with this linker (Hermanson et al., 1992).

The addition of lysine linkers to the SAMs was proposed to decrease rigidity (Figure 8.2**B**) by the following two methods: firstly, as stated above, by allowing for enzymes to be linked in a less denaturing conformation through the increased linker mobility, and secondly by increasing the space between the attached protein and the electrode surface. Since proteins have been shown to alter their conformation from a solvated to a bound

conformation when contacting a solid surface (Mungikar and Forcinti, 2004), an increase in the length between the bound protein film and the electrode would enable a better retention of the solvated conformation (Bayramoğlu and Arica, 2008). A larger degree of protein solvation would increase the amount of coupled water occurring within the film, effectively increasing the amount of bound mass of the protein film and increasing the dissipative effect of the film. Thus, an increase in spacer length would simultaneously lower the V.I and increase the bound mass gain, respectively.

The possibility of cross-linking occurring between linker molecules must also be considered. As linker mobility increases with linker length, there occurs an increasing probability of linkers interacting with one-another, decreasing available covalent linkages to protein. This is a potential explanation behind the lowered final mass gain that appeared between SAM 1.2 and SAM 1.3 (323 $ng.cm^{-2}$ and 296 $ng.cm^{-2}$ respectively, while possessing similar standard deviations of $\pm$ ~30 $ng.cm^{-2}$). A similar effect between SAM 2.3 and SAM 2.2 does not occur, possibly since the inter-cysteamine space was greatly decreased in SAM 2, resulting in less overall linker mobility. As stated above, the inclusion of coupled water would produce a large wet-weight of the protein film, but very little actual bound protein contributing to the mass of this film (Voinova et al., 1998) while the low rigidity (and larger height) of this film may decrease the amount of apparent mass monitored by the Sauerbrey formalism (Voinova et al., 2002) accounting for discrepancies in mass between SAM 1.2 and SAM 1.3.

By itself, the V.I. is a fairly data-poor indicator of the effects undergone by the layer. The reliance on a single harmonic overtone to investigate the film properties produced a higher degree of uncertainty in the determination of bound mass by the Sauerbrey formalism, compared to the mass calculated from the Voigt-modeled film height (Figure 8.2**A**). In addition, relatively high uncertainties in the determination of V.I. values exist (Figure 8.2**B**), making comparisons between closely-related sub-protein films (e.g. SAM 1.1 and 1.2) problematic. Frequency and dissipation measurements are useful, but not considered reliable indicators of film properties and several important assumptions are ignored when merely using these two results as an

indicator of film properties (Johannsmann, 2008). The following section highlights this phenomenon, when considering the rheological modeling of the various surfaces using the Voigt-element modeling of viscoelasticity.

8.5.1.4 Rheological parameters of the attached film:

Table 8.2 displays the viscoelastic parameters elucidated from the pseudo-stable wash-off phase of the laccase attachment utilizing Voigt modeled mass gains. The modeling system used was unable to accurately determine the parameters of the post-SDS wash phase for some of the films presented here without a high degree of uncertainty, hence the inclusion of the pre-SDS, buffer-rinsed protein layer. This also presents valuable information regarding the alteration of the film after exposure to SDS (and thus, a sub- to full monolayer of protein, as opposed to the semi-multilayer of protein that a simple buffer rinse leaves on the crystal).

Table 8.2: Shear modulus, film viscosity and film thickness of the surfactant-washed film determined using Voigt modeling using data drawn from the QCM-D measurements

Surface[a]		Mass gain[b] ($ng.cm^{-2}$)	Film thickness (nm)	Shear Modulus ($10^5 N.m^{-3}$)	Viscosity ($10^{-3} N.s.m^{-3}$)
Gold	- prior	569 ± 58	5.17	0.42 ± 0.23	2.9 ± 0.7
	- post	298 ± 35	2.71	0.26 ± 0.09	2.6 ± 0.1
SAM 1	- prior	611 ± 34	5.56	0.33 ± 0.06	2.7 ± 0.3
(phys)	- post	382 ± 20	3.48	0.16 + 0.05	2.5 ± 0.1
SAM 1.1	- prior	571 ± 88	5.19	7.31 ± 1.78	8.3 ± 1.2
	- post	392 ± 22	3.56	6.69 ± 0.76	6.6 ± 0.8
SAM 1.2	- prior	545 ± 35	4.96	3.44 ± 1.35	4.7 ± 0.5
	- post	490 ± 35	4.46	5.21 ± 0.84	3.3 ± 0.4
SAM 1.3	- prior	691 ± 76	6.29	0.30 ± 0.06	2.3 ± 0.4
	- post	415 ± 14	3.78	1.42 ± 0.29	3.1 ± 0.2
SAM 2.1	- prior	413 ± 59	3.76	10.40 ± 3.80	7.6 ± 2.2
	- post	255 ± 37	2.32	11.50 ± 3.29	8.33 ± 1.30
SAM 2.2	- prior	458 ± 48	4.17	11.25 ± 1.92	7.25 ± 1.49
	- post	391 ± 31	3.56	12.60 ± 0.09	7.20 ± 1.48
SAM 2.3	- prior	438 ± 22	3.99	5.19 ± 2.90	6.43 ± 2.09
	- post	386 ± 39	3.51	9.50 ± 2.50	6.56 ± 0.46

[a] "Prior" refers to values drawn from the end of the wash-off stage prior to treatment of the film with SDS ("B_1" phase in Figure 1 of this Chapter) and "post" to values drawn from a stable response during buffer rinse after SDS exposure ("B_2").

[b] As calculated by multiplying the film thickness by the modeled film density (1100 $kg.m^{-3}$).

Uncertainties represent standard deviations from the mean. Number of independent measurements, $n \geq 3$.

QCM-D has been previously coupled with rheological-modelling software to describe both the mechanical properties of viscoelastic proteinaceous thin-films and alterations undergone by said films (e.g. Voinova et al., 1999; Höök et al., 2001; Gurdak et al., 2005; Feiler et al., 2007; Lubarsky et al., 2007; Malmström et al., 2007; Dutta et al., 2008). A good correlation with validative techniques, such as AFM and SPR have been noted once corrections have been made to accommodate the effects of bound and/or coupled water (Lubarsky et al., 2007; Reimhult et al., 2004).

Mass gains determined by Voigt modeling were consistently higher than those estimated by the use of the Sauerbrey Equation, as displayed in Figure 8.2**A**, a finding which is supported by the literature (Höök et al.,

1998b). The Voigt modeling takes into account viscous energy loss arising from a non-rigid film (Höök et al., 1998b) where the dissipative effect of a viscoelastic film (such as a protein layer) causes an underestimation of the mass / film thickness in the Sauerbrey relation. Additionally, the Sauerbrey equation does not take into account film swelling through solvent intercalation (Voinova et al., 2002). Mass and film thickness are interrelated as described in the footnote of Table 8.2. This value is assumed to be relatively independent of the estimated film density as determined by Larsson et al, 2003. Since the film density was used as a constant between the surfaces examined, it is expected that the greatest areas of alteration (i.e. film viscosity and elastic shear modulus) be substantially different between surfaces, and thus may not be truly representative of these actual values, but still remain useful as a means of comparison.

In Table 8.2 the film thicknesses themselves seem very low relative to expected values from a packed protein surface, however flattening of protein has been noted previously in QCM research (Lojou et al., 2004) and can be attributed to either flattening under sub-monolayer coverage or to conformational changes extant between crystalline protein and immobile protein. Teichroeb et al. (2008) provide evidence to suggest that a monolayer of BSA protein adsorbed onto support deforms dimensions indicated in the crystallographic data.

The two controls used highlight the detail of the information that may be gained from the use of the modeling system used herein (Table 8.2). Even though comparable mass gains / film thicknesses were observed in both phases (569 and 611 $ng.cm^{-2}$ prior to the SDS rinse and 298 and 382 $ng.cm^{-2}$ after the SDS rinse for laccase physically-adsorbed onto the gold surface (Au and SAM 1, respectively) between the controls, higher viscosity and shear modulus values were observed for the gold surface than the SAM-coated gold surface. This indicates either a greater degree of proteinaceous packing, and/or an increased denaturation of the protein at the surface-solvent interface, due to the decreased hydrophilicity of the unmodified gold surface (Mungikar and Forcinti, 2004). A greater degree of distortion/denaturation occurring at the laccase molecule as it interacts with a surface should decrease the amount of surface-facing hydrophilic/ionizeable residues, but allowing predominantly protein-protein interactions through

hydrophobic interactions, but decreasing protein-solvent interactions (Otzen, 2008). Logically, as the amount of coupled or bound water in the protein film decreases, the viscosity and elastic shear modulus of the film would increase as the film increases its cohesiveness, a similar phenomenon to that noted with the binding of streptavidin to a biotin layer (Reimhult et al., 2004). Therefore, a viscosity or shear increase could indicate that either (1) a greater degree of protein packing (as a function of mass) relative to the bound water in the film, (2) an increased strength of attachment between surface and protein or (3) an increased average level of denaturation / conformational alteration undergone by the attached protein or a fusion of the aforementioned factors (Reimhult et al., 2004).

The activation of SAM 1 with glutaraldehyde greatly increased both the viscosity and shear of the protein film (Table 8.2), even though only a 10 $ng.cm^{-2}$ difference in modelled mass was observed. The viscosity increased from an anticipated 2.5 to 6.6 x 10^{-3} $N.s.m^{-3}$ and the shear from 0.16 to 6.69 x 10^{5} $N.m^{-3}$ for physically-adsorbed laccase and covalently-bound laccase after the SDS rinse. This change was expected and attributed to the covalent linkages formed between the protein film and the sensor surface, causing increased protein film rigidity. The increase of protein-binding cysteamine residues between SAM 1 and SAM 2 causes a similar increase in viscosity and shear modulus. This phenomenon is further highlighted in Table 3, where the rheological parameters are normalized to the bound mass of the protein film.

As shown in Table8.2, the covalent addition of L-lysine to the SAM components as a linker caused an increase in the mass / film thickness among surfaces studied compared to their basal SAMs i.e. SAMs 1.1 and 2.1. Generally, the shear and viscosity of the final protein film initially decreases concomitantly with an increase in the number of L-lysine between the SAM and the protein. This function may also be attributable to the further inclusion of water at the protein film (especially when monitoring differences in film thickness and mass). However the statistical significance of the trends of these decreases is questionable.

Similar uncertainties in the rheological properties have been noted for QCM-D viscoelastic modeling (Liu and Kim, 2009) due to the analytical problems associated with viscoelastic modeling in the absence of external information regarding film thickness (Johannsmann, 2008), while the determination of film thickness itself is less affected. Hence, in Table 8.3, shear and viscosity of the protein films (determined at the post-SDS rinse phase) are divided by the Voigt film mass in order to further explore differences extant between the surfaces.

Table 8.3: Rheological parameters calculated relative to the final mass of the protein films following an SDS rinse.

Surface	Shear modulus (10^3N.cm^2.ng^{-1}.m^{-3})	Viscosity (10^{-5}N.s.cm^2.ng^{-1}.m^{-3})	V.I.$_{n=9}$
Gold	0.08 ± 0.01	8.9 ± 1.1	37.2 ± 3.9
SAM 1 (phys)	0.04 ± 0.01	8.2 ± 0.5	22.0 ± 8.3
SAM 1.1	2.07 ± 0.23	16.8 ± 2.3	35.6 ± 2.1
SAM 1.2	0.92 ± 0.18	6.8 ± 0.9	32.2 ± 6.6
SAM 1.3	0.34 ± 0.07	7.5 ± 0.6	29.9 ± 3.3
SAM 2.1	4.51 ± 1.67	32.7 ± 6.9	44.1 ± 2.3
SAM 2.2	3.21 ± 0.18	18.4 ± 3.9	40.1 ± 4. 9
SAM 2.3	2.46 ± 0.70	17.0 ± 2.1	36.3 ± 4.4

Uncertainties represent standard deviations from the mean, with number of independent measurements, $n \geq 3$

Table 3 satisfactorily shows that these parameters tend to decrease when related to the average film mass following SDS desorption. This indicates that the use of L-lysine to separate the attached protein from the surface tends to decrease the shear and viscosity of the protein film (i.e. increase the degree of solvation of the attached protein molecules) *per unit mass added*. This was the anticipated effect of the addition of the linkers to the surfaces examined. Hence, this indicates that, not only does the amount of proteinaceous mass increase with increasing length of linkers, but that the addition of linkers tends to decrease the extent of denaturation exhibited by the attached protein films. In other studies, retention of enzyme activity has been reported for laccase bound through zirconium phopshonate functional groups (Mazur et al., 2007).

It is important to note at this juncture that a higher protein loading does not necessarily entail a better biorecognition element for a protein-based biosensor. When considering the effects of a packed-protein layer, certain issues such as the decreased protein flexibility (due to steric hindrance caused by the presence of other bound biomolecules and/or electrostatic repulsions caused by same), the covalent method of attachment and the resultant non-optimal catalytic conformations that the proteins adopt for the aforementioned reasons could impede the function of the biosensor (Hammes, 2002). For the same reasons, a decreased accessibility of the substrate/s to the enzymes (internal diffusional resistance) and (by inference) decreased accessibility of the products to the electrode surface and the slower diffusional rates that these cause may all influence the efficacy of a protein film when considering its application to a biosensor. This shows that one cannot rely on a single parameter (such as mass gain) in order to determine which the best protein immobilisation method is. In this case, viscosity and shear data derived from QCM-D data may be invaluable indicators of, not only (1) the level of distortion and potential denaturation arising from both the immobilisation method and subsequent protein-surface interactions but also of (2) film properties arising from the lateral interactions of the biomolecules with one another.

8.5.2 Kinetic analysis of laccases immobilized on SAM surfaces

A satisfactory biorecognition signal was transduced from the surfaces investigated within the nanoampere range (Figure 8.3), allowing for accurate modelling of the parameters of the immobilized biomolecule layer to take place (Table 8.4).

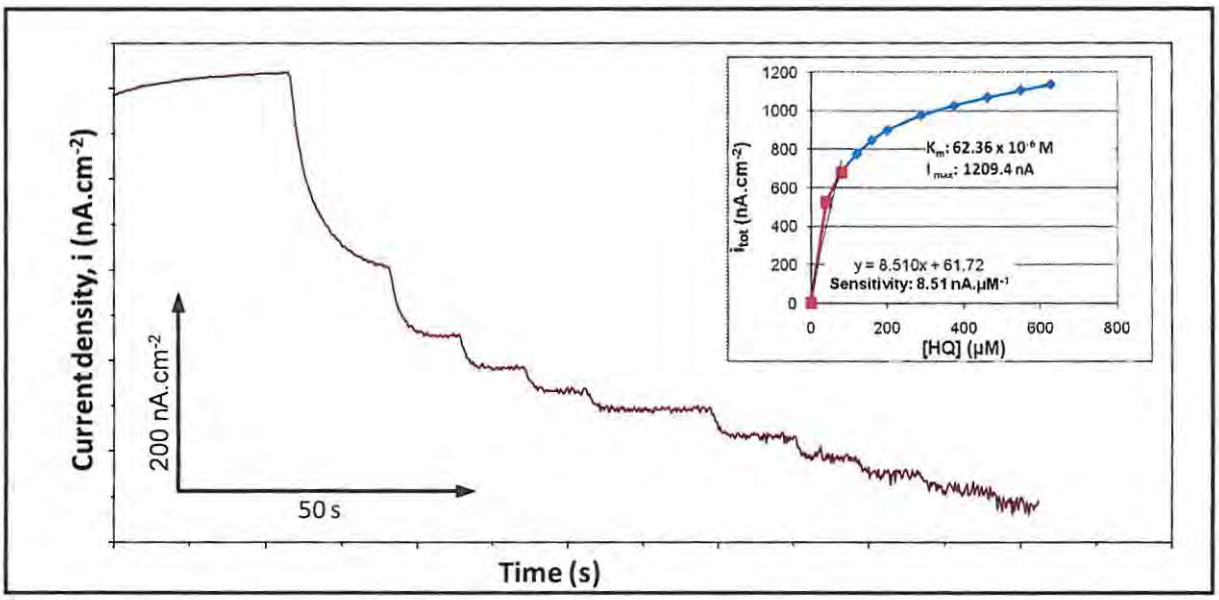

Figure 8.3: Chronoamperogram (current values adjusted to account for surface area) generated through the use of laccase immobilized to a gold electrode through the use of SAM 1.1

Scales of the current-time values for this biosensor are represented in the bottom-left corner. Current plateaus indicate the time of the addition of 2.5 µl of 100 mM HQ to the electrochemical vessel (an increase in concentration of approx. 50 µM) and the double-headed arrows indicate the addition of 5 µl of the same concentration of HQ.

Inset diagram: The current-concentration curve drawn from this data, and the K_m, biosensor sensitivity and I_{max} values determined from same from use of the modeling software

Since the transduced current of the biosensor is in the sub- to low-µA range, the substrate turnover is estimated to be in the pmol.min^{-1} range (As in Eq. 6.1) when using substrate concentrations starting at the µM range. Hence, steady-state enzyme kinetics were assumed to dominate and enzyme kinetics modeling proceeded as normal, as the total change in substrate concentration throughout the analysis was assumed to be far less than 1% of the bulk substrate concentration (in fact, a factor of at least 10^4 separated the bulk solution from the velocity of enzyme reaction).

As Figure 8.3 demonstrates, a rapid current response (> 10 s) to changes in substrate concentration are noted (from stable current-baseline to stable baseline) when using this electrode. However, it provides a very low sensor response, and suffers from a particularly high noise-to-signal ratio for that reason. This becomes more pronounced as the substrate concentration increases, making it difficult to detect changes in the current at very high substrate concentrations.

8.5.2.2 Overview of data obtained from modeling procedures:

Table 8.4 displays the immobilized enzyme kinetic parameters for the various surfaces investigated in the course of this study.

Table 8.4: Operational kinetics parameters determined for immobilized laccase films with regard to the detection of HQ

Surface	Detection sensitivity ($nA.\mu M^{-1}.cm^{-2}$)	i_{max} ($nA.cm^{-2}$)	K_m (μM)	Degree of sigmoidality (b)
Au	3.94 ± 0.53	429 ± 86	132 ± 19	1.00 ± 0.07
SAM 1	2.59 ± 0.29	544 ± 44	224 ± 29	0.92 ± 0.05
SAM 1.1	4.77 ± 0.86	1009 ± 57	205 ± 24	0.90 ± 0.01
SAM 1.2	8.42 ± 0.49	808 ± 85	95 ± 18	1.02 ± 0.09
SAM 1.3	11.8 + 0.75	1404 ± 105	101 ± 3	0.90 ± 0.01
SAM 2.1	2.32 ± 0.17	404 ± 28	196 ± 8	0.97 ± 0.03
SAM 2.2	4.52 ± 0.40	495 ± 57	127 ± 21	0.95 ± 0.03
SAM 2.3	5.30 ± 0.29	677 ± 41	112 ± 14	0.9 ± 0.00

The findings reported in Table 8.4 above indicate that both i_{max} and HQ detection sensitivity were highest for SAM 1 films, relative to any other surface. The increase in cysteamine SAM residues between SAM 2.1 and SAM 1.1 decreased the i_{max} and sensitivities, considerably, while not affecting the K_m to a statistically significant amount, in agreement with the intuition of results obtained from rheological monitoring of the films via QCM-D (Section 8.5.1.3) in which increases in shear and viscosity were attributed to increased levels of denaturation undergone by attaching proteins during immobilization.

While the addition of linkers in both SAMs 1 and SAMs 2 increased both i_{max} and sensitivity and lowered K_m, relative to SAMs 1.1 and SAMs 2.1, respectively, this increase is less for SAM 2 films (i.e. SAM 1.1 – 1.3) than for films amended from SAM 1.1. The sole exception to this trend occurred for the i_{max} values of SAM 1.2. However, this decrease in the i_{max} value for SAM 1.2 (relative to SAM 1.1), does not affect the increase in sensitivity noted between these two surfaces (an increase from 4.8 to 8.4 $nA.\mu M^{-1}.cm^{-2}$). This, in turn, is attributed to the decrease in the apparent K_m values (Table 8.4) of SAM 1.2 surfaces, relative to SAM 1.1 This is in concordance with previous findings reported in Chapters 4 and 5 of this Thesis. To this purpose, Figure 8.5 compares the logarithms of detection sensitivity to that of i/K (i_{max}/K_m) values, as was reported for other biosensor configurations in Chapters 4 and 5 of this Thesis.

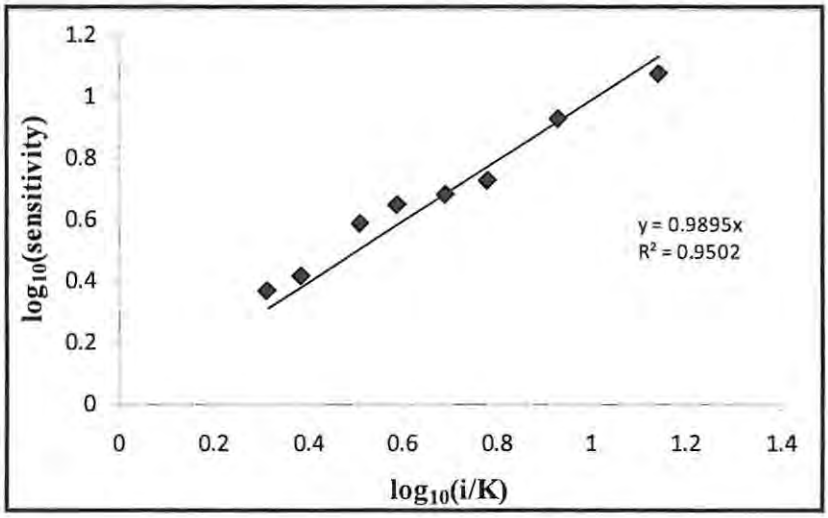

Figure 8.5: Logarithm of hydroquinone detection sensitivity compared to the modeled i/K values for the surfaces examined in this study.

Figure 8.5 indicates that the correlation existing between the detection sensitivities and the i/K values extend the argument put forward earlier in this Thesis that influences of the biosensors' operation represented by i_{max} and K_m parameters themselves influence the detection sensitivity.

A comparison between Tables 8.4 and 8.2 serves to indicate that biosensor performance (i_{max} and biosensor sensitivity) is enhanced with those surfaces that exhibit decreased shear/viscosity (e.g. SAMs 1.1 – 1.3), and that increasing rigidity tends to decrease biosensor performance, independently of bound mass. K_m however

appears to decrease to approximately the same extent with an increase in linker length, regardless of the degree of rigidity/shear/viscosity evaluated from the films. Previous studies performed by Lowe (1977) show that, when using linkers of increasing length to covalently attach an enzyme to the support, there is a concomitant decrease in the K_m accompanied by an increase in the specific activity of the enzyme (Lowe, (1977). The aforementioned study linked these effects to both the increasing distance between enzyme and support (decreasing surface-enzyme bonding interactions which result in deformation of the enzyme structure) and increasing penetration of the enzyme into the diffusion layer (decreasing the diffusional distance undergone by substrate molecules) (Lowe, 1977), both of which are anticipated to occur with the inclusion of linkers. The decrease in K_m and increase in activity expected in the literature are supported by the findings of this study as in Table 8.4.

8.5.3 Integration of QCM-D data analysis with electrochemical kinetic parameters:

Of great interest to this research was examining whether the rheological data provided through the QCM-D data (Section 8.5.1) could be reconciled with the kinetic parameters elucidated through electroanalysis of the fabricated biosensors (Section 8.5.2). Due to the differences inherent in both the immobilisation method (with SAM 1 and Au electrodes making use of physical adsorption as the attachment parameter) and the film properties, trends in this section were only tracked between 3 categories: (1) differences between physically adsorbed and covalently-attached protein films (2) between SAM surface of with differing linker lengths i.e. SAMs 1.1 – 1.3 and SAMs 2.1 – 2.3, respectively and (3) differences occurring between SAM 1 surfaces and SAM 2 surfaces.

Of the two rheological parameters (shear and viscosity) extracted from QCM-D measurement, viscosity was selected for the comparison between physical film parameters and immobilized enzyme kinetics. The reasons for this selection are two-fold: firstly, increases in solution viscosity have been linked to the denaturation of dissolved proteins in previous research (Tanford et al., 1955; McKenzie et al., 1963; Tamia et al., 1985) for cited reasons of protein aggregation (McKenzie et al., 1963; Tamia et al., 198) and conformational changes

between the native and denatured state (Tanford et al., 1955; Tamia et al., 1985). Secondly, literature has cited concerns regarding the accurate determination of shear modulus through the Voigt-model (Johannsmann, 2008), namely that viscosity measurements, while typically deviations of viscosity are ± 10% between crystals, the estimation of shear modulus has a much larger frequency-dependence than viscosity when the crystals are immersed in liquids, such as was performed for this research. Shear modulus values are therefore used as general indicators of film rigidity, rather than absolute numerical values henceforth.

Figure 8.6 depicts relational values of three separate parameters of the protein films: the K_m, film viscosity and the average film viscosity per unit mass (as reported in Table 8.3) values.

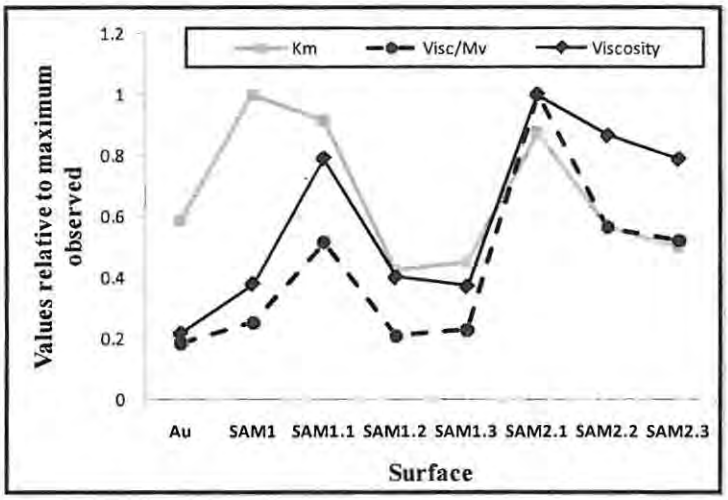

Figure 8.6: Relative values of the immobilized film parameters Viscosity, Viscosity / Voigt Mass (Visc/Mv) and average K_m

Data plotted in black indicates values drawn from QCM-D analysis of immobilized enzyme films. Data plotted in grey indicates values drawn from kinetic estimation of immobilized films catalytic oxidation of HQ

While similar trends in values are noted between the film viscosity and the K_m value extracted from kinetic estimations of the immobilized film for the surfaces studies, a better trend is noted when comparing the average film viscosity per unit mass bound ($Visc/M_V$) with the K_m. If one interprets viscosity as consisting of contributions arising from both the method of attachment and the extent of protein unfolding following

immobilization, then the relationship between the viscosity (normalized relative to the bound mass) will provide an indication of the degree of denaturation undergone by attaching proteins, when categorised by the different surface types (i.e. adsorbed vs. covalent attachment, SAM type 1 vs. SAM type 2). The degree of denaturation undergone would also be represented as differences between K_m. Figure 8.7 displays a comparison of the K_m values to the [mass-normalised] viscosity values obtained during QCM-D analysis for these three categories.

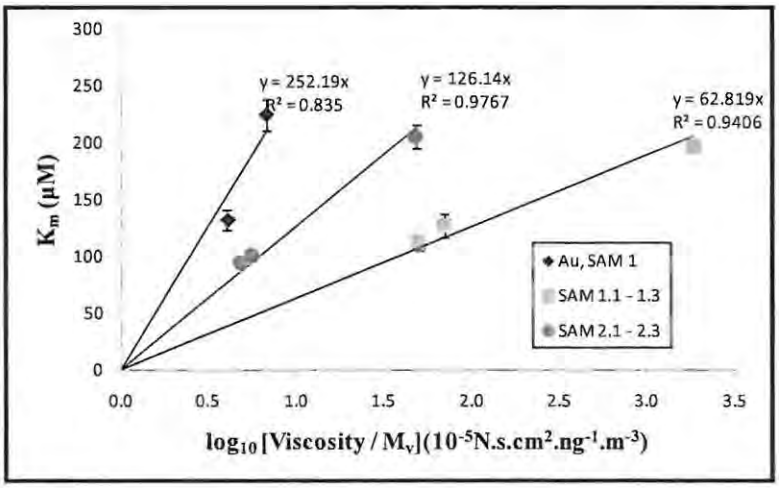

Figure 8.7: Comparison between the K_m values (extracted from immobilized enzyme kinetics) determination to the logarithm of the average viscosity per unit mass of surfaces (extracted from QCM-D studies)

Y-intercepts forced through the origin for linear regression of the data

Figure 8.7 displays that strong linear behaviour is noted between the surface types when comparing the K_m to the mass-normalised film viscosities. Linear correlations for 4-point fits for enzyme films immobilised SAM types 1 and 2 have R^2 values > 0.94, and the 3-point correlation for the physically-adsorbed enzyme films have R^2 > 0.8. The findings of Figures 8.6 and 8.7 indicate that decreases in film viscosity observed through the use of linkers (Table 8.2 and 8.3) are linked to the decreases of K_m values observed at the same SAM amendments (Table 8.4), although the trends observed are restricted between the basal surfaces used for further modification prior to protein immobilization. Due to the increase in viscosity brought about through the method of immobilization used (Table 8.2)and the different surfaces (e.g. SAM 1.1 vs. SAM 2.1,

Table 8.2), these trends are restricted to the various surface classes used, rather than being a global trend, but a satisfactory trend between these classes indicates similar principles governing the correlation between viscosity and K_m. This strongly indicates that the anticipated decrease in enzyme denaturation due to linker inclusion is represented, in part, by the decreases in film rigidity/viscosity noted for during rheological comparison of the films immobilized onto the different surfaces.

While the Sauerbrey Mass (M_S) contains a contribution from trapped/coupled water within the protein film, the Voigt Mass (M_V) is considered to be a more accurate estimation as it corrects for the viscoelasticity of the film. Increasing film softness results in an underestimation of M_S; in addition to which is acknowledged that the M_S imperfectly accounts for film swelling in the solvent (Johannsmann, 2008). Thus, to a very limited extent, the ratio of M_V compared to M_S provides some index of the relative softness and degree of film swelling exhibited by the immobilized enzyme films. Since both of these factors have contributions arising from protein-solvent interaction, M_V/M_S could therefore be taken as a crude estimation of the ratio of viscoelastic mass compared to the rigid mass. In this instance, this can be interpreted as the relative degree of solvation of the immobilized proteins, at least, when considering surfaces differing by the number of linkers connecting proteins to the gold electrode. Similar data treatments for estimating the level of film hydration via the differences occuring between M_V and M_S have been advanced in the literature (Paul et al., 2008).

When comparing the ratio of (M_V/M_S) to the i/K values for immobilized laccase films, two opposing trends are evident – an inverse trend between (M_V/M_S) and HQ detection sensitivity for immobilized films exhibiting low shear modulus (i.e. low rigidity) properties and a positive trend for those possessing higher shear values, as determined by modeling of QCM-D results. Figure 8.8 depicts the relational trends occurring between film shear (normalized to mass gain, as was performed for viscosity in this section), the (M_V/M_S) ratio and the detection sensitivities for the surfaces examined.

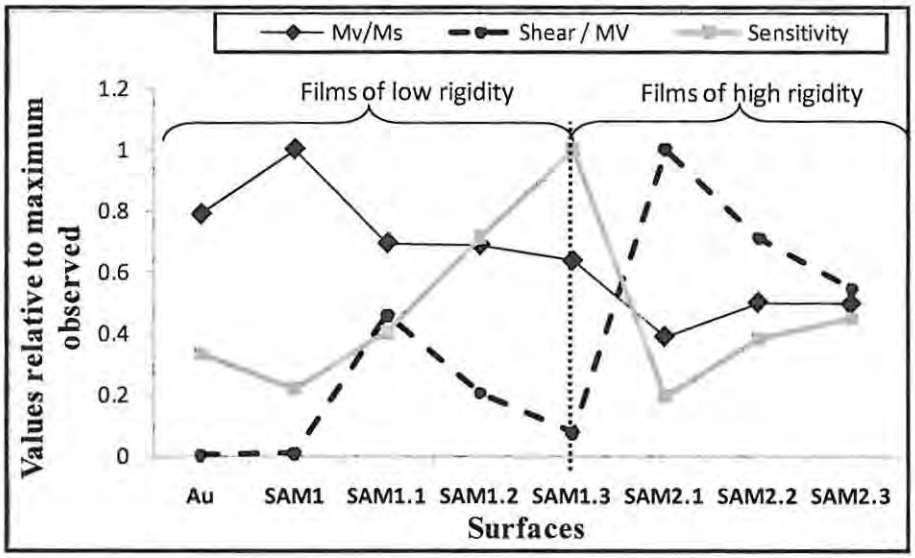

Figure 8.8: Relative values of the immobilized film parameters shear modulus as a function of bound mass (Shear / MV), ratio of Voigt mass to Sauebrey Mass (Mv/Ms) and average detection sensitivities of the films with regard to HQ detection (Sensitivity).

Data plotted in black indicates values drawn from QCM-D analysis of immobilized enzyme films. Data plotted in grey indicates values drawn from kinetic estimation of immobilized films catalytic oxidation of HQ

Figure 8.9**A** displays comparisons between i/K values and the ratio of M_V/M_S (here putatively termed "relative film hydration") obtained for the surfaces studies, while Figure 8.9**B** displays the reciprocal of i/K $(i/K)^{-1}$ against the reciprocal of M_V/M_S i.e. the relative protein levels present in films.

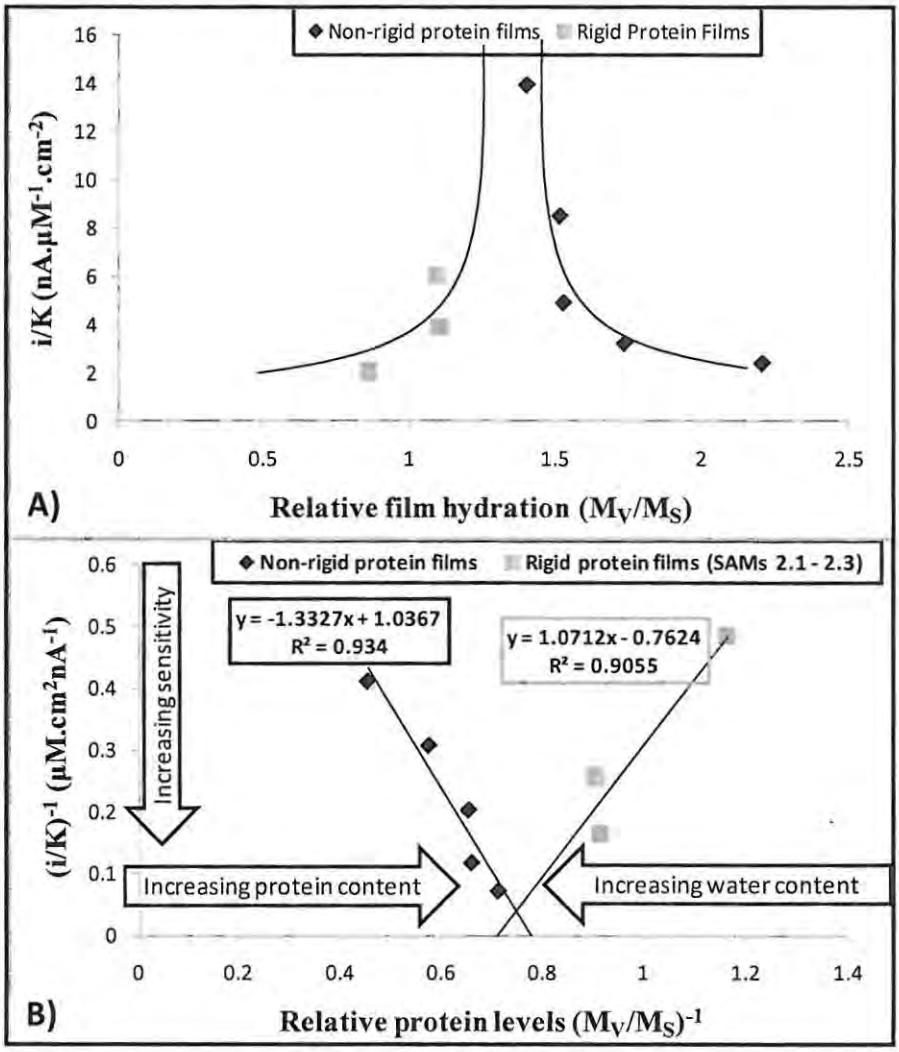

Figure 8.9: Comparisons between i/K and relative film hydration values (M_v/M_s) obtained for the studied surfaces

A) i/K vs. (M_V/M_S)

Lines drawn here are intended to show the asymptotic behaviour of the two separate film structures (rigid and non-rigid protein layers) to guide the user

B) Reciprocal of (i/K) plotted against the reciprocal of (M_V/M_S)

Arrows depict trends in values discussed further on in-text.

Due to the exponential dependence of i/K against the relative hydration levels (Figure 8.9**A**), the reciprocal of both values were plotted against each other in order to linearise the noted dependences (Figure 8.9**B**).

Strongly linear, but opposing trends were noted when comparing the reciprocal of the i/K value to the relative protein content of the film (Figure 8.9**B**). These two separate trends result from the two separate behaviours noted in Figure 8.9**B**. Firstly, a decrease in relative hydration levels within non-rigidly attached films (i.e. an increase in relative protein mass of highly-solvated films) increases the detection sensitivity, most likely through the inclusion of more catalytic protein within the film. This correlation occurs for both laccases attached to the electrode surfaces via physical adsorption, and for SAMs 1.1 – 1.3. However, in the case of rigidly-attached (i.e. distorted/partially denatured) protein films, an increase in relative hydration levels also increases the i/K values, through a decrease in the degree of denaturation undergone by catalytic proteins during the attachment process.

8.6 Conclusions:

It must be noted at this juncture that the scope of this research was not to design a satisfactory biosensor for its functionality – this form of biosensor is primarily fabricated in order to contrast the operating parameters of the functional biosensor with the salient rheological parameters and the other film properties determined from the QCM-D. Hence, the use of this laccase in this instance fulfills the function of a "model" protein-film system.

QCM-D technology, coupled with rheological modeling of the results, showed consistent alterations in the physical properties of attached laccase films occuring between the surfaces examined in this study. Film rigidity (V.I.), bound mass, viscosity and shear modulus values increased when protein was attached to the surface via glutaraldehyde-cysteamine covalent bonds (SAM 1.1), compared to laccase attached by physical adsorption (SAM 1 and Au). Rigidity, viscosity and shear modulus values further increased when the density of cysteamine in the SAM surface was increased (SAM 2.1). Differences between SAM 2.1 and SAM 1.1

surfaces show that the presence of further reactive binding sites on the SAM surface as for SAM 2 do not, by themselves, increase the amount of mass gained at the electrode, but greatly influence the rigidity of the attached protein film (due to the number of increased bonds occurring between the attaching proteins and the electrode surface). The addition of lysine linkers between the piezoelectric sensor and the protein film was shown to decrease the rigidity of the attached protein film and increase the mass gain at the electrode surface above that found at electrodes without lysine. This is more evident in the rheological parameters once they are related to the mass gain at the electrode surface, which show a consistent decrease in the modeled viscosity and shear moduli with increasing lysine-glutaraldehyde linkers for SAMs containing low surface density of cysteamine (SAM 1.1 - 1.3) and for those containing higher surface densities of cysteamine (SAM 2.1 – 2.3). This evidence strongly suggests that the extent of distortion undergone by the proteins during attachment to the surface decreases as a function of linker addition. When combined with the concomitant decrease in film rigidity that was observed with the addition of lysine the increase in bound mass with increasing linker length indicated in this instance, that the increase is caused by the desirable addition of both additional protein and film-associated water.

It was of great interest to examine whether differences in the physical parameters of the film were indicative of alterations in the kinetic functioning of the laccase molecules when attached (in the manners outlined above) to an electrochemical transducer in a biosensor-like configuration.

Analysis of the biochemical kinetics of laccase attached to the various surfaces investigated indicated that, for both SAM 1-type and SAM 2-type surfaces, an increase in linker length lead to a significant decrease in the apparent K_m values of the enzyme film, accompanied by a significant increase of the detection sensitivity for the detection of HQ substrate. Additionally, a general increase in i_{max} was noted with an increase in linker length (SAMs 2.1 - 2.3, SAM 1.3 compared to SAM 1.1) and the concomitant decrease in rigidity, viscosity and shear that was associated with the inclusion of further water into the film. i_{max} values and detection sensitivities were found to increase with a decrease in the lateral density of linkers (SAMs 1 compared to SAMs 2). Biosensor sensitivities increase significantly with the addition of linkers for all surfaces

investigated, most likely due to the significant decreases in K_m values noted with increasing spacer-arm length. Derivatives of SAM 2 surfaces shows overall decreased sensitivities compared to SAM 1 surfaces, probably due to the aforementioned multiple attachments occurring between surface and enzymes. Indeed, HQ detection sensitivity for laccases immobilized onto SAM 1.3 surfaces is nearly 6 times that of SAM 2.1 and more than three times that of the physically-adsorped surfaces (Au and SAM 1).

Analyses of the combined data extracted from QCM-D and the immobilized enzyme kinetics indicate considerations of bound protein mass alone are insufficient to predict the final parameters of the bound macromolecules and that inclusion of the rheological parameters obtained from QCM-D are necessary in order to correlate the enzyme kinetics of laccase films with the physical film parameters. Trends observed between QCM-D and immobilized enzyme kinetic studies indicate that biosensor performance (i_{max} and biosensor sensitivity) is enhanced with those surfaces that exhibit decreased shear/viscosity (e.g. SAMs 1.1 – 1.3), and that increasing rigidity tends to decrease biosensor performance, independently of bound Voigt mass.

Protein film viscosity was found to influence the K_m of the resultant laccase-bound surfaces. When viscosity (in the form of the average viscosity per unit bound mass) was related to the K_m, a positive correlation was observed between the K_m and mass-normalised viscosity was found to occur, although this trend was restricted between surface types and the method of protein attachment used. Nevertheless, this is an indication that film viscosity, when assessed carefully, can predict the level of denaturation undergone by the proteins during the attachment phase. The degree of protein hydration (indicated by the ratio of Voigt-modelled mass to Sauerbrey mass) was found to correlate to the detection sensitivity. For non-rigid protein films, a decrease in this value (i.e. an increase in film protein content) trended with an increase in detection sensitivity, while an increase in the hydration level at very rigid protein films (SAMs 2.1 – 2.3) resulted in an increase in detection sensitivity. The addition of rheological parameters appears to better nuance the differences arising in bound enzyme kinetics due to the differences between immobilization strategies and allow for more in-depth comparisons that determinations of the bound mass alone cannot show.

While other studies have also linked the film structure of a monolayer of immobilized protein to its function, QCM-D offers the opportunity to assess the physical characteristics of that film in a more direct fashion than some of the other methods (AFM, STM, Raman-UV-Vis-Spec, etc). Integrating both the inferred rheological properties of the film derived from QCM-D and comparing them with those determined by electrochemical monitoring of the immobilized laccase monolayer is a potentially viable tool in biosensor design.

From these findings, it can be concluded that monitoring of the film formation using QCM-D, both assessing the mass bound and the relevant rheological properties, can be used in predicting the extent of denaturation undergone by catalytic proteins during immobilisation. When constructing and optimising thin-film biosensors, the QCM-D may prove to be a valuable apparatus for monitoring fundamental film parameters that will impact on the operational properties of the said biosensor/s.

Chapter 8: Monitoring fundamental film characteristics of immobilized laccase monolayers

Chapter 9: Overall Conclusions

This Thesis describes the fabrication of a laccase-based biosensor which possesses a high degree of substrate-detection sensitivity and fabrication consistency towards the monitoring of phenolic compounds. The laccase was sourced from a commercial supplier and used without purification, which demonstrated the wide applicability and ease-of-fabrication of the type of biosensor outlined in this Thesis. The biosensor fabricated was used in the detection of a variety of substrates, and the prediction of substrate-dependent detection sensitivity performed using a combined, novel, parameter that integrated both biochemical and electrochemical measurements of substrate-dependant characteristics. Selective, simultaneous determination of a mixed sample of phenolic substrates was demonstrated in principle, through the use of a second transducer surface type. Finally, alterations to enzyme monolayers (glucose oxidase and laccase enzymes) during immobilisation processes were monitored using QCM-D technology and related to the apparent kinetics of the immobilised proteins.

Regarding the knowledge gaps laccase biosensor technology identified in Chapter 1 (Section 1.3), the following research outcomes are summarised:

9.1 Sensor reproducibility:

The selection of an appropriate cleaning strategy for glassy carbon electrodes (GCEs) was performed. Anodic pretreatment of the electrode as a cleaning strategy resulted in electrode surfaces showing high degrees of electrode-response reproducibility, using both Faradaic and non-Faradaic current measurements as a means of establishing reproducibility. The high degree of non-Faradaic reproducibility indicated a consistent chemical composition of the surface, and the technique used in monitoring was validated using an established method of determining electrode surface capacitance, both in an analytical matrix previously described in literature and the electrolyte system used throughout the research reported on in this Thesis. This method of electrode pretreatment was used throughout the

research reported in this Thesis, when GCEs were used as the transducer surface type. Details of this are available in Chapter 3 of this Thesis.

Laccase activity assays indicated a non-linear dependence on spectrophotometrically-determined activity with the concentration of suspended laccase (Chapter 3). This dependence was not considered to be due to the experimental conditions under which assaying took place; rather, it is an inherent property of highly-concentrated solutions of laccase and is not considered to be of consequence in immobilised laccases. Subsequent to these findings, laccase solutions used for enzyme immobilisation were assayed at low concentrations of enzyme in order to more accurately determine the specific activity.

The inclusion of Bovine Serum Albumin (BSA) into cross-linked films of laccase (Chapter 4) produced biosensors with very consistent current-concentration responses, between sensors. This was concluded to arise from the consistent protein addition to the electrode surface during immobilisation, which adjusted for differences in specific activity of laccases sourced in different batches from the supplier.

9.2 Detection sensitivity:

(a) A variety of different immobilisation strategies were performed and the strategy producing the best measured biosensor response (cross-linking of laccase) was selected for further optimisation (Chapter 4). The inclusion of BSA during immobilisation resulted in the significant enhancement of biosensor operational parameters and resulted in the fabrication of a sensor that produced comparable detection sensitivities to those already reported on in the literature. The alterations to sensor responses upon altering the amounts of laccase or BSA during immobilisation were detailed and discussed in Chapter 4. The role of BSA on the sigmoidality of current-concentration responses was investigated and sigmoidality was assigned to be a by-product caused by the presence of BSA and its inherent ability to bind to substrate oxidation products. Re-use of the cross-linked laccase biosensors, when considering catechol as a substrate, resulted in a significant increase in biosensor operational parameters, which was concluded to arise from both the cessation of BSA binding oxidation products and the tendency of products to attach to the electrode surface, enhancing subsequent biosensor response by increasing the maximal laccase-generated current, i_{max}. The attachment of oxidation products to the electrode surface

was found to be restricted to the GCE surfaces studied and does not occur with gold electrode surfaces, which themselves do not evidence any significant increases in i_{max}.

The effect of the selection of enzyme immobilisation strategy at a monolayer level is described in Chapters 7 and 8 of this Thesis. Chapter 7 demonstrates proof-of-principle for the use of QCM-D in monitoring the formation of immobilised monolayers (both of TCACoPC and Glucose Oxidase) onto gold electrode surfaces, demonstrating that QCM-D measurements can be used to assess these formations under real-time conditions for the purposes of biosensor fabrication studies. In Chapter 8, the measurement of fundamental physical film parameters was undertaken, using a variety of surfaces that differed by their means of attaching laccase monolayers. This was performed in order to determine the extent to which enzyme-support interactions dictate the enzyme kinetic parameters of the immobilised enzymes. The findings from Chapter 8 demonstrated that measurement of the rheological parameters of the film can be used in predicting the physical-kinetic relationship for immobilised enzyme thin-films. In particular, the measurement of film viscosity was linked to the resultant changes in K_m, indicating that the extent of protein denaturation may be assessed through this means. The measured indicator of relative film hydration also showed correlation with the hydroquinone-detection sensitivity of the films immobilised on these surfaces. From the findings in Chapter 8, it can be concluded that monitoring of the film formation using QCM-D, both assessing the mass bound and the relevant rheological properties, can be used in predicting the extent of denaturation undergone by catalytic proteins during immobilisation.

9.3 Inter-substrate selectivity

Chapter 5 demonstrated that substrate-dependent detection sensitivity of the optimised biosensor configuration (Chapter 4) is affected by both electrochemical and biochemical considerations of the substrate. Selected substrates were assessed both electrochemically, at unmodified GCEs and biochemically, using the aforementioned biosensor and assigned categories of reversibility on the basis of the findings of their respective electrochemical characterisation. Readily-reversible substrates exhibited the highest detection sensitivities, quasi-reversible the next-highest, and irreversible substrates exhibited the lowest substrate-dependent detection sensitivities. This was considered to be due to a combination of both biokinetic and electrochemical originating factors. A novel parameter that takes

both of these factors into account (%I/K_m) was found to correlate to the detection sensitivity, and provided more information than the conventional electrochemical method of determining substrate oxidation rates (substrate-dependent oxidation potential). Studies conducted primarily using reversible substrates under conditions of varying electrolyte pH confirmed the previous statement.

Chapter 6 offers proof-of-principle that MPCA can be successfully deployed to produce substrate-specific, representative and separate biosensor response currents that arise from the laccase-based oxidation of several phenolic species present in the same analytical sample.

9.4 Fouling:

Chapter 4 demonstrated that the attachment of oxidation products to the electrode does not necessarily lead to attenuation of biosensor current, but could conceivably be used to enhance biosensor response. Chapter 5 further demonstrated this, when considering the detection of those substrates designated as reversible. For all other substrates investigated during the course of this research, an attenuation in biosensor response was noted upon re-use and the tendency of a given substrate to passivate the electrode surface correlated with the occurrence of fouling, as assessed at bare GCEs.

9.5 Future recommendations:

The following research questions raised in the course of investigation are considered pertinent to better understanding and exploiting the mechanisms by which laccase-based biosensors operate. These are presented in order of the Chapter under which the original research is reported:

From Chapter 3: The assessment as to whether the surface area estimations outlined in this Chapter can be used in assessing further surface amendments that are outlined here. A salient example lies in the conjugation of nanoparticles to the electrodes surface: for a similar purpose behind the inclusion of TCACoPc in Chapter 7, nanoparticles are currently being widely-investigated for inclusion within current biosensor technology and the formation of nanocomposite sensors. A rapid means of establishing whether a surface is sufficiently modified would be of benefit in this technology.

From Chapter 4: Further optimisation of the immobilisation strategy is recommended. In particular, a method whereby sensor re-use response (which showed significantly enhancements in the biosensor operational parameters) can be consistently and routinely applied to biosensors prior to detection would be of great benefit in enhancing the detection sensitivity of fabricated biosensors. In particular, the link between the attachment of oxidation products of reversible substrates to the electrode surface bears further investigation and a more complete understanding of the mechanism governing sensor increase should be investigated in order to better exploit this phenomenon to enhance both sensor response and the degree of inter-analysis response reproducibility.

Chapter 5: Testing of the correlation of ($\%I/K_m$) value with detection sensitivity should be conducted with a greater number of substrates than were investigated during the course of this research. While effort was made to include substrates on the basis of widely-different electrochemical and chemical characteristics, the determined correlation should be broadened in order to demonstrate its applicability in predicting sensor response to a given substrate. To this recommendation is added the inclusion further substrates in pH studies, for similar reasons. The interesting comparisons between the quasi-reversible (GOL) and the irreversible (GA) substrates selected for comparison indicate that there exists further scope for investigation of the interrelatedness of electrochemical and biochemical interactions.

Chapter 6: While Chapter 6 provided convincing evidence that simultaneous signal detection arising from the presence of multiple substrates can be provided through the use of MPCA, the applicability of this waveform will be hampered by the relative proximity of the reducing potentials, and the corresponding sacrifice in sensitivity that occurs at the behest of selectivity. The example of HQ in this Chapter suffices to demonstrate this. A broader study that includes further substrates is recommended in order to critically assess the resolving power of this waveform, as well as to improve upon work presented in this Thesis.

Chapter 8: The measurement of viscoelastic QCM-D is somewhat hampered by the non-trivial concerns of the modelling process – as four separate parameters are modelled simultaneously from the raw data, some parameters (notably shear) provide less accurate and consistent results between measurements, while it is noted that film thickness measurements and viscosity are more consistent and accurate. The use of another analytical method to assess the physical structure of attached films in order to produce a more nuanced understanding of the film structure is recommended.

Appendix 1: Data Treatments of biosensor responses and general modelling considerations

A1.1 Overview

The first section of this appendix (A1.2) demonstrates how the sensor response to substrate concentration curves (current-concentration functions) was calculated. These values were used as the primary basis of assessing biosensor performance, through the calculation of current response to increases in substrate concentration. The final sections provide a brief explanatory overview on how the Solver add-in was executed in order to obtain the kinetic parameters presented henceforth (A1.3), as well as contrasting the two major parameters used in minima-seeking (Sum of Squared Differences vs. Chi-Squared Statistic), and providing background as to their respective strengths and weaknesses as indications of compliance between the modelled parameters and the experimental functions (A1.4).

A1.2 Biosensor response: data treatment and modelling.

A1.2.1 Current-responses analysis for chronoamperometry of electrochemical biosensors

At portions of a steady-state (i.e. linear) current-time response caused by the addition of substrate to the electrochemical cells, the resultant change in current is measured as ΔI. Figure A1.1 displays a section of a typical substrate-dependant chronoamperometric response by a laccase modified electrode.

Appendix 1: Data treatments and general modelling considerations

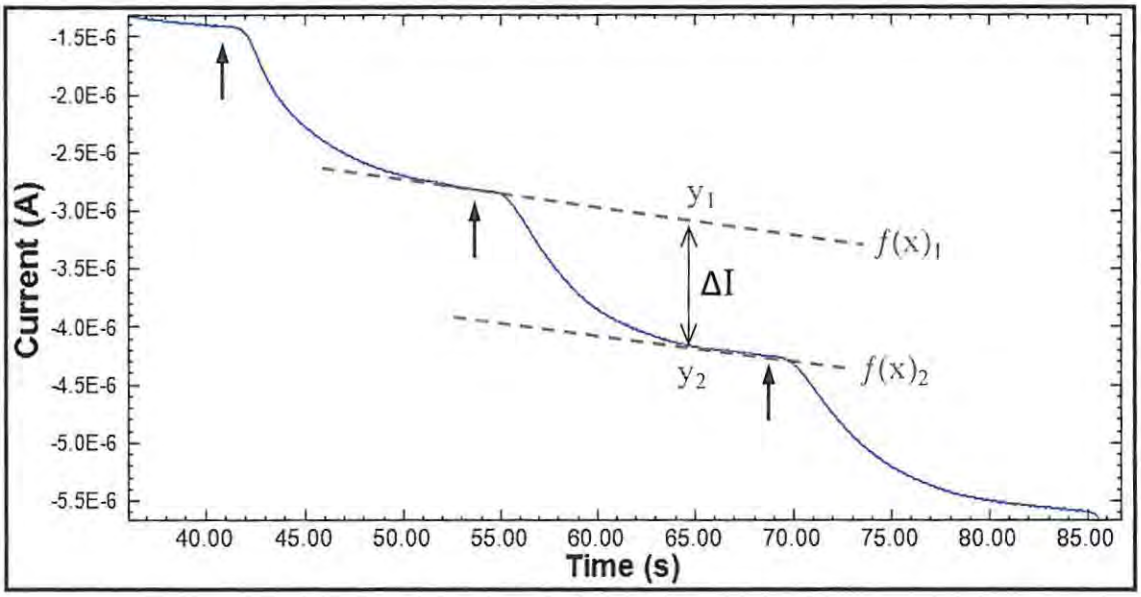

Figure A1.1: Typical biosensor response as assessed by chronoamperometry.

Arrows indicate times at which aliquots of substrate (catechol) were added. The electrode was poised at -0.17 V vs. Ag/AgCl and the solution was stirred throughout the experiment. Dashed lines indicate linear regressions used to determine ΔI i.e. $f(x)_1$ and $f(x)_2$. 800U/ml, GCE 2 (cond.) (2)

By extracting the linear-regressional parameters from the steady-state response at each substrate addition, the change of current caused by increase in substrate concentration was calculated as in Eq. A1.1:

$$y_a - y_{a-1} = x(m_a - m_{a-1}) + (c_a - c_{a-1}) = \Delta I_a \qquad \text{Eq. A1.1}$$

And the total current at a given substrate (I_{tot}) concentration calculated as:

$$I_{tot} = \sum_{i=0}^{n} (\Delta I_i) \qquad \text{Eq. A1.2}$$

A1.3. Options settings of the Excel Solver add-in for meta-modelling parameters

For all the analyses henceforth reported on in this Thesis, the following modelling parameters were used in minima-seeking of the parameter dictating the goodness-of-fit (see proceeding section):

- The Maximum number of successive iterations for modelling was set to at least 1000 iterations / analysis, and modelling was repeated if an unsatisfactory correlation between experimental data and modelled data was seen to take place.
- Precision of modelled parameters was set to 10^{-4} (i.e. 0.0001).
- Tolerance was set to 0.5%
- Convergence was assumed to have occurred if a maximum difference in the modelled goodness-of-fit parameter was less than 10^{-4} of the absolute value of that procedure.
- Automatic Scaling was activated.
- Estimate method was set at "Quadratic"
- Derivatives were "Central"
- The search algorithm was "Conjugate"

The various meaning of the individual parameters adjusted above have been previously discussed by Walsh and Diamond (1994). For the purposes of visual summary, Figure A1.2 is a screenshot depicting the format in which these options were set within the Options menu in the Solver add-in.

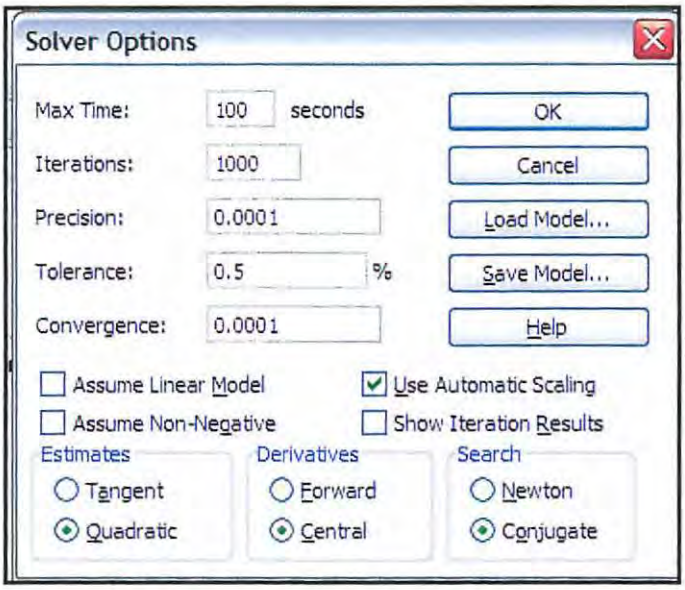

Figure A1.2: Options selected for modelling meta-parameters for the Solver add-in. Microsoft Excel version: 2007.

Figure A1.3, below, shows the relevant sections of data modelling using the Solver Add-in, in this instance, that of biosensor response modelling (Section 1 of this Chapter). The differences between the different goodness-of-fit parameters are outlined in the proceeding Section of this Chapter.

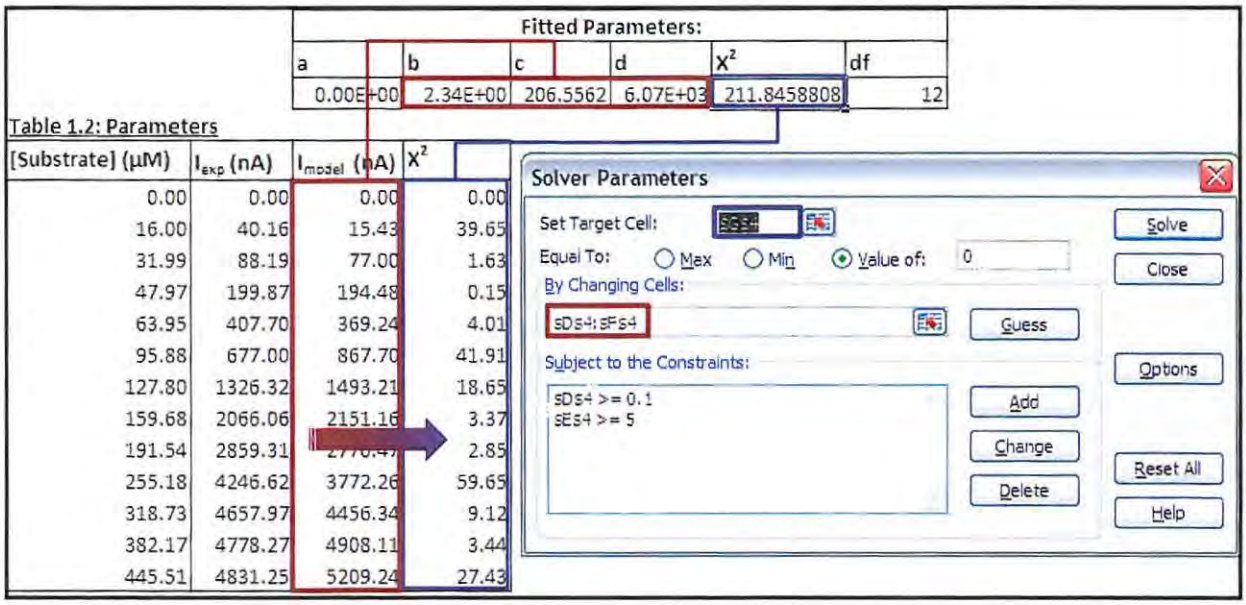

Fitted Parameters:					
a	b	c	d	X^2	df
0.00E+00	2.34E+00	206.5562	6.07E+03	211.8458808	12

Table 1.2: Parameters

[Substrate] (μM)	I_{exp} (nA)	I_{model} (nA)	X^2
0.00	0.00	0.00	0.00
16.00	40.16	15.43	39.65
31.99	88.19	77.00	1.63
47.97	199.87	194.48	0.15
63.95	407.70	369.24	4.01
95.88	677.00	867.70	41.91
127.80	1326.32	1493.21	18.65
159.68	2066.06	2151.16	3.37
191.54	2859.31	[illegible]	2.85
255.18	4246.62	3772.26	59.65
318.73	4657.97	4456.34	9.12
382.17	4778.27	4908.11	3.44
445.51	4831.25	5209.24	27.43

Figure A1.3: Screenshot of Solver functions and fitted parameters.

The χ^2 statistic ("X^2", outlined in purple) is used as a measure of goodness-of-fit (see below section) and is the sum of the χ^2 values in Table 1.2. Alterations of the Fitted Parameters (red boxes) alter the modelled current responses I_{model} in Table 1.2, which in turn alters the calculated individual χ^2 values, altering the resultant χ^2 statistic. Re-iterative altering of fitted parameters drives the χ^2 statistic to a minimum to equate model-to-experimental convergence.

A1.4 Modelling "Goodness-of-fit":

For all electrochemical/enzyme kinetics modelling procedures that were undertaken, goodness-of-fit indicators, either the Sum of Squared Differences (SSD) or χ^2 statistic were required. Briefly, for each individual data-point, the difference between the experimental data and the data as predicted by the modelled parameters was measured by a goodness-of-fit indicator in order to measure the modelled parameter's accuracy of determination. The intersection of parameter values where goodness-of-fit criteria underwent their minima were considered to be accurately estimated values.

In presenting modelled kinetics data in this Thesis, goodness-of-fit is sometimes presented as sample variance (SSD in this thesis, more commonly referred to as s^2), calculated as in Eq. A1.3, adapted from Rosner, 2000.

$$s^2 = \frac{1}{n-1} \sum_{i=1}^{n} (x_{i,exp} - x_{i,model})^2 \qquad \text{Eq. A1.3}$$

Where n is the number of observations (experimental determinations in each model), n-1 is the degree of freedom, $x_{i,exp}$ is the experimentally-determined value at independent value = i and $x_{i,model}$ is the modelled data value (Rosner, 2000).

This method has the advantage of providing unbiased data-comparison regardless of the number of samples used in attaining the standard deviation and allowing for comparison to occur between analyses of differing sample numbers (Rosner, 2000). This was used to obtain comparisons between different sensor configurations in which varying concentration aliquots of substrate were required to reach near-saturation conditions for the attached biorecognition layer(s).

For certain applications, goodness-of-fit was also calculated through the use of the Chi-squared statistic (χ^2). χ^2 was determined as in Eq. A1.4, adapted from Rosner, 2000:

$$\chi^2 = \sum_{i=1}^{n} \frac{(x_{i,exp} - x_{i,model})^2}{x_{i,model}} \qquad \text{Eq. A1.4}$$

The above symbols have the same meaning as found in Eq. A1.3. The use of this comparative method has the advantage of including $x_{i,model}$ as a divisor. This allows equal weighting of determined χ^2 values to be made throughout the possible range of x_i values i.e. if at datapoint = i, $x_{i,model}$ is small, the squared difference between $x_{i,model}$ and $x_{i,exp}$ should be equally small – if not, this deviation will be represented in an unweighted format regardless of the actual value of $x_{i,exp}$ (Rosner, 2000). This was of especial importance in the determination of noise effects and was the main method of determining linear regressional information in chronoamperometry, from which sensor responses are calculated.

Appendix 1: Data treatments and general modelling considerations

Appendix 2: Chronoamperometric determination of double-layer capacitance – computer-driven modelling and effects

A2.1 Validation of modelling systems for short-interval, non-Faradaic chronamperometry

In order to validate the modelling methodology, current samples were varied from between 0.2 and 1.0 ms and the modelling system described in Eq. 4.13 were applied. In two separate modelling experiments, R_S was set at 100 Ω and C_{DL} was varied in order to minimise the χ^2 statistic for the ln values of the modelled and experimental currents (Model I), while the second experiment varied both R_S and C_{DL} (Model II)

In order to minimise modelling, χ^2 was performed on the logarithmic modelled current vs. the logarithm of the experimental data, linearising both datasets and offsetting model-fitting prejudice that arises as the current exponentially fell (Figure A2.1). By modelling prejudice, we mean to say that model-fitting is predisposed towards fitting the larger current values preferentially to the lower current values.

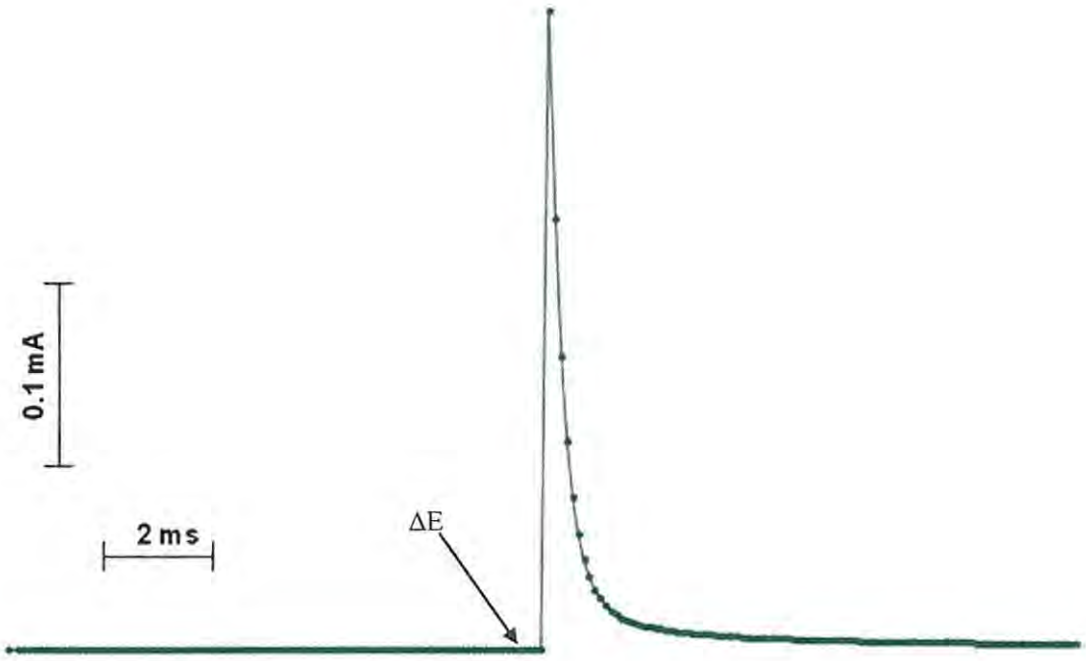

Figure A2.1: Typical current-time data plotted for the non-faradaic processes, primarily electrical double-layer charging.

Potential was altered from + 0.45 V to + 0.5 V vs. Ag/AgCl. The GCE was anodically cleaned, followed by ultrasonication in subsequent solutions of absolute ethanol and water and subsequently analysed in 0.1M KCl solution. This typical chronamperogram is drawn from the third data-set, GCE 3, prior to electrochemical cycling. The arrow indicates the time at which the potential was switched.

The values of C_{DL}, R_S and the χ^2 values were fitted against the current-time curves generated by double-step chronoamperometry. Modelling of the parameters was varied from 2 data-points used to fit the parameters, to 9.

Figures A2.2 and A2.3 display data drawn from this set and show trends when both models converge and when they diverge from one another. Dashed lines indicate parameters extracted with two-parameter model fitting and solid lines indicate values using C_{DL} fitting, alone. The dashed-line inset box displays the average R_S calculated from the two-parameter fitting models. Please note that χ^2 values are presented in a logarithmic format, in order to represent the range through which this variable travels under different modelling processes.

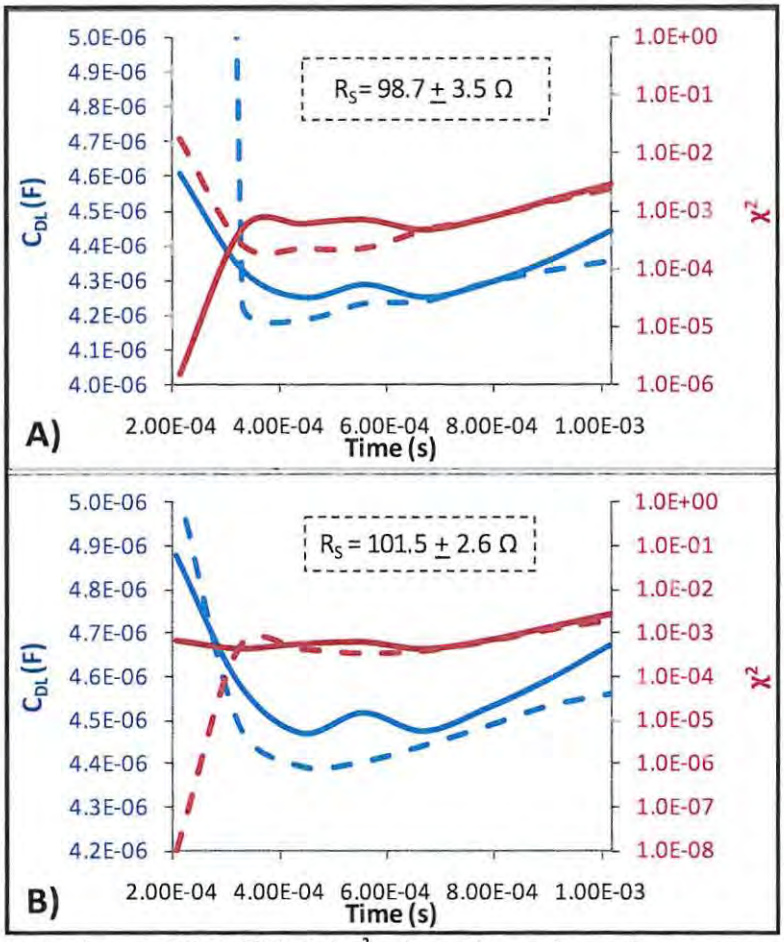

Figure A2.2: Graph plotting modelled CDL and χ^2 values with an increasing amount of time (datapoints) when modelled R_S values converge.

A) Before cycling in 0.1M KCl

B) After cycling.

Modelled parameters drawn from Model I are plotted as solid lines, values drawn from Model II are plotted as dashed lines. Inset box: Average R_S values as calculated by Model II, including standard deviation from the mean.

As is evident from the graphs, there is a large dependence on the time i.e. number of data-points on the calculated C_{DL}. This is, as has been previously mentioned, due to the difficulties in short-time resolutions. However, after 0.4 ms has elapsed (5 data-points), the C_{DL} values for both modelling systems undergo minima, followed by an increase in both plotted C_{DL} values and $\chi 2$ after ± 0.8 ms (for all data examined). The differences occurring in the calculated R_S and C_{DL} values between electrode cycling (Figures A1.2**A** and A1.2**B**) indicates that electrode cycling in 0.1M KCl does slightly alter the surface properties of the electrodes, increasing both C_{DL} and the R_S (in the above instance, C_{DL} increased from an average of 4.27×10^{-6} F to 4.47×10^{-6} F).

This dataset was represented in order to demonstrate the models' closeness of fit between Model I and Model II when R_S values between these sets are nearly equivalent. Calculated C_{DL} values for both Model I and Model II follow very closely, and the χ^2 values are also very close. Figure A2.3 shows model data in which R_S, as calculated by model II, deviates away from the 100 Ω set in Model I.

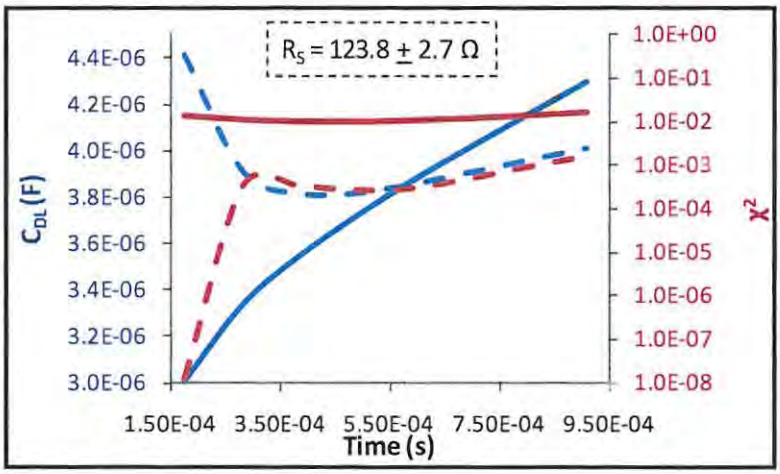

Figure A2.3: Graph plotting modelled C_{DL} and χ^2 values with an increasing amount of time (datapoints) when modelled R_S values diverge.

Modelled parameters drawn from Model I are plotted as solid lines, values drawn from Model II are plotted as dashed lines. Inset box: Average R_S values as calculated by Model II, including standard deviation from the mean.

As is displayed in Figure A2.3, in instances where the R_S calculated by Model II is not equivalent to that of Model I, there is a significant difference in the calculated C_{DL}. C_{DL} values calculated by Model II are much more stable, deviating less with an increase in time / datapoints after ± 0.3 ms (Figure A2.3) than values drawn from Model I (Figure A2.2). By contrast, the calculated C_{DL} values drawn from Model I increased dramatically with increasing time/datapoints, showing an almost linear increase that ranged from 3.4 μF at 0.35 ms to 4.2 μF at 0.935 ms. In addition, the χ^2 values determined using Model II remain 10-fold less than those calculated by Model I.

Model II, for six of the nine random samples, showed more robust calculations for C_{DL} regardless of the apparent difference in RS. While in both models used, there was a tendency for CDL to increase with increasing time/datapoints, this trend is usually less pronounced in Model II than Model I (Figures A2.2 and A2.3), with a slight increase in apparent R_S recorded in Model II in place of the large C_{DL} increases noted when using Model I. In those examples where R_S values from Model I coincided with Model II, there was little apparent difference in the calculated C_{DL}.

Hence, Model II was preferred as the method to determine C_{DL} values. Data drawn from the onset of the potential switch to $\pm$ 0.6 ms were employed to determine the C_{DL} values of the various surfaces in Chapter 3 of this thesis.

A2.2: Effect of electrode cycling on calculated non-Faradaic parameters:

The differences occurring in the calculated R_S and C_{DL} values between electrode cycling (Figure A2.2, (A) and (B)) indicates that electrode cycling in 0.1M KCl does slightly alter the surface properties of the electrodes, increasing both C_{DL} and the R_S (in the above instance, C_{DL} increased from an average of 4.27×10^{-6} F to 4.47×10^{-6} F). However, an examination of the calculated C_{DL} and R_S values of anodically-pretreated electrodes before and after cycling reveals (Figure A2.4) that no substantial alteration of these parameters occurs over the entire population.

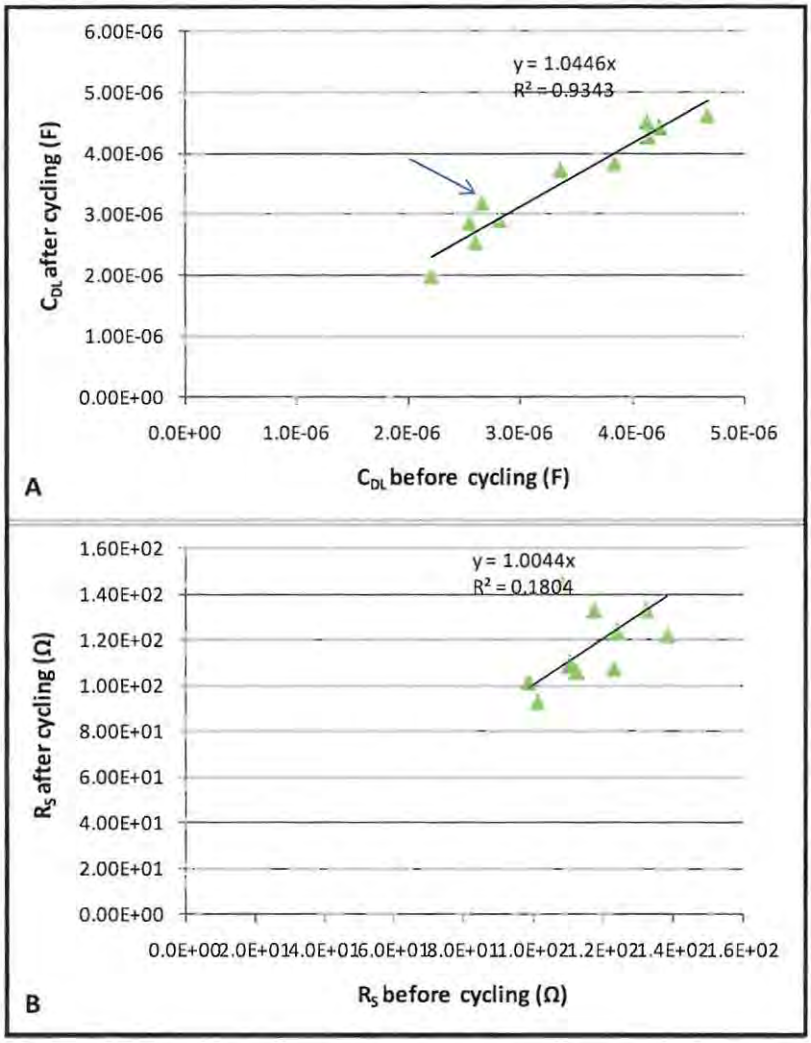

Figure A2.4: Alterations of the calculated (A) C_{DL} and (B) R_S of anodically-pretreated electrodes before and after cycling in 0.1M.

For these graphs, intercepts were forced through the origin in order to produce information regarding the slopes of these graphs. Number of observations, n = 11.

As an examination of the slope in Figure A2.4**A** shows, there is little alteration in the values of C_{DL} after cycling beyond a slight tendency (m = 1.05) to increase when the entire population (n = 12) is assessed. While there is a larger degree of scatter for the calculated R_S (Figure A2.4**B**)and a corresponding drop in the linearity of the function ($R^2 = 0.18$), the degree of scatter is evenly distributed around a slope of 1.0044, indicating little change of the calculated solution resistance after cycling.

From this, we can conclude that cycling of the electrode in 0.1 M KCl does not greatly affect the double-layer charging characteristics of the electrode, and that comparative surfaces are present both before and after cycling of the electrode.

Appendix 2: Chronoamperometric determination of double-layer capacitance

Appendix 3: Goodness-of-fit indicators with increasing sigmoidality of modelled biosensor current response:

Two separate criterion dictating the modelled parameters' goodness-of-fit were performed in parallel throughout the analyses requiring the use of the sigmoidal model – the Sum of Square Differences (SSD) and the Chi-Square statistic. The selection of the criterion for the goodness-of-fit was somewhat complicated during the analysis of highly-sigmoidal (i.e. b > 2.5 for models fitted using SSD minima) sensor response curves. As Figure A4.1 displays, significant differences are in evidence when biosensor current response was modelled using either the Chi-squared statistic (χ^2) or the Sum-of-Square Difference (SSD) parameters were used as indications of the model's goodness-of-fit.

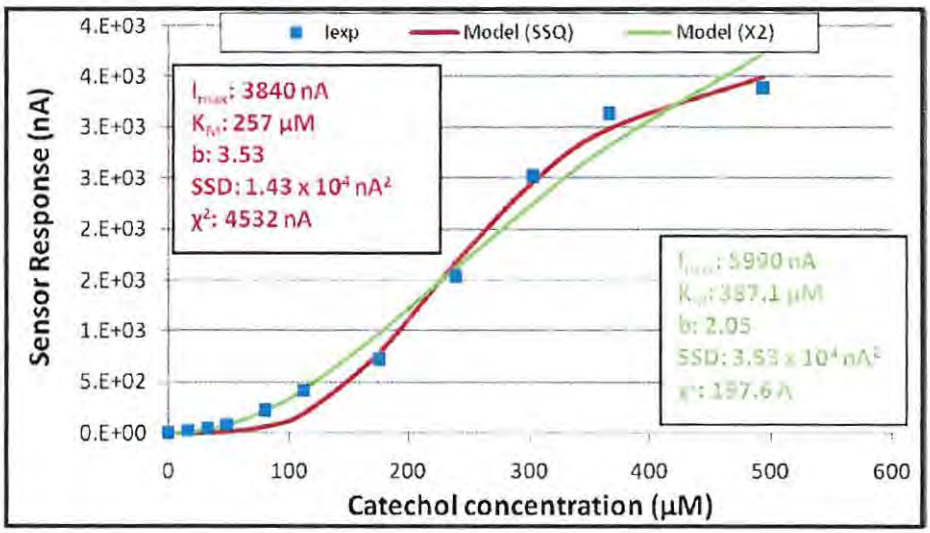

Figure A3.1: Comparison of modelled current contrasting experimental (blue squares) versus modelled current responses when using SSD (red line) or χ^2 (green line) as a measure of goodness-of-fit in highly sigmoidal sensor responses.

Legend: Iexp - experimentally-determined current response, Model(SSD) - current responses as calculated through the use of the minima of the Sum-of-Square Difference, Model(X2) - current responses as determined through the use of χ^2-minima.

Inset boxes present the model parameters extracted from the modelled data at the minima of the goodness-of-fit parameter. Bottom-right, green text = χ^2-minima and upper-left, red text = SSD minima

Sensor used in example: 0.4 U laccase, 100 µg BSA, GCE (1). Data not adjusted for surface area, as is presented in Chapter 4.

Summaries of the differences in applicability of these two statistics as indicators of the model's goodness-of-fit are available in Appendix 1, Section A1.4. As Figure A3.1 indicates, there exists significant differences in both the shape of the modelled current responses and the parameters extracted from the model when using either of these statistics as indicators of goodness-of-fit. By evenly weighting

the data irrespective of the scale of the current response, the use of the χ^2 statistic underestimates the sigmoidality of the sensor response, thus overestimating the modelled i_{max} (in the absence of surface area normalisation, this is referred to as I_{max})and K_m values (Figure A3.1). A much closer degree of fitting when comparing the experimental data to the modelled data is observed at lower concentration/current values through use of χ^2. Use of the SSD minima as the goodness-of-fit criterion shows the converse i.e. a better degree of fitting at higher concentration/current values, with more reasonable I_{max} and K_m values extracted when compared to the experimentally-obtained data. The differences extant between these models are represented by the differences in the calculated SSD and χ^2 values determined when using either criterion as an indication of goodness-of-fit (Figure 4.6 text boxes), with ~30-fold differences evident between the models arrived at using either statistic.

This phenomenon becomes less evident in sensor responses exhibiting either lower degrees of sigmoidalities, or lower apparent K_m values i.e. when the modelled K_m value is less than half the final concentration sensor response was assayed at (508 μM catechol concentration). Lower degrees of sigmoidality provide a greater consensus between the modelled 'b' parameter arrived at through use of either indicators, allowing for greater unification between the other modelled parameters. Similarly, lower apparent K_m values presuppose a larger dataset in which $[S] >> K_m$ (hence that v approches v_{max}), allowing for a preferential weighting of χ^2 values within this range. This, in turn, is beneficial in uniting parameters elicited from χ^2 with those obtained from SSD. Figure A4.2 shows a very good overlap with modelled parameters using either statistic as goodness-of-fit indicators when both of the aforementioned criteria are met.

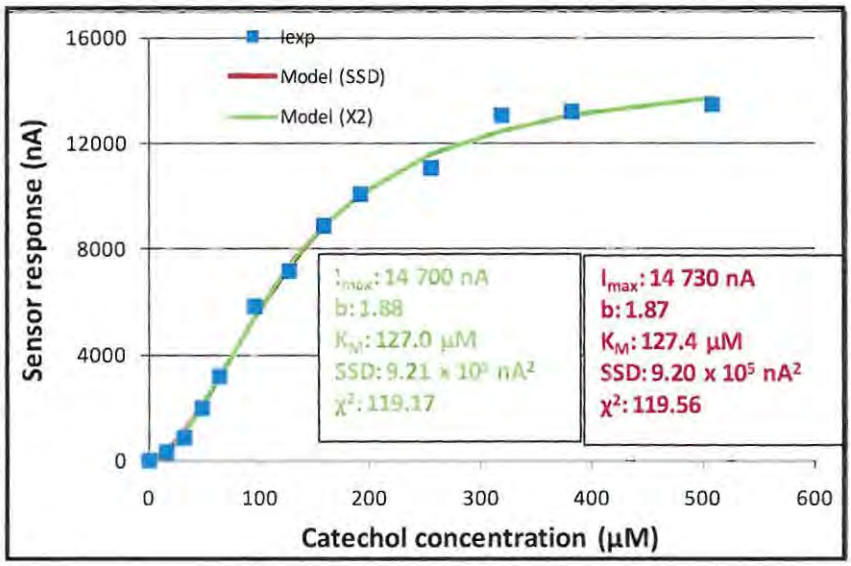

Figure A3.2: Comparison of modelled current contrasting experimental (blue squares) versus modelled current responses when using SSD (red line) or χ^2 (green line) as a measure of goodness-of-fit in systems exhibiting a low degree of sigmoidality in biosensor responses.

Legend as in Figure A4.1

Sensor used: 0.8 U laccase, 20 µg BSA. Data not adjusted for surface area, as is presented in Chapter 4.

For the reasons outlined above, Figure 4.7 shows that, when modelling sensors of lower sigmoidality, either statistic method provides very similar values that seem to accurately model the response of the biosensor as determined experimentally. In order to provide a model fitting that both took into account the lower current responses, while adequately describing the shape of the sigmoid curve, parameters determined using both goodness-of-fit criteria were performed on each data-set in order to compromise between the advantages that these two criteria offer the fitting of the data.

Appendix 4: Tabulated data of pH-dependent substrate investigations at bare GCEs and laccase biosensors.

This section is intended to supplement Chapter 5, Section 5.4.3, which discusses the alteration of biosensor kinetics for the substrates, BZT,3-MC,HQ,CAT, GA and GOL with alterations of electrolyte pH. Presented in this section is a tabulated summary of the biosensor operational kinetics that forms the basis for the interpretation of results presented in the aforementioned section.

Table A4.1: Summary of substrate oxidation/reduction parameters assessed via cyclic voltammetry at unmodified GCEs under conditions of varying electrolyte pH

	%I (Bare GCE)			$E_{p,a}$:bare GCE (V)[a]			$E_{p,a}$: biosensor (V)[a]		
Substrate	**3.5**	**4.5**	**5.5**	**3.5**	**4.5**	**5.5**	**3.5**	**4.5**	**5.5**
Pristine sensors									
BZT	102.3	90.4	78.1	0.217	0.149	0.060	0.222	0.157	0.086
HQ	96.4	94.3	98.2	0.320	0.284	0.203	0.349	0.299	0.214
3-MC	88.6	89.3	91.8	0.394	0.348	0.268	0.385	0.350	0.28
CAT	86.9	85.3	88.8	0.452	0.370	0.293	0.504	0.421	0.343
GOL	32.5	34.8	27.3	0.701	0.681	0.590	0.754	0.704	0.65
GA	3.9	1.2	0.42	0.446	0.358	0.260	0.462	0.401	0.339

All values reported here are drawn from a minimum of 3 independent observations. Unless otherwise indicated. Those with standard errors $\simeq$ 10% are highlighted in light grey. All potentials are reported herein with $<$ 10 mV standard deviation from the mean, and all current yields are reported $\pm$ 1 %, except in the case of GA, which is reported $\pm$ 0.1%.

[a] - vs. Ag/AgCl reference electrode.

Table A4.2: Summary of biosensor operational parameters obtained using laccase biosensors for each substrate, under conditions of varying pH.

	i_{max} ($\mu A.cm^{-2}$)			K_m (μM)			Sensitivity ($nA.\mu M.cm^{-2}$)		
Substrate	**3.5**	**4.5**	**5.5**	**3.5**	**4.5**	**5.5**	**3.5**	**4.5**	**5.5**
BZT	374.9	379.7	303.6	63.4	79.3	49.7	2756	2714	2948
HQ	379.1	342.7	334.3	119.9	87.0	114.4	1621	1903	1468
3-MC	317.7	221.6	283.6	133.3	106.0	58.23	1181	1155	2453
CAT	290.5	236.9	192.0	253.1	125.6	68.00	743	964	1371
GOL	159.3	160.9	138.5	219.3	215.3	219.9	359	340	449
GA	115.0	74.85	84.56	344.9	344.9	423.5	174.07	117.81	101.83

All values reported here are drawn from a minimum of 3 independent observations and generated using pristine biosensors.

Unless otherwise indicated, parameters are reported with a standard error <10% of the mean value reported above, with most having a standard error ~ 5 %. Those with standard errors ≃ 10% are highlighted in light grey.

[a]- vs. Ag/AgCl reference electrode.

Chapter 11: Reference List

Acerenza, L. and Mizraji, E., 1997. Cooperativity: a unified view. Biochim. et Biophys. Acta. 1339, 155-166

Agboola, B., Westbroek, P., Ozoemena, K.I., Nyokong, T., (2007). Voltammetric characterisation of the self-assembled monolayers (SAMs) of benzyl- and dodecyl-mercapto tetra substituted metallophthalocyanines complexes, Electrochem. Comm., 9, 310-316

Ahn et al, 2007a: Ahn, Y.G., Shin, J.H., Kim, H.-Y., Khim, J., Lee, M.-K., and Hong, J., 2007. Application of solid-phase extraction coupled with freezing-lipid filtration clean-up for the determination of endocrine-disrupting phenols in fish. Anal. Chim. Acta 603, 67-75.

Ahn et al., 2007b: Ahn, M-Y., Zimmerman, A.R., Martínez, C.E., Archibald, D.D., Bollag, J-M. and Dec, J., 2007. Characteristics of Trametes villosa laccase adsorbed on aluminum hydroxide. Enz. Microb. Tech. 41, 141-148

Ahuja, T. Mira, I.A., Rajesh, D.K. (2007). Biomolecular immobilization on conducting polymers for biosensing applications, Biomat. 28, 791 - 805

Alberts, B., Johnson, A., Lewis, J., Raff, M., Roberts, K, and Walter, P., 2002. Chapter 2: Cell Chemistry and Biosynthesis. In: *Molecular Biology of the Cell.* 4th Edition. Alberts et al., (eds.). Garland Science, Taylor & Francis Group, United States of America. pp. 47-128

Anandhakumar, S., Chandrasekaran, M. and Noel, M., 2010. Anodic oxidation of chlorophenols in micelles and microemulsions on glassy carbon electrode: the medium effect on electroanalysis and electrochemical detoxification. J. Appl. Electrochem. 40, 303–310

Anderegg, J.W., Beeman, W.W., Shulman S. and Kaesburg, P., 1955. An Investigation of the Size, Shape and Hydration of Serum Albumin by Small-angle X-Ray Scattering. J. Am. Chem. Soc. 77 2927-2937

Andersson, M., Andersson, J., Sellborn, A., Berglin, M., Nilsson, B. and Elwing, H. (2004). Quartz crystal microbalance-with dissipation monitoring (QCM-D) for real time measurements of blood coagulation density and immune complement activation on artificial surfaces, Biosens. Bioelectron., 21, 79-86

Antonyraj, C.A., Gandhi, M. and Kannan, S., 2010. Phenol Hydroxylation over Cu-Containing LDHs and Their Calcined Forms: Profound Cobivalent Metal Influence. Ind. Eng. Chem. Res. 49, 6020-6026

Aptula, , A.O., Roberts, D.W., Cronin, M.T.D. and Schultz, T.W., 2005. Chemistry-Toxicity Relationships for the Effects of Di- and Trihydroxybenzenes to Tetrahymena pyriformis. Chem. Res. Toxicol. 18, 844-854

Arias, F. Godinez, L.A., Wilson, S.R., Kaifer A.E., and Echegoyen, L., Interfacial Hydrogen Bonding. Self-Assembly of a Monolayer of a Fullerene-Crown Ether Derivative on Gold Surfaces Derivatized with an Ammonium-Terminated Alkanethiolate, J. Am. Chem. Soc., 118, 6086 -6087

Arora, A., Nair, M.G., Strasburg, G.M., 1998. Structure–activity relationships for antioxidant activities of a series of flavonoids in a liposomal system. Free Radic. Biol. Med. 24, 1355–1363.

Ashely, K., 2003. Review: Developments in electrochemical sensors for occupational and environmental health applications. J. Haz. Mat. 102, 1-12.

Aytar, B.S. and Bakir, U., 2008. Preparation of cross-linked tyrosinase aggregates. Proc. Biochem. 43, 125-131.

Bain, C.D., Evall, J., and Whitesides, G.M., 1989. Formation of Monolayers by the Coadsorption of Thiols on Gold: Variation in the Head Group, Tail Group, and Solvent, J. Am. Chem. Soc., 111, 7155-7164

Bakker, E. and Telting-Diaz, M., 2002. Electrochemical Sensors. Anal. Chem. 74, 2781-2800

Baldrian, P., 2006. Fungal laccases: occurrence and properties. FEMS Microbiol. Rev. 30, 215 – 240

Barceló, D. and Hennion, M.-C., 1995. Review: On-line sample handling strategies for the trace-level determination of pesticides and their degradation products in environmental waters. Anal. Chim. Acta. 318, 1-41

Bard, A.J. and Faulkner, L.R., 2001a. *Chapter 5: Basic Potential-step Methods*. In: Electrochemical Methods: Fundamentals and Applications. Bard, A.J. and Faulkner, N.R. (eds.) . 2nd Edition. John Wiley and Sons (Inc), United States of America

Bard, A.J. and Faulkner, N.R., 2001b. *Chapter 1: Introduction and overview of electrode processes.* In: Electrochemical Methods – Fundamentals and Applications. Bard, A.J. and Faulkner, N.R. (eds.) 2nd Edition. John Wiley and Sons (Inc), United States of America

Bard, A.J. and Faulkner, N.R., 2001c. *Chapter 14: Electroactive layers and Modified Electrodes.* In: Electrochemical Methods – Fundamentals and Applications. Bard, A.J. and Faulkner, N.R. (eds.) 2nd Edition. John Wiley and Sons (Inc), United States of America

Bartlett, P.N. and Pratt, K.F.E., 1993. Modelling of processes in enzyme electrodes. Biosens. Bioelectron. 8 451-462

Bayramoğlu G and Arica M.Y., 2008. Enzymatic removal of phenol and p-chlorophenol in enzyme reactor: Horseradish peroxidase immobilized on magnetic beads. J. Haz. Mat. 156, 148-155

Bayramoğlu G., Altınok, H., Bulut, A., Denizli, A., and Arıca, M.Y., 2003. Preparation and application of spacer-arm-attached poly(hydroxyethyl methacrylate-co-glycidyl methacrylate) films for urease immobilization. React. Funct. Polym. 56, 111-121

Bayramoğlu, G., Arica, M.Y., 2008. Enzymatic removal of phenol and p-chlorophenol in enzyme reactor: Horseradish peroxidase immobilized on magnetic beads. J Hazard. Mater. 156, 148-155

Bayramoglu, G., Yilmaz, M. and Arica, M.Y., 2010. Preparation and characterization of epoxy-functionalized magnetic chitosan beads: laccase immobilized for degradation of reactive dyes. Bioprocess. Biosyst. Eng. 33, 439-448

Bebeselea, A., Manea, F., Burtica, G., Nagy, L.and Nagy, G., 2009. The electrochemical determination of phenolic derivates using multiple pulsed amperometry with graphite based electrodes. Talanta 80, 1068-1072

Benfield, G., Bocks, S.M., Bromley, K. and Brown, B.R., 1964. Studies of Fungal and Plant Laccases. Phytochem. 3, 79-88

Berchane, N.S., Andrews, M.J., Kerr, S., Slater, N.K.H and Jebrail, F.F., 2008. On the mechanical properties of bovine serum albumin (BSA) adhesives. J. Mater. Sci.: Mater. Med. 19, 1831–1838

Berríos, C., Marco, J.F., Gutiérrez, C., Ureta-Zañartu, M.S., 2009. Electro-oxidation of chlorophenols at glassy carbon electrodes modified with polyNi(II)complexes. Electrochim. Acta 54, 6417-6425

Birlhani, E. and Yesilada, O., 2010. Enhanced production of laccase in repeated-batch cultures of Funalia trogii and Trametes versicolor. Biochem. Engin. J. 52, 33-37

Bobacka, J., Lewenstam, A. and Ivaska, A., 2000. Electrochemical impedance spectroscopy of oxidized poly(3,4-ethylenedioxythiophene) film electrodes in aqueous solutions. J. Electroanal. Chem. 489, 17-27

Bollag et al., 1996a: Bollag, D.M., Rozycki, M. D., Edelstein, S.J. 1996b. Hanging Drop Crystallisation, pg. 356-359, Chapter 12, In: *Protein Methods*, Second Edition, Wiley-Liss Inc., 605 Third Avenue, New York, United States of America

Bollag et al., 1996b: Bollag, D.M., Rozycki, M.D. and Edelstein, S.J., 1996a. Chapter 1: Preparation for Protein Isolation. In: Protein Methods. 2nd Edition. Bollag, D.M., Rozycki, M.D. and Edelstein, S.J (eds.) John Wiley & Sons, Inc., United States of America. pp. 20-22

Bollag et al., 1996c: Bollag, D.M., Rozycki, M.D. and Edelstein, S.J., 1996b. Chapter 8: Immunoblotting. In: Protein Methods. 2nd Edition. Bollag, D.M., Rozycki, M.D. and Edelstein, S.J (eds.) John Wiley & Sons, Inc., United States of America. pp. 206-210.

Bourassa, P., Kanakis, C.D., Tarantilis, P., Pollisiou, M.G. and Tajmir-Raihi, H.A., 2010. Resveratrol, Genistein, and Curcumin Bind Bovine Serum Albumin. J. Phys. Chem. B 114, 3348–3354

Bourbannais, R., Paice, M.G., Reid, D., Lanthier, P. and Yaguchi, M., 1995. Lignin Oxidation by Laccase Isozymes from Trametes versicolor and Role of the Mediator 2,29-Azinobis(3-Ethylbenzthiazoline-6-Sulfonate) in Kraft Lignin Depolymerization. App. Environ. Micro. 61, 1876-1880

Bowers, M.L., Hefter, J., Dugger, D.L. and Wilson, R., 1990. Solid-state analytical characterization of electrochemically-modified glassy carbon electrodes. Anal. Chim. Acta 248, 127-142

Bratkovskaja, I., Vidziunaite, R. and Kulys, J., 2004. Oxidation of Phenolic Compounds by Peroxidase in the Presence of Soluble Polymers. Biochem. (Mosc.) 69, 985-992

Buckman, N.G., Hill, J.O. and Magee, R.J., 1984. Separation of Substituted Phenols, including Eleven Priority Pollutants Using High Performance Liquid Chromatography.

Bumm, L.A.., Arnold, J.J.., Charles, L.F., Dunbar, T.D., Allara, D.L., and Weiss, P.S., 1999. Directed Self-Assembly to Create Molecular Terraces with Molecularly Sharp Boundaries in Organic Monolayers. J. Am. Chem. Soc., 121, 8017-8021

Busca, G., Berardinelli, S., Resini, C. and Arrighi, L., 2008. Review: Technologies for the removal of phenol from fluid streams: A short review of recent developments. J. Haz. Mat. 160, 265-288.

Byfield, M.P. and Abuknesha, R.A., 1994. Review: Biochemical aspects of biosensors. Biosens. Bioelectron. 9, 373-400

Cabaj, J., Sołoducho, J., Chyla, A., Bryjak, J., Zynek, K., 2009. The characterization of ordered thin films built of immobilized phenoloxidases. Sens. Actu. B: Chem, 136, 425–431

Cabana, H., Alexandre, C., Agathos, S.N. and Jones, J.P., 2009. Immobilization of laccase from the white rot fungus Coriolopsis polyzona and use of the immobilized biocatalyst for the continuous elimination of endocrine disrupting chemicals. Biores. Tech. 100, 3447-3458

Cabana, H., Jones, J.P. and Agathos, S.N., 2007. Preparation and characterization of cross-linked laccase aggregates and their application to the elimination of endocrine disrupting chemicals. J. Biotech. 132, 23-31

Call, H., and Mücke, I., 1997. History, overview and applications of mediated lignolytic systems, especially laccase-mediator-systems (Lignozym®-process). Journal of Biotechnology 53 , 163-202.

Calvo, E.J., Etchenique, R., Danilowicz, C., and Diaz, L., (1996). Electrical Communication between Electrodes and Enzymes Mediated by Redox Hydrogels, Anal. Chem., 68, 4186-4193

Canfora, L., Iamarino, G., Roa, M.A and Ginfreda, L., 2008. Oxidative Transformation of Natural and Synthetic Phenolic Mixtures by Trametes versicolor Laccase. J. Agric. Food Chem. 56, 1398-1407

Cao, L., 2005. Immobilised Enzymes: Science or Art? Curr. Opin. Chem. Bio. 9, 217 - 265

Céspedes, C.L., El-Hafidi, M., Pavon, N. and Alarcon, J., 2008. Antioxidant and cardioprotective activities of phenolic extracts from fruits of Chilean blackberry Aristotelia chilensis (Elaeocarpaceae), Maqui. Food Chem. 107, 820–829

Chakroun, H., Mechici, T., Martinez, M.J., Dhouib, A. and Sayadi, S., 2010. Purification and characterization of a novel laccase from the ascomycete Trichoderma atroviride: Application on bioremediation of phenolic compounds. Proc. Biochem. 45, 507-513

Chang, B.S., Mahoney, R.R., 1995. Enzyme thermostabilization by bovine serum albumin and other proteins: evidence for hydrophobic interactions. Biotechnol. Appl. Bioc. 22, 203–214

Chen, H., Yao, J., Wang, F., Choi, M.M.F., Bramanti, E. and Zaray, G., 2009. Study on the toxic effects of diphenol compounds on soil microbial activity by a combination of methods. J. Haz. Mat. 167, 846-851.

Chen, L. and Gorski, W., (2001). Bioinorganic Composites for Enzyme Electrodes, Anal. Chem., 73, 2862-2868

Ciolkosz, M.K. and Jordan, J., 1993. Comparison of Spectrophotometric and Amperometric Rate Parameters of Enzymatic Reactions. Anal. Chem. 65, 164-168

Claus, H., 2004. **Review**: Laccases: structure, reactions, distribution. Micron 35, 93-96

Collins, P.J., Kotterman, M.J.J., Field, J.A. and Dobson, A.D.W., 1996. Oxidation of Anthracene and Benzo[a]pyrene by Laccases from Trametes versicolor. App. Environ. Micro. 62, 4563-4567

Coons, D.M., Boulton, R.B. and Bisson, L.F., 1995. Computer-assisted nonlinear regression analysis of the multicomponent glucose uptake kinetics of *Saccharomyces cerevisiae*. J. Bact., 177, 3251-3258

Costentin, C., Robert, M. and Savéant, J-M., 2010. Concerted Proton-Electron Transfers: Electrochemical and Related Approaches. Acc. Chem. Res. 43, 1019-1029

Couto, S.G., and Herrera, J.L.T., 2006. Industrial and Biotechnological Application of Laccases: A Review. Biotech. Adv. 24, 500-513.

d'Acunzo, F., Galli, C. and Masci, B., 2002. Oxidation of phenols by laccase and laccase-mediator systems. Solubility and steric issues. Eur. J. Biochem. 269, 5330–5335

Davies, M.I., 1999. Review: A review of microdialysis sampling for pharmacokinetic applications. Anal. Chim. Acta 379, 227-249

de Pascual-Teresa, S., Moreno, D.A. and Garca-Viguera, C., 2010. Flavanols and Anthocyanins in Cardiovascular Health: A Review of Current Evidence. Int. J. Mol. Sci., 11, 1679-1703

Dec, J., Haider, K. and Bollag, J-M., 2003. Release of substituents from phenolic compounds during oxidative coupling reactions. Chemosph. 52, 549-556.

Delgado, M., Spanka, C., Kerwin, L.D., Wentworth, P. Jr. and Janda, K.D., 2002. A Tunable Hydrogel for Encapsulation and Controlled Release of Bioactive Proteins. Biomacromolec. 3, 262-271

Demant, E.J.F., 1996. Covalent complexed between serum albumin and 7-hydroxycourmarin-4-acetic acid: synthesis and applications in the spectrophotometric detection of long-chain fatty acids. Biochim. et Biophys. Acta 1304, 43-55

Diaconu, M., Litescu, S.C. and Radu, G.L., 2010. Laccase–MWCNT–chitosan biosensor—A new tool for total polyphenolic content evaluation from in vitro cultivated plants. Sens. Actuat. B: Chem. 145, 800-806

Ding, Y., Ayon, A. and García, C.D., 2007. Electrochemical detection of phenolic compounds using cylindrical carbon-ink electrodes and microchip capillary electrophoresis. Anal. Chim. Acta 584, 244-251

Dong, T., Zhao, L., Huang, Y., and Xin, T., 2010. Preparation of cross-linked aggregates of aminoacylase from *Aspergillus melleus* by using bovine serum albumin as an inert additive. Biores. Tech. 101, 6569-6571

Dorfner, R., Ferge, T., Kettrup, A., Zimmermann, R. and Yeretzian, C, 2003. Real-time monitoring of 4-vinylguaiacol, guaiacol, and phenol during coffee roasting by resonant laser ionization time-of-flight mass spectrometry. J. Agr. Food Chem. 51, 5768–5673.

Durán, N., Esposito, E., 2000. Potential applications of oxidative enzymes and phenoloxidase-like compounds in wastewater and soil treatment: a review. App. Cat. B: Environ. 28, 83-99.

Durán, N., Rosa, M.A., D'Annibale, A., Gianfreda, L., 2002. Applications of laccases and tyrosinases (phenoloxidases) immobilized on different supports: a review. Enz. Microb. Tech. 31, 907-931

Dutta, A.K. Nayak, A.K. and Belfort, G.., 2008. Viscoelastic properties of adsorbed and cross-linked polypeptide and protein layers at a solid–liquid interface. J. Coll Interf. Sci. 324, 55-60

Eisert, R. and Levsen, K., 1996. Review: Solid-phase microextraction coupled to gas chromatography: a new method for the analysis of organics in water. J. Chromatogr. A 733, 143-157

El-Deab, M.S. and Ohsaka, T. (2004). Molecular-level design of binary self-assembled monolayers on polycrystalline gold electrodes, Electrochim. Acta, 49, 2189–2194

Engstrom, R.C., 1982. Electrochemical Pretreatment of Glassy Carbon Electrodes. Anal. Chem. 54, 2310-2314

Fåhraeus, G. and Ljunggren, H., 1960. Substrate Specificity of a Purified Fungal Laccase. Biochim. Biophys. Acta. 46, 22-32

Farré, M., Brix, R. and Barceló, D., 2005. Screening water for pollutants using biological techniques under European Union funding during the last 10 years. Tr. Anal. Chem. 24, 531-545

Feiler, A.A. , Sahlholm, A., Sandberg, T., and Caldwell, K.D. 2007. Adsorption and viscoelastic properties of fractionated mucin (BSM) and bovine serum albumin (BSA) studied with quartz crystal microbalance (QCM-D). J Coll. Interf. Sci. 315, 475-481

Ferrara, F., Fabietti, F., Delise, M., Bocca, A.P, and Funari, E., 2001. Alkylphenolic Compounds in Edible Molluscs of the Adriatic Sea (Italy). Environ. Sci. Technol. 35, 3109-3112

Ferrat, L., Pergent-Martini, C. and Roméo, M., 2003. Assessment of the use of biomarkers in aquatic plants for the evaluation of environmental quality: application to seagrasses. Aqua. Toxicol. 65, 187-204

Ferreira, M., Varela, H., Torresi, R.M. and Tremiliosi-Filho, G., 2006. Electrode passivation caused by polymerization of different phenolic compounds. Electrochim. Act. 52, 434 - 442

Firuzi, O., Lacanna, A., Petrucci, R., Marrosu, G. and Saso, L., 2005. Evaluation of the antioxidant activity of flavonoids by "ferric reducing antioxidant power" assay and cyclic voltammetry. Biochim. Biophys. Acta 1721, 174-184.

Forde, J., Tully, E., Vakuroy, A., Gibson, T.D., Millner, P. and Ó'Fágáin, C., 2010. Chemical modification and immobilisation of laccase from Trametes hirsuta and from Myceliophthora thermophila. Enz. Microb. Tech. 46, 430-437

Frasconi, M., Favero, G., Boer, H., Koivula, A. and Mazzei, F., 2010. Kinetic and biochemical properties of high and low redox potential laccases from fungal and plant origin. Biochim. Biophys. Acta 1804, 899-908

Freire, R.S., Durán, N. and Kubota, L.T., 2001. Effects of fungal laccase immobilization procedures for the development of a biosensor for phenol compounds. Talanta 54, 681-686

Freire, R.S, Duran, N. and Kubota, L.T., 2002. Development of a laccase-based flow injection electrochemical biosensor for the determination of phenolic compounds and its application for monitoring remediation of Kraft E1 paper mill effluent. Anal. Chim. Acta 463, 229-238.

Freire, R.S., Ferreira, M.M.C., Durán, N. and Kubota, L.T., 2003. Dual amperometric biosensor device for analysis of binary mixtures of phenols by multivariate calibration using partial least squares. Anal. Chim. Acta 485, 263-269.

Freixo, M.do R., Karmali, A., Frazão, C. and Arteiro, J.M., 2008. Production of laccase and xylanase from Coriolus versicolor grown on tomato pomace and their chromatographic behaviour on immobilized metal chelates. Proc. Biochem. 43, 1265-1274

Gamella, M., Campuzano, S., Reviejo, A.J. and Pingarrón, J.M., 2006. Electrochemical Estimation of the Polyphenol Index in Wine Using a Laccase Biosensor. J. Agric. Food Chem. 54, 7960-7967

Garret and Grisham, 1999a. Garrett, R.H. and Grisham, C.M., 1999. Chapter 15: Enzyme Specificity and Regulation. In: Biochemistry. 2nd Edition. Garret, R.H. and Grisham, C.M. (eds.), Saunders College Publishing, United States of America.

Garrett and Grisham, 1999b. Garrett, R.H. and Grisham, C.M., 1999. Chapter 5: Proteins: Their Biological Functions and Primary Structure. pgs. 128 - 131. In: Biochemistry. 2nd Edition. Garret, R.H. and Grisham, C.M. (eds.), Saunders College Publishing, United States of America.

Garrett and Grisham, 1999c: Garrett, R.H. and Grisham, C.M., 1999. *Chapter 34: The Reception and Transmission of Extracellular Information.* In: Biochemistry. 2nd Edition. Garret, R.H. and Grisham, C.M. (eds.), Saunders College Publishing, United States of America.

Garzillo, A.M.V., Colao, M.C., Caruso, C., Caporale, C., Celetti, D. and Buonocore, V., 1998. Laccase from the white-rot fungus Trametes trogii. Appl. Microbiol. Biotechnol. 49, 545 - 551

Gaskell., M., McLuckie, K.I.E and Farmer, P.B., 2005. Comparison of the repair of DNA damage induced by the benzene metabolites hydroquinone and p-benzoquinone: a role for hydroquinone in benzene genotoxicity. Carcinogen. 26, 673-680.

Gianfreda, L., Sannino, F., Filazzola, M.T. and Leonowicz, A., 1998. Catalytic behavior and detoxifying ability of a lactase from the fungal strain Cerrena unicolor. J. Mol. Cat. B: Enz. 4, 13-23

Giardina, P., Autore, F., Faraco, V., Festa, G., Palmieri, G., Piscitelli, A. and Sannia, G., 2007. Structural characterization of heterodimeric laccases from Pleurotus ostreatus. Appl. Microbiol. Biotechnol. 75, 1293-1300

Goi, A., Trapido, M and Tuhkanen, T., 2004. A study of toxicity, biodegradability, and some by-products of ozonised nitrophenols. Adv. Environ. Res. 8, 303-311

Goldbeter, A., 1975. Kinetic Cooperativity in the Concerted Model for Allosteric Enzymes. Biophys. Chem. 4 159-167.

Gomes, S.A.S.S., Nogueira, J.M.F. and Rebelo, M.J.F., 2004. An amperometric biosensor for polyphenolic compounds in red wine. Biosens. Bioelectron. 20, 1211-1216

Gonçalves, D., Faria, R.C., Yonashiro, M. and Bulhões, L.O.S., 2000. Electrochemical oxidation of o-aminophenol in aqueous acidic medium: formation of film and soluble products. J. Electroanal. Chem. 487, 90 – 99

González-Molina, E., Domínguez-Perles, R., Moreno, D.A. and García-Viguera, C., 2010. Review: Natural bioactive compounds of Citrus limon for food and health. J. Pharmaceut. Biomed. Anal. 51, 327–345

Gooding, J.J., Erokhin, P., Brynn Hibbert, D., 2000. Parameters important in tuning the response of monolayer enzyme electrodes fabricated using self-assembled monolayers of alkanethiols. Biosens. Bioelectron. 15, 229-239

Göpel, W., and Heiduschka, P., 1995. Interface analysis in biosensor design. Biosens. Bioelectron. 10, 853-883.

Goudar, C.T., Harris, S.K., McInerney, M.J., Suflita, J.M., 2004. Progress curve analysis for enzyme and microbial kinetic reactions using explicit solutions based on the Lambert W function. J. Microb. Meth. 59, 317-326

Gouthamchandra, K., Mahmood, R. and Manjunatha, H., 2010. Free radical scavenging, antioxidant enzymes and wound healing activities of leaves extracts from Clerodendrum infortunatum L. Environ. Toxic. Pharmacol. 30, 11-18

Gurdak, E., Dupont-Gillain, C.C., Booth, J., Roberts, C.J. and Rouxhet, P.G., 2005. Resolution of the Vertical and Horizontal Heterogeneity of Adsorbed Collagen Layers by Combination of QCM-D and AFM, Langmuir 21 10684-10692

Gutés, A., Ibáñez, A.B., Céspedes, F., Alegret, S. and del Valle, M., 2005. Simultaneous determination of phenolic compounds by means of an automated voltammetric "electronic tongue". Anal. Bioanal. Chem. 382, 471-476

Györik, M., Herpai, Z., Szécsényi, I., Varga, L. and Szigeti, J., 2003. Rapid and Sensitive Determination of Phenol in Honey by High-Performance Liquid Chromatography with Fluorescence Detection. J. Agric. Food Chem. 51, 5222-5225

Haghighi, B., Gorton, L., Ruzgas, T., and Jönsson, L.J., 2003. Characterization of graphite electrodes modified with laccasenext term from Trametes versicolor and their use for bioelectrochemical monitoring of phenolic compounds in flow injection analysis. Anal. Chim. Acta 487, 3-14

Hammes, G.G., 2002. Multiple Conformational changes in Enzyme Catalysis. Biochem. 41, 8221-8228

Hamoudi, S., Belkacemi, K and Larachi, F., 1999. Catalytic oxidation of aqueous phenolic solutions catalyst deactivation and kinetics. Chem. Eng. Sci. 54, 3569-3576

Harnly, J.M., Bhagwat, S. and Lin, L.-Z., 2007. Review: Profiling methods for the determination of phenolic compounds in foods and dietary supplements. Anal. Bioanal. Chem. 389, 47–61

Harris, E.L.V. (2001), *Concentration of the extract*, pg 134-135, Chapter 6, In: *Protein Purification techniques*, S. Roe (ed.), Oxford University Press, Oxford, England

Heberer, T. and Stan, H.-J., 1997. Detection of more than 50 substituted phenols as their t-butyldimethylsilyl derivatives using gas chromatography-mass spectrometry. Anal. Chim. Acta 341, 21-34.

Hecht, H.J. and Schomburg, D. (1993), The 3D structure of glucose oxidase from Aspergillus niger: Implications for the use of GOD as a biosensor enzyme, Biosens. Bioelectron., 8, 197-203

Heim, K.E., Tagliaferro, A.R. and Bobilya, D.J., 2002. Review: Flavonoid antioxidants: chemistry, metabolism and structure-activity relationships. J. Nutrit. Biochem. 13, 572-584

Hemmersam, A. G., Foss, M., Chevallier J., and Besenbacher, F. (2005) Adsorption of fibrinogen on tantalum oxide, titanium oxide and gold studied by the QCM-D technique, Coll. Surf. B, 43, 208-215

Hermann, R., Jaenicke, R. and Rudolph, R., Analysis of the Reconstitution of Oligomeric Enzymes by Cross-Linking with Glutaraldehyde: Kinetics of Reassociation of Lactic Dehydrogenase. Biochem. 20, 5195-5201

Hermanson, G.T., Mallia, A.K., and Smith, P.K., 1992. Chapter 2. In: *Immobilised Affinity Ligand Techniques*, Academic Press, Inc. pp., 77-90

Hong, F., Jönsson, L.J., Lundquist, K. and Wei, Y., 2006. Oxidation Capacity of Laccases and Peroxidases as Reflected in Experiments With Methoxy-Substituted Benzyl Alcohols. App. Biochem. Biotech. 129-132, 303 - 319

Hoogvliet, J.C., van den Beld, C.M.B. and van der Poel, C.J., 1986. Influence of Polishing and of Electrochemical Pretreatment on the Performance of Glassy-Carbon Electrodes in Electrochemical Detection. J. Electroanal. Chem. 201., 11-21

Hook et al., 1998a: F. Höök, M. Rodahl, P. Brzezinski, and B. Kasemo (1998) Energy Dissipation Kinetics for Protein and Antibody–Antigen Adsorption under Shear Oscillation on a Quartz Crystal Microbalance. Langmuir, 14, 729 – 734

Höök et al., 1998b: F. Höök, M. Rodahl, B. Kasemo and P. Brzezinski (1998), Structural changes in haemoglobin during adsorption to solid surfaces: Effects of pH, ionic strength, and ligand binding . P. Proc. Natl. Acad. Sci. U.S.A 95, 12271

Höök, F. and Kasemo, B., 2001. Variations in Coupled Water, Viscoelastic Properties, and Film Thickness of a Mefp-1 Protein Film during Adsorption and Cross-Linking: A Quartz Crystal Microbalance with Dissipation Monitoring, Ellipsometry, and Surface Plasmon Resonance Study, Anal. Chem., 73, 5796-5804

Höök, F., Kasemo, B., Nylander, T., Fant, C., Sott, K. and Elwing, H., 2001. Variations in coupled water, viscoelastic properties, and film thickness of a Mefp-1 protein film during adsorption and cross-linking: A quartz crystal microbalance with dissipation monitoring, ellipsometry, and surface plasmon resonance study, Anal. Chem. 73, 5796–5804.

Huang, B.X. and Kim, H.-Y., 2004. Probing Three-Dimensional Structure of Bovine Serum Albumin by Chemical Cross-Linking and Mass Spectrometry. J. Am. Soc. Mass. Spectrom. 15, 1237–1247

Huang, D., Ou, B. and Prior, R.L., 2005. Reviews: The Chemistry Behind Antioxidant Capacity Assays. J. Agric. Food Chem. 53, 1841-1856

Hüsken, L.E., Beeftink, R., de Bont, J.A.M. and Wery, J., 2001. High-rate 3-methylcatechol production in Pseudomonas putida strains by means of a novel expression system. App. Microb. Tech. 55, 571 – 577

Hüsken, L.E., Beeftink, R., de Bont, J.A.M. and Wery, J., 2001. High-rate 3-methylcatechol production in Pseudomonas putida strains by means of a novel expression system. App. Microb. Tech. 55, 571 – 577

Hwang, S., Lee, C-H. and Ahn, I-S., 2008. Product identification of guaiacol oxidation catalyzed by manganese peroxidase. J. Ind. Eng. Chem. 14, 487-492

Ibrahim, V., Mendoza, L., Mamo, G. and Hatti-Kaul, R., 2010. Short communication: Blue laccase from Galerina sp.: Properties and potential for Kraft lignin demethylation. Proc. Biochem. Article In Press.

Iliev, V. and Ileva, A., (1995). Oxidation and photooxidation of sulfur-containing compounds in the presence of water soluble phthalocyanine complexes, J. Mol. Catal. A: Chem, 103, 147-153

Jaenicke, R., 1982. Review: Folding and Association of Proteins. Biophys. Struct. Mech. 8, 231-256

Jarosz-Wilkołazka, A., Ruzgas, T. and Gorton, L., 2004. Use of laccase-modified electrode for amperometric detection of plant flavonoids. Enz. Microb. Tech. 35, 238-241

Jarosz-Wilkołazka, A., Ruzgas, T., and Gorton, L., 2006. Amperometric detection of mono- and diphenols at Cerrena unicolor laccase-modified graphite electrode: correlation between sensitivity and substrate structure. Talanta 66, 1219-1224

Jarząbek, G., and Borkowska, Z., 1996. On the real surface area of smooth solid electrodes. Electrochim. Acta 42, 2915-2918

JEM, author unknown, 2003. It's a bug's life: biosensors for environmental monitoring. J. Environ. Monit. 5, 109-113.

Johannsmann, D., 2008. Viscoelastic, mechanical, and dielectric measurements on complex samples with the quartz crystal microbalance. ChemPhysChem., 10, 4516-4534

Johnson, K.A., 2003. *Chapter 1: Introduction to Kinetic Analysis of Enzyme Systems, in:* Johnson, K.A. (ed.), Kinetic analysis of Macromolecules, Oxford University Press, United Kingdom, 2003

Jordaan, J., Pletschke, B.I. and Leukes, W.D., 2004. Purification and partial characterization of a thermostable laccase from an unidentified basidiomycete. Enz. Microb. Tech. 34, 635-641

Jung, H., Xu, F. and Li, K., 2002. Purification and characterization of laccase from wood-degrading fungus Trichophyton rubrum LKY-7. Enz. Microb. Tech. 30, 161-168

Jürgen, D. and Steckhan, E., 1992. Influence of the Supporting Electrolyte and the pH on the Electrooxidative Activation of Glassy Carbon Electrodes. J. Electronal. Chem. 333, 177-193.

Kahoun, D., Řezková, S., Veškrnová, K., Královský, J. and Holčapek, M., 2008. Determination of phenolic compounds and hydroxymethylfurfural in meads using high performance liquid chromatography with coulometric-array and UV detection. J. Chromatogr. A., 1202, 19-33.

Kamau, G.N., 1989. Review: Surface Preparation of Glassy Carbon Electrodes. Anal. Chim. Acta 207, 1-16.

Karamyshev, A.V., Shleev, S.V., Koroleva, O.V., Yaopolov, A.I and Sakharov, I.Y., 2003. Laccase-catalyzed synthesis of conducting polyaniline. Enz. Microb. Tech. 33., 556-564

Karovičová, J., and Šimko, P., 2000. Review: Determination of synthetic phenolic antioxidants in food by high-performance liquid chromatography. J. Chromatogr. A. 882, 271-281

Kiema, G.K., Mirwais, A. and McDermott, M.T., 2003. Preparation of reproducible glassy carbon electrodes by removal of polishing impurities. J Electroanal. Chem. 540, 7-15

Kim, G-Y., Cuong, N.M., Cho, S-H., Shim, J., Woo, J-J. and Moon, S-H., 2007. Improvement of an enzyme electrode by poly(vinyl alcohol) coating for amperometric measurement of phenol. Talanta 71, 129-135

Kim, G-Y., Cuong, N.M., Cho, S-H., Shim, J., Woo, J-J., Moon, S-H., 2007. Improvement of an enzyme electrode by poly(vinyl alcohol) coating for amperometric measurement of phenol. Talanta, 71, 129-135

Klis et al., 2006a: Klis, M., Maicka, E., Michota, A., Bukowska, J., Sek, S., Rogalski, J. and Beliwicz, R., 2007. Electroreduction of laccase covalently bound to organothiol monolayers on gold electrodes. Electrochim. Acta 52, 5591-5598

Klis et al., 2006b: Klis, M., Rogalski, J. and Bilewicz, R., 2007. Voltammetric determination of catalytic reaction parameters of laccase based on electrooxidation of hydroquinone and ABTS. Bioelectrochem. 71, 2-7

Konopka, S.J. and McDuffie, B. (1970), Diffusion Coefficients of Ferri- and Ferrocyanide Ions in Aqueous Media, Using Twin-Electrode Thin-layer Electrochemistry, Anal. Chem., 42, 1741-1746

Koschorreck, K., Richtera, S.M., Swierczek, A., Beifuss, U., Schmid, R.D. and Urlacher, V.B., 2008. Comparative characterization of four laccases from Trametes versicolor concerning phenolic C–C coupling and oxidation of PAHs. Arch. Biochem. Biophys. 474, 213 - 219

Kulys, J. and Vidziunaite, R., 2003. Amperometric biosensors based on recombinant laccases for phenols determination. Biosens. Bioelectron. 18, 319 – 325

Kulys, J., Krikstopaitis, K., Ziemys, A. and Schneider, P., 2002. Laccase-catalyzed oxidation of syringates in presence of albumins. J. Mol. Catal. B: Enz. 18, 99–108

Kun, R., Kis, L. and Dékány, I., 2010. Hydrophobization of bovine serum albumin with cationic surfactants with different hydrophobic chain length. Coll. Surf. B: Biointerf. 79, 61-68

Kurganov, B.I., Lobanov, A.V., Borisov, I.A. and Reshetilov, A.N., 2001. Criterion for Hill equation validity for description of biosensor calibration curves. Anal. Chim. Acta. 427 11-19.

Kuznetsova, N.A., Gretsova, N.S. Derkacheva, V.M., Kaliya, O.L. and Lukyanets, E.A. (2003), Sulfonated phthalocyanines: aggregation and singlet oxygen quantum yield in aqueous solutions, J. Porphyrins Phthalocyanines, 7, 147-154

Lam, K. B., Irwin, E. F., Healy, K. E., and Lin, L., (2006). Bioelectrocatalytic self-assembled thylakoids for micro-power and sensing applications, Sens. Actuators B, 117, 480–487

Larsson, C., Bramfeldt, H., Wingren, C., Borrebaeck, C. and Höök, F., 2005. Gravimetric antigen detection utilizing antibody-modified lipid bilayers, Anal. Biochem, 345, 72-80

Larsson, C., Rodahl, M., and Höök , F., 2003. Characterization of DNA Immobilization and Subsequent Hybridization on a 2D Arrangement of Streptavidin on a Biotin-Modified Lipd Bilayer Supported on SiO_2. Anal. Chem. 75, 5080-5087

Leatherbarrow, R.J., 1990. Using linear and non-linear regression to fit biochemical data. Trends Biochem. Sci., 15, 455-458

Lee, K.R., Dipaolo, B., and Ji, X., 2000. Calibration and LOD/LOQ estimation of a Chemiluminescent Hybridisation Assay for Residual DNA in Recombinant Protein Drugs Expressed in E. coli Using a Four-Parameter Logistic Model. Drug Dev. Indust. Pharm. 26, 661-669

Lee, Y-G., and Chang, K-S., 2005. Application of a flow type quartz crystal microbalance immunosensor for real time determination of cattle bovine ephemeral fever virus in liquid. *Talanta* 65, 1335-1342

Léger, C.L., Torres-Rasgadol, E., Fouret, G., Lauret, C. and Carbonneau, M-A., 2009. Ellagic acid and its methyl-derivatives inhibit a newly found nitratase activity. Fund. Clin. Pharmacol. 24, 115-119

Lei, C. and Deng, J., 1996. Hydrogen Peroxide Sensor Based on Coimmobilized Methylene Green and Horseradish Peroxidase in the Same Montmorillonite-Modified Bovine Serum Albumin-Glutaraldehyde Matrix on a Glassy Carbon Electrode Surface. Anal. Chem. 68, 3344-3349

Leontievsky, A.A., Myasoedoval, N.M., Baskunov, B.P., Evans, C.S. and Golovleval, L.A., 2000. Transformation of 2,4,6-trichlorophenol by the white rot fungi Panus tigrinus and Coriolus versicolor. Biodegrad. 11, 331-340

Li, J.-M., Meng, X.-G., Hu , C.-W. and Du, J., 2009. Adsorption of phenol, *p*-chlorophenol and *p*-nitrophenol onto functional chitosan. Biores. Tech. 100, 1168-1173

Lian, J., Lui, J.X. and Wei, Y.S., 2009. Fate of nonylphenol polyethoxylates and their metabolites in four Beijing wastewater treatment plants. Sci. Tot. Environ. 407, 4261-4268

Limson, J. Odunuga, O.O., Green, H., Höök, F. and Blatch, G.L., 2004. The use of Quartz Crystal Microbalance with Dissipation (QCM-D) for the measurement of protein-protein interactions: a qualitative and quantitative analysis of the interactions between molecular chaperones. S. Afr. J. Sci., 100, 678-682.

Lin, C.-F., Liu, S.-H. and Hao, O.J., 2001. Effect of Functional Groups of Humic Substances on UF Performance. Wat. Res. 35, 2395–2402

Lin, C-W., Chen S-Y., Cheng, Y-W., 2006. Effect of metals on biodegradation kinetics for methyl tert-butyl ether., Biochem. Eng. Journ., 32, 25-32

Liu, Y., Qu, X., Guo, H., Chen, H., Liue, B., and Don, S., 2006. Facile preparation of amperometric laccase biosensor with multifunction based on the matrix of carbon nanotubes–chitosan composite. Biosens. Bioelectron. 21, 2195-2201

Llorca-Pórcel, J., Martínez-Parreño, M., Martínez-Soriano, E. and Valor, I., 2009. Analysis of chlorophenols, bisphenol-A, 4-tert-octylphenol and 4-nonylphenols in soil by means of ultrasonic solvent extraction and stir bar sorptive extraction with in situ derivatisation. J. Chromatog. A 1216, 5955-5961

Lojou, E., and Bianco, P.J., 2004. Quartz crystal microbalance and voltammetry monitoring for layer-by-layer assembly of cytochrome c3 and poly(ester sulfonic acid) films on gold and silver electrodes. J. Electroanal. Chem. 573 159-167

Lord, M.S. C. Modin, M. Foss, M. Duch, A. Simmons, F. S. Pedersen, B. K. Milthorpe and F. Besenbacher, (2006), Monitoring cell adhesion on tantalum and oxidised polystyrene using a quartz crystal microbalance with dissipation, Biomat., 27, 4529-4537

Löster, K. and Josíc, D. 1997. Review: Analysis of protein aggregates by combination of cross-linking reactions and chromatographic separations. J. Chromatog. B. 699, 439-461

Lowe, C.R., 1977. Immobilized lipoamide dehydrogenase 2. Properties of the enzyme immobilized to agarose through spacer molecules of various lengths. Eur. J. Biochem, 76, 401-409

Lubarsky, G.V., Davidson, M.R., and Bradley, R.H., 2007. Hydration-dehydration of adsorped protein films studied by AFM and QCM-D. Biosens. Bioelectron., 1275-1281

Mafatle, T. and Nyokong, T., 1997. Use of cobalt(II) phthalocyanine to improve the sensitivity and stability of glassy carbon electrodes for the detection of cresols, chlorophenols and phenol. Anal. Chim. Acta 354, 307-314.

Majer, V., Veselý, J., and Štulík, 1973. The Potentiometric Response of some Carbonaceous Electrodes. J. Electroanal. Chem and Interfac. Electrochem. 45, 113-125.

Malaveille, C., Hautefeuille, A., Pignatelli, B., Talaska, G., Vineis, P. and Bartchs, H., 1998. Antimutagenic dietary phenolics as antigenotoxic substances in urothelium of smokers. Mutat. Res. 402, 219-224

Malmström, J., Agheli, H., Kingshott, P., and Sutherland, D.S., 2007. Viscoelastic Modeling of Highly Hydrated Laminin Layers at Homogeneous and Nanostructured Surfaces: Quantification of Protein Layer Properties Using QCM-D and SPR, Langmuir 23, 9760-9768

Mansoor, S., Gupta, N., Luczy-Bachman, G., Limb, A., Kuppermann, B.D. and Kenney, M.C., 2010. Protective effects of memantine and epicatechin on catechol-induced toxicity on Müller cells in vitro. Toxicol. 271, 107-114.

Marozzi, C.A. and Chialvo, A.C., 1996. Periodic current signals of very low frequency and amplitude for real surface area measurements: (I) Theoretical Analysis. Electrochim. Acta 41, 15, 2351-2359

Martínez, D., Cugat, M.J., Borrull, F. and Calull, M., 2000. Review: Solid-phase extraction coupling to capillary electrophoresis with emphasis on environmental analysis. J. Chromatogr. A 902, 65–89

Marx, K.A., Zhou, T., Montrone, A. McIntosh, D. and Braunhut, S.J. (2006), A comparative study of the cytoskeleton binding drugs nocodazole and taxol with a mammalian cell quartz crystal microbalance biosensor: Different dynamic responses and energy dissipation effects, Anal. Biochem., Available in press

Mashazi, P.N., Ozoemena, K.I. and Nyokong, T., (2006). Tetracarboxylic acid cobalt phthalocyanine SAM on gold: Potential applications as amperometric sensor for H_2O_2 and fabrication of glucose biosensor, Electrochim. Acta, 52, 177-186

Mateo, C., Grazú, V., Pessela, B.C.C., Montes, T., Palomo, J.M., Torres, R., López-Gallego, F., Fernández-Lafuente, R., Guisán, J.M., 2007. Advances in the design of new epoxy supports for enzyme immobilization–stabilization. Biochem. Soc. Transact. 35, 1593-1601

Mateo, C., Palomo, J.M., Fernandez-Lorente, G., Guisan, J.M. and Fernandez-Lafuente, R., 2007. Review: Improvement of enzyme activity, stability and selectivity via immobilization techniques. Enz. Microb. Tech. 40, 1451-1463

Matijošytė, I., Arends, I.W.C.E., Sheldon, R.A. and de Vries, S., 2008. Pre-steady state kinetic studies on the microsecond time scale of the laccase from Trametes versicolor. Inorg. Chim. Acta. 361, 1202-1206

Mattheissen, P., and Law, R.J., 2002. Contaminants and their effects on estuarine and coastal organisms in the United Kingdom in the late twentieth century. Environ. Pollut. 120, 739-757

Max, B., Salgado, J.M., Cortés, S. and Domínguez, J.M., 2010. Extraction of Phenolic Acids by Alkaline Hydrolysis from the Solid Residue Obtained after Prehydrolysis of Trimming Vine Shoots. J. Agric. Food Chem. 58, 1909-1917

Mazur, M., Krysiński, P., Michota-Kamińska, A., Bukowska, J., Rogalski, J., Blanchard, G.J., 2007. Immobilization of laccase on gold, silver and indium tin oxide by zirconium–phosphonate–carboxylate (ZPC) coordination chemistry. Bioelectrochem. 71, 15- 22.

McCreery, R.L. and Cline K.K., 1996. *Chapter 10: Carbon Electrodes.* In: Laboratory Techniques in Electroanalytical Chemistry. 2nd Edition. Kissinger, P.T. and Heineman, W.R. (eds). Marcel Dekker, Inc. United States of America. pp., 293-332

McManus, J.P., Davis, K.G., Beart, J.E., Gaffney, S.H., Lilley, T.H. and Haslam, E., 1985. Polyphenol Interactions. Part 1. Introduction; Some Observations on the Reversible Complexation of Polyphenols with Proteins and Polysaccharides. J. Chem. Perkin. Trans. 2, 1429-1438

McMurry, J., 2000a: McMurry, J., 2000. *Ch 17: Alcohols and Phenols.* In: Organic Chemistry, McMurry, J. (ed), 5th edition. Brooks/Cole, Thomson Learning, United States of America.

McMurry, J., 2000b: McMurry, J., 2000. *Ch 15: Benzene and aromaticity.* In: Organic Chemistry, McMurry, J. (ed), 5th edition. Brooks/Cole, Thomson Learning, United States of America.

McMurry, J., 2000c: McMurry, J., 2000. *Ch 16: Chemistry of Benzene: Electrophilic aromatic substitution.* In: Organic Chemistry, McMurry, J. (ed), 5th edition. Brooks/Cole, Thomson Learning, United States of America.

Miaw, L.-H. L. and Perone, S.P., 1979. Theoretical and Experimental Studies of the Effects of Charging Currents in Potential-Step Voltammetry. Anal. Chem. 51, 1645-1650

Miller, A. and Tanner, J., 2008. *Kinetics and Catalysis.* Chapter 8. In: Essentials of Chemical Biology – Structure and Dynamics of Biological Macromolecules, 2008. Miller, A. and Tanner, J. (eds). John Wiley & Sons, Ltd, England.

Modin, C., Stranne, A.-L., Foss, M., Duch, M., Justesen, J., Chevallier, J., Andersen, L.K., Hemmersam, A.G., Pedersen, F. S. and Besenbache, F. (2006). QCM-D studies of attachment and differential spreading of pre-osteoblastic cells on Ta and Cr surfaces, Biomat. 27, 1346-1354

Mondal, K., and Gupta, M.N.., 2006. The affinity concept in bioseparation: Evolving paradigms and expanding range of applications. Biomol. Engin. 23, 59-76

Monterali, M.R., Della Seta, L., Vastarella, W. and Pilloton, R., 2009. A disposable Laccase–Tyrosinase based biosensor for amperometric detection of phenolic compounds in must and wine. J. Mol. Catal. B: Enz.

Moulton, S.E., Barisci, J.N., Bath, A., Stella, R., and Wallace, G.G., 2004. Studies of double layer capacitance and electron transfer at a gold electrode exposed to protein solutions. Electrochim. Acta 49, 4223-4230

Moyo, M., Ndhlala, A.R., Finnie, J.F and Van Staden, J., 2010. Phenolic composition, antioxidant and acetylcholinesterase inhibitory activities of Sclerocarya birrea and Harpephyllum caffrum (Anacardiaceae) extracts. Food Chem. 123, 69-76.

Mudnic, I., Modun, D., Rastija, V., Vukovic, J., Brizic, I., Katalinic, V., Kozina, B., Medic-Sarc, M., and Boban, M., 2010. Antioxidative and vasodilatory effects of phenolic acids in wine. Food Chem. 119, 1205-1210

Müller, M and Kastening, B., 1994. The double layer of activated carbon electrodes. Part 1. The contribution of ions in the pores. J. Electroanal. Chem. 374, 149-158.

Mungikar, A.A. and Forciniti, D. 2004. Conformational Changes of Peptides at Solid/Liquid Interfaces: A Monte Carlo Study, Biomacromol. 5, 2147-2159

Munteanu, F-D., Basto, C., Gübitz, G.M. and Cavaco-Paulo, A., 2006. Staining of wool using the reaction products of ABTS oxidation by Laccase: Synergetic effects of ultrasound and cyclic voltammetry. Ultrason. Sonochem. 14, 363-367

Murphy, L., 2006. Biosensors and bioelectrochemistry, Curr. Opin. Chem. Biol., 10, 77-184

Nam, K., Kimura, T. and Kishida, A., 2007. Preparation and characterization of cross-linked collagen–phospholipid polymer hybrid gels. Biomat. 28, 1 – 8

Navarra, C., Goodwin, C., Burton, S., Danieli, B. and Riva, S., 2010. Laccase-mediated oxidation of phenolic derivatives. J. Mol. Catal. B: Enz. 65, 52-57

Navarra, C., Goodwin, C., Burton, S., Danieli, B. and Riva, S., 2010. Laccase-mediated oxidation of phenolic derivatives. J. Mol. Catal. B: Enz. 65, 52-57

Nematollahi, D. and Goodrazi, H., 2001. Electrochemical study of catechol and some of 3-substituted catechols in the presence of 1,3-diethyl-2-thio-barbituric acid. Application to the electro-organic synthesis of new dispirothiopyrimidine derivatives. J. Electroanal. Chem. 510, 108 - 114

Nematollahi, D. and Goodrazi, H., 2001. Electrochemical study of catechol and some of 3-substituted catechols in the presence of 1,3-diethyl-2-thio-barbituric acid. Application to the electro-organic synthesis of new dispirothiopyrimidine derivatives. J. Electroanal. Chem. 510, 108 - 114

Northrop, D.B., 1998. On the Meaning of K_m and V/K in Enzyme Kinetics. J. Chem. Ed. 75, 1153-1157

Oakley, L., and Mulcahy, P., 2004. Immobilised cofactor derivatives for kinetic-based enzyme capture strategies: Direct coupling of NAD(P)+. Analytical Biochemistry, 335, 316-325. Anal. Biochem. 335, 316-325

Oikari, A., Kukkonen, J., and Virtanen, V., 1992. Acute toxicity of chemicals to Daphnia magna in humic waters. Sci. Total Environ. 117/118, 367-377

Omura, K., 2008. Electron Transfer between Protonated and Unprotonated Phenoxyl Radicals. J. Org. Chem. 73, 858-867.

Otzen, D., 2008. Differential adsorption of variants of the *Thermomyces lanuginosus* lipase on a hydrophobic surface suggests a role for local flexibility. Coll. Surf. B: Biointerf. 64, 223-238

Palmieri, G., Giardina, P., Bianco, C., Fontanella, B. and Sannia, G., 2000. Copper Induction of Laccase Isoenzymes in the Ligninolytic Fungus Pleurotus ostreatus. Appl. Environ. Microbiol. 66, 920-924

Pałys, B., Marzec, M. and Rogalski, J., 2010. Poly-o-aminophenol as a laccase mediator and influence of the enzyme on the polymer electrodeposition. Bioelectrochem. 80, 43-48

Paul, S., Paul, D., Basova, T. and Ray, A.K., 2008. Studies of Adsorption and Viscoelastic Properties of Proteins onto Liquid Crystal Phthalocyanine Surface Using Quartz Crystal Microbalance with Dissipation Technique. J. Phys. Chem. C 112, 11822–11830

Pauliukaite, R., Zhylyak, G., Citterio, D. and Spichiger-Keller, U.E., 2006. L-Glutamate biosensor for estimation of the taste of tomato specimens. Anal. Bioanal. Chem. 386, 220–227

Pazarlıoğlu, N.K., Sariişik, M. and Telefoncu, A., 2005. Laccase: production by Trametes versicolor and application to denim washing. Proc. Biochem. 40, 1673 - 1678

Peng, Y., Ye, J. and Kong, J., 2005. Determination of Phenolic Compounds in Perilla frutescens L. by Capillary Electrophoresis with Electrochemical Detection. J. Agric. Food Chem. 53, 8141-8147

Phizicky, E.M. and Fields, S., 1995. Review: Protein-Protein Interactions: Methods for Detection and Analysis. Microbiol. Rev. 59, 94-123

Piontek, K., Antorini, M. and Choinowski, T., 2002. Crystal Structure of a Laccase from the Fungus Trametes versicolor at 1.90-Å Resolution Containing a Full Complement of Coppers. J. Bio. Chem. 277, 37663–37669

Pocurull, E., Marcé, R.M. and Borrull, F., 1996. Determination of phenolic compounds in natural waters by liquid chromatography with ultraviolet and electrochemical detection after on-line trace enrichment. J. Chromatogr. A. 738, 1-9

Prabhu, V.G., Zarapkar, L.R. and Dhaneshwar, R.G. (1981), Electrochemical studies of hydrogen peroxide at a platinum disc electrode, Electrochim. Acta. 26, 725-729

Qiu, H., Xu, C., Huang, X., Ding, Y., Qu, Y. and Gao, P., 2008. Adsorption of Laccase on the Surface of Nanoporous Gold and the Direct Electron Transfer between Them. J. Phys. Chem. 112, 14781-14785

Quan, D., Kim, Y. and Shin, W., 2003. Characterization of an amperometric laccase electrode covalently immobilized on platinum surface. J. Electroanal. Chem. 561, 181-189

Quintana, M.C. and Ramos, L., 2008. Sample preparation for the determination of chlorophenols. Tr. Anal. Chem. 27, 418-436

R. Pauliukaite, G. Zhylyak, D. Citterio and U. E. Spichiger-Keller (2006) *L-glutamate biosensor for estimation of the taste of tomato specimens*. Anal. Bioanal. Chem. 386, 220-227

Rabinovich, M.L., Bolobova, A.V. and Vasil'chenko, L.G., 2004. Fungal Decomposition of Natural Aromatic Structures and Xenobiotics: A Review. App. Biochem. Microbio. 40, 5-23.

Rahman, Md. A., Noh, H-B., Shim, Y-B., 2008. Direct Electrochemistry of Laccase Immobilized on Au Nanoparticles Encapsulated-Dendrimer Bonded Conducting Polymer: Application for a Catechin Sensor. Anal Chem. 80, 8020-8027

Ray, K.G. III, McCreery, R. L., 1999. Characterization of the surface carbonyl and hydroxyl coverage on glassy carbon electrodes using Raman spectroscopy. J. Electroanal. Chem. 469, 150-158

Razee, S. and Masujima, T., 2002. Uptake monitoring of anilines and phenols using modified zeolites. Anal. Chim. Acta 464, 1-5.

Reimhult, E., Larsson, C., Kasemo, B., and Höök, F., 2004. Simultaneous Surface Plasmon Resonance and Quartz Crystal Microbalance with Dissipation Monitoring Measurements of Biomolecular Adsorption Events Involving Structural Transformations and Variations in Coupled Water. Anal. Chem. 76, 7211-7220

Rice, R., Allred, C. and McCreery, R., 1989. Fast ehterogenous electron transfer rates for glassy carbon electrodes without polishing or activation procedures. J. Electroanal. Chem. 263, 163-169.

Robards, K., 1992. Review: Analytical Applications of liquid-phase chemiluminescence. Anal. Chim. Acta 266, 147-173.

Robbins, R.J., 2003. Phenolic Acids in Foods: An Overview of Analytical Methodology. J. Agr. Food Chem. 51, 2866-2887

Robles, A., Lucas, R., Martínez-Cañamero, M., Ben Omar, N., Pérez, R. and Gálvez, A., 2002. Characterisation of laccase activity produced by the hyphomycete Chalara (syn. Thielaviopsis) paradoxa CH32. Enz. Microb. Tech. 31, 516-522

Rodríguez-Bernaldo de Quirós, A., Frecha-Ferrero, S., Vidal-Pérez, A.M. and López-Hernández, J., 2010. Antioxidant compounds in edible brown seaweeds. Eur. Food Res. Technol. 231, 495–498

Rødtjer, A., Skibsted, L.H., Andersen, M.L., 2006. Identification and quantification of phenolics in aromatic bitter and cherry liqueur by HPLC with electrochemical detection. Eur Food Res Technol 223, 663–668

Roessl, U. Nahálka, J., and Nidetzky, B., 2010. Review: Carrier-free immobilized enzymes for biocatalysis. Biotechnol. Lett. 32, 341-350

Rosner, B., 2000. *Chapter 6: Estimation.* In: Fundamentals of Biostatistics. 5th Edition. Rosner, B. (ed.). Duxbury, Brooks/Cole, United States of America. pp., 185-198

Rothman, N ., Bechtold, W.E., Yin, S.-N., Dosemeci, M., Li, G.-L., Wang, Y.-Z., Griffith, W.C., Smith, M.T. and Hayes, R.B., 1998. Urinary excretion of phenol, catechol, hydroquinone, and muconic acid by workers occupationally exposed to benzene. Occup. Environ .Med. 55, 705–707

Roy, J.J and Abraham, T.E., 2004.Review: Strategies in Making Cross-Linked Enzyme Crystals. Chem. Rev. 104, 3705-3722

Roy, J.J. and Abraham, T.E., 2006. Preparation and characterization of cross-linked enzyme crystals of laccase. J. Mol. Catal. B: Enz. 38, 31–36

Royer, G.P., 1982. Immobilised Enzymes in: Royer, G.P. (Ed.) Fundamentals of Enzymology: Rate enhancement, specificity, control and applications, John Wiley and Sons Ltd., United States of America, pp. 181 - 194

Roza, L., de Vogel, N., van Delft, J.H.M., 2003. Lack of clastogenic effects in cultured human lymphocytes treated with hydroquinone, Food Chem. Toxicol. 41, 1299–1305.

Sadeghi, S.J., Tsotsou, G.E., Fairhead, M., Meharenna, Y.T. and Gilard, G., 2002. Rational design of P450 enzymes for biotechnology. Chapter 3. In: Physics and Chemistry Basis of Biotechnology, Volume 7. De Cuyper, M. and Bulte, J.W.M. (eds.), Kluwer Academic Publishers, New York, United States of America, pp 88-91

Sagnella, G.A., 1985. Fitting linear models to structure-activity data. Trends Biochem. Sci. 10, 100-103

Sahoo, B.K., Ghosh, K.S. and Dasgupta, S., 2008. Investigating the binding of curcumin derivatives to bovine serum albumin. Biophys. Chem.132, 81–88

Saito, T., Hong, P., Kato, K., Okazaki, M., Inagaki, H., Maeda, S. and Yokogawa, Y., 2003. Purification and characterization of an extracellular laccase of a fungus (family Chaetomiaceae) isolated from soil. Enz. Microb. Tech. 33, 520-526

Sakihama, Y., Cohen, M.F., Grace, S.C., Yamasaki, H., 2002. Plant phenolic antioxidant and prooxidant activities: phenolics-induced oxidative damage mediated by metals in plants. Toxicol. 177, 67-80.

Salis, A., Pisano, M., Monduzzi, M., Solinas, V., Sanjust, E., 2009. Laccase from Pleurotus sajor-caju on functionalised SBA-15 mesoporous silica: Immobilisation and use for the oxidation of phenolic compounds. J. Mol. Cat. B: Enz. 58, 175-180

Santos, F.J. and Galceran, M.T., 2003. Review: Modern developments in gas chromatography– mass spectrometry based environmental analysis. J. Chromatrogr. A. 1000, 125-151.

Schwiegert, N., Zehnder, A.J.B. and Eggen, R.I.L., 2001. Minireview: Chemical properties of catechols and their molecular modes of toxic action in cells, from microorganisms to mammals. Environ. Microbio. 3, 81-91

Scouten, W.H., Luon, J.H.T. and Brown, R.S., 1995. Reviews: Enzyme or protein immobilization techniques for applications in biosensor design. TIBTECH 13, 178-185

Shi, K., Hu, K., Wang, S., Lau, C-Y. and Shiu, K.K., 2007. Structural studies of electrochemically activated glassy carbon electrode: Effects of chloride anion on the redox responses of copper deposition. Electrochim. Acta. 52, 5907-5913

Shleev et al., 2006a: Shleev, S.S., Shumakovich, G., Mazhugo,Y., Yaropolov, A., Ruzgas, T., and Gorton, L., 2006. Interaction of fungal laccases and laccase-mediatornext term systems with lignin. Enz. Microb. Tech. 39, 841 – 847

Shleev et al., 2006b: Shleev, S., Reimann, C. T., Serezhenkov, V., and Dosymzhan, B. 2006. Autoreduction and aggregation of fungal laccase in solution phase: possible correlation with a resting form of laccase. Biochimie 88 , 1275–1285.

Shleev et al., 2006c: Shleev, S., Persson, P., Shumakovich, G., Mazhugo, Y., Yaropolov, A., Ruzgas, T. and Gorton, L, 2006. Laccase-based biosensors for monitoring lignin. Enz. Microb. Tech. 39, 835-840

Shleev, S.V., Morozova, O.V., Nikitina, O,V,m Gorshina, E.S., Rusinova, T.V., Serezhenkov, V.A., Burbaev, D.S., Gazaryan, I.G. and Yaropolov, A.I., 2004. Comparison of physico-chemical characteristics of four laccases from different basidiomycetes. Biochimie 86, 693-703

Shuttleworth, K.L. and Bollag, J.M., 1986. Soluble and immobilized laccase as catalysts for the transformation of substituted phenols. Enz. Microb. Tech. 8, 171-177

Siebert, K.J., 1999. Reviews: Effects of Protein-Polyphenol Interactions on Beverage Haze, Stabilization, and Analysis. J. Agric. Food Chem. 47, 353-362

Smith, M.T., Zhang, L., Jeng, M., Wang, Y., Guo, W., Duramad, P., Hubbard, A.E., Hofstadler, G. and Holland, N.T., 2000. Hydroquinone, a benzene metabolite, increases the level of aneusomy of chromosomes 7 and 8 in human CD34-positive blood progenitor cells. Carcinogen. 21, 1485-1490

Smith, R.K., Lewis, P.A. and Weiss, P.S., 2004. Patterning self-assembled monolayers. Prog. Surf. Sci. 75, 1-68

Smyrl, W.H., Atanasoski, R.T., Atanososka, L., Hartshorn, L., Lien, M., Nygren, K. and Fletcher, E.A., 1989. Morphology changes due to anodic treatment of glassy carbon electrodes. J. Electroanal. Chem. 264, 301-304

Soares, A., Guieysse, B.,Jefferson, B., Cartmell, E. and Lester, J.N., 2008. Review article: Nonylphenol in the environment: A critical review on occurrence, fate, toxicity and treatment in wastewaters. Environ. Internat. 34, 1033-1049.

Solńa, R., Dock, E., Christenson, A., Winther-Nielsen, M., Carlsson, C., Emnéus, J., Ruzgas, T. and Skládal, P., 2005. Amperometric screen-printed biosensor arrays with co-immobilised oxidoreductases and cholinesterases. Anal. Chim. Acta 528, 9-19

Stalikas, C.S., 2007. Review: Extraction, separation, and detection methods for phenolic acids and flavonoids. J. Sep. Sci. 30, 3268 – 3295

Stojan, J., 1997. Analysis of Progress Curves in an Acetylcholinesterase Reaction: A Numerical Integration Treatment. J. Chem. Inf. Comput. Sci. 37, 1025-1027

Sugama, T., 2000. Antioxidants for retarding hydrothermal oxidation of polyphenylenesulfide coatings in geothermal environments. Mat. Lett. 43, 185-191.

Suliman, F.E., Al-Kindi, S.S., Al-Kindy, S. M.Z., Al-Lawati, H.A.J., 2006. Analysis of phenols in water by high-performance liquid chromatography using coumarin-6-sulfonyl chloride as a fluorogenic precolumn label. J. Chromatogr. A 1101,179–184

Suzuki, N., Quesenberry, M.S., Wang, J.K., Lee, R.T., Kobayashi, K. and Lee, Y.C., 1997. Efficient Immobilization of Proteins by Modification of Plate Surface with Polystyrene Derivatives. Anal. Biochem. 247, 412-416

Swain, G.M., 2007. Chapter 5: Solid Electrode Materials: Pretreatment and Activation. In: Handbook of Electrochemistry. 1st Edition. Zoski, C.G. (ed.) Elsevier B.V., Netherlands. pp., 114-131

Tallon, G.R. and Hepner, R.D., 1958. Determination of p-Cresol in Industrial Waste Waters. Anal. Chem. 30, 1521-1524

Tan, Y., Deng, W., Ge, B., Xie, Q., Huang, J. and Yao, S., 2009. Biofuel cell and phenolic biosensor based on acid-resistant laccase–glutaraldehyde functionalized chitosan–multiwalled carbon nanotubes nanocomposite film. Biosens. Bioelectron. 24, 2225 – 2231

Tan, Y., Deng, W., Ge, B., Xie, Q., Huang, J. and Yao, S., 2009. Biofuel cell and phenolic biosensor based on acid-resistant laccase–glutaraldehyde functionalized chitosan–multiwalled carbon nanotubes nanocomposite film. Biosens. Bioelectron. 24., 2225-2231

Tanford, C., Swanson, S.A. and Shore, W.S., 1955. Hydrogen Ion Equilibria of Bovine Serum Albumin. J. Am. Chem. Soc. 77, 6414–6421.

Teichroeb, J.H., Forrest, J.A., Jones, L.W., Chan, J., and Dalton, K., 2008. Quartz crystal microbalance study of protein adsorption kinetics on poly(2-hydroxyethyl methacrylate) J Coll. Interf. Sci. 325 157-164)

Tian, J., Liu, J., Hu, X. and Chen, X., 2005. Interaction of wogonin with bovine serum albumin. Bioorg. Med. Chem. 13, 4124-4129

Timur, S., Pazarıoğlu, Pilloton, R. and Telefoncu, A., 2004. Thick film sensors based on laccases from different sources immobilized in polyaniline matrix. Sens. Actuat. B 97, 132–136

Tokmakov, I.V., Kim, G.-S., Kislov, V.V., Mebel, A.M. and Lin, M.C., 2005. The Reaction of Phenyl Radical with Molecular Oxygen: A G2M Study of the Potential Energy Surface. J. Phys. Chem. A 109, 6114-6127

Tranchimand, S., Tron, T., Gaudin, C. and Iacazio, G., 2006. Synthesis of bis-lactone lignans through laccase catalysis. J. Mol. Cat. B: Enzym. 42, 27-31.

Trasatti, S. and Petrii, O.A., 1991. Real surface area measurements in electrochemistry. J. Electroanal. Chem 327, 353-376

Ureta-Zañartu, M.S., Bustos, P., Diez, M.C., Mora, M.L. and Gutiérrez, C., 2001. Electro-oxidation of chlorophenols at a gold electrode. Electrochim. Acta 46, 2545-2551

Uthandi, S., Saad, B., Humbard, M.A. and Maupin-Furlow, J.A., 2010. LccA, an Archaeal Laccase Secreted as a Highly Stable Glycoprotein into the Extracellular Medium by Haloferax volcanii. App. Environ. Microbiol. 76, 733-743.

Vega, D., Agüí, L., González-Cortés, A., Yáñez-Sedeño, P. and Pingarrón, J.M., 2007. Electrochemical detection of phenolic estrogenic compounds at carbon nanotube-modified electrodes. Talanta 71, 1031-1038.

Vianello, F., Cambria, A., Ragusa, S., Cambria, M.T., Zennaro, L., Rigo, A., 2004. A high sensitivity amperometric biosensor using a monomolecular layer of laccase as biorecognition element. Biosens. Bioelectron. 20, 315-321

Villaverde, A., 2003. Minireview: Allosteric enzymes as biosensors for molecular diagnosis. FEBS Lett. 554, 169-172

Voinova, M.V., Rodahl, M., Jonson, M., and Kasemo, B., 1999. Viscoelastic Acoustic Response of Layered Polymer Films at Fluid-solid Interfaces: Continuum Mechanics Approach. Phys. Script. 59, 391-396

Voinova, M.V., Jonson, M., and Kasemo, B., 2002. 'Missing mass' effect in biosensor's QCM applications. Biosens. Bioelectron. 17, 835-841

Voinova, M.V., Rodahl, M., Jonson, M., Kasemo, B., 1999. Viscoelastic Acoustic Response of Layered Polymer Films at Fluid-solid Interfaces: Continuum Mechanics Approach. Phys. Script. 59, 391-396

Walsh, R., Martin, E., Darvesh, S., 2007. A versatile equation to describe reversible enzyme inhibition and activation kinetics: Modeling β-galactosidase and butyrylcholinesterase. Biochim. Biophys. Acta, 1770 733–746

Walsh, S., Diamond, D., 1994. Non-linear curve fitting using Microsoft Excel *Solver*. Talanta, 42, 561-572

Wang, J. and Lin, M.S., 1988. In Situ Electrochemical Renewal of Glassy Carbon Electrodes. Anal. Chem. 60, 499-502

Wang, J. and Martinez, T., 1991. Scanning tunneling microscopic investigation of surface fouling of glassy carbon surfaces due to phenol oxidation. J. Electroanal. Chem. 313, 129-140

Wang, J. and Martinez, T., 1991. Scanning tunneling microscopic investigation of surface fouling of glassy carbon surfaces due to phenol oxidation. J. Electroanal. Chem. 313, 129-140

Wang, J., 1994. *Chapter 1: Fundamental Concepts*. In: Analytical Electrochemistry. 2nd Edition. Wang, J. (ed.). VCH, New York. pp 15-42

Wang, J., Jiang, M. and Lu, F., 1998. Short Communication: Electrochemical quartz crystal microbalance investigation of surface fouling due to phenol oxidation. J. Electroanal. Chem. 444, 127-132

Wang, J., Liu, J. and Cepra, G., 1997. Thermal Stabilization of Enzymes Immobilized within Carbon Paste Electrodes. Anal. Chem. 69, 3124-3127

Wang, Y.-J., Lee, C.-C., Chang, W.-C., Liou, H.-B. and Ho, Y.-S., 2001. Oxidative stress and liver toxicity in rats and human hepatoma cell line induced by pentachlorophenol and its major metabolite tetrachlorohydroquinone. Toxicol. Lett. 122, 157–169

Wasinki, F.A.H. and Andersson, J.T., 2007. Qualitative analysis of phenols and alcohols in complex samples after derivatization to esters of ferrocene carboxylic acid by gas chromatography with mass spectrometric detection. J. Chromatogr. A 1157, 376-385

Weiss, J.N., 1997. The Hill equation revisited: uses and misuses. FASEB J. 11, 835-841

Wheeler, S.K., Coury, L.A. and Heineman, W.R., 1990. Fouling-resistant, polymer-modified graphite electrodes. Anal. Chim. Acta. 237, 141-148

Whitehead, E.P., 1978. Co-operativity and the Methods of Plotting Binding and Steady-State Kinetic Data. Biochem. J. 171, 501-504.

Xu, C., Zhang, Y., Cao, L. and Lu, J., 2010. Phenolic compounds and antioxidant properties of different grape cultivars grown in China. Food Chem. 119, 1557-1565

Xu, F., 2005. Applications of oxidoreductases: Recent progress. Industrial Biotechnology 1, 38-50.

Xu, F., 1996. Oxidation of Phenols, Anilines, and Benzenethiols by Fungal Laccases: Correlation between Activity and Redox Potentials as Well as Halide Inhibition. Biochem. 35, 7608-7614

Xu, F., 1997. Effects of Redox Potential and Hydroxide Inhibition on the pH Activity Profile of Fungal Laccases. J. Biol. Chem. 272, 924-928

Xu, F., 2001. Dioxygen Reactivity of Laccase: Dependence on Laccase Source, pH, and Anion Inhibition. App. Biochem. Biotech. 95, 125 – 133

Xu, F., Kulys, J.J., Duke, K., Li, K., Krikstopaitis, K., Duessen, H-J. W., Abbate, E. and Galinyte, V., 2000. Redox Chemistry in Laccase-Catalyzed Oxidation of N-Hydroxy Compounds. App. Environ. Microb. 66, 2052-2056

Yang, F., Ruan, C., Xu, J.Lei, C. and Deng, J., 1998. An amperometric biosensor using toluidine blue as an electron transfer mediator intercalated in α-zirconium phosphate-modified horseradish peroxidase immobilization matrix. J. Anal. Chem. 361, 115–118

Yaropolov, A.I., Shleev, S.V., Morozova, O.V., Zaitseva, E.A., Marko-Varga, G., Emneus, J. and Gorton, L., 2005. An Amperometric Biosensor Based on Laccase Immobilized in Polymer Matrices for Determining Phenolic Compounds. J. Anal. Chem. 60, 553 - 557

Yaver, D.S., Xu, F., Golightly, E.J., Brown, K.M., Brown, S.H., Rey, M.W., Schneider, P., Halkier, T., Mondorf, K. and Dalbøge, H., 1996. Purification, Characterization, Molecular Cloning, and Expression of Two Laccase Genes from the White Rot Basidiomycete Trametes villosa.

Yin, Y., Bilek, M.M.M., McKenzie, D.R., Nosworthy, N.J., Kondyurin, A., Youssef, H., Byrom, M.J. and Yang, W., 2008. Acetylene plasma polymerized surfaces for covalent immobilisation of dense bioactive protein monolayers. Surf. Coat. Tech. 203, 1310-1316

Ying, G.-G., Williams, B. and Kookana, R., 2002. Environmental fate of alkylphenols and alkylphenol ethoxylates—a review. Environ. Internat. 28, 215-226.

Yu, J. and Liu, C.-C., 2010. Microfabricated Thin Film Impedance Sensor & AC Impedance Measurements. Sensors 10, 5845-5855

Zagal, J. H., (1992). Metallophthalocyanines as catalysts in electrochemical reactions. Coordin. Chem. Rev. 119, 89-136

Zhang, X., Liu, T., Sreekumar, T.V., Kumar, S., Moore, V.C., Hauge, R.H. and Smalley, R.E. (2003). Poly(vinyl alcohol)/SWNT Composite Film, Nano Lett. 3, 1285-1288

Zhang, Y., Zeng, G.-M., Tang, L., Huang, D.-L., Jiang, X.-Y. and Chen, Y.-N., 2006. A hydroquinone biosensor using modified core–shell magnetic nanoparticles supported on carbon paste electrode. Biosens. Bioelectron. 22, 2121-2126

Zhang, Y.-Z., Zhou, B., Zhang, X.-P., Huang, P., Li, C.-H. and Liu, Y., 2009 Interaction of malachite green with bovine serum albumin: Determination of the binding mechanism and binding site by spectroscopic methods. J. Haz. Mat. 163, 1345–1352

Zhao, Q-L., Zhang, Z-L., Bao, L. and Pang, D-W., 2008. Surface structure-related electrochemical behaviors of glassy carbon electrodes. Electrochem. Comm. 10, 181-185

Zhi, J-F., Wang, H-B., Nakashima, T., Rao, T.N. and Fujishima, A., 2003. Electrochemical Incineration of Organic Pollutants on Boron-Doped Diamond Electrode. Evidence for Direct Electrochemical Oxidation Pathway. J. Phys. Chem. B 107, 13389-13395

Zhi, J-F., Wang, H-B., Nakashima, T., Rao, T.N. and Fujishima, A., 2003. Electrochemical Incineration of Organic Pollutants on Boron-Doped Diamond Electrode. Evidence for Direct Electrochemical Oxidation Pathway. J. Phys. Chem. B 107, 13389-13395

Zhu, X. and Williamson, P.R., 2004. Role of laccase in the biology and virulence of Cryptococcus neoformans. FEMS Yeast Res. 5, 1-10.

Zoppellaro, G., Sakurai, N., Kataoka, K., Sakurai, T. 2004. The reversible change in the redox state of type I Cu in Myrothecium verrucaria bilirubin oxidase depending on pH, Biosci. Biotechnol. Biochem. 68, 1998–2000.